JOURNAL OF CONDENSED MATTER NUCLEAR SCIENCE

Experiments and Methods in Cold Fusion

VOLUME 11, April 2013

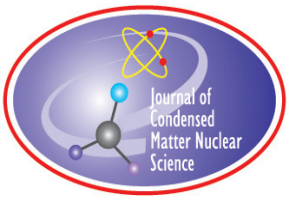

JOURNAL OF CONDENSED MATTER NUCLEAR SCIENCE

Experiments and Methods in Cold Fusion

Editor-in-Chief
Jean-Paul Biberian
Marseille, France

Editorial Board

Peter Hagelstein
MIT, USA

George Miley
Fusion Studies Laboratory, University of Illinois, USA

Xing Zhong Li
Tsinghua University, China

Michael McKubre
SRI International, USA

Edmund Storms
KivaLabs, LLC, USA

Akito Takahashi
Osaka University, Japan

JOURNAL OF CONDENSED MATTER NUCLEAR SCIENCE

Volume 11, April 2013

© 2013 ISCMNS. All rights reserved. **ISSN 2227-3123**

This journal and the individual contributions contained in it are protected under copyright by ISCMNS and the following terms and conditions apply.

Electronic usage or storage of data

JCMNS is an open-access scientific journal and no special permissions or fees are required to download for personal non-commercial use or for teaching purposes in an educational institution.

All other uses including printing, copying, distribution require the written consent of ISCMNS.

Permission of the ISCMNS and payment of a fee are required for photocopying, including multiple or systematic copying, copying for advertising or promotional purposes, resale, and all forms of document delivery.

Permissions may be sought directly from ISCMNS, E-mail: CMNSEditor@iscmns.org. For further details you may also visit our web site: http:/www.iscmns.org/CMNS/

Members of ISCMNS may reproduce the table of contents or prepare lists of articles for internal circulation within their institutions.

Orders, claims, author inquiries and journal inquiries

Please contact the Editor in Chief, CMNSEditor@iscmns.org or webmaster@iscmns.org

J. Condensed Matter Nucl. Sci. 11 (2013) 1–156
©2013 ISCMNS. All rights reserved. ISSN 2227-3123

JOURNAL OF CONDENSED MATTER NUCLEAR SCIENCE

Volume 11 2013

CONTENTS

PREFACE

It is my pleasure to announce the publication of the 11th volume of the "*Journal of Condensed Matter Nuclear Science*". This new volume comprises eight papers of theoretical and experimental studies. The growing number of publications in the journal indicates that the field is becoming more and more active.

Again in this volume, I had to make a decision regarding a paper by Edmund Storms. The referee did not agree with the reviewer, therefore we decided to publish the paper along with the comments of the referee. I know that this is not a common way of including the comments of referee in scientific journals, but this field is very uncommon, and deserves an unusual openness to ideas and suggestions.

Jean-Paul Biberian
April 2013

J. Condensed Matter Nucl. Sci. 11 (2013) 1–7

Obituary Note

On Martin Fleischmann: An Obituary and More

J.O'M. Bockris *

Haile Plantation, Gainesville, FL 32608, USA

Abstract

After receiving a Ph.D. Degree from Imperial College, Fleischmann (F) went to work in the University of Newcastle in the U.K. and spent productive years there (metal deposition, micro-electrodes, and electrochemical extraction from mixtures metals). His reputation grew at a time (1950–1960) when electrochemistry was a popular subject for university research. British Electricity saw their chance to get a star performer down to Southampton University as professor, so they paid for a chair for a person who could attract research support and found that F could fill the job, although it was open to other candidates. Fleischmann occupied the chair for only a few years, less than had been foreseen, and retired from university life some years before it is usual. By this time he already was a Fellow of the Royal Society and also a director of the Max Planck Institute in Berlin. Fleischmann made a colleague of Stanley Pons, head of the Chemistry Department in the University in Utah. Pons (P) was of independent means and could fund research which the two of them might think out together. Fusion means coming together and F saw in electrochemistry a high performance way whereby this might be done. What they found was that the heat evolved in a particular deuterium solution when they passed current through it was larger than it should have been according to known chemical theory. In addition to this they observed some neutrons. They suggested that the extra heat was due to an unknown nuclear reaction. What was unusual about the next step was that F&P got on the McNeil–Lehrer Hour and announced that they had been the first to carry out a nuclear reaction in the cold. After a short time, the nuclear chemists of the world turned against F&P and said that their claims must be all nonsense. The anti-Fleischmann opinion expressed at meetings was so great that they decided that it would be a good thing to escape to some other country. They had a friendship with a very wealthy man, Mr. Toyota, and he had already founded some laboratories in the South of France. He offered F and P laboratory space there and they could move their operation to it free of the negative atmosphere which reigned in America. At first the news which came from the laboratory in France was good. Alas, this was not maintained and after two years they split up and P retired to live in France whilst F retired to Tisbury in the U.K. But F's creativity would not lie down and he was soon to apply something new, Quantum Electrodynamics. He made a colleagueship with a well-known Italian physicist Preparata. However, fate was not kind to F and he discovered that he was suffering from Parkinson 's disease. This is a slow disease but it's incurable. However, for a couple of years F continued to attend meetings and make intelligent remarks at them. He died on 3 August 2012. Was F a brilliant theorist who did not have time to realize his true vision or had Jack the Flash, his nickname, flashed too much? The field that could have been his greatest is now called condensed matter nuclear reactions.
© 2013 ISCMNS. All rights reserved. ISSN 2227-3123

Keywords: Eagerness, Ideas, Imperial College, Quantum electrodynamics, Royal Society

*E-mail: jbockris@cox.net

© 2013 ISCMNS. All rights reserved. ISSN 2227-3123

1. Introduction

My first memory of Martin Fleischmann was a letter of application to me, then a young faculty member at the Imperial College of Science and Technology in London, to become a graduate student working under my direction.

I was only a few years past my own Ph.D. and already had 10 graduate students. I thought it would be a bit too much to take on another. I deflected Fleischmann's application to another person who was around the same degree of development as I. This man was Dr. J.F. Herringshaw and turned out to have a temperament which was the opposite of that of Fleischmann's, a pipe sucker, and he let it be known that he thought that the objective of his job was giving of lectures rather than the supervision of research.

The first impression one got of Martin Fleischmann in those days, and he changed little in appearance and manner throughout all the 67 years in which I knew him, was, well, I can choose two words, "eagerness, flashy."[a]

2. Imperial College

[b] Dr. Herringshaw's office was about a three minute walk from mine and Martin Fleischmann of course had his experimental bench in Herringshaw's office, but it was not long before Martin found out that there were quite a few fellows within a five-minute walk of the office in which he worked who were capable of providing discussions which was more than you could say for Dr. Herringshaw. I myself was available for discussion too, and there were several occasions in which Martin Fleischmann asked me directly if he could discuss a point with me and we took out for the stone corridor outside my room and walked up and down there: my usual platform for discussions with graduate students.

Roger Parsons and Brian Conway were both my graduate students at this time, but they were already recognized as advanced and could discuss too, so I think that Fleischmann got plenty of advice as he built up his Ph.D. thesis.

My corridor in the imposing modern looking Victorian constructed buildings holding the Chemistry and Physics Departments at Imperial College was a long one and the floor was made of stone. One could work as long as one wanted and seldom get interrupted and that's why I preferred to begin many discussions with my graduate students by pacing the corridor with anyone discussion-worthy.

Martin Fleischmann was seen often in my corridor and with my group, particularly on the weekends off and trips which we took together for social reasons[c], so that it seemed to be understood, as I have been told in later years that

[a] After I had left London in 1953, F was in the University of Newcastle and I heard, "from the grapevine," that he had developed there the nickname "jack the flash."

[b] It's worth saying a word about Imperial College where both Fleischmann and I got our Ph.D.'s. It is the nearest that the Brits have to MIT and certainly the principal education establishment in England which tends to look towards applications as well as giving a sound education in the fundamentals. Imperial College surrounded itself with high barriers. In the days in which I was teaching there entry students were selected by considering only those who could prove that they had come out first in their high school in chemistry. After that the firsts were called to London in the examination halls. There they underwent a stiff examination in chemistry, - all 500 of them, - and we selected the best 50 for further training and perhaps to graduate work. I had one year in which I was an examiner of this barrier and it certainly wasn't an easy exam. So we had the cream of the cream.

[c] Our trips were salted with girls and we used to collect them from the local nurses training institute which was around the corner from Imperial College Chemistry where we worked. Unfortunately the building in which they lived received a direct hit around about 1944 when Martin was still an undergraduate and as I was a member of the fire brigade of Imperial College Chemistry had to stand by while their building burned down. We didn't have any more girls from there!

part of the discussion and therefore the direction of Martin Fleischmann's thesis depended upon me as well as upon Herringshaw. However, I must admit that I don't remember much of it now.

One of the ways in which Martin Fleischmann helped me as much as I helped him, was with visitors.

In England the feeling is that the scientists who all have teaching positions at the great universities, government rewarded, should be open to serious citizens who would call in and ask a few questions.

When the discussions with the visitors began taking too much of my time, I would call on Martin Fleischmann and see if he had time to meet these people.

After stating the subject which they wanted to talk about, I would retreat to my desk and continue my work.

The story was the same for all of them. It was impressive how often Martin conjured up some theoretical hypothesis to meet the type of result that they were trying to expand on. Of course the level at which Fleischmann would present his ideas was a rather high one and sometimes involved beginning with a second order differential equation and some applications of Fick's law. It took about five minutes for the visitors to think that they had no place in this and make an excuse for catching the earlier train.

I would like to give you two more snippets from my contacts with Martin Fleischmann in his graduate student days.

First of all, I would like to stress that in my knowledge of him I never experienced harsh words. He was a smooth talker and bountifully possessed with ideas, though some of them were not clearly stated.

Long after the time when he got his Ph.D. and moved to Southampton and had several years there he was awarded with what most chemists regard as not quite the Nobel Prize but a good substitute indeed, A Fellowship of the Royal Society! He visited America about this time and of course came to see me. At this time I was at the Texas A&M University which is better financed than MIT because of the large amount of oil money which is at the disposal of the Board of Directors.

Martin, just after his FRS, and talking to me in the visit never mentioned it and jumped right into a scientific discussion. Before he left I briefly congratulated him on his attainment and all he said was, "oh, well..."

One story I would like to tell relates to the early seventies and I had been on a trip to Moscow to see Frumkin. In those days flights directly from Moscow to New York were absent and one had to change in London and this I did and thought well, why not go and see Fleischmann and have a talk with him. I met with Martin on a Saturday morning and we had lunch in a pub and I tried to discuss the electrochemical problem which was worrying me. We retreated to my rental car that I had used for coming down from Heathrow and I tried to engage Martin to open up some fundamental ideas, but it was difficult. He never wanted to engage with me and kept on telling me that I was quite right, excellent, etc., but of course that was not what I was looking for. What I wanted was intellectual engagement. I had had many with him when he was a graduate student. When I got home to Philadelphia I looked back on the day in Southampton as a waste of time.

So it was not easy to get Martin Fleischmann to open up and it may well have been that he objected to giving his ideas to other people, but I think it was a different thing. I think he needed to be alone and as with many people including myself in open discussions with people except with very rare people like Brian Conway or Srinivasen, seldom develop in an original way.

This next instant comes from the 1950s whilst I was still in London and Martin Fleischmann had his Ph.D. I want to describe to you his persona at that time which I remember well. He really did look like a "European intellectual." He was dressed usually in a jacket which certainly wasn't made in London. His most frequent phrase in those times, "what a gas," was to the fore in his conversation and he smiled and laughed a lot. He was a jovial sort of fellow to be with.

Of course, there is no doubt that one of Martin's faults was that he overstated himself, but do not think for a moment that I am suggesting that there wasn't behind the overstatement a REAL BRAIN, but he did not agree with the British habit of understatement.

Well, let us now shift a bit in the direction of the McNeil Lehrer Hour (1989) and all the unpleasant times that we

had to go through then. We haven't met Stanley Pons yet.

3. Fleischmann after Imperial College

I think that Martin's thesis must have gone through around about 47 or 48. In spite of my relationship in the work before the thesis I do not remember reading it, but I do remember that the first job he had after he left with a Doctor's title was an academic job in Newcastle and those who are only faintly familiar with the UK, you can think of Newcastle as about three-quarters of the way up the eastern side of Great Britain.

Reginald Thirsk was the man with whom Martin collaborated there and Thirsk had his day as a leading electrochemist in the country a little bit before the time Martin gathered with him in Newcastle. He was a slow speaking man and not one who would rush at a new idea, but there's no doubt that Reginald Thirsk was a full-time electrochemist and had a good reputation for solid work.

There was indeed a time around about 1960 when my own co-workers Damjanovic from Belgrade and Asa Despic from the same city were collaborating with me and my colleagues particularly in the early stages of metal deposition and Thirsk and Fleischmann were doing something very similar. It wasn't metal deposition at its complex multi crystalline, but was what happened when you turned a current on and metal ions deposited on the surface of the originating metal and we made it simple by having, for example, silver on silver, because if, of course as we did later, you had A depositing on B then everything was a good deal more complicated.

Here I think Martin Fleischmann's ability to handle equations which showed up with the visitors, came out in full and how much he helped Thirsk and how much Thirsk helped him I cannot say, but I suspect that the equational part was at least in a fair amount due to Martin Fleischmann because he was facile with manipulations of the type that you need when you are considering surface diffusion of metal atoms, meeting growth sites and rotating spiral.

Another thing that Martin Fleischmann did and became well known for in those days, the late sixties, was to help with the equations for porous electrodes. It is of course completely wrong to tackle fuel cell electrodes while assuming that the depositing substrate is a plain surface. It's all pores that you have to deal with and most of the porous electrodes used in fuel cells have some kind of catalyst deposited in the pores. So you have to consider the pores, the diffusion in them, the growing resistance of the solution with depth of the pore and finally the electron transfer and redox reaction which occurs on this metal catalyst.

Then there was another line which Martin Fleischmann developed. There was the micro electrode field. This was something which I had to teach myself I think independently of Martin Fleischmann, mainly the fact that below a certain radius you can get a much higher current density on the tip of a porous electrode so that dendrites can be developed quite easily and sometimes you can make some interesting looking patterns especially if you show how they can easily dissolve again and etc., but Martin Fleischmann made a useful kind of short book on micro-electrodes in which he published around about 1980. You can see how the micro electrodes and the diffusion problems which gather there towards the tip do have relevance to the porous electrodes. Its all electrode kinetics but not just depositing on a plain surface.

One of the fields which Martin Fleischmann helped a lot in his later days in Southampton was the use of spectroscopy on the surface of electrodes. Obviously the major problem is the liquid which prevents one using the many methods used in a vacuum.[d]

[d]Whilst I am talking or hinting at Fleischmann's character let me tell you a memory from early times when I knew him well in London in the graduate days. We all had nicknames. I am talking about this first group that's in the famous picture of 1947 and I do not know how these nicknames get made but they're remarkably accurate in many cases. We called Fleischmann "ephemeral transient and diffuse." I think this does get the middle part of Fleischmann, the lower part being that he would just be diffuse and not really tell you anything and the upper part being that he had the good ideas, some which he had developed with Thirsk.

Most of the time Martin bloomed and the work that got his FRS perhaps was done when I was away in America or Australia, but I did keep an interest in it and looked at his publications not only on those he sent me but I searched for them. Roger Parsons is the man who knows most about those days and I expect he will write something about them in the same volume to be published.

4. The McNeil Lehrer Hour and what Followed

We are now in the 1980s and Martin Fleischmann has retired early from the University of Southampton and taken up a moreorless freelance position to tackle whatever he wanted to do. I expect that until Stanley Pons's writes his version about it all we shall not know too much what happened in those days at the University of Utah. They talked about going for long walks and discussing what interested them most and this of course was fusion. At this time, fusion was a much sought after but totally mercurial and unavailable source of energy. Because of the bomb everyone thought that taming fusion would be the ideal way for getting more energy for the future. There are still a few people who think that, but two methods failed. One attempted to hold mixtures of hydrogen isotopes at temperatures near those of the sun in a magnetic field!

Another idea was to hit the mixtures of deuterium and tritium with a tremendous whack delivered by a laser which was two houses long and that failed too. The laser was set up at great cost and it failed. I remember being in the University of California just after the trial of the laser method was found to be a failure and hearing that the calculations now said that the power of the laser would have to be increased by ten times! It was news like this that delivered great blows to the attainment of fusion but it made a person like Martin Fleischmann more and more eager to contribute and his goal was to find out if it was possible to make a fusion reaction work in ordinary temperatures.

I suppose that the failures of these high pressure super energized methods was the basis of Martin's thinking that he would go in the opposite direction and try something with very little energy but with some thought behind it. Maybe that would work.

What Stan Pons and Martin came out with in March of 1989 was the electrolysis of deuterium oxide in which they had dissolved LiOD, lithium deuteride. Electrolyzing it they found something which excited them. It was, and everybody else thought this was all just due to instrumental error, that when they measured the heat of the reaction more heat was being given off than was classically possible. It was not much, perhaps 30% of the total heat energy which was evolved in the normal functioning of the electrolysis of deuterium oxide, but if the calorimeter worked well, it was significant.

Well, after the announcement on the McNeil Lehrer Hour there was a great counter reaction and much of it went on trying to hit Fleischmann and Pons' calorimetry. It took a great time, perhaps as much as five years for many who were expert in the calorimetry area really to believe that the calorimetry that F and P used was good enough. Eventually with EPRI support in his hands, it was Mike McKubre who built the ultimate calorimeter and his results were really believed.

So at this stage we were left with, as Martin and Stan put it an unknown nuclear reaction. Why was it called nuclear? Well, for one reason there did not seem anything else. Also there were a few neutrons.

I myself wrote a paper entitled "Eight Explanations of the Pons' and Fleischmann Effect," and in it I made simple calculations of all sorts of things that could happen and none of them came up to the needed heat and so although the title of my paper sounds threatening to F&P, it's the other way around. It looked as though there was no other explanation except something nuclear.

So I think it would all right to put the time now as somewhere about 1990. I was at Texas A&M University but it was getting late to be there because I was being punished so much by those who said that my support of Pons and Fleischmann had condemned me. "Obviously he must be wrong because everybody knows you cannot get fusion and Bockris is supporting them." I had to bear a very great deal of criticism because of this and indeed the criticism

spread to the university who then subjected me to two academic trials, and although the final answer was very good. Nevertheless, it's like having mud slung at your face and it's difficult to wipe it off.[e]

In the meantime (1991) Fleischmann and Pons had developed a relationship with Toyota and Mr. Toyoda offered the two miscreants an escape. They could leave all the mucky stuff behind in England and America and go and enjoy themselves in Southern France and of course prove their point because they would have excellent laboratory facilities and money and help there which they couldn't get elsewhere and so it seemed to be the ideal escape. Now they were in the Japanese/French laboratory for 2.5 years and I am glad to tell you that things looked good enough for two years. Looked good means that they were able to get more efficiency heat which is what they wanted. Ideally they wanted enough heat to make something commercial, but then, I do not know if either of them have an explanation, things began to go wrong. They could not get the results they had had in 1989.

One of the difficulties of their situation was due to poor management on the part of the Japanese funders.

A man like Martin Fleischmann will not work well if he is restricted in what he does or if he is told what to do. Now he was under supervision and made to write reports and do what the sponsors wanted so Jack did not flash anymore. Whether there was a bad interaction between Fleischmann and Pons I do not know. I suspect there was. Martin Fleischmann could be dictatorial and the man who says what had to be done. Stanley Pons saw that things were failing and it may be that at last he turned against the man in whom he had put his trust and walked out on Martin Fleischmann? I do not know. Something of both?

Anyway, it broke up and Martin Fleischmann headed for Bury Lodge, Tisbury, whilst Stanley Pons, he was independently wealthy, settled down in France more or less on the French Riviera, a pretty good place to retire in.

5. Fleischmann and Preparata

After he had retired to England, Martin Fleischmann was not to be forgotten and not to stop work. He continued to attend the meetings on Cold Fusion and usually made some pithy comments at them although I only attended up to the one in Vancouver, but Martin Fleischmann, keen on high sounding theory had developed an interest in quantum electrodynamics and he found in Professor Preparata a soul mate. This is the kind of stuff Preparata liked indeed and Preparata had an attractive model which was a good thing for discussion. It consisted of the idea that in solids there would be patches in which all atoms reacted together and gave rise to a glow and this was of course the heat observed. This was the type of thing to which Martin Fleischmann contributed after he returned to England. I don't know whether it produced anything permanent but at any rate it was joyful to them both and to those who were watching and hoping.

Preparata died first and then Martin Fleischmann entered his long illness.

6. Fleischmann after Preparata

Until he was stricken with Parkinson's, Fleischmann kept up regular attendance at the international meetings on Cold Fusion and as said by those who were present at such meetings he usually made some consequent comments and often praised the younger men coming up with new results.

I think that as I remember, perhaps far back on this matter than most, Martin Fleischmann was really keen on trying to get people to infer that that was how he had come to his great conclusion about fusion, but I think it was an entirely different idea. What would happen in the Nernstian Equations if we went to high pressures and I think that was the origins of his thoughts about fusion when he first talked to an American audience? But to say that your basic idea came

[e]My wife did much to help me. A lawyer's daughter, she supplied my lawyers with legal points which made onlookers see there was two sides to this mudslinging game. But one thing she said spread among the governing body of the University. She had spent a year in Vienna under Nazi rule, forbidden education, and she said that her years at Texas A&M were worse for her than that that Nazi rule.

from a Nernst Equation 1903 was not good. It was much better to quote quantum electrodynamics which we had heard about for some years after 1990.

I have four long letters from Martin Fleischmann after 1990 and I have given copies to a man who said he is interested in the history of this whole development. The letters I have from Martin were very interesting. They dealt really with politics and philosophy.

One of Martin's ideas which I believe is false was that the military had to do with delays and obstructions. I do not know whether he thought of CIA or the British MI5 but I believe both of those organizations worked together but it would not be worth developing as I am sure that his idea was not correct.[f]

Parkinson's disease is a death sentence but it is slow and I knew something about it because Ernie Yeager, one of my closest colleagues in electrochemistry, died from it. The early stages in Parkinson's is easy on the patient and by taking the right kind of drug, he can have normal behavior for maybe three hours, give lectures, etc., but of course as with all drugs you have to take more and more until it becomes impractical and you have to prepare for adventures in the next plane as the spiritualists call it. So Martin Fleischmann took a path quite parallel about ten years behind Ernie Yeager.

I found that no visits at the end time are a good idea. I had known both men for so long and so I never saw either man in their setting sun days and I think it's a good way to end this obituary by saying that when the sun shone on them, it seemed very, very good.

[f]The fact that there is a relationship between the CIA and AISIO the Australian equivalent was proved in my own case. When I was in Australia I developed producing hydrogen with light and had I succeeded a bit more than I did and increased the efficiency of recovery from the 9.6% to say 15 or even 18%, I might have challenged Exxon itself. So it was not particularly surprising when one of my co-workers who was keen on Japanese fighting styles, dressed up in his Japanese Togs, one night about midnight saw that my light was on when he came across the bridge joining my part of the Flinders University to another. He thought I might be working late and so he wanted to say goodnight Prof so he opened my door and said: "Good…" Before he could say a second word he found there were two men at my desk taking photographs. They decided that rapid exit was the next part of the program and so they dashed past my graduate student, knocking him aside and made it outside the university and I suppose they had a car and went home, but my own interpretation of the event that was that that was ASIO and I suspect that somewhere deep buried in the record is that CIA had told them to "See what Bockris is doing." In case you think this is absurd, you should recall what would happen if somebody found an easy way of getting hydrogen out of light and water. In fact there is a group in the California Institute of Technology at this time who has got very strong funding just to do that, and of course if it is done and accepted and the whole thing worked our financially then the oil companies would have to shiver. In fact I used to have several dinners per year with the reigning CIA man in Philadelphia and when I told him that I was going to immigrate to Australia he said (typically) that of course he knew that and he thought that "we might be in contact later". I think that that meeting of my graduate student and the men at my desk were the result of what he said.

J. Condensed Matter Nucl. Sci. 11 (2013) 8–14

Research Article

Destruction of Radioactivity by Stimulation of Nuclear Transmutation Reactions

L.A. Bernstein *

BLL Inc., 1725B South Hayes Street, Arlington, Virginia 22202, USA

Abstract

Modern science considers properties of radioactive decay as intrinsic characteristics of each isotope that cannot be affected by changes in the surroundings. Here, we present an approach for stimulation of nuclear transmutation reactions leading to accelerated destruction of radioactive isotopes that allows expedited disposal of radioactive materials.
© 2013 ISCMNS. All rights reserved. ISSN 2227-3123

Keywords: Destruction of radioactivity, Nuclear transmutation reactions, Radioactive waste disposal, Thermal desorption, Tritium

1. Introduction

The disposal of radioactive materials is one of the most important tasks to be resolved by the humankind. This process can be started only after radioactivity has decayed enough to allow further utilization via decontamination of the radioactive materials and subsequent return of the decontaminated materials and removed radioactive isotopes for a second use and/or storage. Therefore, accelerating the reduction of radioactivity is an economically viable option of radioactive waste treatment in the nuclear industry.

2. Background

In theory, accelerating the reduction of waste radioactivity is possible through transmutation nuclear reactions of the radioactive isotopes present in the waste by stimulating the radioactive decay of the isotopes and/or nuclear reactions of the radioactive isotopes with other isotopes to form stable isotopes. Transmutation of any radioactive isotopes leading to the formation of stable isotopes when no radioactivity is produced results in destruction of radioactivity.However, it is necessary not just to prove that it is possible but also to find a stimulus acceptable from practical view to accelerate the reduction of waste radioactivity.

Modern science considers rates of radioactive decay as intrinsic characteristics of each isotope that cannot be affected by changes in the surroundings. The radioactive decay of an isotope is measured in terms of “half-life,” the duration

*E-mail: bllinc@comcast.net; Tel.: +1- 703-200-4062; Fax: +1-703-271-8243

© 2013 ISCMNS. All rights reserved. ISSN 2227-3123

of a period necessary to reduce the radioactivity of the isotope by half. The half-life values of the most common decay processes are well known. However, an analysis of published scientific literature shows that certain direct and indirect experimental data challenge this approach.

One of the first methods of changing the half-life of isotopes [1] involved heating an isotope to a very high temperature (2E+8 K), which caused a part of the ^{176}Lu to decay to ^{176}Hf by passing the conventional slow route, and going into an isomeric state with a half-life of only 3.68 h. Another approach was patented by Backer [2]. He suggested that applying electrical potential of 50–500 kV to contaminated metals that contain alpha, beta, or gamma radioactivity and have been placed as a target in a Van de Graph accelerator would significantly accelerate decay. It was shown that the decay for alpha emitter, thorium 230 ($_{90}$Th^{230}), can be accelerated by a factor of 4.49×10^4 while for beta minus emitter, thallium 204 ($_{81}$Tl^{204}), a respective acceleration factor of just 15 was measured. This significant difference can be explained by the fact that alpha decay process is controlled by the Coulomb barrier, which was modified by applying electrical potential, while beta decay is controlled by electron–nucleus contact. Jung et al. [3] found conditions to transmute even a stable atom of ^{163}Ds$_{66}$ to ^{163}Ho$_{67}$ with a half-life of 47 days in a storage ring. The conditions allowed obtaining a bare ^{163}Ds$_{66}^{66+}$- ion with 294 MeV/u, which decays into ^{163}Ho$_{67}^{66+}$- ion. Due to the only electron of Ho-ion, this ion could be quantitatively detected in a mixture with Ds-ion. Beta-bound decay has been experimentally demonstrated in the rhenium–osmium (^{187}Re–^{187}Os) system. Stable Re was transmuted to Os with a half-life of 33 years in a storage ring [4]. All of these examples do not have any practical application because their implementation requires a lot of energy. For example, in order to produce ions with kinetic energy of 294 MeV achieved in storage ring, it is necessary to heat the gas to 2.3E+12K. However, it is proven in these experiments that beta-decay rate varies under certain conditions.

3. Review of Experimental Studies on Detritiation of Tritium-contaminated Samples

The utilization of tritium-contaminated waste is very important, especially due to the fact that tritium is the fuel for ITER-International Thermonuclear Experimental Reactor, a new nuclear reactor that is being constructed in France by the global scientific and technical communities. Tritium decay with the generally accepted half-life of 12.32 years is based on the transmutation reaction resulting in formation of $_2$He^3, beta particle, and an antineutrino. This transmutation reaction can be monitored by measuring the amounts of He^3 formed and/or beta particles released. Most researchers have been measuring beta particles because it is much easier in many experimental conditions. However, measuring He^3 would make it easier to reach a conclusion about a rate of tritium decay.

Torikai et al. [5] studied the detritiation of tritium contaminated stainless steel samples using various purging gases (argon, air and argon +3 vol% H_2) and interpreted the results of the experiments assuming that a half-life of tritium decay has a generally accepted value. They purged samples heated up to a temperature of 673 K, collected tritium removed from these samples (hereafter, the removed tritium), determined the activity of the removed tritium, and stated that all sorbed tritium was removed from the sample. They determined an initial concentration of tritium in a sample indirectly based on the tritium content measured for another sample loaded at the same time, i.e., they did not know the exact amount of tritium sorbed in the sample studied, which made it very difficult to verify tritium balance after the test. They also did not measure the residual tritium activity of the sample after the completion of the detritiation, which made it impossible to verify the tritium balance during the test. However, they stated without any experimental proof that all sorbed tritium could be thermally released during heating the sample at a temperature higher than 673 K, which makes it difficult to accept their interpretation of tritium decay.

Akulov and Mamyrin [6] used mass-spectrometry for measuring He^3 concentration in gas phase during tritium decay experiments. They proved that the half-life for molecular tritium was by 11.5 days longer than the half-life for atomic tritium. Based on experimental data for atomic tritium decay and their model for possible atomic tritium decay reactions, they also calculated triton decay half-life that turned out to be by 9.5 days shorter than the half-life for atomic tritium decay. These data also prove that the experimental surrounding can affect beta decay rates.

Reifenschweller [7], in his experiments with tritium, counted beta particles formed during tritium decay and concluded that decelerated decay for beta radioactive tritium during the detritiation of a titanium sample (of 48 mg) consisting of mono-crystalline particles of about 15 nm in diameter arranged in chains and loaded with tritium in the hydrogen form (100 mCi T_2) was the only possible explanation for his experimental data. This study deserves a detailed discussion. The sample was slowly heated to 450°C within 10 h (at a specific rate per sample unit mass of 15.6°C/(min*g)), and the electron current was measured and attributed to beta particles released to gas phase of the volume where the required pressure was kept using a diffusion pump. It was shown that the electron current went down sharply to 72% of its initial value in a temperature range of 115–160°C followed by a slower decrease to 60% at 275°C. With a further temperature increase, the current returned to its initial value at 360°C, and then went down due to the complete decomposition of the titanium preparation, which indicated that most of tritium was removed from the metal sample. In another experiment, another sample was heated five times faster (at a specific rate per sample unit mass of 78.1°C/(min*g)) and there was no reduction in the electron current measured. The author stated that no tritium escaped from the titanium layer in the temperature range of 115–275°C, and this statement inevitably led him to conclude that the tritium decay constant decreases in this temperature range. The statement that "no tritium escaped from titanium layer in the temperature range of 115–275°C" was based on the fact that an increase in a temperature from 275°C to 360°C led to "re-increase of count rate." In order to prove this statement, it was needed to estimate tritium activity balance at each step of the process; however, the residual tritium inventory in titanium particles and a quantity of tritium released during the detritiation process and pumped out of the volume by the diffusion pump were not analyzed. Considering a small mass of titanium and its low tritium activity, it was probably impossible to measure in those experiments a concentration of tritium removed with the gas phase, a residual tritium activity of the sample, and/or a concentration of He^3 formed during tritium decay and remained in the sample after completion of the experiments. Finding tritium in the metal would be a proof that no tritium "disappearance" occurs, and a balance of the tritium activity in the experiments would allow one to estimate whether the tritium decay constant was changed. However, if the tritium balances for the experiments were not converged, and analytical procedures used for detection and measurement of tritium in all phases involved in the experiments were correct, it would be possible to conclude that beta bound decay or other nuclear reactions involving tritium occurred. However, there was no experimental proof there that the tritium decay constant was reduced.

Analysis of the aforementioned publications leads one to a conclusion that radioactive decay acceleration is possible dependent on the experimental surrounding and by applying an electrical potential to radioactive metals or accelerating the atoms to a very high speed. In contrast to previously suggested conclusions that the low temperature heating of metals either does not change a half-life of tritium [5], or even increases it [7], we demonstrate below that apparent tritium decay constant shows a completely opposite trend.

We are unaware about any study on transmutation of solid radioactive waste through nuclear reactions at low temperatures. However, the transmutation nuclear reaction could be one of the possible interpretations of the results of the research related to decontamination of tritium-contaminated metals [8]. We demonstrate below that it is possible to destroy radioactive isotopes by stimulating nuclear transmutation reactions.

4. Present Detritiation Experiments, Results and Discussion

The experiments described in details in [8] were conducted with stainless steel (dimension of 12.0 cm ×12.0 cm × 4.9 cm; mass of 5645 g), copper alloy Cu–Cr–Zr (dimension of 6.0 cm × 6.0 cm × 2.2 cm; mass of 710 g), tungsten (dimension of 4.0 cm × 4.0 cm × 1.0 cm; mass of 309 g), and beryllium (dimension of 3.0 cm × 3.0 cm × 1.0 cm; mass of 17 g). A brief summary of experimental setup is given below

The samples of the materials were cleaned using the same procedure as in the study [8] and loaded into the chamber, which was then pumped down and purged with argon to eliminate presence of residual air. The samples were heated

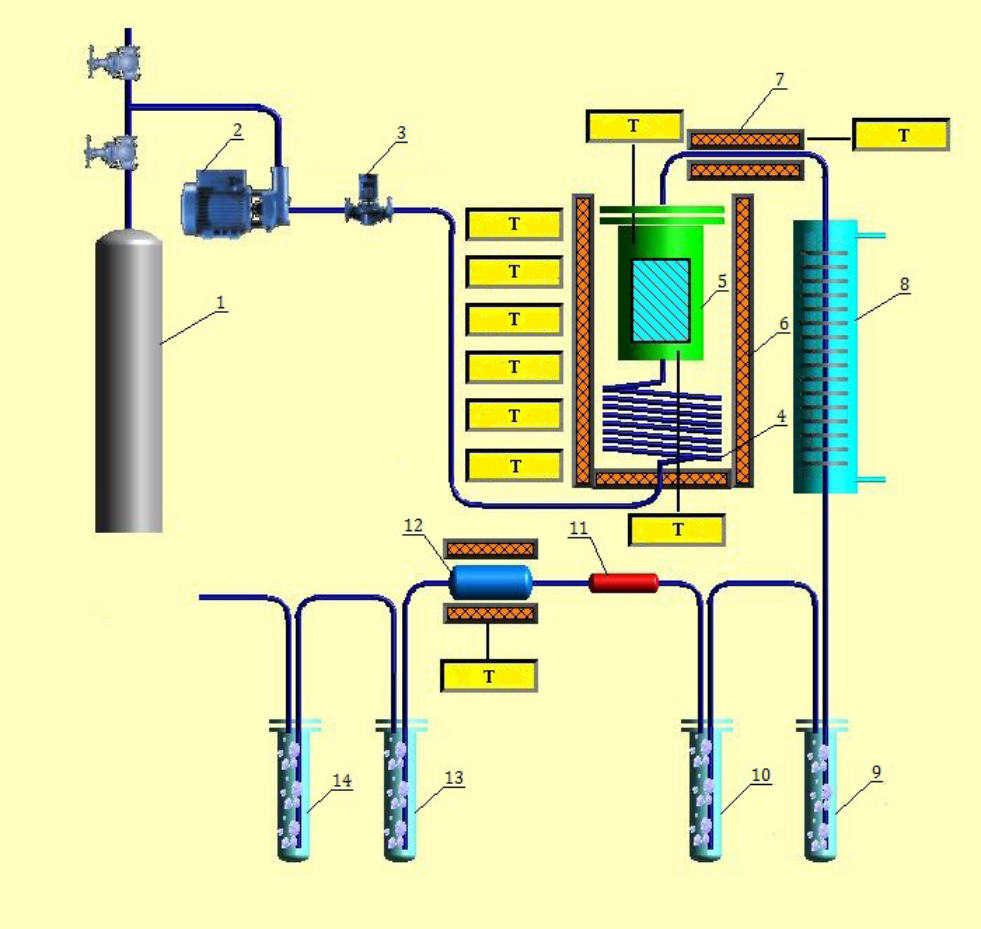

Figure 1. A block diagram of a facility for detritiation of metals: 1 – Cylinder with purging gas; 2 – Membrane pump/compressor; 3 – Gas flow meter; 4 – Heat exchanger; 5 – Chamber with a sample; 6 – Resistance oven; 7 – Heated communication lines; 8 – Condenser; 9, 10, 13, 14 – Bubblers; 11 – Dryer with absorbent; 12 – Catalytic reactor with heater.

for 10 h at a temperature of 773 K under a residual gas pressure of 10^{-4} Pa to remove gases dissolved in the metals. Samples were loaded with tritium by exposing them to a gaseous D–T mixture (48.3% of tritium, 50.6% of deuterium and 1.1% of protium) at a temperature of 473 K and a pressure around 0.05 MPa for 24 h. The temperature was maintained uniformly through the whole chamber. The D–T gas mixture was rapidly evacuated from the chamber at the end of the exposure, and the chamber was immediately cooled down and purged with argon prior to opening.

Each detritiation experiment was conducted with one metal sample placed into a chamber where it was heated to a given temperature at a temperature increase rate of 10^{o}C/min and simultaneously purged with a purge agent supplied to control a gas exchange rate (Fig. 1). The mixtures of 95 vol% argon + 5 vol% hydrogen, 95 vol% nitrogen + 5 vol% hydrogen, and argon + water vapor were used as purge agents. When a required operation temperature was achieved, the detritiation process continued for a duration ranging from 24 to 90 h, and the operation temperature was held stable during this period. The selection of a temperature increase rate of 10 ^{o}C/min was limited by the equipment capability.

Considering that (i) the mass of the smallest sample in our experiments exceeds by a factor of 350 the mass of each individual sample in Reifenschweller's experiments [7] and (ii) the operation temperature was steadily maintained in our experiments while was not steadily maintained in Reifenschweller's experiments, we concluded that a rate of the temperature increase in our experiments cannot affect the detritiation process because the duration of temperature increase period required to heat samples to the operation temperature contributed no more than 5.5% to the overall time of the detritiation process

The detritiation of each metal was studied at three different temperatures: 200°C, 500°C, and 800°C, with the three aforementioned purge agents supplied at various flow rates. A change in flow rate affects the kinetics of tritium desorption from metals and as such can affect other possible processes occurred inside the metal. During the detritiation experiments, the tritium transferred to gas phase was removed from the chamber with the flow of the purge agent and was collected in a tritium collection system consisting of a series of bubblers (9, 10, 13 and 14, Fig. 1) installed downstream of the chamber. The first pair of bubblers in a series was placed in between the chamber and the catalytic reactor filled with copper oxide. These bubblers trap tritium released in form of water vapor. The catalytic reactor operated at a temperature of about 770 K to oxidize gaseous hydrogen to water vapor. The second pair of bubblers was placed downstream to trap this water vapor that included tritium released by the samples in the form of gaseous hydrogen and converted in the catalytic reactor. The bubblers were designed to produce small bubbles of air and in order to ensure a high efficiency of the tritium collection.

The balance of tritium activity for each experiment was determined based on the following formula that represents material balance of that tritium in the experiment: A = B + C + D, where A is the initial tritium inventory in a metal; B is the residual tritium inventory in the metal after the experiment; C is the tritium inventory transferred to gas phase and collected during the experiment; and D is the possible tritium activity that could escape during the length of the experiment due to, for example, leakage through faulty air-tight barriers of an experimental system, and/or diffusion through the walls of the chamber. The radioactive decay of tritium is not considered here due to very short durations of the experiments when compared to the generally accepted half-life of 12.32 years.

Initial (A) and residual (B) tritium inventory and distribution in the samples were determined using radioluminography [9]. Tritium stripped from the metal in the detritiation experiments was very efficiently collected in the tritium collection system, and tritium content in both molecular hydrogen and water vapor forms was measured individually using the liquid scintillation counting method. The sum of tritium activity in its molecular hydrogen and water vapor forms (C) was calculated.

Before the experiments, the chamber with a metal sample loaded with tritium was checked with a helium leak detector and showed no leakage. During the experiments, the radiation level was measured in the premises surrounding the experimental system and was at a background level. After all experiments were completed, the walls of the chamber were cut, and the tritium activity and its distribution inside the walls of the reactor were measured. The result showed that tritium activity in the walls of the chamber was at a background level. These facts demonstrate that, within an accuracy of the measurements, the term D in the formula above is insignificant and was neglected in further analyses. Therefore, the difference between an initial inventory of tritium in a metal sample (A) and a sum of the residual inventory of tritium in the metal sample (B) and collected activity removed from the metal sample (C) was determined. This difference determined as percentage of A as [1-(B+C)/A]$\times$ 100% is referred to hereafter as disbalance.

All metal samples studied had a tritium disbalance, which increased with an increase in temperature. Despite significant mass of the samples and tritium activity in them, the concentration of He^3 formed was so low that it was impossible to detect it. Tritium disbalances are dependent on gas exchange rates (the first number shown in parentheses is the optimal rate, after which a further increase does not improve tritium removal from the metals) at a temperature of 800°C as follows:

- Stainless steel – 47–95.2% (6.0–0.1 h^{-1})

- Cu – 77–99.6% (6.0–0.1 h^{-1})
- W – 63-96.7% (6.0–0.1 h^{-1})
- Be – 87–95.3% (80–0.1 h^{-1})

Tritium disbalances at temperatures of 200°C and 500°C and optimal gas exchange rates determined at 800°C for each metal specified (the latter figures are shown in the parentheses) are:

- Stainless steel – 78.8% (200°C, 6 h^{-1}) and 74.9% (500°C, 6 h^{-1})
- Cu – 45.8% (200°C, 6 h^{-1}) and 87.5% (500°C, 6 h^{-1})
- W – 39.1% (200°C, 6 h^{-1}) and 85.3% (500°C, 6 h^{-1})
- Be – 45.7% (200°C, 80 h^{-1}) and 94.6% (500°C, 80 h^{-1})

Attributing disbalance in the material balance equation shown above to the nuclear transmutation of tritium (via unspecified nuclear reactions and/or beta bound decay) and applying the exponential formula of the radioactive decay to these experimental results allows one to determine the half-life parameter describing the kinetics of tritium destruction achieved during the detritiation process ($T_{1/2\text{cal}}$) and compare it to the generally accepted half-life of tritium radioactive decay of 12.32 years. The ratios between the generally accepted half-life of tritium and the half-life parameter of tritium destruction obtained for various metals studied in these detritiation processes are in the following ranges:

- Stainless steel: 4.0E+3 – 2.0E+4 with the average ratio of $12.32/T_{1/2\text{cal}}$ = 1.0E+4
- Cu: 4.0E+3 – 3.5E+4 with the average ratio of $12.32/T_{1/2\text{cal}}$ = 1.6E+4
- W: 3.2E+3 – 2.5E+4 with the average ratio of $12.32/T_{1/2\text{cal}}$ = 1.5E+4
- Be: 3.9E+3 – 2.0E+4 with the average ratio of $12.32/T_{1/2\text{cal}}$ = 1.5E+4

This means that the destruction of tritium as a radioactivity source via nuclear transmutation occurs in these experiments at a rate that is significantly faster than the generally accepted rate for the radioactive decay of tritium, i.e., the conditions of the experiments facilitate an acceleration of nuclear transmutation of tritium.

Exact mechanism of nuclear reactions involving tritium – accelerated radioactive decay and/or transmutation nuclear reactions with tritium participation – remains uncertain. However, regardless this mechanism, the observed phenomenon could be used for decontamination of tritium in tritium-contaminated metals in a controlled manner (partially recovering tritium for re-use and destroying the residual tritium).

Using the half-life parameters obtained for tritium destruction in stainless steel and considering a standard tritium decay mechanism only (with an average energy of β particles of 5.7 keV), energy released by 1 g of tritium per day will be very significant (4.4E+5 kJ/g), almost 10 000 times greater than for the same amount of practically any other fuel. As no experimental proof of this phenomenon is obtained, this conclusion should be considered as tentative. However, it hints for potential use of tritium energy released during destruction of tritium to self-sustain a process of tritium waste decontamination/destruction [10].

5. Conclusion

Tritium disbalances observed in these experiments can be explained by stimulated nuclear transmutation reactions and we are unable to offer another explanation of the experimental results. This phenomenon can be used for controlled decontamination of metals contaminated with tritium, and, tentatively, for self-sustaining a process of tritium waste decontamination/destruction by energy released there.

References

[1] F. Kappeler, H. Beer and K. Wisshak, S-process nucleosynthesis—nuclear physics and the classical model, *Reports Prog. Phys.* **52** (1989) 945–1013.

[2] W. Backer, U.S. Pat. No 5,076,971, Method for enhancing alpha decay in radioactive materials, issued on 31 December 1991 (filed 28 August 1989).

[3] M. Jung et al., First observation of bound-state β^- Decay, *Phy. Rev. Lett.* **69** (N15) (1992) 2164–2167.

[4] F. Bosch et al., Observation of bound-state β^- decay of fully ionized ^{187}Re, *Phy. Rev. Lett.* **77**(N26) (1996) 5190–5193.

[5] Y. Torikai, R.-D. Penzhorn, M. Matsuyama and K. Watanabe, Tritium Uptake by SS316 and its Decontamination, *J. Nucl. Materials* **329–333** (2004) 1624–1628.

[6] Yu. A. Akulov and B.A. Mamyrin, Isotopic-helium mass-spectrometry method of tritium beta-decay study, *UspehiPhizicheskihNauk* **173** (N11) (2003) 1187–1197 (in Russian).

[7] O. Reifenschweller, Reduced radioactivity of tritium in small titanium particles, *Phys. Lett. A* **184** (1994) 149–153.

[8] A.N. Perevezentsev, L.A. Bernstein and L.A. Rivkis *et al*., Study of out-gassing and removal of tritium from metallic construction materials of ITER vacuum vessel components (In preparation).

[9] A.N. Perevezentsev, A.C. Bell and L.A. Rivkis *et al.*, Comparative study of the tritium distribution in metals, *J. Nucl. Materials* **372** (2,3) (2008) 263–276.

[10] L.A. Bernstein, US non-provisional patent application "Method of acceleration of nuclear transmutation of isotopes by carrying out exothermic reactions,"filed on 9/6/2012, application number 13605032; provisional patent application filed on 10/26/2011, application number 61/551,652.

J. Condensed Matter Nucl. Sci. 11 (2013) 15–58

Research Article

Central and Tensor Contributions to the Phonon-exchange Matrix Element for the $D_2/^4He$ Transition

Peter L. Hagelstein *

Research Laboratory of Electronics, Massachusetts Institute of Technology, Cambridge, MA 02139, USA

Irfan U. Chaudhary

Department of Computer Science and Engineering, University of Engineering and Technology. Lahore, Pakistan

Abstract

The biggest theoretical problem associated with excess heat in the Fleischmann–Pons experiment in our view has been the absence of energetic particles in amounts commensurate with the energy produced. In response we have pursued models in which the large nuclear energy quantum is fractionated into a great many lower energy quanta. To connect these idealized models to the physical system we need to evaluate the associated coupling matrix elements. Recently we have found a new coupling mechanism that arises when a lattice model is derived starting from a Dirac description of individual nucleons; this coupling mechanism can be considered a generalization of spin-orbit coupling and produces interactions between the center of mass dynamics and internal nuclear degrees of freedom. In this work we develop a simplified model for ^4He and molecular D_2 states with which we evaluate the phonon exchange matrix element for $D_2/^4He$ transitions based on the new interaction. We restrict our calculation to the central and tensor contributions of the Hamada–Johnston nucleon-nucleon potential, which are the strongest, and find coupling between ground state ^4He and triplet P and F molecular states. This interaction matrix element can be used in generalized lossy spin–boson models for the calculation of excess heat production in the Fleischmann–Pons experiment..
© 2013 ISCMNS. All rights reserved. ISSN 2227-3123

Keywords: $D_2/^4H$ phonon exchange matrix element, Excess heat, Fleischmann–Pons effect, Nuclear physics calculation, Phonon exchange, Selection rules

1. Introduction

We have for many years pursued the development of a theoretical model [1] to account for excess heat in the Fleischmann–Pons experiment [2–4]. From our perspective the biggest challenge for theory is the absence of energetic nuclear products in amounts commensurate with the energy produced [5]. Such an effect is unprecedented in nuclear physics, although there are effects which might be considered to be distant analogs in other areas of physics.

*E-mail: plh@mit.edu

© 2013 ISCMNS. All rights reserved. ISSN 2227-3123

We have studied new models in which efficient coherent energy exchange occurs between quantum systems with strongly mismatched characteristic energies [6–9]. These models are based on two-level systems coupled with an oscillator in the presence of strong loss effects. While these basic models have been under investigation now for more than a decade, it has been problematic connecting them with the physical system. In the model most relevant for excess heat production [10], there is a set of two-level systems that are weakly coupled to the oscillator; these stand in for a proposed $D_2/^4He$ transition. In addition there is a set of two-level systems that are strongly coupled to the oscillator; until recently it has not been clear what transitions in the physical system these might represent, since the coupling needed to be sufficiently strong that all reasonable electron–nuclear and electron–electron transitions could be ruled out (as too weak to fractionate the large MeV quantum).

The only transitions which could be sufficiently strong to make the model relevant to experiment are internal nuclear transitions, but until recently it was not obvious that there could be phonon exchange in such a transition. Earlier this year we developed a new fundamental lattice Hamiltonian that took as a starting point a Dirac model for electrons and nucleons, and we obtained an appropriate nonrelativistic limit that included mass effects as well as a new coupling between the center of mass an internal nuclear states [11]. In this model lattice vibrations are coupled to internal nuclear transitions as a result of relativistic effects, with the result that all compound nuclei have transitions that are candidates to fractionate a large quantum within the lossy spin–boson models.

In the Fleischmann–Pons experiments deuterium is loaded into palladium, so the most obvious candidates for the strongly coupled transitions are the deuterons and host Pd nuclei. In the two-laser experiments compressional optical phonon modes are implicated, suggesting that our focus should be on the deuterons since they move much more than the Pd nuclei when optical phonon modes are excited. We recently evaluated the deuteron coupling matrix element within the model [12], with the result that the coupling is very strong – much stronger than for any conventional (electron–nuclear or electron–electron) transition. Unfortunately, when we evaluated coherent energy exchange rates to compare with experiment we found that the coupling was still too weak. Recent work to be published shortly starts from a fundamental Hamiltonian based on quarks and electrons (instead of nucleons and electrons), which results in much larger coupling matrix elements. The model that results appears to be much more closely connected with experiment.

With a possible solution to the problem of the strongly-coupled transition in hand, our attention turns back to the $D_2/^4He$ system, where the coupling mechanism and associated phonon exchange have been of great interest. In nuclear physics the $d(d,\gamma)^4He$ reaction is known [13], and is weak since an electromagnetic interaction is involved [14] (the much stronger $d(d,n)^3He$ and d(d,p)t reactions are mediated by the strong force [15]). We had thought for many years that there might be a strong force mediated version of the $D_2/^4He$ transition with phonon exchange involved in the Fleischmann–Pons excess heat effect. The basic argument was that the difference between a local molecular D_2 and ^4He is sufficiently large that one would expect a very high probably for phonon exchange if the lattice is highly excited. A weakness of the argument is that the nuclear system on the fermi scale is very close to the vacuum system, so that one would expect the transition to be forbidden without some additional coupling.

If so, then we must return to the issue of how such a transition might occur consistent with physical law and the requirements of the lossy spin–boson models. There are a number of approaches that might be considered. We might contemplate electromagnetic coupling between the transition and the local electrons, which could be expected to lead to phonon exchange since the electronic orbitals respond to atomic motion associated with vibrations. Over the past year we have been wrestling with a similar approach in the case of nuclear excitation, where we explored many transitions mediated by electron–nuclear coupling. In general we found that the associated phonon exchange coupling matrix elements were small, and there is no reason not to think that the electron–nuclear coupling analog in the $D_2/^4He$ transition would not similarly be small. Given the recent computation of phonon exchange in the case of the $\mathbf{a} \cdot c\mathbf{P}$ coupling for the deuteron [12], which produced an interaction many orders of magnitude larger than possible for electron–nuclear coupling, it seems that we would do best by focusing on $\mathbf{a} \cdot c\mathbf{P}$ coupling for the $D_2/^4He$ transition.

The computation implied from this line of argument then is one in which we would evaluate the interaction matrix

element between a molecular D_2 state in the lattice, and the ground state ^{4}He state also in the lattice. In a relativistic model we could imagine evaluating the $\mathbf{a} \cdot c\mathbf{P}$ matrix element directly; in the nonrelativistic case we have available a reduction of the operator that we might use [11]. Unfortunately the nuclear four-body problem is much more complicated than the two-body problem was, and to carry out such a calculation even in the case of a simple nuclear potential model (such as the Hamada–Johnston potential [16]) involves considerable work.

An alternate approach in this case might instead be to carry out a much simpler calculation that assumes an approximate (not self-consistent) ^{1}S configuration for the ^{4}He, and use approximate molecular deuteron–deuteron fixed core wavefunctions based on reduced ^{3}S wavefunctions for individual deuterons. Within such an approach we might develop an approximate description that could be evaluated with a much more modest effort level. A more sophisticated calculation could be pursued in the future.

In what follows in this lengthy paper is a presentation of the associated calculation, with documentation of the associated details. In the nuclear physics literature in general the details of this kind of calculation do not get published. There are many reasons for this; for example, specific results for one potential in one formulation of a particular system do not extend to other systems, and as such they are not inherently interesting; and in the case of more complicated potential models the number of terms becomes very large, so that a documentation of the details would result in a very long paper. Here, we are dealing with one of the simpler potentials (and restricting our focus to only central and tensor contributions), so that we are not overwhelmed by a large number of contributions to the interaction. Also, this is the first calculation of the phonon exchange matrix element for the $D_2/^4$He transition, so we expect some interest in just how the coupling works and what is in the model. The relative absence of specific details about how one carries out such a calculation in the literature provided a hindrance to us in our calculations, so we are motivated here to present them in case others are interested in what we have done.

Some discussion of the calculation itself may be useful. The matrix element calculation involves spatial parts, spin parts, and isospin parts. Historically Racah algebra has been used to sort out the spin and isospin parts, and there is no reason that we should not make use of Racah algebra here. In practice, it seemed simpler to make use of Mathematica for a direct brute force evaluation of the spin and isospin parts of the matrix elements. A very large number of spatial integrals result from the reduction of the spin and isospin part of the problem, and we found that because of the high degree of symmetry of the spatial wavefunctions that they reduce down to only a few cases. As a result, by the end of the analysis we end up with relatively simple explicit formulas for the associated matrix element; for fixed center of mass momentum P (and no magnetic field coupling) we can write for the central potential contribution to the $l = 1$ matrix element a result of the form

$$M_{\rm C}^{(S,M_{\rm S})} \;=\; (cP)\left[{\rm e}^{-G}\sqrt{\frac{R_0}{\langle R\rangle}\frac{(\Delta R)^2}{\langle(\Delta R)^2\rangle}}\right]_{l=1}\sum_{\kappa} A_{\rm C}^{\kappa}I_{\rm C}^{\kappa} + B_{\rm C}^{\kappa}J_{\rm C}^{\kappa} + C_{\rm C}^{\kappa}K_{\rm C}^{\kappa} + D_{\rm C}^{\kappa}L_{\rm C}^{\kappa},$$

which makes all parts of the problem explicit. The spin and isospin part of the problem now appears in the $A_{\rm C}$, $B_{\rm C}$, $C_{\rm C}$ and $D_{\rm C}$ expansion coefficients, which we tabulate. The spatial integrals show up as the $I_{\rm C}$, $J_{\rm C}$, $K_{\rm C}$ and $L_{\rm C}$ terms; since they are four-dimensional, there is no need to expand them in a series (as was typical in years past) because we can do the integrals numerically in this day and age with ease. We see that the Gamow factor associated with tunneling shows up explicitly as a prefactor; we also see prefactors associated with the relative molecular volume referenced to the molecule in vacuum. Finally, we have termed the interaction an $\mathbf{a} \cdot c\mathbf{P}$ interaction, so we see the cP part of the interaction explicitly in the prefactor (for z-directed motion), with the remaining terms combining to make up the associated a_z-matrix element.

2. Construction of the ^{4}He state

Since empirical nucleon-nucleon potentials depend explicitly on isospin, it is convenient to work with nuclear wavefunctions constructed using antisymmetric wavefunctions from space, spin and isospin pieces. In general we may write for such wavefunctions

$$\Psi \;=\; \sum_j c_j [R]_j [S]_j [T]_j , \tag{1}$$

where the $[R]_j$ are spatial terms, where the $[S]_j$ are spin-dependent terms, and where the $[T]_j$ are isospin-dependent terms [16,17].

In the case of the ^{4}He wavefunction, we can take advantage of the symmetric group construction. This allows us to identify the space, spin, and isospin terms directly with irreducible representations of the symmetric group, which we can write in terms of Yamanouchi symbols. Such a construction is also possible for the molecular D_2 wavefunction; however, the resulting expression is more complicated than what is possible from a simple factorization of the antisymmetrized wavefunction. Because of this, and also because our evaluation of the spin and isospin algebra will be done by brute force (so that we are not taking advantage of the nice properties of the Yamanouchi symbols), it will be convenient to work in terms of $[R]_j$, $[S]_j$, and $[T]_j$ functions.

2.1. Symmetric group construction of the helium ^{1}S state

We begin with a specification of the helium ^{1}S state wavefunction, which can be expanded as

$$\Psi_{^1\mathrm{S}} \;=\; [4321]_{RST} \;=\; [1111]_R [4321]_{ST} . \tag{2}$$

This formula may require some explanation in order to understand the associated construction. Nuclear wavefunctions in the isospin scheme are subject to the generalized Pauli principle that requires them to be antisymmetric upon exchange of any two nucleons. The first Yamanouchi symbol that appears ($[4321]_{RST}$) is one that says that the wavefunction made up of spatial (R), spin (S) and isospin (T) components must be fully antisymmetric upon substitution of any two nucleons $[4321]_{RST}$. On the right hand side is the decomposition into a fully symmetric spatial piece $[1111]_R$ and a fully antisymmetric spin and isospin piece $[4321]_{ST}$.

It is possible to decompose the fully antisymmetric spin and isospin piece into two different terms of mixed symmetry

$$[4321]_{ST} \;=\; \frac{1}{\sqrt{2}} \Big([2211]_S [2121]_T - [2121]_S [2211]_T \Big) . \tag{3}$$

This will allow us later on to separate the spin and isospin calculations. Overall, we may write the ^{4}He wavefunction as

$$\Psi_{^1\mathrm{S}} \;=\; \frac{1}{\sqrt{2}} [1111]_R \Big([2211]_S [2121]_T - [2121]_S [2211]_T \Big) . \tag{4}$$

2.2. Definition of $[R]$, $[S]$, and $[T]$ terms

The wavefunction described above is composed of two terms which we will denote as

$$\Psi_{^1S} = \sum_{j=1}^{2} c_j [R]_j [S]_j [T]_j, \tag{5}$$

where

$$c_1 = \frac{1}{\sqrt{2}}, \qquad c_2 = -\frac{1}{\sqrt{2}}, \tag{6}$$

$$[R]_1 = [R]_2 = [1111]_R, \tag{7}$$

$$[S]_1 = [2211]_S, \qquad [T]_1 = [2121]_T, \tag{8}$$

$$[S]_2 = [2121]_S, \qquad [T]_2 = [2211]_T. \tag{9}$$

2.3. Spin pieces

We have available explicit representations of the spin functions for the singlet ($S = 0$) case (which for $M_S = 0$); these can be written as

$$[2211]_S = \frac{1}{\sqrt{12}}\Big[2\alpha(1)\alpha(2)\beta(3)\beta(4) + 2\beta(1)\beta(2)\alpha(3)\alpha(4) - \alpha(1)\beta(2)\alpha(3)\beta(4) - \beta(1)\alpha(2)\alpha(3)\beta(4) - \alpha(1)\beta(2)\beta(3)\alpha(4) - \beta(1)\alpha(2)\beta(3)\alpha(4)\Big], \tag{10}$$

$$[2121]_S = \frac{1}{2}\Big[\alpha(1)\beta(2)\alpha(3)\beta(4) - \beta(1)\alpha(2)\alpha(3)\beta(4) + \beta(1)\alpha(2)\beta(3)\alpha(4) - \alpha(1)\beta(2)\beta(3)\alpha(4)\Big]. \tag{11}$$

The notation here can be understood as defining whether a specific nucleon has an up or down spin

$$\alpha(j) = |\uparrow\rangle_j = \left|s = \frac{1}{2}, m_s = \frac{1}{2}\right\rangle, \tag{12}$$

$$\beta(j) = |\downarrow\rangle_j = \left|s = \frac{1}{2}, m_s = -\frac{1}{2}\right\rangle. \tag{13}$$

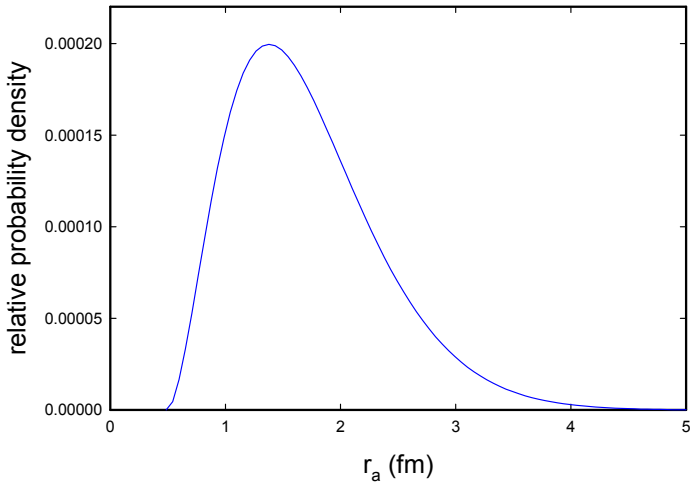

Figure 1. Relative probability distribution for nucleon–nucleon separation.

2.4. Isospin pieces

These basic formulas for the spin Yamanouchi symbols can be taken over to isospin directly (since the total isospin is zero) with the replacements

$$\alpha(j) \;\rightarrow\; \left| t = \frac{1}{2}, m_t = \frac{1}{2} \right\rangle, \tag{14}$$

$$\beta(j) \;\rightarrow\; \left| t = \frac{1}{2}, m_t = -\frac{1}{2} \right\rangle. \tag{15}$$

2.5. Spatial part

The symmetry properties can be made clear using the notation

$$[R]_1 \;=\; [1111]_R \;=\; \Phi_S(\mathbf{r}_1, \mathbf{r}_2, \mathbf{r}_3, \mathbf{r}_4). \tag{16}$$

The requirement that Φ_S is fully symmetric can be written

$$\Phi_S(\mathbf{r}_1, \mathbf{r}_2, \mathbf{r}_3, \mathbf{r}_4) \;=\; \Phi_S(\mathbf{r}_2, \mathbf{r}_1, \mathbf{r}_3, \mathbf{r}_4) \;=\; \Phi_S(\mathbf{r}_3, \mathbf{r}_2, \mathbf{r}_1, \mathbf{r}_4) \;=\; \cdots, \tag{17}$$

where the $\cdots$ includes all permutations.

We adopt a symmetric wavefunction of the form

$$[R]_1 \;=\; N_S\, u(r_{21})u(r_{31})u(r_{41})u(r_{32})u(r_{42})u(r_{43}). \tag{18}$$

The form of the radial wavefunction $u(r)$ is

$$u(r) \;=\; (r - r_0)\mathrm{e}^{-\beta r} \tag{19}$$

with

$$\beta \;=\; 0.928\ \mathrm{fm}^{-1}, \qquad r_0 \;=\; 0.485\ \mathrm{fm}, \qquad N_S \;=\; 0.7476\ \mathrm{fm}^{-21/2}. \tag{20}$$

These parameters were selected so that the mean square radius is matched to the equivalent radius for point nucleons from experiment

$$\sqrt{\langle |\mathbf{r} - \mathbf{R}|^2 \rangle} \;=\; 1.42\ \mathrm{fm}. \tag{21}$$

The normalization N_S is determined relative to a nine-dimensional integral expressed in molecular coordinates (to be discussed later on in this paper). The relative probability as a function of nucleon–nucleon separation for this model is shown in Fig. 1; it compares reasonably well to the relative probability for accurate wavefunctions (see [19]).

3. Construction of Molecular D_2 States

Our focus in this work will be on interaction matrix elements coupling to the molecular D_2 triplet states, since coupling to these states occur for the transition matrix element in connection with the central and tensor contributions to the Hamada–Johnston potential. However, more generally we are interested in coupling to the other states as well, and it is convenient to develop a systematic construction here for the other states as well.

3.1. Construction of anti-symmetrized wavefunctions

We would like to construct the nuclear wavefunctions for molecular D_2 using the generalized Pauli principle in the isospin scheme, since the empirical nucleon–nucleon potentials that we will be using are written explicitly in terms of isospin operators. The approach that we will use involves first constructing a suitable unsymmetrized wavefunction that has appropriate space, spin, and isospin components; and then make use of an antisymmetrization operator to produce a fully antisymmetric wavefunction. In general, we may write this as

$$\Psi \;=\; \mathcal{A}\Big\{[R][S][T]\Big\}, \tag{22}$$

where $[R]$, $[S]$, and $[T]$ denote space, spin, and isospin components, respectively.

3.2. Isospin component

The two nucleons that make up a deuteron in the ground state are in an isospin singlet state, so in all cases we may write

$$[T] \;=\; \frac{1}{2}\Big[\alpha(1)\beta(2) - \beta(1)\alpha(2)\Big]_T\Big[\alpha(3)\beta(4) - \beta(4)\alpha(3)\Big]_T, \tag{23}$$

where nucleons 1 and 2 are in one deuteron, and where nucleons 3 and 4 are in the other.

3.3. Spin components

Individual deuterons within the molecular are in triplet states, so we will make use of Clebsch–Gordan coefficients to construct the different spin states; we may write

$$|S_1 S_2 S M_S\rangle \;=\; \sum_{M_1+M_2=M_S} \langle S_1 S_2 M_1 M_2 | S_1 S_2 S M_S\rangle |S_1 S_2 M_1 M_2\rangle, \tag{24}$$

where $S_1 = S_2 = 1$. For the singlet case, we have

$$|S=0, M_S=0\rangle \;=\; \frac{1}{\sqrt{3}}\Big[|1,1\rangle_1|1,-1\rangle_2 - |1,0\rangle_1|1,0\rangle_2 + |1,-1\rangle_1|1,1\rangle_2\Big]. \tag{25}$$

For the three triplet cases, we may write

$$|S=1, M_S=-1\rangle \;=\; \frac{1}{\sqrt{2}}\Big[|1,0\rangle_1|1,-1\rangle_2 - |1,-1\rangle_1|1,0\rangle_2\Big], \tag{26}$$

$$|S=1, M_S=0\rangle \;=\; \frac{1}{\sqrt{2}}\Big[|1,1\rangle_1|1,-1\rangle_2 - |1,-1\rangle_1|1,1\rangle_2\Big], \tag{27}$$

$$|S=1, M_S=1\rangle \;=\; \frac{1}{\sqrt{2}}\Big[|1,1\rangle_1|1,0\rangle_2 - |1,0\rangle_1|1,1\rangle_2\Big]. \tag{28}$$

For the quintet states, we have

$$|S=2, M_S=-2\rangle \;=\; |1,-1\rangle_1|1,-1\rangle_2, \tag{29}$$

$$|S=2, M_S=-1\rangle \;=\; \frac{1}{\sqrt{2}}\Big[|1,0\rangle_1|1,-1\rangle_2 + |1,-1\rangle_1|1,0\rangle_2\Big], \tag{30}$$

$$|S=2, M_S=0\rangle \;=\; \frac{1}{\sqrt{6}}\Big[|1,1\rangle_1|1,-1\rangle_2 + 2|1,0\rangle_1|1,0\rangle_2 + |1,-1\rangle_1|1,1\rangle_2\Big], \tag{31}$$

$$|S=2, M_S=1\rangle \;=\; \frac{1}{\sqrt{2}}\Big[|1,1\rangle_1|1,0\rangle_2 + |1,0\rangle_1|1,1\rangle_2\Big], \tag{32}$$

$$|S=2, M_S=2\rangle \;=\; |1,1\rangle_1|1,1\rangle_2. \tag{33}$$

3.4. Spatial components

The associated spatial wavefunction should be of the form

$$[R] \;=\; \phi_d(r_{21})\phi_d(r_{43})R(r)Y_{lm}(\theta,\phi) \;=\; R(12;34). \tag{34}$$

We write for the molecular wavefunction the product $R(r)Y_{lm}(\theta,\phi)$ where r, θ, and ϕ are the spherical coordinates associated with the molecular relative coordinate $\mathbf{r}$ defined according to

$$\mathbf{r} \;=\; \frac{\mathbf{r}_3+\mathbf{r}_4}{2} - \frac{\mathbf{r}_1+\mathbf{r}_2}{2}. \tag{35}$$

For the spin triplet case l must be odd; for the singlet and quintet cases l must be even.

3.5. Antisymmetric molecular singlet state

We have used Mathematica to analyze the (unnormalized) antisymmetric singlet wavefunction, and we find that it simplifies to

$$\begin{aligned}
\mathcal{A}\Big\{[R][S][T]\Big\} \;=\;& R(12;34)\Big[(\alpha(1)\beta(2)-\beta(1)\alpha(2))(\alpha(3)\beta(4)-\beta(3)\alpha(4))\Big]_T \\
&\Big[2\alpha(1)\alpha(2)\beta(3)\beta(4)-\alpha(1)\beta(2)\alpha(3)\beta(4)-\alpha(1)\beta(2)\beta(3)\alpha(4) \\
&-\beta(1)\alpha(2)\alpha(3)\beta(4)-\beta(1)\alpha(2)\beta(3)\alpha(4)+2\beta(1)\beta(2)\alpha(3)\alpha(4)\Big]_S \\
&-R(13;24)\Big[(\alpha(1)\beta(3)-\beta(1)\alpha(3))(\alpha(2)\beta(4)-\beta(2)\alpha(4))\Big]_T \\
&\Big[2\alpha(1)\beta(2)\alpha(3)\beta(4)-\alpha(1)\alpha(2)\beta(3)\beta(4)-\alpha(1)\beta(2)\beta(3)\alpha(4) \\
&-\beta(1)\beta(2)\alpha(3)\alpha(4)-\beta(1)\alpha(2)\alpha(3)\beta(4)+2\beta(1)\alpha(2)\beta(3)\alpha(4)\Big]_S \\
&+R(14;23)\Big[(\alpha(1)\beta(4)-\beta(1)\alpha(4))(\alpha(2)\beta(3)-\beta(2)\alpha(3))\Big]_T \\
&\Big[2\alpha(1)\beta(2)\beta(3)\alpha(4)-\alpha(1)\beta(2)\alpha(3)\beta(4)-\alpha(1)\alpha(2)\beta(3)\beta(4) \\
&-\beta(1)\beta(2)\alpha(3)\alpha(4)-\beta(1)\alpha(2)\beta(3)\alpha(4)+2\beta(1)\alpha(2)\alpha(3)\beta(4)\Big]_S.
\end{aligned} \tag{36}$$

We can write the resulting antisymmetrized wavefunction as a summation of the form

$$\Psi \;=\; \sum_{j=3}^{5} c_j[R]_j[S]_j[T]_j, \tag{37}$$

where we will work with $[R]_j$, $[S]_j$, and $[T]_j$ components that are individually normalized. For the isospin functions, we may write

$$[T]_3 \;=\; \frac{1}{2}\Big[(\alpha(1)\beta(2)-\beta(1)\alpha(2))(\alpha(3)\beta(4)-\beta(3)\alpha(4))\Big]_T, \tag{38}$$

$$[T]_4 \;=\; \frac{1}{2}\Big[(\alpha(1)\beta(3)-\beta(1)\alpha(3))(\alpha(2)\beta(4)-\beta(2)\alpha(4))\Big]_T, \tag{39}$$

$$[T]_5 \;=\; \frac{1}{2}\Big[(\alpha(1)\beta(4)-\beta(1)\alpha(4))(\alpha(2)\beta(3)-\beta(2)\alpha(3))\Big]_T. \tag{40}$$

For the spatial wavefunctions, we have

$$[R]_3 \;=\; R(12;34), \qquad [R]_4 \;=\; R(13;24), \qquad [R]_5 \;=\; R(14;23). \tag{41}$$

In the case of the expansion coefficients, we have

$$c_3 \;=\; c_5 \;=\; \frac{1}{\sqrt{3}}, \qquad c_4 \;=\; -\frac{1}{\sqrt{3}}. \tag{42}$$

The spin functions are different for the three cases; we may write

$$\begin{aligned}[S]_3 \;=\; \frac{1}{\sqrt{12}}\Big[&2\alpha(1)\alpha(2)\beta(3)\beta(4)-\alpha(1)\beta(2)\alpha(3)\beta(4)-\alpha(1)\beta(2)\beta(3)\alpha(4)\\ &-\beta(1)\alpha(2)\alpha(3)\beta(4)-\beta(1)\alpha(2)\beta(3)\alpha(4)+2\beta(1)\beta(2)\alpha(3)\alpha(4)\Big]_S,\end{aligned} \tag{43}$$

$$\begin{aligned}[S]_4 \;=\; \frac{1}{\sqrt{12}}\Big[&2\alpha(1)\beta(2)\alpha(3)\beta(4)-\alpha(1)\alpha(2)\beta(3)\beta(4)-\alpha(1)\beta(2)\beta(3)\alpha(4)\\ &-\beta(1)\beta(2)\alpha(3)\alpha(4)-\beta(1)\alpha(2)\alpha(3)\beta(4)+2\beta(1)\alpha(2)\beta(3)\alpha(4)\Big]_S,\end{aligned} \tag{44}$$

$$\begin{aligned}[S]_5 \;=\; \frac{1}{\sqrt{12}}\Big[&2\alpha(1)\beta(2)\beta(3)\alpha(4)-\alpha(1)\beta(2)\alpha(3)\beta(4)-\alpha(1)\alpha(2)\beta(3)\beta(4)\\ &-\beta(1)\beta(2)\alpha(3)\alpha(4)-\beta(1)\alpha(2)\beta(3)\alpha(4)+2\beta(1)\alpha(2)\alpha(3)\beta(4)\Big]_S.\end{aligned} \tag{45}$$

3.6. Systematic construction of the molecular states

It is possible to develop a systematic construction for all of the molecular states using

$$\Psi \;=\; \frac{1}{\sqrt{3}}\Big([R]_3[S]_3[T]_3 - [R]_4[S]_4[T]_4 + [R]_5[S]_5[T]_5 \Big). \tag{46}$$

Based on the same c_j, $[R]_j$, and $[T]_j$ definitions given above for the singlet case. The spin functions $[S]_j$ are different, and we have tabulated unnormalized spin functions for all cases in Table 1. The notation we have used is as follows:

$$\begin{array}{llll}
s_1 = \alpha(1)\alpha(2)\alpha(3)\alpha(4), & s_2 = \alpha(1)\alpha(2)\alpha(3)\beta(4), & s_3 = \alpha(1)\alpha(2)\beta(3)\alpha(4), & s_4 = \alpha(1)\alpha(2)\beta(3)\beta(4), \\
s_5 = \alpha(1)\beta(2)\alpha(3)\alpha(4), & s_6 = \alpha(1)\beta(2)\alpha(3)\beta(4), & s_7 = \alpha(1)\beta(2)\beta(3)\alpha(4), & s_8 = \alpha(1)\beta(2)\beta(3)\beta(4), \\
s_9 = \beta(1)\alpha(2)\alpha(3)\alpha(4), & s_{10} = \beta(1)\alpha(2)\alpha(3)\beta(4), & s_{11} = \beta(1)\alpha(2)\beta(3)\alpha(4), & s_{12} = \beta(1)\alpha(2)\beta(3)\beta(4), \\
s_{13} = \beta(1)\beta(2)\alpha(3)\alpha(4), & s_{14} = \beta(1)\beta(2)\alpha(3)\beta(4), & s_{15} = \beta(1)\beta(2)\beta(3)\alpha(4), & s_{16} = \beta(1)\beta(2)\beta(3)\beta(4).
\end{array} \tag{47}$$

Certainly the various spin states are well known; however, the tabulation of the states in the form of Table 1 makes convenient their use systematically in Mathematica calculations.

Table 1. Tabulation of spin states $[S]^{(S,M_S)}$.

State	s_1	s_2	s_3	s_4	s_5	s_6	s_7	s_8	s_9	s_{10}	s_{11}	s_{12}	s_{13}	s_{14}	s_{15}	s_{16}
$[S]_3^{(0,0)}$	0	0	0	2	0	-1	-1	0	0	-1	-1	0	2	0	0	0
$[S]_4^{0,0}$	0	0	0	-1	0	2	-1	0	0	-1	2	0	-1	0	0	0
$[S]_5^{(0,0)}$	0	0	0	-1	0	-1	2	0	0	2	-1	0	-1	0	0	0
$[S]_3^{(1,-1)}$	0	0	0	0	0	0	0	1	0	0	0	1	0	-1	-1	0
$[S]_4^{(1,-1)}$	0	0	0	0	0	0	0	1	0	0	0	-1	0	1	-1	0
$[S]_5^{(1,-1)}$	0	0	0	0	0	0	0	1	0	0	0	-1	0	-1	1	0
$[S]_3^{(1,0)}$	0	0	0	1	0	0	0	0	0	0	0	0	-1	0	0	0
$[S]_4^{(1,0)}$	0	0	0	0	0	1	0	0	0	0	-1	0	0	0	0	0
$[S]_5^{(1,0)}$	0	0	0	0	0	0	1	0	0	-1	0	0	0	0	0	0
$[S]_3^{(1,1)}$	0	1	1	0	-1	0	0	0	-1	0	0	0	0	0	0	0
$[S]_4^{(1,1)}$	0	1	-1	0	1	0	0	0	-1	0	0	0	0	0	0	0
$[S]_5^{(1,1)}$	0	-1	1	0	1	0	0	0	-1	0	0	0	0	0	0	0
$[S]_3^{(2,-2)}$	0	0	0	0	0	0	0	0	0	0	0	0	0	0	0	1
$[S]_4^{(2,-2)}$	0	0	0	0	0	0	0	0	0	0	0	0	0	0	0	1
$[S]_5^{(2,-2)}$	0	0	0	0	0	0	0	0	0	0	0	0	0	0	0	1
$[S]_3^{(2,-1)}$	0	0	0	0	0	0	0	1	0	0	0	1	0	1	1	0
$[S]_4^{(2,-1)}$	0	0	0	0	0	0	0	1	0	0	0	1	0	1	1	0
$[S]_5^{(2,-1)}$	0	0	0	0	0	0	0	1	0	0	0	1	0	1	1	0
$[S]_3^{(2,0)}$	0	0	0	1	0	1	1	0	0	1	1	0	1	0	0	0
$[S]_4^{(2,0)}$	0	0	0	1	0	1	1	0	0	1	1	0	1	0	0	0
$[S]_5^{(2,0)}$	0	0	0	1	0	1	1	0	0	1	1	0	1	0	0	0
$[S]_3^{(2,1)}$	0	1	1	0	1	0	0	0	1	0	0	0	0	0	0	0
$[S]_4^{(2,1)}$	0	1	1	0	1	0	0	0	1	0	0	0	0	0	0	0
$[S]_5^{(2,1)}$	0	1	1	0	1	0	0	0	1	0	0	0	0	0	0	0
$[S]_3^{(2,2)}$	1	0	0	0	0	0	0	0	0	0	0	0	0	0	0	0
$[S]_4^{(2,2)}$	1	0	0	0	0	0	0	0	0	0	0	0	0	0	0	0
$[S]_5^{(2,2)}$	1	0	0	0	0	0	0	0	0	0	0	0	0	0	0	0

4. Molecular and Nuclear Deuteron Wavefunctions

We require a specification of the relative deuteron–deuteron molecular wavefunctions, and also the relative deuteron wavefunction, in order to evaluate the spatial integrals. For the molecular wavefunction we require estimates for the nuclear and Coulomb potentials, and then we must develop solutions to the radial Schrödinger equation. We will also need to worry about the wavefunction normalization which is made nontrivial due to the sizeable Gamow factors that appear in connection with tunneling through the Coulomb barrier. In the case of the nuclear wavefunction, we will need to develop a useful parameterization of the deuteron relative wavefunction.

4.1. Woods–Saxon potentials

Woods–Saxon potential parameters have been determined previously for deuteron–deuteron scattering. We may write for the different cases

$$V_{WS}^{(S,M_S)}(r) \;=\; \frac{V_S}{1+\mathrm{e}^{(r-r_S)/a_S}}, \tag{48}$$

where the fitting parameters from [20] are listed in Table 2.

4.2. Coulomb potential

The Coulomb potential between two deuterons within the approximation under discussion is given by

$$V_{\rm Coul}(r) \;=\; \left\langle R(12;34)\left|\frac{e^2}{r_{31}}\right|R(12;34)\right\rangle, \tag{49}$$

where the integrations are over the relative deuteron coordinates

$$\begin{aligned} V_{\rm Coul}(r) \;&=\; \left\langle \phi_d(r_{21})\phi_d(r_{43})\left|\frac{e^2}{r_{31}}\right|\phi_d(r_{21})\phi_d(r_{43})\right\rangle \\ &=\; \int \mathrm{d}^3\mathbf{r}_a \int \mathrm{d}^3\mathbf{r}_b\; \phi_d^2(r_a)\phi_d^b(r_b)\;\frac{e^2}{\sqrt{r^2+\left|\frac{\mathbf{r}_a-\mathbf{r}_b}{2}\right|^2}}. \end{aligned} \tag{50}$$

We have carried out a numerical evaluation of the Coulomb potential and fit the results in the form

Table 2. Woods–Saxon potential fitting parameters for deuteron–deuteron scattering.

S	l	V_S (MeV)	r_S (fm)	a_S (fm)
0	0	74	1.70	0.90
0	2	13.5	3.39	0.79
1	1	13.5	5.04	0.79
2	0	15.5	3.59	0.81

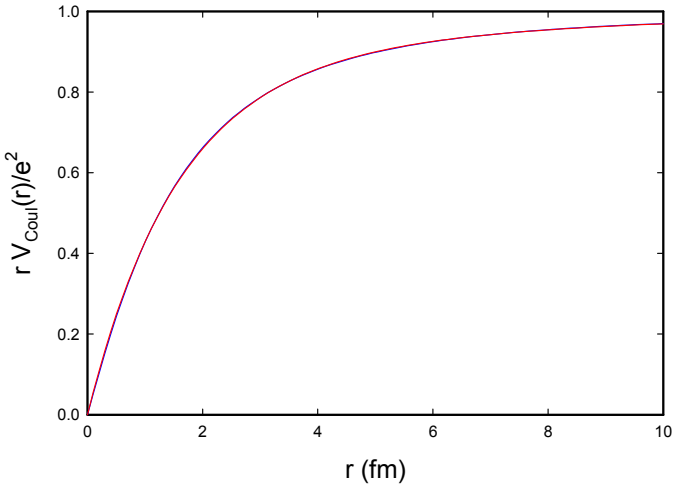

Figure 2. Scaled Coulomb potential between two deuterons; numerical calculation (*blue*); empirical fit (*red*). The two curves are seen to be very close together.

$$V_{\rm Coul}(r) \;=\; \frac{e^2}{r}\Big[1 - a{\rm e}^{-\kappa_1 r} - (1-a){\rm e}^{-\kappa_2 r}\Big] \tag{51}$$

with

$$a \;=\; 0.160807, \quad \kappa_1 \;=\; 0.170843\ {\rm fm}^{-1}, \quad \kappa_2 \;=\; 0.656377\ {\rm fm}^{-1}. \tag{52}$$

This fit is very good as illustrated in Fig. 2.

4.3. Molecular potential model

The deuteron–deuteron potential at short distances is made up of nuclear and Coulomb contributions as discussed above. At larger separation the deuterons see an attractive molecular potential. Since we are interested in the relative radial wavefunction, we will add the centripetal potential to make an effective potential. This allows us to write

$$V_{\rm eff}(r) \;=\; V_{WS}(r) + V_{\rm mol}(r) + \frac{\hbar^2 l(l+1)}{2\mu r^2}. \tag{53}$$

At larger separation we have made use of a molecular H_2 potential proposed by Frost and Musulin [21]

$$V_{\rm mol}(r) \;=\; \begin{cases} V_{\rm Coul}(r), & \text{small } r, \\ \dfrac{e^2}{a_0}{\rm e}^{-ar/a_0}\left(\dfrac{a_0}{r} - b\right), & \text{large } r \end{cases} \tag{54}$$

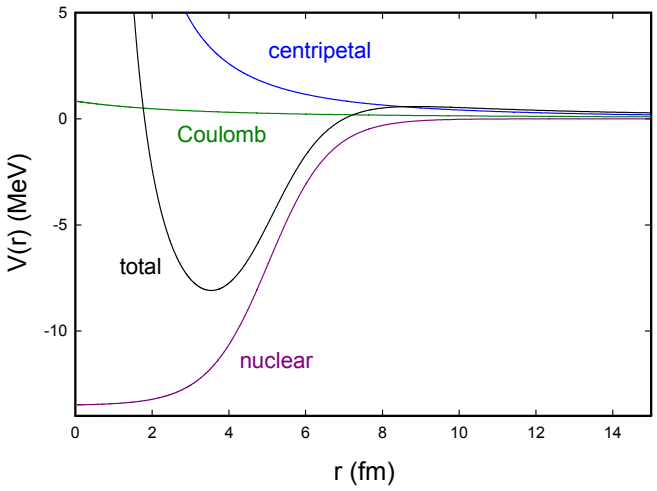

Figure 3. Deuteron–deuteron potential model, showing Wood–Saxon, Coulomb, and centripetal contributions.

with

$$a = 0.886, \qquad b = 1.315. \tag{55}$$

In Fig. 3, we show the different components along with the total deuteron–deuteron potential for the $l = 1$ channel in this model.

4.4. Schrödinger equation for the molecular radial wavefunction

The molecular radial wavefunction satisfies

$$E R(r) = -\frac{\hbar^2}{2\mu}\frac{1}{r^2}\frac{\mathrm{d}}{\mathrm{d}r}\left(r^2\frac{\mathrm{d}}{\mathrm{d}r}R(r)\right) + V_{\mathrm{eff}}(r)R(r), \tag{56}$$

where μ is the reduced mass

$$\mu = \frac{M_D}{2}. \tag{57}$$

4.5. Normalization of the molecular radial wavefunction

The normalization of the radial wavefunction is determined through

$$\int_0^\infty r^2 R^2(r)\mathrm{d}r = 1. \tag{58}$$

The normalization in this case is determined primarily by the wavefunction on the Angstrom scale; because of tunneling the wavefunction is very small on the fermi scale. Because screening effects are known to be important in metal deuterides, we would like to work with a scaled wavefunction near the origin where the tunneling effects have been removed.

We have decided to work with a scaled molecular radial wavefunction defined according to

$$R(r) \;=\; \frac{\mathrm{e}^{-G}}{\sqrt{R_0(\Delta R)^2}}\, F(r). \tag{59}$$

Here G is the Gamow factor

$$G \;=\; \int_{r_{\rm min}}^{r_{\rm max}} \sqrt{\frac{2\mu[V(r)-E]}{\hbar^2}}\mathrm{d}r. \tag{60}$$

The average separation and spread are given by

$$\langle r\rangle \;=\; R_0, \qquad (\Delta R)^2 \;=\; \langle (r-R_0)^2\rangle. \tag{61}$$

Defined in this way, our results will be roughly independent of the details of the particular molecular potential used. If screening is important, it will come in through the Gamow factor; if the molecular separation in the lattice is different, the associated volume effect is taken into account in the terms within the square root.

4.6. Model molecular radial wavefunctions

We have computed the molecular radial wavefunctions normalized as above, and fit them to

Table 3. Fitting parameters for the molecular D_2 wavefunctions; R_0 and ΔR in Angstroms; γ is in fm$^{-1/2}$; A in fm^{-l}; b_1 and c_1 in fm^{-1}; b_2 and c_2 in fm^{-2}; and b_3 and c_3 in fm^{-3}.

Parameter	$S=0$ $l=0$	$S=2$ $l=0$	$S=1$ $l=1$	$S=0$ $l=2$	$S=2$ $l=2$	$S=1$ $l=3$
G	85.63	85.52	88.13	93.84	93.71	99.44
R_0	0.750	0.750	0.751	0.752	0.752	0.754
ΔR	0.0751	0.0751	0.0751	0.0752	0.0752	0.0753
γ	0.445321	0.447246	0.409238	0.367509	0.368575	0.327432
A	47.7563	28.6494	217.299	5.16205	5.12699	2.15563
b_1	-0.0574296	0.188016	-0.0856778	-0.225749	-0.227819	-0.218391
b_2	-0.148166	-0.0807753	0.00478186	0.0326325	0.0305096	0.0285951
b_3	-0.00449984	-0.00219149	1.16077×10^{-5}	3.72936×10^{-5}	3.35009×10^{-5}	2.234×10^{-5}
c_1	0.169052	0.412487	0.285851	-0.0557748	-0.053966	-0.0747202
c_2	0.204056	0.0257346	-0.141624	0.0238128	0.0177579	0.0215395
c_3	0.107872	0.0367975	0.0568277	0.00858995	0.00909683	0.0059147

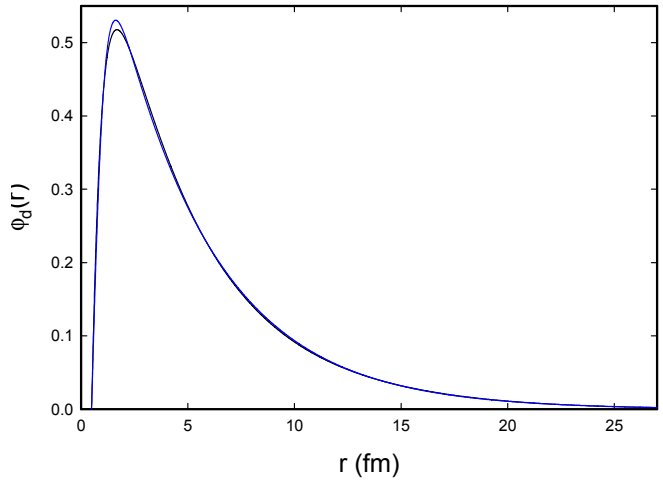

Figure 4. Triplet S channel deuteron wavefunction computed from the coupled-channel equations (*black*); and least squares fit (*blue*).

$$F(r) \;=\; Ar^l \frac{1 + b_1 r + b_2 r^2}{1 + c_1 r + c_2 r^2} \mathrm{e}^{-\gamma(\sqrt{r}+1)}. \tag{62}$$

where the 1 in the exponent is to be understood as $\sqrt{1\ \mathrm{fm}}$. Fitting parameters for the different radial molecular wavefunctions are given in Table 3.

4.7. Deuteron wavefunction

A reasonable approximation for a single deuteron wavefunction S channel is

$$\phi_d(r) \;=\; \begin{cases} 0 & \text{for } r < r_0, \\ N_d \dfrac{\tanh[\gamma(r - r_0)]\ \mathrm{e}^{-\beta r}}{r} & \text{for } r_0 < r \end{cases} \tag{63}$$

From a least squares fit to a numerical solution of the Rarita–Schwinger equation based on the Hamada–Johnston potential, we obtain

$$\beta \;=\; 0.2159\ \mathrm{fm}^{-1}, \qquad \gamma \;=\; 1.460\ \mathrm{fm}^{-1}, \qquad N_d \;=\; 0.2132\ \mathrm{fm}^{-3/2}. \tag{64}$$

This function can provide a good fit to the model deuteron S channel wavefunction that we computed previously, as shown in Fig. 4.

5. Interaction

With a specification of the spin and isospin functions of the initial and final states, and with a clarification of the general form of the spatial wavefunctions, we now turn our attention to a specification of the interaction.

5.1. Relativistic $\mathbf{a} \cdot c\mathbf{P}$ interaction

In previous work we have derived the $\mathbf{a} \cdot c\mathbf{P}$ interaction starting with a many-nucleon Dirac model for the nuclei. In response to comments from a reviewer, we consider this approach under conditions where an external electromagnetic field is present. The relativistic nucleon Hamiltonian in the Dirac phenomenology in this case for a single nucleus can be written as

$$\hat{H} \;=\; \sum_j \boldsymbol{\alpha}_j \cdot c\left[\hat{\mathbf{p}}_j - \frac{e_j}{c}\hat{\mathbf{A}}(\mathbf{r}_j)\right] + \beta_j m_j c^2 + \sum_{j<k} V_{jk}(\mathbf{r}_k - \mathbf{r}_j), \tag{65}$$

where the nucleon–nucleon potential V_{jk} here is intended to include the strong force interaction as well as the electromagnetic interactions between nucleons within the nucleus; and where $\hat{\mathbf{A}}$ describes the external field.

Since the nuclear center of mass momentum is small for the problems of interest to us, we adopt nonrelativistic center of mass and relative coordinates

$$M\mathbf{R} \;=\; \sum_j m_j \mathbf{r}_j, \qquad \boldsymbol{\xi}_j \;=\; \mathbf{r}_j - \mathbf{R}, \tag{66}$$

$$\mathbf{P} \;=\; \sum_j \mathbf{p}_j, \qquad \boldsymbol{\pi}_j \;=\; \mathbf{p}_j - \frac{m_j}{M}\mathbf{P}. \tag{67}$$

Due to the close connection between the momentum and vector potential in the many-nucleon Dirac model, it may be best to adopt an analogous separation in the external field based on the total (charge-weighted) external field

$$\sum_j e_j \hat{\mathbf{A}}(\mathbf{r}_j) \;\rightarrow\; Ze\hat{\mathbf{A}}. \tag{68}$$

This allows us to achieve a separation between center of mass and relative contributions for the Hamiltonian

$$\begin{aligned}\hat{H} \;=\; & \sum_j \frac{m_j}{M}\boldsymbol{\alpha}_j \cdot \left(c\hat{\mathbf{P}} - Ze\hat{\mathbf{A}}\right) \\ & + \sum_j \boldsymbol{\alpha}_j \cdot \left(c\hat{\boldsymbol{\pi}}_j - e_j\hat{A}(\mathbf{r}_j) + \frac{m_j}{M}Ze\hat{\mathbf{A}}\right) + \sum_j \beta_j m_j c^2 + \sum_{j<k} V_{jk}(\boldsymbol{\xi}_k - \boldsymbol{\xi}_j).\end{aligned} \tag{69}$$

The first term includes center of mass interactions, and the remaining can be understood as describing relative interactions. In light of this the relativistic $\mathbf{a} \cdot c\mathbf{P}$ interaction should be

$$\hat{H}_{\rm int} \;=\; \sum_j \frac{m_j}{M}\boldsymbol{\alpha}_j \cdot \left(c\hat{\mathbf{P}} - Ze\hat{\mathbf{A}}\right) \tag{70}$$

instead of what we have used in earlier work where the contribution of the external field has not been included. We are indebted to the reviewer for pointing this out.

Some further discussion is probably helpful in thinking about the model that results. It does not come as a surprise that photon absorption and emission can be included in this kind of formulation (Eq. (69)), and in the separation that we have adopted we can see both center of mass and relative contributions explicitly. Since we are most interested in the center of mass interaction, it becomes important to understand what new physics is now included in the new interaction Hamiltonian of Eq. (70). If we adopt a Coulomb gauge point of view (which is predominant in atomic, molecular and condensed matter physics), then we would associate the new term with magnetic interactions (since Coulomb interactions are not included in the vector potential operator). This is interesting, since it tells us that there is a magnetic analog to the vibrational coupling that we have been focusing on, that we had not considered previously.

In what follows we will continue the analysis as if magnetic field effects can be neglected (working with **P** alone), and then revisit the issue in the conclusions.

5.2. Nonrelativistic $\mathbf{a}\cdot c\mathbf{P}$ Hamiltonian

For the nuclear calculation we adopt the equal mass part of the nonrelativistic expansion [11], which can be written as

$$\hat{H}_{\rm int} = \frac{1}{(2Mc^2)}\frac{1}{(2m_{av}c^2)} \sum_i \left\{ (\boldsymbol{\sigma}_i\cdot c\hat{\mathbf{P}})\left[\sum_{j<k}\hat{V}_{jk}\right](\boldsymbol{\sigma}_i\cdot c\hat{\boldsymbol{\pi}}_i) + (\boldsymbol{\sigma}_i\cdot c\hat{\boldsymbol{\pi}}_i)\left[\sum_{j<k}\hat{V}_{jk}\right](\boldsymbol{\sigma}_i\cdot c\hat{\mathbf{P}})\right\}, \tag{71}$$

where the $\hat{\boldsymbol{\pi}}_j$ operators are nucleon operators without the center of mass contribution.

$$\hat{\boldsymbol{\pi}}_j = \hat{\mathbf{p}}_j - \frac{\hat{\mathbf{P}}}{4}. \tag{72}$$

Note that in general this interaction involves three nucleons.

5.3. Two-body interaction

It appears that it is possible to simplify the interaction some. From an inspection of the interaction Hamiltonian, one sees that there are indices for three nucleons. When the index i matches j or k, we may isolate the contribution as

$$\hat{H}_{\rm int}^{2\,\rm body} = \frac{1}{(2Mc^2)}\frac{1}{(2m_{av}c^2)}\sum_{j<k}\Big\{(\boldsymbol{\sigma}_j\cdot c\hat{\mathbf{P}})\hat{V}_{jk}(\boldsymbol{\sigma}_j\cdot c\hat{\boldsymbol{\pi}}_j) + (\boldsymbol{\sigma}_j\cdot c\hat{\boldsymbol{\pi}}_j)\hat{V}_{jk}(\boldsymbol{\sigma}_j\cdot c\hat{\mathbf{P}})$$

$$+(\boldsymbol{\sigma}_k\cdot c\hat{\mathbf{P}})\hat{V}_{jk}(\boldsymbol{\sigma}_k\cdot c\hat{\boldsymbol{\pi}}_k) + (\boldsymbol{\sigma}_k\cdot c\hat{\boldsymbol{\pi}}_k)\hat{V}_{jk}(\boldsymbol{\sigma}_k\cdot c\hat{\mathbf{P}})\Big\}. \tag{73}$$

5.4. Three-body interaction

If the indices are all different then it seems that the associated operators will commute. In this case we may write

$$\hat{H}_{\rm int}^{\rm 3\,body} = \frac{1}{(2Mc^2)}\frac{1}{(2m_{\rm av}c^2)} \sum_i \sum_{j<k, j\neq i, k\neq i} \left\{ (\boldsymbol{\sigma}_i \cdot c\hat{\mathbf{P}})\hat{V}_{jk}(\boldsymbol{\sigma}_i \cdot c\hat{\boldsymbol{\pi}}_i) + (\boldsymbol{\sigma}_i \cdot c\hat{\boldsymbol{\pi}}_i)\hat{V}_{jk}(\boldsymbol{\sigma}_i \cdot c\hat{\mathbf{P}}) \right\}. \tag{74}$$

In general we expect the operators associated with i to commute with $\hat{V}_{jk}$, which allows us to write

$$\begin{aligned} \hat{H}_{\rm int}^{\rm 3\,body} &= \frac{1}{(2Mc^2)}\frac{1}{(2m_{\rm av}c^2)} \sum_i \sum_{j<l, j\neq i, k\neq i} \hat{V}_{jk} \left[(\boldsymbol{\sigma}_i \cdot c\hat{\mathbf{P}})(\boldsymbol{\sigma}_i \cdot c\hat{\boldsymbol{\pi}}_i) + (\boldsymbol{\sigma}_i \cdot c\hat{\boldsymbol{\pi}}_i)(\boldsymbol{\sigma}_i \cdot c\hat{\mathbf{P}}) \right] \\ &= \frac{1}{(2m_{\rm av}c^2)} \sum_i \frac{\hat{\mathbf{P}} \cdot \hat{\boldsymbol{\pi}}_i}{M} \left[\sum_{j<k, j\neq i, k\neq i} \hat{V}_{jk} \right]. \end{aligned} \tag{75}$$

The three-body interaction vanishes in this case because

$$\sum_i \frac{\hat{\mathbf{P}} \cdot \hat{\boldsymbol{\pi}}_i}{M} = \frac{\hat{\mathbf{P}}}{M} \cdot \sum_i \hat{\boldsymbol{\pi}}_i = 0 \tag{76}$$

since the relative momentum operators sum to zero [11].

5.5. Hamada–Johnston potential

Because the nuclear potential models are very complicated, we have chosen to work with one of the early models that is relatively simple in form. The Hamada–Johnston potential can be written as [15]

$$\hat{V} = V_C + V_T \hat{S}_{12} + V_{LS}(\hat{\mathbf{L}} \cdot \hat{\mathbf{S}}) + V_{LL}\hat{L}_{12}. \tag{77}$$

It will be convenient to rewrite it in the form

$$\hat{V} = (\boldsymbol{\sigma}_1 \cdot \boldsymbol{\sigma}_2)(\boldsymbol{\tau}_1 \cdot \boldsymbol{\tau}_2)v_C(r) + (\boldsymbol{\tau}_1 \cdot \boldsymbol{\tau}_2)\hat{S}_{12}v_T(r) + \left(\frac{\hat{\mathbf{L}} \cdot \hat{\mathbf{S}}}{\hbar^2}\right) v_{LS}(r) + \left(\frac{\hat{L}_{12}}{\hbar^2}\right) v_{LL}(r), \tag{78}$$

where the different terms are described in the Appendix.

6. Reduction of Spin and Isospin for the Central Potential

We can write for the central potential contribution to the interaction matrix element

$$\hat{H}_C = \frac{1}{(2Mc^2)}\frac{1}{(2m_{\rm av}c^2)}\sum_{j<k}\left\{\left\langle\Psi[^4{\rm He}]\right|(\boldsymbol{\sigma}_j\cdot c\hat{\mathbf{P}})(\boldsymbol{\sigma}_j\cdot\boldsymbol{\sigma}_k)(\boldsymbol{\tau}_j\cdot\boldsymbol{\tau}_k)\hat{v}_C(r_{jk})(\boldsymbol{\sigma}_j\cdot c\hat{\boldsymbol{\pi}}_j)\left|\Psi[{\rm D}_2]\right\rangle\right.$$
$$+\left\langle\Psi[^4{\rm He}]\right|(\boldsymbol{\sigma}_j\cdot c\hat{\boldsymbol{\pi}}_j)(\boldsymbol{\sigma}_j\cdot\boldsymbol{\sigma}_k)(\boldsymbol{\tau}_j\cdot\boldsymbol{\tau}_k)\hat{v}_C(r_{jk})(\boldsymbol{\sigma}_j\cdot c\hat{\mathbf{P}})\left|\Psi[{\rm D}_2]\right\rangle$$
$$+\left\langle\Psi[^4{\rm He}]\right|(\boldsymbol{\sigma}_k\cdot c\hat{\mathbf{P}})(\boldsymbol{\sigma}_j\cdot\boldsymbol{\sigma}_k)(\boldsymbol{\tau}_j\cdot\boldsymbol{\tau}_k)\hat{v}_C(r_{jk})(\boldsymbol{\sigma}_k\cdot c\hat{\boldsymbol{\pi}}_k)\left|\Psi[{\rm D}_2]\right\rangle$$
$$\left.+\left\langle\Psi[^4{\rm He}]\right|(\boldsymbol{\sigma}_k\cdot c\hat{\boldsymbol{\pi}}_k)(\boldsymbol{\sigma}_j\cdot\boldsymbol{\sigma}_k)(\boldsymbol{\tau}_j\cdot\boldsymbol{\tau}_k)\hat{v}_C(r_{jk})(\boldsymbol{\sigma}_k\cdot c\hat{\mathbf{P}})\left|\Psi[{\rm D}_2]\right\rangle\right\}. \quad (79)$$

Our interest ultimately is in the interaction as a lattice operator based on the center of mass operator $\hat{\mathbf{P}}$; however, for the specific calculations that we need to carry out to evaluate the nuclear part of the interaction the answers will be the same if we replace the operator $\hat{\mathbf{P}}$ with a constant momentum $\mathbf{P}$. Then, in order to simplify things, we take the center of mass momentum $\mathbf{P}$ to be z-directed

$$\mathbf{P} = P\hat{\mathbf{i}}_z \quad (80)$$

This allows us to write

$$M_C = \frac{P}{2M}\frac{1}{(2m_{\rm av}c^2)}\sum_{j<k}\left\{\left\langle\Psi[^4{\rm He}]\right|(\boldsymbol{\sigma}_j\cdot\hat{\mathbf{i}}_z)(\boldsymbol{\sigma}_j\cdot\boldsymbol{\sigma}_k)(\boldsymbol{\tau}_j\cdot\boldsymbol{\tau}_k)\hat{v}_C(r_{jk})(\boldsymbol{\sigma}_j\cdot\hat{\boldsymbol{\pi}}_j)\left|\Psi[{\rm D}_2]\right\rangle\right.$$
$$+\left\langle\Psi[^4{\rm He}]\right|(\boldsymbol{\sigma}_j\cdot\hat{\boldsymbol{\pi}}_j)(\boldsymbol{\sigma}_j\cdot\boldsymbol{\sigma}_k)(\boldsymbol{\tau}_j\cdot\boldsymbol{\tau}_k)\hat{v}_C(r_{jk})(\boldsymbol{\sigma}_j\cdot\hat{\mathbf{i}}_z)\left|\Psi[{\rm D}_2]\right\rangle$$
$$+\left\langle\Psi[^4{\rm He}]\right|(\boldsymbol{\sigma}_k\cdot\hat{\mathbf{i}}_z)(\boldsymbol{\sigma}_j\cdot\boldsymbol{\sigma}_k)(\boldsymbol{\tau}_j\cdot\boldsymbol{\tau}_k)\hat{v}_C(r_{jk})(\boldsymbol{\sigma}_k\cdot\hat{\boldsymbol{\pi}}_k)\left|\Psi[{\rm D}_2]\right\rangle$$
$$\left.+\left\langle\Psi[^4{\rm He}]\right|(\boldsymbol{\sigma}_k\cdot\hat{\boldsymbol{\pi}}_k)(\boldsymbol{\sigma}_j\cdot\boldsymbol{\sigma}_k)(\boldsymbol{\tau}_j\cdot\boldsymbol{\tau}_k)\hat{v}_C(r_{jk})(\boldsymbol{\sigma}_k\cdot\hat{\mathbf{i}}_z)\left|\Psi[{\rm D}_2]\right\rangle\right\}. \quad (81)$$

6.1. Evaluation based on product formula

The computation of the interaction matrix elements involves spin, isospin, angular momentum and spatial matrix elements which at the outset are mixed together. Since we are using nuclear wavefunctions that are composed of simple products of space, spin and isospin we can take advantage of the factorization of the individual terms in the Hamiltonian. Since individual interactions factor, we may evaluate the contributions to the matrix element using the product formula

$$\langle\Psi_{^1{\rm S}}|\hat{O}_R\hat{O}_S\hat{O}_T|\Psi_{D_2}\rangle = \sum_{j=1}^{2}\sum_{k=3}^{5}c_jc_k\langle[R]_j|\hat{O}_R|[R]_k\rangle\langle[S]_j|\hat{O}_S|[S]_k\rangle\langle[T]_j|\hat{O}_T|[T]_k\rangle. \quad (82)$$

Specific computations that follow have been carried out using Mathematica to evaluate the spin and isospin matrix elements.

6.2. Central potential matrix element for singlet states

We can express the results of the Mathematica calculations for the molecular singlet state in the form

$$M_C^{(0,0)} = \frac{P}{2M}\frac{1}{(2m_{av}c^2)}\sum_{j<k}\sum_{\kappa}\sum_{\iota}\Bigg\{ a_C^{\kappa}(jk;\iota)\Big\langle [R]_1\Big|v_C^{\kappa}(r_{jk})(\hat{\mathbf{i}}_z\cdot\hat{\boldsymbol{\pi}}_j)\Big|[R]_\iota\Big\rangle + b_C^{\kappa}(jk;\iota)\Big\langle [R]_1\Big|\hat{v}_C(r_{jk})(\hat{\mathbf{i}}_z\cdot\hat{\boldsymbol{\pi}}_k)\Big|[R]_\iota\Big\rangle + c_C^{\kappa}(jk;\iota)\Big\langle [R]_1\Big|(\hat{\mathbf{i}}_z\cdot\hat{\boldsymbol{\pi}}_j)v_C^{\kappa}(r_{jk})\Big|[R]_\iota\Big\rangle + d_C^{\kappa}(jk;\iota)\Big\langle [R]_1\Big|(\hat{\mathbf{i}}_z\cdot\hat{\boldsymbol{\pi}}_k)\hat{v}_C(r_{jk})\Big|[R]_\iota\Big\rangle\Bigg\}. \tag{83}$$

A tabulation of explicit values for expansion coefficients in a different form will be presented for contributions that are not zero due to selection rules later on.

6.3. Central potential matrix element for the triplet states

For the triplet case, when $M_S = \pm 1$ we obtain

$$M_C^{(1,\pm1)} = \frac{P}{2M}\frac{1}{(2m_{\rm av}c^2)}\sum_{j<k}\sum_{\kappa}\sum_{\iota}\Bigg\{$$

$$a_C^{\kappa}(jk;\iota)\Big\langle [R]_1\Big|v_C^{\kappa}(r_{jk})\Big[(\hat{\mathbf{i}}_x\pm\hat{\mathbf{i}}_y)\cdot\hat{\boldsymbol{\pi}}_j\Big]\Big|[R]_\iota\Big\rangle + b_C^{\kappa}(jk;\iota)\Big\langle [R]_1\Big|\hat{v}_C(r_{jk})\Big[(\hat{\mathbf{i}}_x\pm\hat{\mathbf{i}}_y)\cdot\hat{\boldsymbol{\pi}}_k\Big]\Big|[R]_\iota\Big\rangle$$

$$+c_C^{\kappa}(jk;\iota)\Big\langle [R]_1\Big|\Big[(\hat{\mathbf{i}}_x\pm\hat{\mathbf{i}}_y)\cdot\hat{\boldsymbol{\pi}}_j\Big]v_C^{\kappa}(r_{jk})\Big|[R]_\iota\Big\rangle + d_C^{\kappa}(jk;\iota)\Big\langle [R]_1\Big|\Big[(\hat{\mathbf{i}}_x\pm\hat{\mathbf{i}}_y)\cdot\hat{\boldsymbol{\pi}}_k\Big]\hat{v}_C(r_{jk})\Big|[R]_\iota\Big\rangle\Bigg\}. \tag{84}$$

The coefficients for both cases $M_S = \pm 1$ are the same. When $M_S = 0$ there is no contribution

$$M_C^{(1,0)} = 0. \tag{85}$$

6.4. Central potential matrix element for the quintet states

Central potential contributions to the interaction matrix element are found for quintet states with $M_S = 0, \pm 1$. For the $M_S = 0$ case we may write

$$M_C^{(2,0)} = \frac{P}{2M}\frac{1}{(2m_{\rm av}c^2)}\sum_{j<k}\sum_{\kappa}\sum_{\iota}\Bigg\{ a_C^{\kappa}(jk;\iota)\Big\langle [R]_1\Big|v_C^{\kappa}(r_{jk})(\hat{\mathbf{i}}_z\cdot\hat{\boldsymbol{\pi}}_j)\Big|[R]_\iota\Big\rangle + b_C^{\kappa}(jk;\iota)\Big\langle [R]_1\Big|\hat{v}_C(r_{jk})(\hat{\mathbf{i}}_z\cdot\hat{\boldsymbol{\pi}}_k)\Big|[R]_\iota\Big\rangle + c_C^{\kappa}(jk;\iota)\Big\langle [R]_1\Big|(\hat{\mathbf{i}}_z\cdot\hat{\boldsymbol{\pi}}_j)v_C^{\kappa}(r_{jk})\Big|[R]_\iota\Big\rangle + d_C^{\kappa}(jk;\iota)\Big\langle [R]_1\Big|(\hat{\mathbf{i}}_z\cdot\hat{\boldsymbol{\pi}}_k)\hat{v}_C(r_{jk})\Big|[R]_\iota\Big\rangle\Bigg\}. \tag{86}$$

In the case of the quintet states with $M_S = \pm 1$, we may write

$$M_C^{(1,\pm 1)} = \frac{P}{2M}\frac{1}{(2m_{\rm av}c^2)}\sum_{j<k}\sum_{\kappa}\sum_{\iota}\Bigg\{$$

$$a_C^\kappa(jk;\iota)\Big\langle [R]_1\Big|v_C^\kappa(r_{jk})\Big[(\hat{\mathbf{i}}_x \pm i\hat{\mathbf{i}}_y)\cdot\hat{\boldsymbol{\pi}}_j\Big]\Big|[R]_\iota\Big\rangle + b_C^\kappa(jk;\iota)\Big\langle [R]_1\Big|\hat{v}_C(r_{jk})\Big[(\hat{\mathbf{i}}_x \pm i\hat{\mathbf{i}}_y)\cdot\hat{\boldsymbol{\pi}}_k\Big]\Big|[R]_\iota\Big\rangle$$

$$+c_C^\kappa(jk;\iota)\Big\langle [R]_1\Big|\Big[(\hat{\mathbf{i}}_x \pm i\hat{\mathbf{i}}_y)\cdot\hat{\boldsymbol{\pi}}_j\Big]v_C^\kappa(r_{jk})\Big|[R]_\iota\Big\rangle + d_C^\kappa(jk;\iota)\Big\langle [R]_1\Big|\Big[(\hat{\mathbf{i}}_x \pm i\hat{\mathbf{i}}_y)\cdot\hat{\boldsymbol{\pi}}_k\Big]\hat{v}_C(r_{jk})\Big|[R]_\iota\Big\rangle\Bigg\}. \quad (87)$$

There is no contribution for the quintet $M_S = \pm 2$ states

$$M_C^{(2,\pm 2)} = 0. \quad (88)$$

6.5. Discussion

As discussed in the introduction, we needed to evaluate the spin and isospin parts of the matrix element; since we are doing the associated calculations by brute force, we needed a complete specification of the initial and final state wavefunctions which was done in the earlier sections. We end up with a very large number of terms here resulting from the reduction of the spin and isospin factors. It would be possible to evaluate all of these terms individually to develop an estimate for the matrix element. However, since there is a great deal of redundancy at this stage, we are motivated to continue further analytic work prior to the computations in order to simplify the calculation.

7. Reduction of Spin and Isospin for the Tensor Interaction

The biggest contribution to the strong force in the Hamada–Johnston potential is from the tensor interaction. We can use Mathematica to systematically reduce the spin and isospin matrix elements also in this case.

7.1. Tensor matrix element for the singlet state

The evaluation of the tensor contribution to the matrix element leads to a result that can be expressed as

$$M_T^{(0,0)} = \frac{P}{2M}\frac{1}{(2m_{\rm av}c^2)}\sum_{j<k}\sum_{\kappa}\sum_{\iota}\Bigg\{\Big\langle [R]_1\Big|\Big[-a_T^\kappa(jk;\iota)+\tilde{a}_T^\kappa(jk;\iota)\frac{z_{jk}^2}{r_{jk}^2}\Big]v_T^\kappa(r_{jk})(\hat{\mathbf{i}}_z\cdot\hat{\boldsymbol{\pi}}_j)\Big|[R]_\iota\Big\rangle$$

$$+\Big\langle [R]_1\Big|\Big[-b_T^\kappa(jk;\iota)+\tilde{b}_T^\kappa(jk;\iota)\frac{z_{jk}^2}{r_{jk}^2}\Big]\hat{v}_C(r_{jk})(\hat{\mathbf{i}}_z\cdot\hat{\boldsymbol{\pi}}_k)\Big|[R]_\iota\Big\rangle$$

$$+\Big\langle [R]_1\Big|(\hat{\mathbf{i}}_z\cdot\hat{\boldsymbol{\pi}}_j)\Big[-c_T^\kappa(jk;\iota)+\tilde{c}_T^\kappa(jk;\iota)\frac{z_{jk}^2}{r_{jk}^2}\Big]v_C^\kappa(r_{jk})\Big|[R]_\iota\Big\rangle$$

$$+\Big\langle [R]_1\Big|(\hat{\mathbf{i}}_z\cdot\hat{\boldsymbol{\pi}}_k)\Big[-d_T^\kappa(jk;\iota)+\tilde{d}_T^\kappa(jk;\iota)\frac{z_{jk}^2}{r_{jk}^2}\Big]\hat{v}_C(r_{jk})\Big|[R]_\iota\Big\rangle\Bigg\}. \quad (89)$$

Some of the expansion coefficients are identical to their central potential equivalents (for this case and also for all of the others).

$$a_T^\kappa \;=\; a_C^\kappa, \qquad b_T^\kappa \;=\; b_C^\kappa, \qquad c_T^\kappa \;=\; c_C^\kappa, \qquad d_T^\kappa \;=\; d_C^\kappa. \tag{90}$$

As mentioned above, we defer a presentation of explicit value for the expansion coefficients; later on results will be presented for the cases that are not forbidden in a different form.

7.2. Tensor matrix element for the triplet states

In the case of the triplet states, we find for $M_S = \pm 1$ that

$$\begin{aligned} M_T^{(1,\pm 1)} \;=\; \frac{P}{2M}\frac{1}{(2m_{\rm av}c^2)}\sum_{j<k}\sum_\kappa\sum_\iota \Bigg\{ &\left\langle [R]_1 \left| \left[-a_T^\kappa(jk;\iota) + \tilde{a}_T^\kappa(jk;\iota)\frac{z_{jk}^2}{r_{jk}^2}\right] v_T^\kappa(r_{jk}) \left[(\hat{\mathbf{i}}_x \pm i\hat{\mathbf{i}}_y)\cdot\hat{\boldsymbol{\pi}}_j \right] \right| [R]_\iota \right\rangle \\ &+\left\langle [R]_1 \left| \left[-b_T^\kappa(jk;\iota) + \tilde{b}_T^\kappa(jk;\iota)\frac{z_{jk}^2}{r_{jk}^2}\right] \hat{v}_C(r_{jk}) \left[(\hat{\mathbf{i}}_x \pm i\hat{\mathbf{i}}_y)\cdot\hat{\boldsymbol{\pi}}_k \right] \right| [R]_\iota \right\rangle \\ &+\left\langle [R]_1 \left| \left[(\hat{\mathbf{i}}_x \pm i\hat{\mathbf{i}}_y)\cdot\hat{\boldsymbol{\pi}}_j \right] \left[-c_T^\kappa(jk;\iota) + \tilde{c}_T^\kappa(jk;\iota)\frac{z_{jk}^2}{r_{jk}^2}\right] v_C^\kappa(r_{jk}) \right| [R]_\iota \right\rangle \\ &+\left\langle [R]_1 \left| \left[(\hat{\mathbf{i}}_x \pm i\hat{\mathbf{i}}_y)\cdot\hat{\boldsymbol{\pi}}_k \right] \left[-d_T^\kappa(jk;\iota) + \tilde{d}_T^\kappa(jk;\iota)\frac{z_{jk}^2}{r_{jk}^2}\right] \hat{v}_C(r_{jk}) \right| [R]_\iota \right\rangle \Bigg\}. \end{aligned} \tag{91}$$

For $M_S = 0$ the contribution vanishes

$$M_T^{(1,0)} \;=\; 0. \tag{92}$$

7.3. Tensor matrix element for the quintet states

In the case of the $M_S = 0$ quintet state we can write for the tensor contribution to the interaction matrix element

$$\begin{aligned} M_T^{(2,0)} \;=\; \frac{P}{2M}\frac{1}{(2m_{\rm av}c^2)}\sum_{j<k}\sum_\kappa\sum_\iota \Bigg\{ &\left\langle [R]_1 \left| \left[-a_T^\kappa(jk;\iota) + \tilde{a}_T^\kappa(jk;\iota)\frac{z_{jk}^2}{r_{jk}^2}\right] v_T^\kappa(r_{jk}) (\hat{\mathbf{i}}_z\cdot\hat{\boldsymbol{\pi}}_j) \right| [R]_\iota \right\rangle \\ &+\left\langle [R]_1 \left| \left[-b_T^\kappa(jk;\iota) + \tilde{b}_T^\kappa(jk;\iota)\frac{z_{jk}^2}{r_{jk}^2}\right] \hat{v}_C(r_{jk}) (\hat{\mathbf{i}}_z\cdot\hat{\boldsymbol{\pi}}_k) \right| [R]_\iota \right\rangle \\ &+\left\langle [R]_1 \left| (\hat{\mathbf{i}}_z\cdot\hat{\boldsymbol{\pi}}_j) \left[-c_T^\kappa(jk;\iota) + \tilde{c}_T^\kappa(jk;\iota)\frac{z_{jk}^2}{r_{jk}^2}\right] v_C^\kappa(r_{jk}) \right| [R]_\iota \right\rangle \\ &+\left\langle [R]_1 \left| (\hat{\mathbf{i}}_z\cdot\hat{\boldsymbol{\pi}}_k) \left[-d_T^\kappa(jk;\iota) + \tilde{d}_T^\kappa(jk;\iota)\frac{z_{jk}^2}{r_{jk}^2}\right] \hat{v}_C(r_{jk}) \right| [R]_\iota \right\rangle \Bigg\}. \end{aligned} \tag{93}$$

In the case of the $M_S = \pm 1$ states, we may write

$$M_T^{(2,\pm 1)} = \frac{P}{2M}\frac{1}{(2m_{\rm av}c^2)}\sum_{j<k}\sum_{\kappa}\sum_{\iota}\left\{\left\langle [R]_1\left|\left[-a_T^\kappa(jk;\iota)+\tilde{a}_T^\kappa(jk;\iota)\frac{z_{jk}^2}{r_{jk}^2}\right]v_T^\kappa(r_{jk})\left[(\hat{\mathbf{i}}_x \pm i\hat{\mathbf{i}}_y)\cdot\hat{\boldsymbol{\pi}}_j\right]\right|[R]_\iota\right\rangle\right.$$

$$+\left\langle [R]_1\left|\left[-b_T^\kappa(jk;\iota)+\tilde{b}_T^\kappa(jk;\iota)\frac{z_{jk}^2}{r_{jk}^2}\right]\hat{v}_C(r_{jk})\left[(\hat{\mathbf{i}}_x \pm i\hat{\mathbf{i}}_y)\cdot\hat{\boldsymbol{\pi}}_k\right]\right|[R]_\iota\right\rangle$$

$$+\left\langle [R]_1\left|\left[(\hat{\mathbf{i}}_x \pm i\hat{\mathbf{i}}_y)\cdot\hat{\boldsymbol{\pi}}_j\right]\left[-c_T^\kappa(jk;\iota)+\tilde{c}_T^\kappa(jk;\iota)\frac{z_{jk}^2}{r_{jk}^2}\right]v_C^\kappa(r_{jk})\right|[R]_\iota\right\rangle$$

$$\left.+\left\langle [R]_1\left|\left[(\hat{\mathbf{i}}_x \pm i\hat{\mathbf{i}}_y)\cdot\hat{\boldsymbol{\pi}}_k\right]\left[-d_T^\kappa(jk;\iota)+\tilde{d}_T^\kappa(jk;\iota)\frac{z_{jk}^2}{r_{jk}^2}\right]\hat{v}_C(r_{jk})\right|[R]_\iota\right\rangle\right\}. \quad (94)$$

There is no contribution for $M_S = \pm 2$

$$M_T^{(2,\pm 2)} = 0. \quad (95)$$

7.4. Discussion

Similar comments can be made here as was done at the end of the previous section. The big issue here is that the tensor contribution is more complicated than the central contribution, so we end up with twice as many integrals, and these spatial integrals are going to take more effort to compute.

8. Molecular Coordinates

The evaluation of the interaction matrix element involves spin, isospin, angular momentum and multi-dimensional spatial terms. In previous sections we have dealt with the spin and isospin terms, and next we are interested in the reduction of the radial and angular part of the problem. Since there are four nucleons, each with three spatial degrees of freedom, there are in principle twelve degrees of freedom possible. The elimination of the center of mass dependence reduces this to nine degrees of freedom.

It will be convenient to implement the integrations using molecular coordinates. Two of these coordinates $\mathbf{r}_a$ and $\mathbf{r}_b$ are associated with the relative separation of the nucleons in deuterons that make up the D_2 molecule, and one $\mathbf{r}$ is the relative coordinate between the two deuterons. The nine degrees of freedom can be reduced into three radial and six angular degrees of freedom. We will have to integrate the three radial degrees of freedom numerically, and also at least one of the angular degrees of freedom. Some of the integrals will evaluate to zero due to the angular part of the integration, or due to the spatial part of the integration.

In this section we are concerned with coordinates and momentum operators, which we will use in the following sections to evaluate the spatial operators and integrals.

8.1. Molecular coordinates

To isolate the angular integration, we need to work in terms of coordinates relevant to the molecular part of the problem. We begin by defining them systematically in terms of the individual nucleon coordinates:

$$\mathbf{R} = \frac{\mathbf{r}_1 + \mathbf{r}_2 + \mathbf{r}_3 + \mathbf{r}_4}{4}, \tag{96}$$

$$\mathbf{r}_a = \mathbf{r}_2 - \mathbf{r}_1, \tag{97}$$

$$\mathbf{r}_b = \mathbf{r}_4 - \mathbf{r}_3, \tag{98}$$

$$\mathbf{r} = \frac{\mathbf{r}_3 + \mathbf{r}_4}{2} - \frac{\mathbf{r}_1 + \mathbf{r}_2}{2}. \tag{99}$$

Using these coordinates we may write for the spatial part of the D_2 wavefunction

$$R(12;34) = N_P \phi_d(r_a)\phi_d(r_b)R(r)Y_{lm}(\theta,\phi). \tag{100}$$

We see that this wavefunction does not depend on the center of mass coordinate $\mathbf{R}$, as is also the case for the ^{4}He wavefunction.

8.2. Coordinate transformations

We can specify the molecular coordinates in terms of nucleon coordinates using a matrix notation to write

$$\begin{pmatrix} \mathbf{R} \\ \mathbf{r}_a \\ \mathbf{r}_b \\ \mathbf{r} \end{pmatrix} = \begin{pmatrix} \frac{1}{4} & \frac{1}{4} & \frac{1}{4} & \frac{1}{4} \\ -1 & 1 & 0 & 0 \\ 0 & 0 & -1 & 1 \\ -\frac{1}{2} & -\frac{1}{2} & \frac{1}{2} & \frac{1}{2} \end{pmatrix} \begin{pmatrix} \mathbf{r}_1 \\ \mathbf{r}_2 \\ \mathbf{r}_3 \\ \mathbf{r}_4 \end{pmatrix}. \tag{101}$$

This can be inverted to produce

$$\begin{pmatrix} \mathbf{r}_1 \\ \mathbf{r}_2 \\ \mathbf{r}_3 \\ \mathbf{r}_4 \end{pmatrix} = \begin{pmatrix} 1 & -\frac{1}{2} & 0 & -\frac{1}{2} \\ 1 & \frac{1}{2} & 0 & -\frac{1}{2} \\ 1 & 0 & -\frac{1}{2} & \frac{1}{2} \\ 1 & 0 & \frac{1}{2} & \frac{1}{2} \end{pmatrix} \begin{pmatrix} \mathbf{R} \\ \mathbf{r}_a \\ \mathbf{r}_b \\ \mathbf{r} \end{pmatrix}. \tag{102}$$

8.3. Absence of angular momentum in the ^{4}He wavefunction

We know that the ^{4}He wavefunction has zero angular momentum associated with $\mathbf{r}$. It is helpful to seen how this happens with the ^{4}He wavefunction is written in terms of molecular coordinates. To this end, we write

$$\begin{aligned}\Phi_S(\mathbf{r}_1,\mathbf{r}_2,\mathbf{r}_3,\mathbf{r}_4) &= N_S\, u(r_{21})u(r_{31})u(r_{41})u(r_{32})u(r_{42})u(r_{43}) \\ &= N_S\, u(r_a)u\left(\left|\mathbf{r}+\frac{\mathbf{r}_a-\mathbf{r}_b}{2}\right|\right)u\left(\left|\mathbf{r}+\frac{\mathbf{r}_a+\mathbf{r}_b}{2}\right|\right)u\left(\left|\mathbf{r}-\frac{\mathbf{r}_a+\mathbf{r}_b}{2}\right|\right)u\left(\left|\mathbf{r}+\frac{\mathbf{r}_b-\mathbf{r}_a}{2}\right|\right)u(r_b). \quad (103)\end{aligned}$$

We can verify that this has no net angular momentum by considering as an example

$$\left|\mathbf{r}+\frac{\mathbf{r}_a-\mathbf{r}_b}{2}\right|^2 = |\mathbf{r}|^2+\mathbf{r}\cdot(\mathbf{r}_a-\mathbf{r}_b)+\frac{|\mathbf{r}_a-\mathbf{r}_b|^2}{4}. \quad (104)$$

Since

$$\mathbf{r}\cdot\mathbf{r}_a = \mathbf{r}\cdot\mathbf{r}_b = 0, \quad (105)$$

we may write

$$\left|\mathbf{r}+\frac{\mathbf{r}_a-\mathbf{r}_b}{2}\right|^2 = |\mathbf{r}|^2+\frac{|\mathbf{r}_a-\mathbf{r}_b|^2}{4}. \quad (106)$$

The relative distances in this case depends only on the magnitude $|\mathbf{r}|$, which means that the ^{4}He spatial wavefunction explicitly has no angular momentum associated with $\mathbf{r}$ as expected.

8.4. Relative coordinates

It is convenient to introduce nucleon coordinates with the center of mass removed

$$\boldsymbol{\xi}_j = \mathbf{r}_j-\mathbf{R}. \quad (107)$$

Note that there are only three independent coordinates since

$$\boldsymbol{\xi}_1+\boldsymbol{\xi}_2+\boldsymbol{\xi}_3+\boldsymbol{\xi}_4 = 0. \quad (108)$$

8.5. Momentum operators in terms of molecular coordinates

To isolate the angular momentum associated with the molecular coordinates, we will need to work with momentum operators written for the molecular coordinates. As an example consider $\hat{\mathbf{p}}_1$ which can be written as

$$\hat{\mathbf{p}}_1 = -i\hbar\left(\hat{\mathbf{i}}_x\frac{\partial}{\partial x_1}+\hat{\mathbf{i}}_y\frac{\partial}{\partial y_1}+\hat{\mathbf{i}}_z\frac{\partial}{\partial z_1}\right). \quad (109)$$

The derivative in x_1 can be written in terms of molecular coordinates as

$$\begin{aligned}\frac{\partial}{\partial x_1} &= \left(\frac{\partial x_a}{\partial x_1}\right)\frac{\partial}{\partial x_a} + \left(\frac{\partial x_b}{\partial x_1}\right)\frac{\partial}{\partial x_b} + \left(\frac{\partial x}{\partial x_1}\right)\frac{\partial}{\partial x} + \left(\frac{\partial X}{\partial x_1}\right)\frac{\partial}{\partial X} \\ &= (-1)\,\frac{\partial}{\partial x_a} + (0)\,\frac{\partial}{\partial x_b} + \left(-\frac{1}{2}\right)\frac{\partial}{\partial x} + \left(\frac{1}{4}\right)\frac{\partial}{\partial X}. \end{aligned} \tag{110}$$

This can be generalized to

$$\nabla_1 = (-1)\,\nabla_a + (0)\,\nabla_b + \left(-\frac{1}{2}\right)\nabla + \left(\frac{1}{4}\right)\nabla_{\mathbf{R}}, \tag{111}$$

$$\nabla_2 = (1)\,\nabla_a + (0)\,\nabla_b + \left(-\frac{1}{2}\right)\nabla + \left(\frac{1}{4}\right)\nabla_{\mathbf{R}}, \tag{112}$$

$$\nabla_3 = (0)\,\nabla_a + (-1)\,\nabla_b + \left(\frac{1}{2}\right)\nabla + \left(\frac{1}{4}\right)\nabla_{\mathbf{R}}, \tag{113}$$

$$\nabla_4 = (0)\,\nabla_a + (1)\,\nabla_b + \left(\frac{1}{2}\right)\nabla + \left(\frac{1}{4}\right)\nabla_{\mathbf{R}} \tag{114}$$

or in matrix form as

$$\begin{pmatrix}\nabla_1\\ \nabla_2\\ \nabla_3\\ \nabla_4\end{pmatrix} = \begin{pmatrix}-1 & 0 & -\frac{1}{2} & \frac{1}{4}\\ 1 & 0 & -\frac{1}{2} & \frac{1}{4}\\ 0 & -1 & \frac{1}{2} & \frac{1}{4}\\ 0 & 1 & \frac{1}{2} & \frac{1}{4}\end{pmatrix}\begin{pmatrix}\nabla_a\\ \nabla_b\\ \nabla\\ \nabla_{\mathbf{R}}\end{pmatrix}. \tag{115}$$

We can relate the momentum operators in the same way

$$\begin{pmatrix}\hat{\mathbf{p}}_1\\ \hat{\mathbf{p}}_2\\ \hat{\mathbf{p}}_3\\ \hat{\mathbf{p}}_4\end{pmatrix} = \begin{pmatrix}-1 & 0 & -\frac{1}{2} & \frac{1}{4}\\ 1 & 0 & -\frac{1}{2} & \frac{1}{4}\\ 0 & -1 & \frac{1}{2} & \frac{1}{4}\\ 0 & 1 & \frac{1}{2} & \frac{1}{4}\end{pmatrix}\begin{pmatrix}\hat{\mathbf{p}}_a\\ \hat{\mathbf{p}}_b\\ \hat{\mathbf{p}}\\ \hat{\mathbf{P}}\end{pmatrix}. \tag{116}$$

Finally, we arrive at the relations

$$\begin{aligned}\hat{\boldsymbol{\pi}}_1 &= -\hat{\mathbf{p}}_a - \frac{1}{2}\hat{\mathbf{p}}, \qquad \hat{\boldsymbol{\pi}}_2 = \hat{\mathbf{p}}_a - \frac{1}{2}\hat{\mathbf{p}},\\ \hat{\boldsymbol{\pi}}_3 &= -\hat{\mathbf{p}}_b + \frac{1}{2}\hat{\mathbf{p}}, \qquad \hat{\boldsymbol{\pi}}_4 = \hat{\mathbf{p}}_b + \frac{1}{2}\hat{\mathbf{p}}. \end{aligned} \tag{117}$$

8.6. Discussion

The $\mathbf{a} \cdot c\mathbf{P}$ interaction is expressed in terms of individual nucleon momentum operators, but we would like to do the spatial integrals in molecular coordinates. As a result, we needed the individual momentum operators expressed in terms of molecular coordinates. Now that we have the associated definitions and relations, we can work on the spatial integrals.

9. Reduction of the Spatial Integrals

We expect that some of the matrix elements will vanish because of angular momentum selection rules or because of the symmetry of the spatial wavefunctions and operators. We also expect that many of the integrals with different numbering will end up being identical, which will allow us to obtain reduced expressions to evaluate. In this section we will focus on these issues.

9.1. Reduction of one of the central potential integrals

We begin by considering the reduction of a specific integral from the singlet case of the central potential interaction

$$\left\langle [R]_1 \left| v_C^\kappa(r_{21})(\hat{\mathbf{i}}_z \cdot \hat{\boldsymbol{\pi}}_1) \right| [R]_3 \right\rangle = \int \mathrm{d}^3\mathbf{r} \int \mathrm{d}^3\mathbf{r}_a \int \mathrm{d}^3\mathbf{r}_b \, [R]_1 v_C^\kappa(r_{21})(\hat{\mathbf{i}}_z \cdot \hat{\boldsymbol{\pi}}_1)[R]_3. \tag{118}$$

To proceed we need to make clear the dependence of the different terms on the molecular coordinates. We may write

$$[R]_1 = \Phi_{4\,\mathrm{He}}(r, r_a, r_b, \theta_{ab}), \tag{119}$$

$$[R]_3 = \frac{\mathrm{e}^{-G}}{\sqrt{R_0(\Delta R)^2}} \phi_d(r_a)\phi_d(r_b)F(r)Y_{lm}(\theta, \phi), \tag{120}$$

$$r_{21} = r_a, \tag{121}$$

$$(\hat{\mathbf{i}}_z \cdot \hat{\boldsymbol{\pi}}_1) = \hat{\mathbf{i}}_z \cdot \left(-\hat{\mathbf{p}}_a - \frac{1}{2}\hat{\mathbf{p}} \right) = i\hbar \left(\frac{\mathrm{d}}{\mathrm{d}z_a} + \frac{1}{2}\frac{\mathrm{d}}{\mathrm{d}z} \right). \tag{122}$$

We see in the last of these that there will be two different two contributions to the integral, each with different selection rules. We consider first

$$-\left\langle [R]_1 \left| v_C^\kappa(r_{21})(\hat{\mathbf{i}}_z \cdot \hat{\mathbf{p}}_a) \right| [R]_3 \right\rangle = i\hbar \frac{\mathrm{e}^{-G}}{\sqrt{R_0(\Delta R)^2}} \int \mathrm{d}^3\mathbf{r} \int \mathrm{d}^3\mathbf{r}_a \int \mathrm{d}^3\mathbf{r}_b$$

$$\Phi_{4\mathrm{He}}(r, r_a, r_b, \theta_{ab}) v_C^\kappa(r_a) \left[\frac{\mathrm{d}}{\mathrm{d}z_a}\phi_d(r_a) \right] \phi_d(r_b)F(r)Y_{lm}(\theta, \phi) = 0. \tag{123}$$

Since the integrand is odd in z_a, the integral vanishes.

In the case of the other integral, we have

$$-\frac{1}{2}\left\langle [R]_1 \left| v_C^\kappa(r_{21})(\hat{\mathbf{i}}_z \cdot \hat{\mathbf{p}}) \right| [R]_3 \right\rangle = \frac{i\hbar}{2} \frac{\mathrm{e}^{-G}}{\sqrt{R_0(\Delta R)^2}} \int \mathrm{d}^3\mathbf{r} \int \mathrm{d}^3\mathbf{r}_a \int \mathrm{d}^3\mathbf{r}_b$$

$$\Phi_{4\mathrm{He}}(r, r_a, r_b, \theta_{ab}) v_C^\kappa(r_a) \phi_d(r_a) \phi_d(r_b) \left[\frac{\mathrm{d}}{\mathrm{d}z} F(r) Y_{lm}(\theta, \phi) \right]. \tag{124}$$

This integral vanishes in general for even l (in which case the integrand is odd in z), and will be nonzero only for $l = 1$ and $m = 0$. Since there are no values of S and M_S for which this integral occurs with odd l, we conclude that the integral will vanish for all cases of interest in this calculation.

$$\left\langle [R]_1 \left| v_C^\kappa(r_{21})(\hat{\mathbf{i}}_z \cdot \hat{\boldsymbol{\pi}}_1) \right| [R]_3 \right\rangle = 0 \qquad \text{for even } S. \tag{125}$$

9.2. Interpretation in terms of angular momentum

This result can be understood intuitively in terms of angular momentum. The operator in this case can be understood as having one unit of angular momentum by virtue of the appearance of $(\hat{\mathbf{i}}_z \cdot \hat{\boldsymbol{\pi}}_1)$. Since $\hat{\boldsymbol{\pi}}$ can be decomposed into $-\hat{\mathbf{p}}_a - \hat{\mathbf{p}}/2$, we can say that this unit of angular momentum can apply either to the relative degree of freedom within the first deuteron, or the relative molecule degree of freedom. We can think of

$$v_C^\kappa(r_{21})(\hat{\mathbf{i}}_z \cdot \hat{\boldsymbol{\pi}}_1)$$

in this context as a generalized dipole operator.

The internal deuteron part of the dipole gives no contribution. In the approximation under consideration we model the deuteron using only a spherically symmetric wavefunction $\phi_d(r_a)$, so it has s-symmetry. The ground state ^{4}He wavefunction in this approximation is a four-nucleon correlated ^{1}S wavefunction which has no net angular momentum. It is not the case that there is no angular momentum present associated with the relative $\mathbf{r}_a$ degree of freedom, since the four-nucleon wavefunction is correlated. Instead, the a and b channels are correlated so that when the a channel has one unit of angular momentum (which would lead to a finite integral in $\mathbf{r}_a$), so does the b channel (producing a vanishing integral).

9.3. Selection rule for central potential contributions

We can generalize this argument into a selection rule

$$\left\langle [R]_1 \left| v_C^\kappa(r_{21})(\hat{\mathbf{i}}_z \cdot \hat{\boldsymbol{\pi}}_1) \right| [R]_3 \right\rangle \neq 0 \qquad \text{for } S = 1;\ M_S = \pm 1;\ l = 1;\ m = \mp 1. \tag{126}$$

A further generalization to the other integrals appearing in the central potential contribution to the interaction would lead us to the conclusion

$$M_C = 0 \qquad \text{for all cases except } S = 1;\ M_S = \pm 1;\ l = 1;\ m = \mp 1. \tag{127}$$

9.4. Reduction in the case of an allowed transition

This motivates us to examine the evaluation of a spatial integral under conditions where a finite result is expected. In this case, we consider

$$\left\langle [R]_1 \left| v_C^\kappa(r_{jk}) \left[(\hat{\mathbf{i}}_x \pm i\hat{\mathbf{i}}_y)\cdot\hat{\boldsymbol{\pi}}_1 \right] \right| [R]_3 \right\rangle = \int \mathrm{d}^3\mathbf{r} \int \mathrm{d}^3\mathbf{r}_a \int \mathrm{d}^3\mathbf{r}_b [R]_1 v_C^\kappa(r_{12}) \left[(\hat{\mathbf{i}}_x \pm i\hat{\mathbf{i}}_y)\cdot\hat{\boldsymbol{\pi}}_1 \right] [R]_3. \tag{128}$$

Following the arguments given above, we can immediately reduce it to

$$\left\langle [R]_1 \left| v_C^\kappa(r_{jk}) \left[(\hat{\mathbf{i}}_x \pm i\hat{\mathbf{i}}_y)\cdot\hat{\boldsymbol{\pi}}_1 \right] \right| [R]_3 \right\rangle = \frac{i\hbar}{2} \frac{\mathrm{e}^{-G}}{\sqrt{R_0(\Delta R)^2}} \int \mathrm{d}^3\mathbf{r} \int \mathrm{d}^3\mathbf{r}_a \int \mathrm{d}^3\mathbf{r}_b$$

$$\Phi_{4\mathrm{He}}(r, r_a, r_b, \theta_{ab}) v_C^\kappa(r_a)\phi_d(r_a)\phi_d(r_b) \left[\left(\frac{\mathrm{d}}{\mathrm{d}x} \pm i\frac{\mathrm{d}}{\mathrm{d}y} \right) F(r) Y_{l,\mp 1}(\theta,\phi) \right]. \tag{129}$$

We can evaluate the derivatives for $l = 1$ to obtain

$$\left(\frac{\mathrm{d}}{\mathrm{d}x} \pm i\frac{\mathrm{d}}{\mathrm{d}y} \right) F(r) Y_{1,\mp 1}(\theta,\phi) = \pm\sqrt{\frac{3}{8\pi}} \left[\frac{r^2+z^2}{r^3} + \frac{r^2-z^2}{r^2}\frac{\mathrm{d}}{\mathrm{d}r} \right] F(r). \tag{130}$$

We can use this to write the integral in terms of radial and angular integrals to give

$$\begin{aligned} \left\langle [R]_1 \left| v_C^\kappa(r_{jk}) \left[(\hat{\mathbf{i}}_x \pm i\hat{\mathbf{i}}_y)\cdot\hat{\boldsymbol{\pi}}_1 \right] \right| [R]_3 \right\rangle = {} & \frac{i\hbar}{2} \frac{\mathrm{e}^{-G}}{\sqrt{R_0(\Delta R)^2}} 16\pi^3 \int_0^\infty r^2\mathrm{d}r \int_0^\infty r_a^2\mathrm{d}r_a \int_0^\infty r_b^2\mathrm{d}r_b \\ & \int_0^\pi \sin\theta_{ab}\,\mathrm{d}\theta_{ab}\ \Phi_{4\mathrm{He}}(r, r_a, r_b, \theta_{ab}) v_C^\kappa(r_a)\phi_d(r_a)\phi_d(r_b) \\ & \int_0^\pi \sin\theta\,\mathrm{d}\theta \left[\pm\sqrt{\frac{3}{8\pi}} \left[\frac{1+\cos^2\theta}{r} + \sin^2\theta\frac{\mathrm{d}}{\mathrm{d}r} \right] F(r) \right]. \end{aligned} \tag{131}$$

We integrate over θ to obtain

$$\left\langle [R]_1 \left| v_C^\kappa(r_{jk}) \left[(\hat{\mathbf{i}}_x \pm i\hat{\mathbf{i}}_y)\cdot\hat{\boldsymbol{\pi}}_1 \right] \right| [R]_3 \right\rangle = \pm\frac{i\hbar}{2} \frac{\mathrm{e}^{-G}}{\sqrt{R_0(\Delta R)^2}} 16\pi^3 \sqrt{\frac{8}{3\pi}} \int_0^\infty r^2\mathrm{d}r \int_0^\infty r_a^2\mathrm{d}r_a \int_0^\infty r_b^2\mathrm{d}r_b$$

$$\int_0^\pi \sin\theta_{ab}\,\mathrm{d}\theta_{ab}\ \Phi_{4\mathrm{He}}(r, r_a, r_b, \theta_{ab}) v_C^\kappa(r_a)\phi_d(r_a)\phi_d(r_b) \left(\frac{1}{r} + \frac{1}{2}\frac{\mathrm{d}}{\mathrm{d}r} \right) F(r). \tag{132}$$

The four-dimensional integral that results can be done numerically easily; selected numerical results are listed in Table 4.

Table 4. Numerical values for four dimensional central potential integrals; units are MeV/fm.

Integral	Prefactor	eS	eT	oS	oT
$\left\langle [R]_1 \left\| v_C^\kappa(r_{21})(\hat{\mathbf{i}}_x \pm i\hat{\mathbf{i}}_y)\cdot\hat{\boldsymbol{\pi}}_1 \right\| [R]_3 \right\rangle$	$i\hbar e^{-G}$	1.24×10^{-3}	5.45×10^{-4}	1.36×10^{-4}	-3.12×10^{-4}
$\left\langle [R]_1 \left\| v_C^\kappa(r_{31})(\hat{\mathbf{i}}_x \pm i\hat{\mathbf{i}}_y)\cdot\hat{\boldsymbol{\pi}}_1 \right\| [R]_3 \right\rangle$	$i\hbar e^{-G}$	4.00×10^{-4}	2.43×10^{-4}	1.50×10^{-5}	-7.85×10^{-5}
$\left\langle [R]_1 \left\| v_C^\kappa(r_{41})(\hat{\mathbf{i}}_x \pm i\hat{\mathbf{i}}_y)\cdot\hat{\boldsymbol{\pi}}_1 \right\| [R]_3 \right\rangle$	$i\hbar e^{-G}$	4.00×10^{-4}	2.43×10^{-4}	1.50×10^{-5}	-7.85×10^{-5}

9.5. Checking the $l = 3$ case

It may not be obvious that a strict dipole selection rule is obeyed for this integral, so this motivates us to examine the integral for the next odd l. For $l = 3$ we may write

$$\left(\frac{\mathrm{d}}{\mathrm{d}x} \pm i\frac{\mathrm{d}}{\mathrm{d}y}\right) F(r) Y_{3,\mp1}(\theta,\phi) \;=\; \mp\frac{1}{8}\sqrt{\frac{21}{\pi}}\left[\frac{r^4+6r^2z^2-15z^4}{r^5} + \frac{r^4-6z^2r^2+5z^4}{r^4}\frac{\mathrm{d}}{\mathrm{d}r}\right]F(r). \tag{133}$$

We can use this to write for the integral

$$\begin{aligned}
&\left\langle [R]_1 \left| v_C^\kappa(r_{jk})\left[(\hat{\mathbf{i}}_x \pm i\hat{\mathbf{i}}_y)\cdot\hat{\boldsymbol{\pi}}_j\right] \right| [R]_3 \right\rangle \\
&\qquad = \;\mp\frac{i\hbar}{2}\frac{e^{-G}}{\sqrt{R_0(\Delta R)^2}} 16\pi^3 \frac{1}{8}\sqrt{\frac{21}{\pi}} \int_0^\infty r^2\mathrm{d}r \int_0^\infty r_a^2\mathrm{d}r_a \int_0^\infty r_b^2\mathrm{d}r_b \\
&\int_0^\pi \sin\theta_{ab}\,\mathrm{d}\theta_{ab}\;\Phi_{4\mathrm{He}}(r,r_a,r_b,\theta_{ab}) v_C^\kappa(r_a)\phi_d(r_a)\phi_d(r_b) \\
&\int_0^\pi \sin\theta\,\mathrm{d}\theta\left[\frac{1+6\cos^2\theta-15\cos^4\theta}{r} + (1-6\cos^2\theta+5\cos^4\theta)\frac{\mathrm{d}}{\mathrm{d}r}\right]F(r).
\end{aligned} \tag{134}$$

We evaluate the θ integral to obtain

$$\left\langle [R]_1 \left| v_C^\kappa(r_{jk})\left[(\hat{\mathbf{i}}_x \pm i\hat{\mathbf{i}}_y)\cdot\hat{\boldsymbol{\pi}}_j\right] \right| [R]_3 \right\rangle \;=\; 0. \tag{135}$$

This supports the notion that a dipole selection rule is appropriate for the integral under discussion.

9.6. Symmetry in the spatial integrals

In the numerical results of Table 4 we see that the same numerical values show up for different cases, which motivates us to examine this issue further in the hope that we can simplify things. In general we find that for integrals involving the spatial function $[R]_3$ we get the same magnitude when the two nucleons are in different deuterons (which would occur for the r_{31}, r_{41}, r_{32} and r_{42} cases). If the two nucleons are in the same deuteron (the r_{21} and r_{43} cases) the magnitude is again the same.

We expect a sign difference when $\hat{\boldsymbol{\pi}}_1$ and $\hat{\boldsymbol{\pi}}_2$ appear in the integrand for an $[R]_3$ integral as compared with when $\hat{\boldsymbol{\pi}}_3$ and $\hat{\boldsymbol{\pi}}_4$ show up. This is because of the different dependence on $\hat{\mathbf{p}}$ that appears in Eq. (117). In the case of integrals with $[R]_4$ and $[R]_5$, the nucleons which are in the same deuteron change. We again would expect the the integral to have the same magnitude for the two cases (nucleons in the same deuteron, or in different deuterons).

9.7. Separation of spatial integrals

It will be convenient to take advantage of the separation

$$\left\langle [R]_1 \left| \left[(\hat{\mathbf{i}}_x \pm i\hat{\mathbf{i}}_y)\cdot\hat{\boldsymbol{\pi}}_j \right] v_C^\kappa(r_{jk}) \right| [R]_\iota \right\rangle = \left\langle [R]_1 \left| \left\{ \left[(\hat{\mathbf{i}}_x \pm i\hat{\mathbf{i}}_y)\cdot\hat{\boldsymbol{\pi}}_j \right] v_C^\kappa(r_{jk}) \right\} \right| [R]_\iota \right\rangle + \left\langle [R]_1 \left| v_C^\kappa(r_{jk}) \left[(\hat{\mathbf{i}}_x \pm i\hat{\mathbf{i}}_y)\cdot\hat{\boldsymbol{\pi}}_j \right] \right| [R]_\iota \right\rangle. \tag{136}$$

We see that the second integral that appears on the RHS is of the same form as we have been considering above. This suggests that it should be possible to write for the overall expression

$$\begin{aligned} M_C^{(1,\pm1)} = \frac{P}{2M}\frac{1}{(2m_{\rm av}c^2)} \sum_{j<k}\sum_\kappa\sum_\iota \Bigg\{ & [a_C^\kappa(jk;\iota) + c_C^\kappa(jk;\iota)] \left\langle [R]_1 \left| v_C^\kappa(r_{jk}) \left[(\hat{\mathbf{i}}_x \pm i\hat{\mathbf{i}}_y)\cdot\hat{\boldsymbol{\pi}}_j \right] \right| [R]_\iota \right\rangle \\ & + [b_C^\kappa(jk;\iota) + d_C^\kappa(jk;\iota)] \left\langle [R]_1 \left| \hat{v}_C(r_{jk}) \left[(\hat{\mathbf{i}}_x \pm i\hat{\mathbf{i}}_y)\cdot\hat{\boldsymbol{\pi}}_k \right] \right| [R]_\iota \right\rangle \\ & + c_C^\kappa(jk;\iota) \left\langle [R]_1 \left| \left[\left((\hat{\mathbf{i}}_x \pm i\hat{\mathbf{i}}_y)\cdot\hat{\boldsymbol{\pi}}_j \right) v_C^\kappa(r_{jk}) \right] \right| [R]_\iota \right\rangle \\ & + d_C^\kappa(jk;\iota) \left\langle [R]_1 \left| \left[\left((\hat{\mathbf{i}}_x \pm i\hat{\mathbf{i}}_y)\cdot\hat{\boldsymbol{\pi}}_k \right) \hat{v}_C(r_{jk}) \right] \right| [R]_\iota \right\rangle \Bigg\} \end{aligned} \tag{137}$$

and then simplify it to

$$\begin{aligned} M_C^{(1,\pm1)} = \frac{P}{2M}\frac{1}{(2m_{\rm av}c^2)} \sum_\kappa \Bigg\{ & A_C^\kappa \left\langle [R]_1 \left| v_C^\kappa(r_{21}) \left[(\hat{\mathbf{i}}_x \pm i\hat{\mathbf{i}}_y)\cdot\hat{\boldsymbol{\pi}}_1 \right] \right| [R]_3 \right\rangle \\ & + B_C^\kappa \left\langle [R]_1 \left| \hat{v}_C(r_{31}) \left[(\hat{\mathbf{i}}_x \pm i\hat{\mathbf{i}}_y)\cdot\hat{\boldsymbol{\pi}}_1 \right] \right| [R]_3 \right\rangle \\ & C_C^\kappa \left\langle [R]_1 \left| \left[\left((\hat{\mathbf{i}}_x \pm i\hat{\mathbf{i}}_y)\cdot\hat{\boldsymbol{\pi}}_1 \right) v_C^\kappa(r_{21}) \right] \right| [R]_3 \right\rangle \\ & + D_C^\kappa \left\langle [R]_1 \left| \left[\left((\hat{\mathbf{i}}_x \pm i\hat{\mathbf{i}}_y)\cdot\hat{\boldsymbol{\pi}}_1 \right) \hat{v}_C(r_{31}) \right] \right| [R]_3 \right\rangle \Bigg\}. \end{aligned} \tag{138}$$

Written in this form, we see that the matrix element is made up of 16 individual terms.

9.8. Expressions for the expansion coefficients

To proceed, we require expressions for the expansion coefficients. It seems reasonably clear how to identify the same deuteron and different deuteron cases when dealing with integrals involving $[R]_4$ and $[R]_5$; for example we may write

$$\left\langle [R]_1 \left| v_C^\kappa(r_{21}) \left[(\hat{\mathbf{i}}_x \pm i\hat{\mathbf{i}}_y) \cdot \hat{\boldsymbol{\pi}}_1 \right] \right| [R]_4 \right\rangle = \left\langle [R]_1 \left| v_C^\kappa(r_{31}) \left[(\hat{\mathbf{i}}_x \pm i\hat{\mathbf{i}}_y) \cdot \hat{\boldsymbol{\pi}}_1 \right] \right| [R]_3 \right\rangle, \tag{139}$$

since r_{21} involves nucleons in different deuterons for the spatial wavefunction $[R]_4 = R(13;24)$. A more subtle case is

$$\begin{aligned} \left\langle [R]_1 \left| v_C^\kappa(r_{21}) \left[(\hat{\mathbf{i}}_x \pm i\hat{\mathbf{i}}_y) \cdot \hat{\boldsymbol{\pi}}_2 \right] \right| [R]_4 \right\rangle &= \left\langle [R]_1 \left| v_C^\kappa(r_{31}) \left[(\hat{\mathbf{i}}_x \pm i\hat{\mathbf{i}}_y) \cdot \hat{\boldsymbol{\pi}}_3 \right] \right| [R]_3 \right\rangle \\ &= -\left\langle [R]_1 \left| v_C^\kappa(r_{31}) \left[(\hat{\mathbf{i}}_x \pm i\hat{\mathbf{i}}_y) \cdot \hat{\boldsymbol{\pi}}_1 \right] \right| [R]_3 \right\rangle. \end{aligned} \tag{140}$$

The idea here is that we first renumber the nucleons in order to change $[R]_4$ into $[R]_3$, and then note that a sign change occurs for the $\hat{\mathbf{p}}$ part of $\hat{\boldsymbol{\pi}}_3$ and $\hat{\boldsymbol{\pi}}_1$.

We can use the arguments given above to develop explicit expressions for the expansion coefficients. We may write

$$\begin{aligned} A_C^\kappa = {} & a_C(12;3) - a_C(34;3) - b_C(12;3) + b_C(34;3) \\ & + a_C(13;4) - a_C(24;4) - b_C(13;4) + b_C(24;4) \\ & + a_C(14;5) - a_C(23;5) - b_C(14;5) + b_C(23;5) \\ & + c_C(12;3) - c_C(34;3) - d_C(12;3) + d_C(34;3) \\ & + c_C(13;4) - c_C(24;4) - d_C(13;4) + d_C(24;4) \\ & + c_C(14;5) - c_C(23;5) - d_C(14;5) + d_C(23;5), \end{aligned} \tag{141}$$

$$\begin{aligned} B_C^\kappa = {} & a_C(13;3) + a_C(14;3) + a_C(23;3) + a_C(24;3) \\ & - b_C(13;3) - b_C(14;3) - b_C(23;3) - b_C(24;3) \\ & + a_C(12;4) + a_C(14;4) + a_C(32;4) + a_C(34;4) \\ & - b_C(12;4) - b_C(14;4) - b_C(32;4) - b_C(34;4) \\ & + a_C(12;5) + a_C(13;5) + a_C(42;5) + a_C(43;5) \\ & - b_C(12;5) - b_C(13;5) - b_C(42;5) - b_C(43;5) \\ & c_C(13;3) + c_C(14;3) + c_C(23;3) + c_C(24;3) \\ & - d_C(13;3) - d_C(14;3) - d_C(23;3) - d_C(24;3) \\ & + c_C(12;4) + c_C(14;4) + c_C(32;4) + c_C(34;4) \\ & - d_C(12;4) - d_C(14;4) - d_C(32;4) - d_C(34;4) \\ & + c_C(12;5) + c_C(13;5) + c_C(42;5) + c_C(43;5) \\ & - d_C(12;5) - d_C(13;5) - d_C(42;5) - d_C(43;5), \end{aligned} \tag{142}$$

$$C_C^\kappa = c_C(12;3) - c_C(34;3) + c_C(13;4) - c_C(24;4) + c_C(14;5) - c_C(23;5), \tag{143}$$

$$\begin{aligned} D_C^\kappa &= d_C(13;3) + d_C(14;3) + d_C(23;3) + d_C(24;3) \\ &\quad d_C(12;4) + d_C(14;4) + d_C(32;4) + d_C(34;4) \\ &\quad d_C(12;5) + d_C(13;5) + d_C(42;5) + d_C(43;5). \end{aligned} \tag{144}$$

We draw attention to the ordering of the first two indices in these expressions, since the sign depends on the order.

9.9. Discussion

When we first carried out the reduction of the spin and isospin parts of the matrix elements, we ended up with a very large number of terms. Here we have recognized that many of the associated spatial integrals are zero (on account of angular momentum selection rules), and that the ones that are left are in many cases numerically identical. This allowed us to combine together all the terms that are the same, leading to a dramatic simplification of the overall calculation.

10. Evaluation of the Interaction Matrix Element

We can use the approach outlined above to carry out a systematic evaluation of the interaction matrix element. For each of the interactions, we need to first determine which terms are non-zero, evaluate the associated expansion coefficients, evaluate the associated spatial integrals, and then sum the results.

10.1. Central potential contribution for $l = 1$

In the case of the central potential we may write

$$M_C^{(1,\pm1)} = (cP)\left[\mathrm{e}^{-G}\sqrt{\frac{R_0}{\langle R\rangle}\frac{(\Delta R)^2}{\langle(\Delta R)^2\rangle}}\right]_{l=1}\sum_\kappa A_C^\kappa I_C^\kappa + B_C^\kappa J_C^\kappa + C_C^\kappa K_C^\kappa + D_C^\kappa L_C^\kappa. \tag{145}$$

Results for the expansion coefficients from Mathematica are presented in Table 5. For the spatial integrals $I_C^\kappa(l,m), \cdots$ we may write

$$\begin{aligned} I_C^\kappa(1,\mp1) &= \frac{1}{2Mc}\frac{1}{(2m_{\rm av}c^2)}\left\langle [R]_1\left|v_C^\kappa(r_{21})\left[(\hat{\mathbf{i}}_x \pm \hat{\mathbf{i}}_y)\cdot\hat{\boldsymbol{\pi}}_1\right]\right|\phi_d(r_{21})\phi_d(r_{43})\frac{F(r)}{\sqrt{R_0(\Delta R)^2}}Y_{1,\mp1}(\theta,\phi)\right\rangle \\ &= \pm\,\mathrm{Const}\int_0^\infty r^2\mathrm{d}r\int \mathrm{d}^3\mathbf{r}_a\int \mathrm{d}^3\mathbf{r}_b\ \Phi_{4\mathrm{He}}(r,r_a,r_b,\theta_{ab})\phi_d(r_a)\phi_d(r_b)v_C^\kappa(r_a)\sqrt{\frac{8\pi}{3}}\left[\frac{2}{r}+\frac{\mathrm{d}}{\mathrm{d}r}\right]F(r), \end{aligned} \tag{146}$$

$$\begin{aligned} J_C^\kappa(1,\mp1) &= \frac{1}{2Mc}\frac{1}{(2m_{\rm av}c^2)}\left\langle [R]_1\left|v_C^\kappa(r_{31})\left[(\hat{\mathbf{i}}_x \pm i\hat{\mathbf{i}}_y)\cdot\hat{\boldsymbol{\pi}}_1\right]\right|\phi_d(r_{21})\phi_d(r_{43})\frac{F(r)}{\sqrt{R_0(\Delta R)^2}}Y_{1,\mp1}(\theta,\phi)\right\rangle \\ &= \pm\,\mathrm{Const}\int_0^\infty r^2\mathrm{d}r\int \mathrm{d}^3\mathbf{r}_a\int \mathrm{d}^3\mathbf{r}_b\ \Phi_{4\mathrm{He}}(r,r_a,r_b,\theta_{ab})\phi_d(r_a)\phi_d(r_b)v_C^\kappa(r_{31})\sqrt{\frac{8\pi}{3}}\left[\frac{2}{r}+\frac{\mathrm{d}}{\mathrm{d}r}\right]F(r), \end{aligned} \tag{147}$$

$$\begin{aligned} K_C^\kappa(1,\mp1) &= \frac{1}{2Mc}\frac{1}{(2m_{\rm av}c^2)}\left\langle [R]_1\left|\left\{(\hat{\mathbf{i}}_x \pm i\hat{\mathbf{i}}_y)\cdot\hat{\boldsymbol{\pi}}_1 v_C^\kappa(r_{21})\right\}\right|\phi_d(r_{21})\phi_d(r_{43})\frac{F(r)}{\sqrt{R_0(\Delta R)^2}}Y_{1,\mp1}(\theta,\phi)\right\rangle \\ &= 0, \end{aligned} \tag{148}$$

Table 5. Expansion coefficients for the central potential contribution to the interaction matrix element for $S = 1$ and $M_S = \pm 1$.

Coefficient	eS	eT	oS	oT
A_C^κ	$-\frac{1}{16\sqrt{2}}$	$-\frac{23}{16\sqrt{2}}$	$\frac{69}{16\sqrt{2}}$	$\frac{1}{48\sqrt{2}}$
B_C^κ	0	$-\frac{13}{8\sqrt{2}}$	0	$\frac{35}{24\sqrt{2}}$
C_C^κ	$\frac{1}{16\sqrt{2}}$	$\frac{23}{16\sqrt{2}}$	$-\frac{69}{16\sqrt{2}}$	$-\frac{1}{48\sqrt{2}}$
D_C^κ	0	$\frac{13}{8\sqrt{2}}$	0	$-\frac{35}{24\sqrt{2}}$

$$L_C^\kappa(1,\mp 1) = \frac{1}{2Mc}\frac{1}{(2m_{\rm av}c^2)}\left\langle [R]_1 \left| \left\{ (\hat{\mathbf{i}}_x \pm i\hat{\mathbf{i}}_y)\cdot \hat{\boldsymbol{\pi}}_1 v_C^\kappa(r_{31}) \right\} \right| \phi_d(r_{21})\phi_d(r_{43}) \frac{F(r)}{\sqrt{R_0(\Delta R)^2}} Y_{1,\mp 1}(\theta,\phi) \right\rangle$$
$$= \pm \text{Const} \int_0^\infty r^2 \mathrm{d}r \int \mathrm{d}^3\mathbf{r}_a \int \mathrm{d}^3\mathbf{r}_b \; \Phi_{4\text{He}}(r, r_a, r_b, \theta_{ab})\phi_d(r_a)\phi_d(r_b)F(r)\sqrt{\frac{8\pi}{3}}\frac{r}{r_{31}}\frac{\mathrm{d}}{\mathrm{d}r_{31}}v_C^\kappa(r_{31}), \quad (149)$$

where

$$\text{Const} = \frac{i\hbar}{2}\frac{1}{2Mc}\frac{1}{(2m_{\rm av}c^2)}\frac{1}{\sqrt{R_0(\Delta R)^2}}. \quad (150)$$

We can use the results for the expansion coefficients along with the numerical results for the spatial integrals in Table 6 to obtain

Table 6. Dimensionless spatial integrals for the central potential contribution to the interaction matrix element for the case $S = 1$, $M_S = 1$, $l = 1$, $m = -1$; the integrals for the other case with $M_S = -1$ and $m = 1$ differ only in sign.

Integral	eS	eT	oS	oT
I_C^κ	$i\ 3.48 \times 10^{-8}$	$i\ 1.53 \times 10^{-8}$	$i\ 3.81 \times 10^{-9}$	$-i\ 8.75 \times 10^{-9}$
J_C^κ	$i\ 1.12 \times 10^{-8}$	$i\ 6.80 \times 10^{-9}$	$i\ 4.20 \times 10^{-10}$	$-i\ 2.20 \times 10^{-9}$
K_C^κ	0	0	0	0
L_C^κ	$-i\ 8.81 \times 10^{-9}$	$-i\ 4.53 \times 10^{-9}$	$-i\ 1.34 \times 10^{-11}$	$i\ 2.63 \times 10^{-9}$

$$M_C^{(S,M_S)} = \left[e^{-G\sqrt{\frac{R_0}{\langle R\rangle}\frac{(\Delta R)^2}{\langle(\Delta R)^2\rangle}}} \right]_{l=1} \times \begin{cases} i(cP)\,2.35\times10^{-8} & S=1,\ M_S=-1,\ l=1,\ m=\ 1 \\ 0 & S=1,\ M_S=\ 0,\ l=1,\ m=\ 0 \\ -i(cP)\,2.35\times10^{-8} & S=1,\ M_S=\ 1,\ l=1,\ m=-1 \end{cases} \quad (151)$$

10.2. Tensor potential contribution for $l = 1$

In the case of the tensor potential we may write

$$M_T^{(1,\pm1)} = (cP)\left[e^{-G\sqrt{\frac{R_0}{\langle R\rangle}\frac{(\Delta R)^2}{\langle(\Delta R)^2\rangle}}} \right]_{l=1} \sum_\kappa A_T^\kappa I_T^\kappa + B_T^\kappa J_T^\kappa + C_T^\kappa K_T^\kappa + D_T^\kappa L_T^\kappa + \tilde{A}_T^\kappa \tilde{I}_T^\kappa + \tilde{B}_T^\kappa \tilde{J}_T^\kappa + \tilde{C}_T^\kappa \tilde{K}_T^\kappa + \tilde{D}_T^\kappa \tilde{L}_T^\kappa. \quad (152)$$

The expansion coefficients A_T through D_T can be related to the expansion coefficients of the central potential case

$$A_T^\kappa = -A_C^\kappa, \qquad B_T^\kappa = -B_C^\kappa, \qquad C_T^\kappa = -C_C^\kappa, \qquad D_T^\kappa = -D_C^\kappa. \quad (153)$$

We have used Mathematica to sum contributions for the other coefficients; the results are tabulated in Table 7.

Table 7. Expansion coefficients for the tensor potential contribution to the interaction matrix element for $S = 1$ and $M_S = \pm1$.

Coefficient	eS	eT	oS	oT
$\tilde{A}_C^\kappa$	$-\frac{1}{16\sqrt{2}}$	$-\frac{69}{16\sqrt{2}}$	$\frac{69}{16\sqrt{2}}$	$\frac{1}{16\sqrt{2}}$
$\tilde{B}_C^\kappa$	0	$-\frac{45}{4\sqrt{2}}$	0	$\frac{51}{4\sqrt{2}}$
$\tilde{C}_C^\kappa$	$\frac{1}{16\sqrt{2}}$	$\frac{69}{16\sqrt{2}}$	$-\frac{69}{16\sqrt{2}}$	$-\frac{1}{16\sqrt{2}}$
$\tilde{D}_C^\kappa$	0	$-\frac{15}{4\sqrt{2}}$	0	$-\frac{17}{4\sqrt{2}}$

The spatial integrals $I_T^\kappa, \cdots L_T^\kappa$ have a form very similar to that of the central potential integrals; for example, we may write

$$I_T^\kappa(1,\mp1) = \frac{1}{2Mc}\frac{1}{(2m_{\rm av}c^2)}\left\langle [R]_1 \left| v_T^\kappa(r_{21}) \left[(\hat{\mathbf{i}}_x \pm \hat{\mathbf{i}}_y)\cdot\hat{\boldsymbol{\pi}}_1 \right] \right| \phi_d(r_{21})\phi_d(r_{43}) \frac{F(r)}{\sqrt{R_0(\Delta R)^2}} Y_{1,\mp1}(\theta,\phi) \right\rangle$$
$$= \pm \text{Const} \int_0^\infty r^2 dr \int d^3\mathbf{r}_a \int d^3\mathbf{r}_b\ \Phi_{4\rm He}(r, r_a, r_b, \theta_{ab})\phi_d(r_a)\phi_d(r_b) v_T^\kappa(r_a) \sqrt{\frac{8\pi}{3}} \left[\frac{2}{r} + \frac{d}{dr} \right] F(r) \quad (154)$$

with analogous modifications of the other cases. Results for the four-dimensional numerical integrations are given in Table 8.

Table 8. Dimensionless spatial integrals for the tensor potential contribution to the interaction matrix element for $S = 1$, $M_S = 1$, $l = 1$ and $m = -1$; the matrix elements for the other case with $M_S = -1$ and $m = 1$ differ only by a sign.

Integral	eS	eT	oS	oT
I_T^κ	$i\ 3.66 \times 10^{-8}$	$i\ 2.94 \times 10^{-8}$	$i\ 3.66 \times 10^{-8}$	$i\ 1.88 \times 10^{-8}$
J_T^κ	$i\ 1.57 \times 10^{-8}$	$i\ 1.39 \times 10^{-8}$	$i\ 1.57 \times 10^{-8}$	$i\ 1.10 \times 10^{-8}$
K_T^κ	0	0	0	0
L_T^κ	$-i\ 1.06 \times 10^{-8}$	$-i\ 8.84 \times 10^{-9}$	$-i\ 1.06 \times 10^{-8}$	$-i\ 6.20 \times 10^{-9}$

The other spatial integrals can be written as

$$\begin{aligned}\tilde{I}_T^\kappa(1,\mp1) &= \frac{1}{2Mc}\frac{1}{(2m_{\rm av}c^2)}\left\langle [R]_1\left|\frac{z_{21}^2}{r_{21}^2}v_T^\kappa(r_{21})\left[(\hat{\mathbf{i}}_x \pm \hat{\mathbf{i}}_y)\cdot\hat{\boldsymbol{\pi}}_1\right]\right|\phi_d(r_{21})\phi_d(r_{43})\frac{F(r)}{\sqrt{R_0(\Delta R)^2}}Y_{1,\mp1}(\theta,\phi)\right\rangle \\ &= \pm\,\text{Const}\int_0^\infty r^2{\rm d}r\int {\rm d}^3\mathbf{r}_a\int {\rm d}^3\mathbf{r}_b\ \Phi_{\rm 4He}(r,r_a,r_b,\theta_{ab})\phi_d(r_a)\phi_d(r_b)\frac{z_{21}^2}{r_{21}^2}v_T^\kappa(r_a)\sqrt{\frac{8\pi}{3}}\left[\frac{2}{r}+\frac{\rm d}{{\rm d}r}\right]F(r), \quad (155)\end{aligned}$$

$$\begin{aligned}\tilde{J}_T^\kappa(1,\mp1) &= \frac{1}{2Mc}\frac{1}{(2m_{\rm av}c^2)}\left\langle [R]_1\left|\frac{z_{31}^2}{r_{31}^2}v_T^\kappa(r_{31})\left[(\hat{\mathbf{i}}_x \pm \hat{\mathbf{i}}_y)\cdot\hat{\boldsymbol{\pi}}_1\right]\right|\phi_d(r_{21})\phi_d(r_{43})\frac{F(r)}{\sqrt{R_0(\Delta R)^2}}Y_{1,\mp1}(\theta,\phi)\right\rangle \\ &= \pm\,\text{Const}\int_0^\infty r^2{\rm d}r\int {\rm d}^3\mathbf{r}_a\int {\rm d}^3\mathbf{r}_b\ \Phi_{\rm 4He}(r,r_a,r_b,\theta_{ab})\phi_d(r_a)\phi_d(r_b)v_T^\kappa(r_{31}) \\ &\quad \sqrt{\frac{8\pi}{3}}\left[\left(\frac{4}{5}\frac{r}{r_{31}^2}+\frac{1}{2}\frac{z_{ab}^2}{rr_{31}^2}\right)+\left(\frac{1}{5}\frac{r^2}{r_{31}^2}+\frac{1}{4}\frac{z_{ab}^2}{r_{31}^2}\right)\frac{\rm d}{{\rm d}r}\right]F(r), \quad (156)\end{aligned}$$

$$\begin{aligned}\tilde{K}_T^\kappa(1,\mp1) &= \frac{1}{2Mc}\frac{1}{(2m_{\rm av}c^2)}\left\langle [R]_1\left|\left[(\hat{\mathbf{i}}_x \pm i\hat{\mathbf{i}}_y)\cdot\hat{\boldsymbol{\pi}}_1 v_T^\kappa(r_a)\frac{z_a^2}{r_a^2}\right]\right|\phi_d(r_a)\phi_d(r_b)\frac{F(r)}{\sqrt{R_0(\Delta R)^2}}Y_{1,\mp1}(\theta,\phi)\right\rangle \\ &= 0, \quad (157)\end{aligned}$$

$$\begin{aligned}\tilde{L}_T^\kappa(1,\mp1) &= \frac{1}{2Mc}\frac{1}{(2m_{\rm av}c^2)}\left\langle [R]_1\left|\left[(\hat{\mathbf{i}}_x \pm i\hat{\mathbf{i}}_y)\cdot\hat{\boldsymbol{\pi}}_1 v_T^\kappa(r_{31})\frac{z_{31}^2}{r_{31}^2}\right]\right|\phi_d(r_{21})\phi_d(r_{43})\frac{F(r)}{\sqrt{R_0(\Delta R)^2}}Y_{1,\mp1}(\theta,\phi)\right\rangle \\ &= \pm\,\text{Const}\int_0^\infty r^2{\rm d}r\int {\rm d}^3\mathbf{r}_a\int {\rm d}^3\mathbf{r}_b\ \Phi_{\rm 4He}(r,r_a,r_b,\theta_{ab})\phi_d(r_a)\phi_d(r_b)F(r) \\ &\quad \sqrt{\frac{8\pi}{3}}\left[\left(-\frac{2}{5}\frac{r^3}{r_{31}^4}-\frac{1}{2}\frac{rz_{ab}^2}{r_{31}^4}\right)+\left(\frac{1}{5}\frac{r^3}{r_{31}^3}+\frac{1}{4}\frac{rz_{ab}^2}{r_{31}^3}\right)\frac{\rm d}{{\rm d}r_{31}}\right]v_T^\kappa(r_{31}). \quad (158)\end{aligned}$$

These results (see Table 9) allow us to write

Table 9. Dimensionless spatial integrals for the tensor potential contribution to the interaction matrix element for $S = 1$, $M_S = 1$, $l = 1$ and $m = -1$; the matrix elements for the other case with $M_S = -1$ and $m = 1$ differ only by a sign.

Integral	eS	eT	oS	oT
$\tilde{I}_T^\kappa$	$i\ 1.17 \times 10^{-8}$	$i\ 9.42 \times 10^{-9}$	$i\ 1.17 \times 10^{-8}$	$i\ 6.01 \times 10^{-9}$
$\tilde{J}_T^\kappa$	$i\ 4.87 \times 10^{-9}$	$i\ 4.30 \times 10^{-9}$	$i\ 4.87 \times 10^{-9}$	$i\ 3.42 \times 10^{-9}$
$\tilde{K}_T^\kappa$	0	0	0	0
$\tilde{L}_T^\kappa$	$-i\ 3.75 \times 10^{-9}$	$-i\ 3.20 \times 10^{-9}$	$-i\ 3.75 \times 10^{-9}$	$-i\ 2.36 \times 10^{-9}$

$$M_T^{(S,M_S)} = \left[e^{-G\sqrt{\frac{R_0}{\langle R\rangle}\frac{(\Delta R)^2}{\langle(\Delta R)^2\rangle}}} \right]_{l=1} \times \begin{cases} -i(cP)\ 7.38 \times 10^{-8} & S=1,\ M_S=-1,\ l=1,\ m=\ 1 \\ 0 & S=1,\ M_S=\ 0,\ l=1,\ m=\ 0 \\ i(cP)\ 7.38 \times 10^{-8} & S=1,\ M_S=\ 1,\ l=1,\ m=-1 \end{cases} \tag{159}$$

10.3. Tensor potential contribution for $l = 3$

There is no contribution from the central potential interaction for the $l = 3$ case as discussed above. There is a contribution from the tensor potential, and we may write in this case

$$M_T^{(3,\pm1)} = (cP) \left[e^{-G\sqrt{\frac{R_0}{\langle R\rangle}\frac{(\Delta R)^2}{\langle(\Delta R)^2\rangle}}} \right]_{l=3} \sum_\kappa \tilde{A}_T^\kappa \tilde{I}_T^\kappa + \tilde{B}_T^\kappa \tilde{J}_T^\kappa + \tilde{C}_T^\kappa \tilde{K}_T^\kappa + \tilde{D}_T^\kappa \tilde{L}_T^\kappa, \tag{160}$$

The expansion coefficients are the same as above (see Table 7). The spatial integrals are

$$\tilde{I}_T^\kappa(1,\mp1) = \frac{1}{2Mc}\frac{1}{(2m_{\rm av}c^2)} \left\langle [R]_1 \left| \frac{z_{21}^2}{r_{21}^2} v_T^\kappa(r_{21}) \left[(\hat{\mathbf{i}}_x \pm \hat{\mathbf{i}}_y)\cdot\hat{\boldsymbol{\pi}}_1 \right] \right| \phi_d(r_{21})\phi_d(r_{43}) \frac{F(r)}{\sqrt{R_0(\Delta R)^2}} Y_{3,\mp1}(\theta,\phi) \right\rangle = 0, \tag{161}$$

$$\begin{aligned} \tilde{J}_T^\kappa(1,\mp1) &= \frac{1}{2Mc}\frac{1}{(2m_{\rm av}c^2)} \left\langle [R]_1 \left| \frac{z_{31}^2}{r_{31}^2} v_T^\kappa(r_{31}) \left[(\hat{\mathbf{i}}_x \pm \hat{\mathbf{i}}_y)\cdot\hat{\boldsymbol{\pi}}_1 \right] \right| \phi_d(r_{21})\phi_d(r_{43}) \frac{F(r)}{\sqrt{R_0(\Delta R)^2}} Y_{3,\mp1}(\theta,\phi) \right\rangle \\ &= \pm \text{Const} \int_0^\infty r^2 dr \int d^3\mathbf{r}_a \int d^3\mathbf{r}_b\ \Phi_{4\rm He}(r, r_a, r_b, \theta_{ab})\phi_d(r_a)\phi_d(r_b) v_T^\kappa(r_{31}) \\ &\quad \frac{8\sqrt{21\pi}}{105}\left(4\frac{r}{r_{31}^2} + \frac{r^2}{r_{31}^2}\frac{d}{dr} \right) F(r), \end{aligned} \tag{162}$$

$$\tilde{K}_T^\kappa(1,\mp1) = \frac{1}{2Mc}\frac{1}{(2m_{\rm av}c^2)} \left\langle [R]_1 \left| \left[(\hat{\mathbf{i}}_x \pm i\hat{\mathbf{i}}_y)\cdot\hat{\boldsymbol{\pi}}_1 v_T^\kappa(r_a) \frac{z_a^2}{r_a^2} \right] \right| \phi_d(r_a)\phi_d(r_b) \frac{F(r)}{\sqrt{R_0(\Delta R)^2}} Y_{3,\mp1}(\theta,\phi) \right\rangle = 0, \tag{163}$$

$$\tilde{L}_T^{\kappa}(1,\mp 1) = \frac{1}{2Mc}\frac{1}{(2m_{\rm av}c^2)}\left\langle [R]_1 \left| \left[(\hat{\mathbf{i}}_x \pm i\hat{\mathbf{i}}_y)\cdot\hat{\boldsymbol{\pi}}_1 v_T^{\kappa}(r_{31})\frac{z_{31}^2}{r_{31}^2}\right] \right| \phi_d(r_{21})\phi_d(r_{43})\frac{F(r)}{\sqrt{R_0(\Delta R)^2}}Y_{3,\mp 1}(\theta,\phi)\right\rangle$$
$$= \pm \text{Const}\int_0^{\infty} r^2 \mathrm{d}r \int \mathrm{d}^3\mathbf{r}_a \int \mathrm{d}^3\mathbf{r}_b\ \Phi_{4\rm He}(r,r_a,r_b,\theta_{ab})\phi_d(r_a)\phi_d(r_b)F(r)$$
$$\frac{8\sqrt{21\pi}}{105}\left(-\frac{r^3}{r_{31}^4} + \frac{r^3}{r_{31}^3}\frac{\mathrm{d}}{\mathrm{d}r_{31}}\right) v_T^{\kappa}(r_{31}). \tag{164}$$

Numerical results are presented in Table 10. We can use these results to write

$$M_T^{(S,M_S)} = \left[\mathrm{e}^{-G\sqrt{\frac{R_0}{\langle R\rangle}\frac{(\Delta R)^2}{\langle(\Delta R)^2\rangle}}}\right]_{l=3}$$
$$\times \begin{cases} i(cP)\ 1.45\times 10^{-9} & S=1,\ M_S=-1,\ l=3,\ m=\ 1 \\ 0 & S=1,\ M_S=\ 0,\ l=3,\ m=\ 0 \\ -i(cP)\ 1.45\times 10^{-9} & S=1,\ M_S=\ 1,\ l=3,\ m=-1 \end{cases} \tag{165}$$

11. Summary and discussion

We have computed central and tensor interaction contributions to the phonon exchange matrix elements for $D_2/^4$He transitions based on the new $\mathbf{a}\cdot c\mathbf{P}$ coupling between vibrations and internal nuclear degrees of freedom described in [12], using simplified nuclear models in connection with the Hamada–Johnston nucleon–nucleon potential. We find nonzero coupling to the molecular ^{3}P and ^{3}F states, with the largest interaction in the case of ^{3}P; the interaction Hamiltonian for both the central and tensor interactions together in this model for z-directed motion and/or vector potential is

$$\hat{H}_{\rm int} = i\ 5.03\times 10^{-8}\left(c\hat{P}_z - Ze\hat{A}_z\right)\left[\mathrm{e}^{-G\sqrt{\frac{R_0}{\langle R\rangle}\frac{(\Delta R)^2}{\langle(\Delta R)^2\rangle}}}\right]_{l=1}$$
$$\left\{ \left|\Psi[^4\text{He}]\right\rangle\left\langle\Psi[\text{D}_2\ ^3\text{P}(M_S=1,m=-1)]\right| - \left|\Psi[^4\text{He}]\right\rangle\left\langle\Psi[\text{D}_2\ ^3\text{P}(M_S=-1,m=1)]\right|\right\} + \text{Hc.}, \tag{166}$$

where "Hc." indicates the Hermitian conjugate, for z-directed vibrations. We have augmented the center of mass momentum from the text with the vector potential following the discussion of Section 5. The coupling in the case of the molecular ^{3}F states is more

Table 10. Dimensionless spatial integrals for the tensor potential contribution to the interaction matrix element for $S=1$, $M_S=1$, $l=3$ and $m=-1$; the matrix elements for the other case with $M_S=-1$ and $m=1$ differ only by a sign.

Integral	eS	eT	oS	oT
$\tilde{I}_T^{\kappa}$	0	0	0	0
$\tilde{J}_T^{\kappa}$	$i\ 3.08\times 10^{-9}$	$i\ 2.73\times 10^{-9}$	$i\ 3.08\times 10^{-9}$	$i\ 2.19\times 10^{-9}$
$\tilde{K}_T^{\kappa}$	0	0	0	0
$\tilde{L}_T^{\kappa}$	$-i\ 1.90\times 10^{-9}$	$-i\ 1.61\times 10^{-9}$	$-i\ 1.90\times 10^{-9}$	$-i\ 1.61\times 10^{-9}$

than two orders of magnitude smaller, and there is no coupling to the singlet and quintet molecular states due to central and tensor contributions. The phase factor i that appears is due to the definition of the triplet molecular relative wavefunction as real; other conventions are possible, and subsequent calculations that might involve this interaction potential are not impacted by this phase convention.

It is possible to understand this result in connection with a relative volume argument that we have used previously [22]. Not only do the two deuterons need to tunnel through the Coulomb barrier in order to interact, but they also need to localize from the molecular scale to the nuclear scale. As a result, we can think of the interaction Hamiltonian for a specific transition as

$$\hat{H}_{\rm int} \;=\; \left[{\rm e}^{-G} \sqrt{\frac{v_{\rm nuc}}{v_{\rm mol}}} \right]_{l=1} \; (c\hat{P}_z - ZeA_z)\; i\; (\cdots), \tag{167}$$

where $v_{\rm mol}$ is the characteristic molecular volume, where $v_{\rm nuc}$ is a characteristic nuclear volume, and where $(\cdots)$ is the interaction strength for deuterons localized on a nuclear scale. If we take for the ratio

$$\frac{v_{\rm nuc}}{v_{\rm mol}} \;=\; \frac{\frac{4}{3}\pi r_{\rm nuc}^3}{2\pi^2 R_0 \Delta R^2} \;=\; 6.26 \times 10^{-12} \tag{168}$$

using $r_{\rm nuc} = 5$ fm, then we can estimate

$$|(\cdots)| \;=\; 0.020. \tag{169}$$

Since the $\hat{\mathbf{a}}$ operator of the $\mathbf{a} \cdot (c\mathbf{P})$ interaction is a velocity operator normalized to the speed of light [11], the associated transition matrix element (which has magnitude $|(\cdots)|$) can be no larger than unity. The magnitude of the transition matrix element in the case of coupling to the deuteron was estimated to be about $0.003(cP)$. We might have expected a volume corrected interaction matrix element calculated in this paper to have a similar magnitude (of 0.003); however, the result that we obtained is somewhat larger (due primarily to the effect of the relative deuteron–deuteron potential). Our basic conclusion at this point is that the magnitude of the interaction Hamiltonian calculated in this paper seems to us to be reasonable given the previous calculation for the deuteron transition.

We have focused in this work on the central and tensor contributions to the interaction, since these are the strongest. Our attention might reasonably have been focused on the spin–orbit contribution, which would produce different selection rules (including singlet and quintet coupling, with allowed coupling to the $l = 0$ rotational state). Such a project is of interest, but there are complications. The $\mathbf{a} \cdot c\mathbf{P}$ coupling that we are interested in is closely related to spin–orbit coupling, so it will be necessary to examine the derivation of the new interaction specifically for the spin–orbit interaction (which would involve going to higher order than was done in [11]). In the case of the Hamada–Johnston model, the spin–orbit coupling model is not derived as a normal spin–orbit coupling based on the central and tensor interactions, but is itself independent and empirical. As such, one wonders whether such a model is appropriate for an $\mathbf{a} \cdot c\mathbf{P}$ interaction. Nevertheless we have carried out some exploratory computations for the spin–orbit contribution for the singlet $l = 0$ case, and the relevant spatial integrals appear to be much smaller than for the central and tensor cases.

The advantage of using simplified wavefunctions and the Hamada–Johnston potential in the calculations presented in this paper is primarily that we are able to carry out a reasonable first pass at the largest contribution to the interaction matrix element without too much effort. It is certainly possible to do a better job, and it seems worthwhile to comment on some of the issues that seem important in the calculation. First and foremost seems to be the deuteron–deuteron interaction potential, since the magnitude of the probability amplitude at the fermi scale is very sensitive to this potential (for our calculation we have relied on empirical Woods–Saxon potentials optimized to match experimental phase shifts). The use of simplified ^{4}He and deuteron wavefunctions with no D-state admixture is expected to produce errors in the matrix element perhaps at the 50% level, based on our experience with the coupling matrix element calculation for the deuteron. The simplicity of the assumed product wavefunctions for both the initial and final states will lead to errors. In addition we expect errors associated with the use of the Hamada–Johnston potential (although these are likely small compared to those already mentioned).

It is possible to do a better job in all areas. For example, impressive results have been obtained in recent years with nuclear calculations based on chiral effective field theory [23]. There are by now many modern calculations of ^{4}He, such as described in [24–26]. There is a growing literature that make use of modern potentials and methods for four-nucleon scattering and reaction

calculations. Groups that work in this area would have little difficulty in applying their models to the calculation of the phonon exchange transition matrix element done more simply in this work.

Appendix A. Hamada–Johnston potential

The Hamada–Johnston potential can be written as [15]

$$\hat{V} \;=\; (\boldsymbol{\sigma}_1\cdot\boldsymbol{\sigma}_2)(\boldsymbol{\tau}_1\cdot\boldsymbol{\tau}_2)v_C(r)+(\boldsymbol{\tau}_1\cdot\boldsymbol{\tau}_2)\hat{S}_{12}v_T(r)+\left(\frac{\hat{\mathbf{L}}\cdot\hat{\mathbf{S}}}{\hbar^2}\right)v_{LS}(r)+\left(\frac{\hat{L}_{12}}{\hbar^2}\right)v_{LL}(r). \tag{A.1}$$

Appendix A.1. Central potential

The first term is the central potential with

$$v_C(r) \;=\; 0.08\frac{m_\pi c^2}{3}Y(\alpha r)\Big[1+a_C Y(\alpha r)+b_C Y^2(\alpha r)\Big], \tag{A.2}$$

where $Y(x)$ is defined according to

$$Y(x) \;=\; \frac{\mathrm{e}^{-x}}{x}. \tag{A.3}$$

Appendix A.2. Tensor interaction

The second term is the tensor interaction where

$$v_T(r) \;=\; 0.08\frac{m_\pi c^2}{3}Z(\alpha r)\Big[1+a_T Y(\alpha r)+b_T Y^2(\alpha r)\Big], \tag{A.4}$$

$$\hat{S}_{12} \;=\; 3\frac{(\boldsymbol{\sigma}_1\cdot\mathbf{r})(\boldsymbol{\sigma}_2\cdot\mathbf{r})}{r^2}-(\boldsymbol{\sigma}_1\cdot\boldsymbol{\sigma}_2). \tag{A.5}$$

Appendix A.3. Spin–orbit interaction

The third term is the spin–orbit interaction

$$v_{LS}(r) \;=\; G_{LS}m_\pi c^2 Y^2(\alpha r)\big[1+b_{LS}Y(\alpha r)\big], \tag{A.6}$$

$$\hat{\mathbf{L}} \;=\; (\mathbf{r}_2-\mathbf{r}_1)\times(\mathbf{p}_2-\mathbf{p}_1), \tag{A.7}$$

$$\hat{\mathbf{S}} \;=\; \frac{\hbar}{2}(\boldsymbol{\sigma}_1+\boldsymbol{\sigma}_2). \tag{A.8}$$

Appendix A.4. Quadratic spin–orbit interaction

The last term is a quadratic spin–orbit term with

$$v_{LL}(r) \;=\; G_{LL}m_\pi c^2\frac{Z(\alpha r)}{(\alpha r)^2}\Big[1+a_{LL}Y(\alpha r)+b_{LL}Y^2(\alpha r)\Big], \tag{A.9}$$

$$\hat{L}_{12} \;=\; (\boldsymbol{\sigma}_1\cdot\boldsymbol{\sigma}_2)|\hat{\mathbf{L}}|^2-\frac{1}{2}(\boldsymbol{\sigma}_1\cdot\hat{\mathbf{L}})(\boldsymbol{\sigma}_2\cdot\hat{\mathbf{L}})-\frac{1}{2}(\boldsymbol{\sigma}_2\cdot\hat{\mathbf{L}})(\boldsymbol{\sigma}_1\cdot\hat{\mathbf{L}}). \tag{A.10}$$

The Z function is defined according to

$$Z(x) \;=\; Y(x)\left(1+\frac{3}{x}+\frac{3}{x^2}\right). \tag{A.11}$$

Appendix A.5. Parametrization

The various a and b parameters are channel-dependent fitting coefficients which have been tabulated in [15]. The α parameter in the Hamada–Johnston potential is taken to satisfy

$$\frac{1}{\alpha} \;=\; 1.415 \text{ fm}. \tag{A.12}$$

The pion mass is taken to be

$$m_\pi c^2 \;=\; 139.4 \text{ MeV}. \tag{A.13}$$

The Hamada–Johnston potential is a hard core potential, so the potential is assumed to be infinitely repulsive at small relative position

$$v_{12} \;=\; \infty, \qquad \alpha r < 0.343. \tag{A.14}$$

Appendix A.6. Projection operators

The different potentials in the Hamada–Johnston model depend on whether the spin of the two interacting nucleons is singlet or triple, and whether the relative spatial wavefunction is even or odd. To implement this one can make use of spin and isospin projection operators, by taking advantage of antisymmetry. We know that the wavefunction for two nucleons must be antisymmetric if the two nucleons are exchanged, and that this antisymmetry is reflected in the spatial, spin and isospin components of the wavefunction. So, if the relative spatial wavefunction is even (symmetric), and the nucleon spins are in a triplet configuration (also symmetric), then the isospin wavefunction must be singlet (antisymmetric). We can use this to write

$$\hat{v}_C(r) \;=\; v_C^{eS}(r)\hat{P}_S^{(a)}\hat{P}_T^{(s)} + v_C^{eT}(r)\hat{P}_S^{(s)}\hat{P}_T^{(a)} + v_C^{oS}(r)\hat{P}_S^{(a)}\hat{P}_T^{(a)} + v_C^{oT}(r)\hat{P}_S^{(s)}\hat{P}_T^{(s)}, \tag{A.15}$$

where the $\hat{P}$ operators are projection operators

$$\hat{P}_S^{(a)}(12) \;=\; -\frac{1}{4}\Big[\boldsymbol{\sigma}_1\cdot\boldsymbol{\sigma}_2 - I\Big] \qquad \hat{P}_S^{(s)}(12) \;=\; \frac{1}{4}\Big[\boldsymbol{\sigma}_1\cdot\boldsymbol{\sigma}_2 + 3I\Big], \tag{A.16}$$

$$\hat{P}_T^{(a)}(12) \;=\; -\frac{1}{4}\Big[\tau_1\cdot\boldsymbol{\tau}_2 - I\Big] \qquad \hat{P}_T^{(s)}(12) \;=\; \frac{1}{4}\Big[\boldsymbol{\tau}_1\cdot\boldsymbol{\tau}_2 + 3I\Big]. \tag{A.17}$$

References

[1] P.L. Hagelstein, Bird's eye view of phonon models for excess heat in the Fleischmann—Pons experiment, *J. Condensed Matter Nucl. Sci.* **6** (2011) 169.

[2] M. Fleischmann, S. Pons and M. Hawkins, *J. Electroanal Chem.* **201** (1989) 301; errata, **263** (1990) 187.

[3] M. Fleischmann, S. Pons, M.W. Anderson, L.J. Li and M. Hawkins, *J. Electroanal. Chem.* **287** (1990) 293.

[4] P.L. Hagelstein, M.C.H. McKubre, D.J. Nagel, T.A. Chubb and R.J. Hekman, *Proc. ICCF11*, 2004, p. 23.

[5] P.L. Hagelstein, *Naturwissenschaften* **97** (2010) 345.

[6] P.L. Hagelstein and I.U. Chaudhary, Energy exchange in the lossy spin-boson model, *J. Condensed Matter Nucl. Sci.* **5** (2011) 52.

[7] P.L. Hagelstein and I.U. Chaudhary, Second-order formulation and scaling in the lossy spin-boson model, *J. Condensed Matter Nucl. Sci.* **5** (2011) 87.
[8] P.L. Hagelstein and I.U. Chaudhary, Local approximation for the lossy spin—boson model, *J. Condensed Matter Nucl. Sci.* **5** (2011) 102.
[9] P.L. Hagelstein and I.U. Chaudhary, Coherent energy exchange in the strong coupling limit of the lossy spin-boson model, *J. Condensed Matter Nucl. Sci.* **5** (2011) 116.
[10] P.L. Hagelstein and I.U. Chaudhary, Generalization of the lossy spin—boson model to donor and receiver systems, *J. Condensed Matter Nucl. Sci.* **5** (2011) 140.
[11] P.L. Hagelstein and I.U. Chaudhary, Including nuclear degrees of freedom in a lattice Hamiltonian, *J. Condensed Matter Nucl. Sci.* **7** (2011) 35.
[12] P.L. Hagelstein and I.U. Chaudhary, Coupling between a deuteron and a lattice, *J. Condensed Matter Nucl. Sci.* **9** (2012) 50.
[13] F.J. Wilkinson III and F.J. Cecil, *Phys. Rev. C* **31** (1985) 2036.
[14] H.J. Assenbaum and K. Langanke, *Phys. Rev. C* **36** (1987) 17.
[15] H.J. Boersma, *Nucl. Phys.* **A135** (1969) 609.
[16] T. Hamada and I.D. Johnston, A potential model representation of two-nucleon data below 315 MeV, *Nucl. Phys.* **34** (1962) 382.
[17] I.U. Chaudhary, *Applications of Group Theory to Few-Body Physics*, MIT PhD Thesis (2005).
[18] I.U. Chaudhary and P.L. Hagelstein, Four-body RST general nuclear wavefunctions and matrix elements, *Proc. ICCF12* (2005) 527.
[19] J. Carlson, *Phys. Rev. C* **38** (1988) 1879.
[20] E.L. Tomusiak, W. Leidemann and H.M. Hofmann, *Phys. Rev. C* **52** (1995) 1963.
[21] A.A. Frost and B. Musulin, *J. Chem. Phys.* **22** (1954) 1017.
[22] P.L. Hagelstein, Phonon exchange models: Some new results, *Proc. ICCF11*, 2004, p. 743.
[23] R. Machleidt and D.R. Entem, Chiral effective field theory and nuclear forces, *Physics Reports* **503** (2011) 1.
[24] H. Kamada, A. Nogga, W.Glöckle, E. Hiyama, M. Kamimura, K. Varga, Y. Suzuki, M. Viviani, A. Kievsky, and S. Rosati, Benchmark test calculation of a four-nucleon bound state, *Phys. Rev. C* **64** (2001) 044001.
[25] L. Coraggio, A. Covello, A. Gargano, N. Itaco, T.T.S. Kuo and R. Machleidt, *Phys. Rev. C* **271** (2005) 014307-1.
[26] J. Kirscher, H.W. Griesshammer, D. Shukla and H.M. Hofmann, *Eur. Phys. J. A* **44** (2010) 239.

J. Condensed Matter Nucl. Sci. 11 (2013) 59–92

Research Article

Lossy Spin–boson Model with an Unstable Upper State and Extension to N-level Systems

Peter L. Hagelstein *

Research Laboratory of Electronics, Massachusetts Institute of Technology, Cambridge, MA 02139, USA

Irfan U. Chaudhary

Department of Computer Science and Engineering, University of Engineering and Technology. Lahore, Pakistan

Abstract

In the Fleischmann–Pons experiment, excess heat is thought to have a nuclear origin due to the amount of energy produced, yet there are no commensurate energetic particles. This has motivated us over the years to focus attention on models in which a large quantum is fractionated into a great many small quanta. We have found that many two-level systems with a large transition energy are able to exchange energy coherently with an oscillator with a much smaller characteristic energy as long as decay channels are present in the vicinity of the two-level transition energy. In previous work we analyzed this basic model, and obtained estimates for the coherent energy exchange rate in the strong coupling limit. In this work we consider a version of this model where the upper states of the two-level systems are unstable. In this case, there is no coherent energy exchange, but instead we find a dynamical polarization effect which we have analyzed. We extend the model to the case of three-level systems, and generalize the result to apply to general N-level systems. Coherent energy exchange is possible within the context of a donor and receiver model, where the receiver transitions have unstable upper states. We give results for the donor dynamics in this case. This model provides a foundation for a new kind of model that we put forth recently for which the predictions appear to be closely connected to experiment.
© 2013 ISCMNS. All rights reserved. ISSN 2227-3123

Keywords: Coherent energy exchange, Fleischmann–Pons experiment, Lossy spin–boson model, Theory

1. Introduction

For the past several years we have pursued models involving sets of two-level systems and a highly excited oscillator with linear coupling and loss [1–4]. These models are interesting to us because they show coherent energy exchange between the two different quantum systems under conditions where the two-level transition energy is much greater than the characteristic energy of the oscillator; in essence, the large quantum is “fractionated” in these models [4].

*E-mail: plh@mit.edu

© 2013 ISCMNS. All rights reserved. ISSN 2227-3123

Our motivation for these studies has be to understand physical mechanisms associated with excess heat production in the Fleischmann–Pons experiment [5–7]. What makes the experimental results difficult to understand is that a large amount of energy is released which appears to be of nuclear origin, and yet there are not energetic nuclear particles present in amounts commensurate with the energy produced [8]. If the large nuclear quantum can be fractionated, and the energy coherently coupled to a low energy mode (such as a phonon, plasmon, or perhaps magnon mode), then the physical mechanism would no longer be such a mystery.

The lossy spin–boson models that we have studied exhibit efficient coherent energy exchange under conditions where the large quantum is fractionated. We have proposed a generalization with two sets of two-level systems, in which one set is strongly coupled to the oscillator, and one set is weakly coupled to the oscillator (which we have termed a donor and receiver model) [9]. In such models, the initial excitation is in the weakly coupled two-level systems, which alone cannot fractionate the large two-level system quantum; however, when a strongly-coupled set of two-level systems is also present then the excitation from the weakly coupled systems is transferred to the strongly-coupled systems and fractionated.

We have for years considered this kind of model as a candidate to account for excess heat production in the Fleischmann–Pons experiment [10]. The mechanism that the model implements seems to be what is needed to account for the effect, and there seems to be indirect evidence in the two-laser experiment of Letts and Cravens [11] that the nuclear energy is communicated into specific optical phonon modes [12]. Another indirect connection to experiment is the observation that excess heat is correlated with a deuteron flux within the PdD, as one expects the deuteron flux to generate substantial incoherent optical phonon excitation (which is otherwise difficult to arrange for) [7]. In the donor and receiver models, no reactions occur unless the oscillator is highly excited, so we view the problem of triggering in these experiments in terms of developing strong excitation in high frequency vibrational modes [10].

It seems straightforward to identify the weakly-coupled donor transition in the model with $D_2/^4He$ transitions in the PdD, since the associated matrix element will be small because of tunneling through the Coulomb barrier. However, there have been difficulties for many years in the identification of the strongly-coupled receiver transition. While there has been no lack of candidate transitions, when we analyzed obvious candidates we found that the coupling was too weak to fractionate the large 24 MeV quantum from the donor transition under conditions relevant to experiment [10].

Earlier this year we recognized the existence of a relativistic coupling between lattice vibrations and internal nuclear degrees of freedom that results in a much stronger phonon exchange interaction [13]. This new interaction is important since it predicts a much stronger coupling than can be obtained from indirect electron-nuclear interactions; consequently, we have been optimistic that with this stronger coupling we might be able to finally identify receiver transitions involved in the excess heat experiments. The strongest coupling produced by the new interaction is found in the case of very highly excited nuclear excitation in which the upper state is extremely unstable. Since the donor and receiver model developed previously is based on strongly coupled receiver transitions with stable upper states, we cannot use it to model these transitions with the strongest coupling. To make progress, we need to revisit the basic lossy spin–boson model, and to repeat or extend the analysis for the special case where the upper states are unstable. This is the basic task we address in this work.

The lossy spin–boson model with unstable upper states is fundamentally different than the basic lossy spin–boson model that we analyzed before. Since the upper states are unstable, there cannot be net (real) excitation of the levels; hence, there is no evaluation of the coherent energy exchange rate in this case. Instead, the highly-exited oscillator causes a dynamical polarization of the two-level transitions, somewhat analogous to the dynamical polarization one would expect for a hydrogenic $1s-2p$ transition in a slowly varying electric field (in this case, there is a mixing of the $1s$ and $2p$ states, but there is no real excitation of the $2p$ state). The analogy is not quite precise, since in our model there is an additional loss effect due to the coupling of the oscillator to fast decay channels available for states far off of resonance. In what follows we obtain results for two-level systems, for three-level systems, and for the generalization to N-level systems.

Armed with these results, we are in a position to return to the donor and receiver model which we can extend now to the case of receivers with unstable upper states. We find that the receiver is still able to fractionate a large quantum, at least in principle, and we obtain results for the donor dynamics in the presence of the coupled oscillator and receiver system. The subdivision effect that was present with stable receiver upper states is no longer present in the new model; without stable upper states the receiver must fractionate the large quantum completely. Without the ability to subdivide the large donor quantum, the requirements on the receiver transition are sufficiently severe that it is not possible to find receiver transitions (even with the new relativistic coupling) that can fractionate a 24 MeV quantum under conditions relevant to experiment.

Unfortunately, this result ends up ruling out the basic donor and receiver model as a candidate to account for excess heat in the Fleischmann–Pons experiment. This was disconcerting; we found this result while preparing for a conference (ICCF17), where we wanted to present more positive results. This provided the motivation for seeking some kind of modification of the model which might be more promising. The result of this work was the development of a new kind of model, one which appears to be in agreement with experiment in the cases we have studied so far, and which came into existence just in time to present at ICCF17 [14,15]. The lossy two-level model with unstable upper states considered in this work provides the foundation for this new model.

2. Model

We turn our attention now to a brief discussion of the new basic model. Our immediate goal then is to specify a Hamiltonian that implements a lossy spin–boson model with unstable upper states. However, it seems useful to begin the discussion at an earlier point in order to make the arguments more accessible.

2.1. Basic spin–boson model

We begin with the basic spin–boson model [16–18], which can be written as

$$\hat{H}_{\rm spin-boson} \;=\; \Delta E\frac{\hat{S}_z}{\hbar} + \hbar\omega_0\hat{a}^\dagger\hat{a} + V(\hat{a}+\hat{a}^\dagger)\frac{2\hat{S}_x}{\hbar}. \tag{1}$$

This model includes a set of identical two-level systems with transition energy ΔE and an oscillator with characteristic energy $\hbar\omega_0$, linearly coupled with a coupling strength V. This model has been studied extensively in the literature, and we know that it describes coherent energy exchange between the two-level system and oscillator under conditions where the dressed two-level system energy is an odd multiple of the oscillator energy. The coherent energy exchange effect is weak in the multiphoton regime, and we have discussed previously that this is due to a destructive interference effect [1].

2.2. Lossy spin–boson model

Coherent energy exchange is very much faster in a generalization of the lossy spin–boson model when oscillator loss is present in the vicinity of the two-level system transition energy. We have written for this model the Hamiltonian

$$\hat{H}_{\rm lossy\ spin-boson} \;=\; \Delta E\frac{\hat{S}_z}{\hbar} + \hbar\omega_0\hat{a}^\dagger\hat{a} + V(\hat{a}+\hat{a}^\dagger)\frac{2\hat{S}_x}{\hbar} - i\frac{\hbar\hat{\Gamma}(E)}{2}, \tag{2}$$

where the $i\hbar\hat{\Gamma}(E)/2$ term accounts for the loss in an infinite-order Brillouin–Wigner formalism (described in [1]). We call this model the lossy spin–boson model. There are issues connected to the inclusion of loss in this formalism that were raised by a reviewer; in response we have added an Appendix that discusses such issues.

We have been interested in the model in the strong coupling limit when a large number of two-level systems are present, since in this regime the coherent exchange rate between the two-level systems and oscillator can be reasonably large even when the two-level system quantum is fractionated into a great many oscillator quanta. The model looks deceptively simple, so that one might not anticipate the substantial amount of effort and approximations needed to determine the coherent energy exchange rate. Nevertheless, the coherent energy exchange rate has been determined as discussed in [2–4,19].

2.3. Lossy spin–boson model with an unstable upper state

In view of the discussion in the Introduction, we would like now to consider an extension of the lossy spin–boson model in which the upper state is unstable. We begin by first writing the lossy spin–boson model using a matrix notation

$$\hat{H}_{\text{lossy spin}-\text{boson}} = \frac{\Delta E}{2}\sum_j \begin{pmatrix} 1 & 0 \\ 0 & -1 \end{pmatrix}_j + \hbar\omega_0 \hat{a}^\dagger \hat{a} + V(\hat{a}+\hat{a}^\dagger)\sum_j \begin{pmatrix} 0 & 1 \\ 1 & 0 \end{pmatrix}_j - i\frac{\hbar\hat{\Gamma}(E)}{2} \tag{3}$$

and then adding upper state loss to obtain

$$\hat{H} = \frac{\Delta E}{2}\sum_j \begin{pmatrix} 1 & 0 \\ 0 & -1 \end{pmatrix}_j - i\frac{\hbar\hat{\gamma}(E)}{2}\sum_j \begin{pmatrix} 1 & 0 \\ 0 & 0 \end{pmatrix}_j + \hbar\omega_0 \hat{a}^\dagger \hat{a} + V(\hat{a}+\hat{a}^\dagger)\sum_j \begin{pmatrix} 0 & 1 \\ 1 & 0 \end{pmatrix}_j - i\frac{\hbar\hat{\Gamma}(E)}{2}. \tag{4}$$

In this equation $\hat{\gamma}(E)$ models the decay of the unstable upper state of the two-level system, again within the infinite-order Brillouin–Wigner formalism. We presume in this that the two-level systems remain identical, and the decay rate is determined by the available system energy E consistent with decay processes in the Brillouin–Wigner approach.

2.4. Discussion

This provides us with a starting point for the analysis and extensions that will follow. This basic model by itself does not do very much; for example, we expect a mixing of the two-level and oscillator degrees of freedom that increases with coupling strength; but in general we are not looking for the mixing to lead to significant excitation of the upper state in order to see upper state decay. Our goal in this version of the model is to describe the basic mixing of the degrees of freedom, but otherwise the coupled system just sits there and doesn't do much that seems interesting.

What is interesting about the systems under discussion in this paper is that they provide a more relevant model for the physical systems that we are ultimately interested in. They behave somewhat differently than the lossy spin–boson models considered previously. Before moving on to use them in applications, we need to spend some time analyzing them in order to understand them.

3. Expansion Coefficients

To make progress generally on the problems of interest described in the Introduction we require approximate solutions for the eigenfunctions of the model, especially in the strong coupling regime. In spite of the deceptive simplicity of the basic model, there are subtle issues associated with the eigenfunctions, and exact analytic solutions are not available. We are going to have to make use of approximate and numerical solutions, and these will be pursued most easily if we work in terms of expansion coefficients $c_{m,n}$ in connection with the wavefunction construction

$$\Psi \;=\; \sum_m \sum_n c_{m,n} |S,m\rangle |n\rangle. \tag{5}$$

We recognize the $|S,m\rangle$ states as Dicke states associated with the pseudospin formalism, and $|n\rangle$ are the eigenstates of the simple harmonic oscillator.

3.1. Eigenvalue equation

We assume that Ψ satisfies the time-independent Schrödinger equation

$$E\Psi \;=\; \hat{H}\Psi. \tag{6}$$

The expansion coefficients then satisfy an eigenvalue equation, which we will approximate by

$$\begin{aligned} Ec_{m,n} \;=\; & \left(\Delta E m + \hbar\omega_0 n - i\frac{\hbar}{2}\Gamma(E)\right)c_{m,n} + V\sqrt{n+1}\sqrt{(S-m)(S+m-1)}c_{m+1,n+1} \\ & + V\sqrt{n}\sqrt{(S-m)(S+m-1)}c_{m+1,n-1} + V\sqrt{n+1}\sqrt{(S+m)(S-m+1)}c_{m-1,n+1} \\ & + V\sqrt{n}\sqrt{(S+m)(S-m+1)}c_{m-1,n-1}. \end{aligned} \tag{7}$$

What is missing in this explicit eigenvalue equation is the contribution of the upper state decay; we will take the point of view that the upper state decay is infinitely fast where it occurs, and exclude states from the problem that are unstable (consistent with the associated occupation probability vanishing). This greatly simplifies the problem.

3.2. Limit of large S and n

We are interested in the system when there are many two-level systems, and in general the polarization of the two-level systems will be weak. Under these conditions we may take

$$(S-m+1) \;\rightarrow\; (S-m) \;\rightarrow\; 2S. \tag{8}$$

In addition, we assume that the oscillator is highly excited. The associated notation deserves some comment, as it is perhaps more iconic than mathematical. We assume that the oscillator is excited around some large number of quanta n_0, so that we might write

$$n \;=\; n_0 + \delta n. \tag{9}$$

For n sufficiently large we might write

$$\sqrt{n} \;\rightarrow\; \sqrt{n_0}, \qquad \sqrt{n+1} \;\rightarrow\; \sqrt{n_0}, \tag{10}$$

which removes the n-dependence from the coupling terms. The basis state energies depends on n, so we might write

$$\hbar\omega_0 n \;\rightarrow\; \hbar\omega_0(n_0 + \delta n). \tag{11}$$

All of this would suggest that we should write the eigenvalue equation as

$$\begin{aligned} Ec_{m,n_0+\delta n} &= \left(\Delta Em + \hbar\omega_0(n_0+\delta n) - i\frac{\hbar}{2}\Gamma(E)\right)c_{m,n_0+\delta n} \\ &\quad + V\sqrt{n_0}\sqrt{2S}\left[\sqrt{S+m-1}\left(c_{m+1,n_0+\delta n+1} + c_{m+1,n_0+\delta n-1}\right)\right. \\ &\quad \left. + \sqrt{S+m}\left(c_{m-1,n_0+\delta n-1} + c_{m-1,n_0+\delta n-1}\right)\right]. \end{aligned} \tag{12}$$

Such an eigenvalue equation could be understood from a mathematical point of view directly. However, we would like to work with a simpler notation. Since $\hbar\omega_0 n_0$ is a constant, we can eliminate it with no change in the dynamics (but we should remember that the energy eigenvalue would then be shifted). The $n_0 + \delta n$ appearing in the subscripts will be painful to deal with, so we replace them with n.

In the end, we work with an eigenvalue equation of the form

$$\begin{aligned} Ec_{m,n} &= \left(\Delta Em + \hbar\omega_0 n - i\frac{\hbar}{2}\Gamma(E)\right)c_{m,n} + V\sqrt{n_0}\sqrt{2S} \\ &\quad \times \left[\sqrt{S+m-1}\left(c_{m+1,n+1} + c_{m+1,n-1}\right) + \sqrt{S+m}\left(c_{m-1,n-1} + c_{m-1,n-1}\right)\right]. \end{aligned} \tag{13}$$

In this equation we now think of n as incremental ($\delta n \to n$), and we have decided to go a bit against the literature and maintain the n_0 in the square root. Hopefully with this explanation and this notation things may be less confusing.

3.3. Dimensionless coupling constant

The dimensionless coupling constant that seems natural for this problem is

$$g = \frac{V\sqrt{n_0}\sqrt{2S}}{\Delta E}. \tag{14}$$

This dimensionless coupling constant differs from that of the spin–boson model written using a similar notation [20]

$$g_{\text{spin}-\text{boson}} = \frac{V\sqrt{n_0}}{\Delta E} \tag{15}$$

and also from what we have been using for the lossy spin–boson model [3]

$$g_{\text{lossy spin}-\text{boson}} = \frac{V\sqrt{n_0}\sqrt{S^2-m^2}}{\Delta E}. \tag{16}$$

It is important to note that big difference between the basic (lossless) spin–boson model and the lossy variants we have been interested in is that when loss is introduced the model responds to a dimensionless coupling constant that is greatly increased when many two-level systems are present.

The difference between the earlier lossy spin–boson model and the extension to the unstable upper state case looks to be drastic (going from $\sqrt{S^2-m^2}$ to $\sqrt{2S}$), but this would be misleading. There is a close connection between the earlier lossy spin–boson model and this new model, and the new one would behave very similarly to the old one in the

vicinity of $m \approx -S$. So, writing the dimensionless coupling constant in this way here is more a matter of convenience, and it emphasizes that we are working with problems in which all of the two-level systems are close to being in ground states. When there is substantial excitation in the new model, the average coupling strength between individual states will be much greater than $V\sqrt{n_0}\sqrt{2S}/\Delta E$, and will be much closer instead to $V\sqrt{n_0}\langle\sqrt{S^2-m^2}\rangle/\Delta E$. Unfortunately it will be inconvenient to work with a dimensionless coupling constant that is implicitly defined in terms of itself. For a given solution, we will be able to determine what the suitable averaged dimensionless coupling strength is if we would like to compare with the earlier lossy spin–boson model.

With this definition we may write the normalized eigenvalue equation as

$$\begin{aligned}\epsilon c_{m,n} \;=\; & \left(m + \frac{n}{\Delta n} - i\frac{\hbar}{2\Delta E}\Gamma(\epsilon)\right)c_{m,n} \\ & + g\left[\sqrt{S+m-1}\left(c_{m+1,n+1} + c_{m+1,n-1}\right) + \sqrt{S+m}\left(c_{m-1,n-1} + c_{m-1,n-1}\right)\right],\end{aligned} \tag{17}$$

where

$$\epsilon \;=\; \frac{E}{\Delta E}. \tag{18}$$

3.4. Loss and boundary conditions

In some of our early studies with the lossy spin–boson model we included explicit loss models that included estimates of the decay rates as a function of energy. We found in general that the probability amplitude tended to avoid states with high loss, and that when the dimensionless coupling constant became large, that the boundary appeared sharp on the scale of the overall probability amplitude as a function of m and n. Consequently, when we carried out detailed analyses relevant to the strong coupling limit, it seemed natural to work with an "infinite loss" version of the model in which we simply omitted unstable states [2]. Consistent with the premise of such a model, all basis states with energies below some threshold would be removed from the calculation as a way to approximately model the effect of loss.

We encounter this basic issue anew in the new version of the model with unstable upper states. Since this same loss is present in the new model, we would make a similar approximation by excluding all basis states below a fixed energy. But now we have an additional loss effect in which we need to exclude states that involve real occupation of excited states; this is new and deserves some thought.

Coherent energy exchange in the previous model resulted in real excited states, in which Δn oscillator quanta were lost and one unit of excitation $\Delta E = \hbar\omega\Delta n$ was gained. In the new model this cannot occur since all real excited states are unstable. But suppose that we were to consider states in which less than Δn oscillator quanta were lost, so that an excited state could be formed off of resonance (as a virtual state). Depending on the loss channels available, we would probably still expect it to decay rapidly, although not as rapidly as if it had its full energy. Based on this picture, we should exclude such states as well.

The end result of such a line of argument is that we might implement upper state decay approximately by omitting basis states with an oscillator energy below some threshold value. If so, we would write the normalized eigenvalue equation as

$$\begin{aligned}\epsilon c_{m,n} \;=\; & \left(m + \frac{n}{\Delta n}\right)c_{m,n} \\ & + g\left[\sqrt{S+m-1}\left(c_{m+1,n+1} + c_{m+1,n-1}\right) + \sqrt{S+m}\left(c_{m-1,n-1} + c_{m-1,n-1}\right)\right]\end{aligned} \tag{19}$$

subject to the boundary condition

$$c_{m,n} = 0, \quad n < 0 \tag{20}$$

taking the incremental n to be zero at the cut off.

3.5. Solutions in the weak coupling regime

Based on the discussion above we have arrived at a model that can be analyzed, and one of our first tasks is to consider which of the many possible eigenfunction solutions are of interest. Consider first the situation where the dimensionless coupling strength is small; for example, suppose that

$$\Delta n = \frac{\Delta E}{\hbar\omega_0} = 1000, \tag{21}$$

$$g = 0.03. \tag{22}$$

We can compute solutions numerically, and categorize them usefully by plotting out values of $\langle m+S\rangle$ and $\langle n\rangle$ as shown in Fig. 1. Since the coupling is weak for this example, for the most part we do not expect much to happen. We see that most of the states have $\langle m+S\rangle$ and $\langle n\rangle$ averages which closely match the basis state equivalents. The biggest impact from the coupling can be seen in the lower left corner, where there is some mixing between basis states with $m+S=0$ and with $n=0$ and $n=2$.

All of the states indicated to the right of the first column involve $\langle m+S\rangle$ values on the order of 1 or higher; these states clearly involve one or more excited two-level systems. As such, we would not make use of them for our model, since excited states are unstable.

Based on this, all of the solutions indicated in the first column then are candidate wavefunctions that we might consider using to describe our coupled system. But how do we think about them? We know that the state at the bottom is closest to the cut off, so it will be most impacted by the effect of the boundary. We would expect that once we have gone up the column far enough that we will find states sufficiently removed from the boundary that the boundary will have no impact. The choice of one such state over another in the weak coupling regime appears to then be connected with where the cut off in oscillator quanta is relative to the basis states that make up the eigenfunction. If the coupling is weak this can make a substantial difference, as we can see already in the shifted $\langle n\rangle$ value of the state closest to the boundary.

3.6. Solutions when the coupling is stronger

The situation changes qualitatively when the coupling is stronger. Perhaps the best way to see this simply is to consider the lowest two eigenfunctions when the coupling is not so weak. Consider an example in which

$$\Delta n = \frac{\Delta E}{\hbar\omega_0} = 100, \tag{23}$$

$$g = 0.70. \tag{24}$$

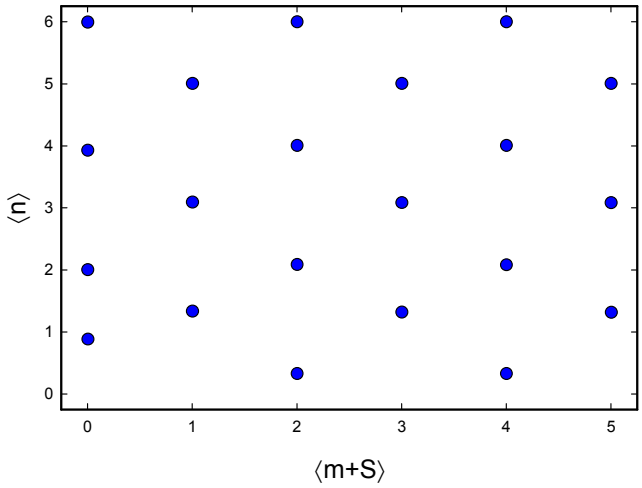

Figure 1. Average values $\langle m+S\rangle$ and $\langle n\rangle$ for low-lying states with even $n+m+S$ basis states in weak coupling.

The lowest two eigenfunctions are shown in Figs. 2 and 3. We see that the situation seems qualitatively different now; these eigenfunctions closest to the boundary are showing a collective effect beyond primarily translation and simple mixing as in the weak coupling limit. We see in these eigenfunctions a ground state and single unit of collective excitation in n, and there is also a solution which shows a similar single unit of excitation in $m+S$. We will be interested in these solutions in a following paper where they will constitute a set of off-resonant intermediate states that will contribute in a coherent dynamics calculation.

3.7. Intermediate regime

We recognize in this discussion that there should occur an intermediate regime. One intermediate regime we might associate with values of g in which the system changes over from the weak coupling regime to the strong coupling regime; another intermediate regime would be expected when the spread in oscillator quanta leads to occupation of states that decay with associated rates that are slow or moderate. The development of models relevant to these regimes will be interesting, especially in the latter case; we consider such endeavors to be outside of the scope of this study.

3.8. Hard and soft boundary conditions

In our earlier work on the lossy spin–boson model we noticed an issue with respect to the "hard" boundary condition discussed above. As a mathematical statement it seems clear that we might draw a line at some value of n and exclude basis states below the line. This is similar to the assumption that we made in our earlier work where we excluded basis states below a fixed energy. We found in that case that the wavefunctions that result were finite at the threshold energy [4].

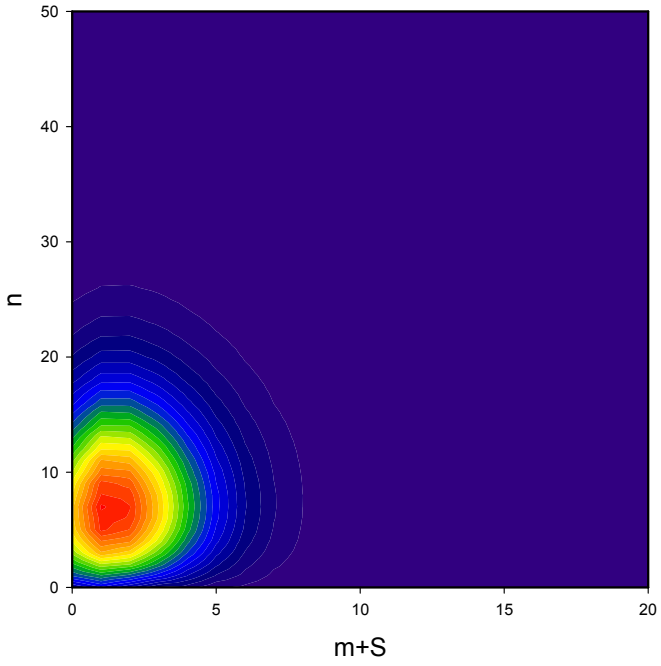

Figure 2. Contour plot of the lowest eigenfunction solution plotted as $(-1)^m c_{m,n}$ as a function of $m + S$ and n.

Since there has been some time since this earlier work, we have had time to think about this assumption and the consequences. One unexpected consequence is that it leads to a discontinuous slope for zero energy exchange in the line shape we compute for the broad x-ray feature in the Karabut experiment. This motivated us to reconsider the boundary condition, and prompts us here to propose a modified boundary condition which we may write as

$$c_{m,0} \;=\; 0 \tag{25}$$

with excluded states for $n < 0$. The idea is that when decay processes occur as the excitation of the lattice decreases, the effect will be gradual with n; we would not expect in the physical system that there will be no decay above some threshold value of n and infinite decay below that threshold.

4. Approximation with Product Wavefunction

It is of interest to see whether an approximate product wavefunction might be useful for this problem, as it would allow us to analyze the strong coupling regime more easily. To proceed, we approximate the expansion coefficients using

$$c_{m,n} \;=\; (-1)^m a_m u_n. \tag{26}$$

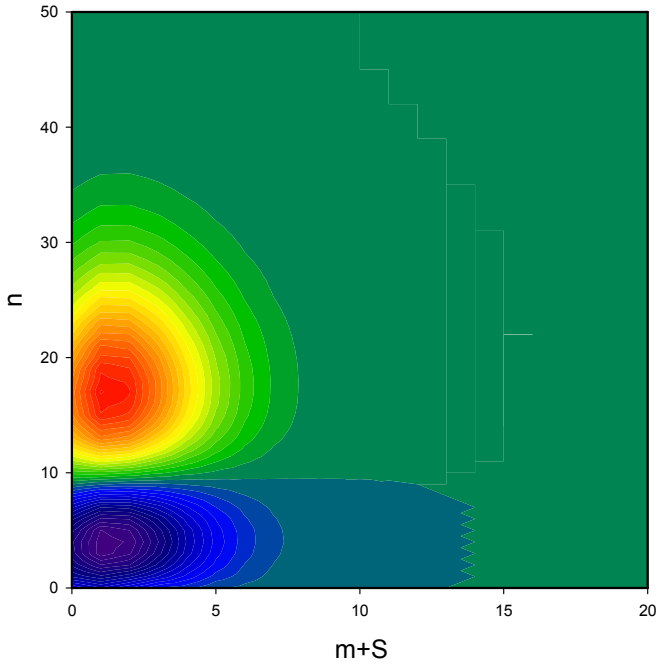

Figure 3. Contour plot of the first excited state plotted as $(-1)^m c_{m,n}$ as a function of $m + S$ and n.

This is analogous the the pulse and amplitude approximation that we pursued in the case of the lossy spin–boson model [21].

4.1. Variational model

The eigenvalue equation for the expansion coefficients can be derived from a variational principle based on

$$I = \sum_{m,n}\left(m+\frac{n}{\Delta n}\right)c_{m,n}^2 - g\sum_{m,n}c_{m,n}\Bigg[\sqrt{S+m-1}\Big(c_{m+1,n+1}+c_{m+1,n-1}\Big) + \sqrt{S+m}\Big(c_{m-1,n-1}+c_{m-1,n-1}\Big)\Bigg] \tag{27}$$

subject to the constraint

$$\sum_{m,n} c_{m,n}^2 = 1. \tag{28}$$

This motivates us to propose a modified variational principle for the approximate product wavefunction

$$J = \sum_m m a_m^2 + \frac{1}{\Delta n}\sum_n n u_n^2 - g\Big[\sum_n u_n(u_{n+1}+u_{n-1})\Big] \times\Bigg[\sum_m\Big(\sqrt{S+m-1}\,a_m a_{m+1}+\sqrt{S+m}\,a_m a_{m-1}\Big)\Bigg] \tag{29}$$

subject to the constraints

$$\sum_m a_m^2 = 1, \tag{30}$$

$$\sum_n u_n^2 = 1. \tag{31}$$

4.2. Optimization of the product wavefunction

We can make J stationary if a_m satisfies the constraint

$$\lambda_a a_m = m a_m - g\Big[\sum_n u_n(u_{n+1}+u_{n-1})\Big]\Big(\sqrt{S+m-1}\,a_{m+1}+\sqrt{S+m}\,a_{m-1}\Big) \tag{32}$$

with the boundary conditions

$$a_m = 0 \qquad \text{for } m < -S, \tag{33}$$

$$a_m \to 0 \qquad \text{for } m \to \infty. \tag{34}$$

In addition, the other function u_n satisfies the constraint

$$\lambda_u u_n = \frac{n}{\Delta n}u_n - g\Big[\sum_m\Big(\sqrt{S+m-1}\,a_m a_{m+1}+\sqrt{S+m}\,a_m a_{m-1}\Big)\Big](u_{n+1}+u_{n-1}) \tag{35}$$

subject to

$$u_n = 0 \qquad \text{for } n < 0, \tag{36}$$

$$u_0 = 0, \tag{37}$$

$$u_n \to 0 \qquad \text{for } n \to \infty. \tag{38}$$

4.3. Comparison

We have carried out computations with the product solution in order to compare with the exact solution for the parameters

$$\Delta n = \frac{\Delta E}{\hbar\omega_0} = 70, \tag{39}$$

$$g = 1.80. \tag{40}$$

We see from Figs. 4 and 5 that the optimized product solution is quite close to the exact numerical solution.

5. Sets of N-level Systems Coupled to an Oscillator

We are also interested in more complicated models than those discussed in the earlier sections. The simplest example of a nucleus interacting with a lattice in the strong coupling regime is the case of internal excitation of the deuteron coupled to highly excited optical phonon modes in PdD. In this case there are three spin states associated with the deuteron, two of which can undergo transitions to different upper states [22]. Most other examples involve coupling to many excited states (transitions in Pd or Ni), and also involve transitions in different isotopes. This provides us with motivation to examine more complicated versions of the model.

To reduce the complexity of the problem that results, we will restrict our attention to two specific issues in what follows: multiple excited states and different interacting systems. In doing so we defer the problem of multiple ground states interacting with common excited states, which makes things substantially more complicated. Our approach will be to focus first on the interaction of two three-level systems (with a single ground state and two unstable excited states) with a highly excited oscillator, as before in the limit that the transition energies are much greater than the characteristic oscillator energy. The analysis of this problem will allow us to generalize in a straightforward way to the case of many N-level systems interacting with a common oscillator, under the restriction that each has only a single ground state.

5.1. Model Hamiltonian

We can write a Hamiltonian for two sets of three-level systems interacting with an oscillator as

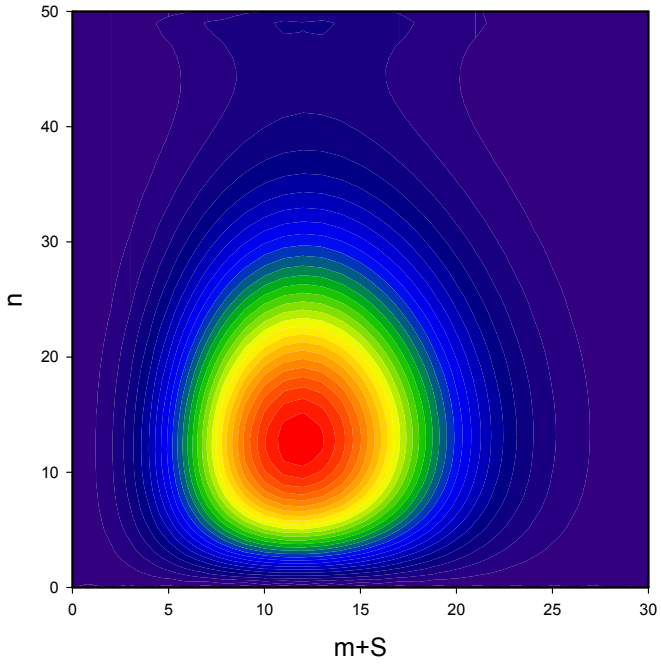

Figure 4. Exact lowest eigenfunction solution plotted as $c_{m,n}$ as a function of $m + S$ and n.

$$\begin{aligned}\hat{H} \;=\; & \sum_j \begin{pmatrix} E_1^{(1)} & 0 & 0 \\ 0 & E_2^{(1)} & 0 \\ 0 & 0 & E_3^{(1)} \end{pmatrix}_j + \sum_k \begin{pmatrix} E_1^{(2)} & 0 & 0 \\ 0 & E_2^{(2)} & 0 \\ 0 & 0 & E_3^{(2)} \end{pmatrix}_k + \hbar\omega_0 \hat{a}^\dagger \hat{a} \\ & + \sum_j \begin{pmatrix} 0 & V_{12}^{(1)} & V_{13}^{(1)} \\ V_{21}^{(1)} & 0 & V_{23}^{(1)} \\ V_{31}^{(1)} & V_{32}^{(1)} & 0 \end{pmatrix}_j (\hat{a} + \hat{a}^\dagger) + \sum_k \begin{pmatrix} 0 & V_{12}^{(2)} & V_{13}^{(2)} \\ V_{21}^{(2)} & 0 & V_{23}^{(2)} \\ V_{31}^{(2)} & V_{32}^{(2)} & 0 \end{pmatrix}_k (\hat{a} + \hat{a}^\dagger) \\ & - \frac{i\hbar}{2} \sum_j \begin{pmatrix} 0 & 0 & 0 \\ 0 & \hat{\gamma}_2^{(1)}(E) & 0 \\ 0 & 0 & \hat{\gamma}_3^{(1)}(E) \end{pmatrix}_j - \frac{i\hbar}{2} \sum_k \begin{pmatrix} 0 & 0 & 0 \\ 0 & \hat{\gamma}_2^{(2)}(E) & 0 \\ 0 & 0 & \hat{\gamma}_3^{(2)}(E) \end{pmatrix}_k - i\frac{\hbar\hat{\Gamma}(E)}{2}. \end{aligned} \tag{41}$$

Note that the notation appropriate for the three-level systems in this case is reversed relative to that of the two-level systems. One set of three-level systems is located at a set of sites denoted by the index j, and the other set of three-level systems is located at sites denoted by k. Single-phonon exchange transitions are included for both sets of three-level

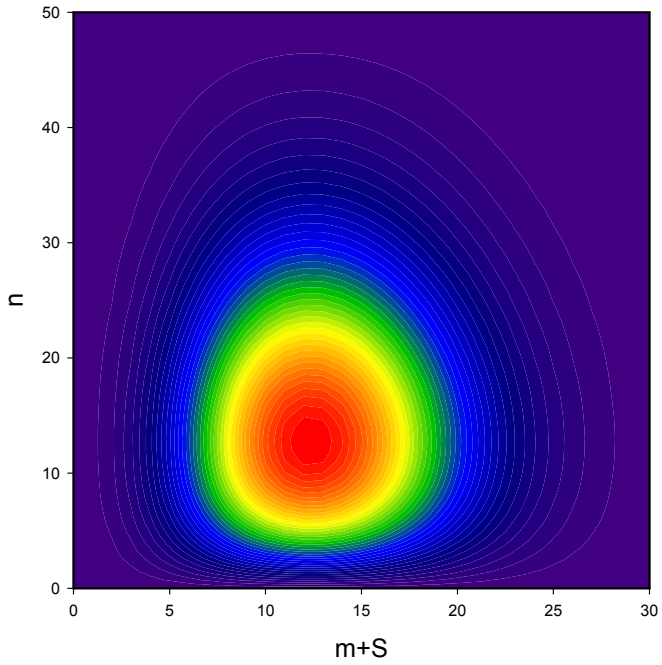

Figure 5. Approximate product lowest eigenfunction solution plotted as $c_{m,n}$ as a function of $m + S$ and n.

systems. Oscillator loss is included as before through a Brillouin–Wigner loss operator $-i\hbar\hat{\Gamma}(E)/2$; and we indicate the loss associated with the unstable upper states through appropriate $\hat{\gamma}(E)$ operators.

5.2. Expansion coefficients

This model is more complicated than the extension of the lossy spin–boson model considered in previous sections; however, we can reduce the complexity some by working with expansion coefficients. We assume a wavefunction for the coupled system of the form

$$\Psi = \sum_n \sum_{N_2^{(1)}} \sum_{N_3^{(1)}} \sum_{N_2^{(2)}} \sum_{N_3^{(2)}} c_{N_1^{(1)},N_2^{(1)},N_3^{(1)},N_1^{(2)},N_2^{(2)},N_3^{(2)},n} \left|N_1^{(1)}, N_2^{(1)}, N_3^{(1)}\right\rangle \left|N_1^{(2)}, N_2^{(2)}, N_3^{(2)}\right\rangle |n\rangle, \tag{42}$$

where the different $|N_1, N_2, N_3\rangle$ states are the generalization of Dicke states for the two three-level systems.

We are interested in developing solutions to the time-independent Schrödinger equation

$$E\Psi \;=\; \hat{H}\Psi. \tag{43}$$

In the case of the basis state expansion above this leads to an eigenvalue equation for the expansion coefficients which is of the form

$$\begin{aligned} E\, c_{N_1^{(1)},N_2^{(1)},N_3^{(1)},N_1^{(2)},N_2^{(2)},N_3^{(2)},n} \;=\; & \Big[E_1^{(1)}N_1^{(1)} + E_2^{(1)}N_2^{(1)} + E_3^{(1)}N_3^{(1)} \\ & + E_1^{(2)}N_1^{(2)} + E_2^{(2)}N_2^{(2)} + E_3^{(2)}N_3^{(2)} + n\hbar\omega_0\Big] c_{N_1^{(1)},N_2^{(1)},N_3^{(1)},N_1^{(2)},N_2^{(2)},N_3^{(2)},n} \\ & + V_{12}^{(1)}\sqrt{N_1^{(1)}(N_2^{(2)}+1)}\Big[\sqrt{n+1}c_{N_1^{(1)}+1,N_2^{(1)}-1,N_3^{(1)},N_1^{(2)},N_2^{(2)},N_3^{(2)},n+1} \\ & + \sqrt{n}c_{N_1^{(1)}+1,N_2^{(1)}-1,N_3^{(1)},N_1^{(2)},N_2^{(2)},N_3^{(2)},n-1}\Big] \\ & + V_{21}^{(1)}\sqrt{(N_1^{(1)}+1)N_2^{(2)}}\Big[\sqrt{n+1}c_{N_1^{(1)}-1,N_2^{(1)}+1,N_3^{(1)},N_1^{(2)},N_2^{(2)},N_3^{(2)},n+1} \\ & + \sqrt{n}c_{N_1^{(1)}-1,N_2^{(1)}+1,N_3^{(1)},N_1^{(2)},N_2^{(2)},N_3^{(2)},n-1}\Big] \\ & + \cdots, \end{aligned} \tag{44}$$

where the $\cdots$ denotes a very large number of interaction terms similar to the ones included, and where we include loss through appropriate boundary conditions as above.

5.3. Limit of large n, large $N_1^{(1)}$ and $N_1^{(2)}$

Even though we are interested in the strong coupling regime, we expect the occupation of the ground state to dominate for both sets of three-level systems. Since the interaction terms are present proportional to the appropriate Dicke factors (such as $\sqrt{(N_1^{(1)}+1)N_2^{(2)}}$) we see that interactions with the ground states will be favored. This suggests that we might simplify things by retaining only interactions involving ground states, and using the large N approximations

$$\sqrt{N_1+1} \;\rightarrow\; \sqrt{N_1}, \tag{45}$$

$$\sqrt{n+1} \;\rightarrow\; \sqrt{n_0}. \tag{46}$$

In addition, it will be convenient to adopt a phase convention in which all of the coupling matrix elements from ground states are real, so

$$V_{12} \;=\; V_{21} \quad \text{(real)}, \tag{47}$$

$$V_{13} \;=\; V_{31} \quad \text{(real)}. \tag{48}$$

This leads to an approximate eigenvalue equation of the form

$$
\begin{aligned}
E\, c_{N_1^{(1)},N_2^{(1)},N_3^{(1)},N_1^{(2)},N_2^{(2)},N_3^{(2)},n} \;=\; & \Big[E_2^{(1)} N_2^{(1)} + E_3^{(1)} N_3^{(1)} \\
& + E_2^{(2)} N_2^{(2)} + E_3^{(2)} N_3^{(2)} + n\hbar\omega_0 \Big] c_{N_1^{(1)},N_2^{(1)},N_3^{(1)},N_1^{(2)},N_2^{(2)},N_3^{(2)},n} \\
& + V_{12}^{(1)} \sqrt{n_0} \sqrt{N_1^{(1)}} \Bigg\{ \sqrt{N_2^{(2)}+1} \Big[c_{N_1^{(1)}+1,N_2^{(1)}-1,N_3^{(1)},N_1^{(2)},N_2^{(2)},N_3^{(2)},n+1} \\
& + c_{N_1^{(1)}+1,N_2^{(1)}-1,N_3^{(1)},N_1^{(2)},N_2^{(2)},N_3^{(2)},n-1} \Big] \\
& + \sqrt{N_2^{(2)}} \Big[c_{N_1^{(1)}-1,N_2^{(1)}+1,N_3^{(1)},N_1^{(2)},N_2^{(2)},N_3^{(2)},n+1} \\
& + c_{N_1^{(1)}-1,N_2^{(1)}+1,N_3^{(1)},N_1^{(2)},N_2^{(2)},N_3^{(2)},n-1} \Big] \Bigg\} \\
& + \cdots ,
\end{aligned}
\tag{49}
$$

where we have taken the ground state energy E_1 for the two three-level systems to be zero.

5.4. Approximate product solution

Based on the utility of the approximate product solution described above, we would like to generalize it to the present case. We consider an approximate product solution of the form

$$
c_{N_1^{(1)},N_2^{(1)},N_3^{(1)},N_1^{(2)},N_2^{(2)},N_3^{(2)},n} \;=\; (-1)^{N_1^{(1)}+N_2^{(1)}+N_1^{(2)}+N_2^{(2)}} a^{(1)}_{N_2^{(1)}} b^{(1)}_{N_3^{(1)}} a^{(2)}_{N_2^{(2)}} b^{(2)}_{N_3^{(2)}} u_n . \tag{50}
$$

There are selection rules for the expansion coefficients (half of them are zero) as was the case for the two-level version of the problem considered above. Within the product wavefunction approximation we lose the selection rule, but we face no difficulties with this in applications later on. It is possible to impose selections rule once the various terms in the product wavefunction are optimized if needed.

5.5. Variational principle

To proceed, we would like to optimize the product solution based on a variational principle. We begin by considering the variational principle associated with the original expansion coefficients $c_{N_1^{(1)},N_2^{(1)},N_3^{(1)},N_1^{(2)},N_2^{(2)},N_3^{(2)},n}$. We write

$$
\begin{aligned}
I \;=\; & \sum_n \sum_{N_2^{(1)}} \sum_{N_3^{(1)}} \sum_{N_2^{(2)}} \sum_{N_3^{(2)}} \Big[E_2^{(1)} N_2^{(1)} + E_3^{(1)} N_3^{(1)} \\
& + E_2^{(2)} N_2^{(2)} + E_3^{(2)} N_3^{(2)} + n\hbar\omega_0 \Big] c^2_{N_1^{(1)},N_2^{(1)},N_3^{(1)},N_1^{(2)},N_2^{(2)},N_3^{(2)},n} \\
& + V_{12}^{(1)} \sqrt{n_0} \sqrt{N_1^{(1)}} \sum_n \sum_{N_2^{(1)}} \sum_{N_3^{(1)}} \sum_{N_2^{(2)}} \sum_{N_3^{(2)}} \Big\{ \sqrt{N_2^{(2)}+1}\, c_{N_1^{(1)},N_2^{(1)},N_3^{(1)},N_1^{(2)},N_2^{(2)},N_3^{(2)},n} \\
& \Big[c_{N_1^{(1)}+1,N_2^{(1)}-1,N_3^{(1)},N_1^{(2)},N_2^{(2)},N_3^{(2)},n+1} + c_{N_1^{(1)}+1,N_2^{(1)}-1,N_3^{(1)},N_1^{(2)},N_2^{(2)},N_3^{(2)},n-1} \Big] \\
& + \sqrt{N_2^{(2)}}\, c_{N_1^{(1)},N_2^{(1)},N_3^{(1)},N_1^{(2)},N_2^{(2)},N_3^{(2)},n} \\
& \Big[c_{N_1^{(1)}-1,N_2^{(1)}+1,N_3^{(1)},N_1^{(2)},N_2^{(2)},N_3^{(2)},n+1} + c_{N_1^{(1)}-1,N_2^{(1)}+1,N_3^{(1)},N_1^{(2)},N_2^{(2)},N_3^{(2)},n-1} \Big] \Big\} \\
& + \cdots
\end{aligned}
\tag{51}
$$

subject to

$$
\sum_n \sum_{N_2^{(1)}} \sum_{N_3^{(1)}} \sum_{N_2^{(2)}} \sum_{N_3^{(2)}} c^2_{N_1^{(1)},N_2^{(1)},N_3^{(1)},N_1^{(2)},N_2^{(2)},N_3^{(2)},n} \;=\; 1 \tag{52}
$$

Based on this, we consider the optimization of the product wavefunction based on

$$
\begin{aligned}
J \;=\; & \sum_{N_2^{(1)}} E_2^{(1)} [a^{(1)}_{N_2^{(1)}}]^2 + \sum_{N_3^{(1)}} E_3^{(1)} [b^{(1)}_{N_3^{(1)}}]^2 + \sum_{N_2^{(2)}} E_2^{(2)} [a^{(2)}_{N_2^{(2)}}]^2 + \sum_{N_3^{(2)}} E_3^{(2)} [b^{(2)}_{N_3^{(2)}}]^2 + \sum_n \hbar\omega_0 n u_n^2 \\
& - V_{12}^{(1)} \sqrt{n_0} \sqrt{N_1^{(1)}} \sum_{N_2^{(1)}} a^{(1)}_{N_2^{(1)}} \Big(\sqrt{N_2^{(1)}+1}\, a^{(1)}_{N_2^{(1)}+1} + \sqrt{N_2^{(1)}}\, a^{(1)}_{N_2^{(1)}-1} \Big) \sum_n u_n \Big(u_{n+1} + u_{n-1} \Big) \\
& - V_{13}^{(1)} \sqrt{n_0} \sqrt{N_1^{(1)}} \sum_{N_3^{(1)}} b^{(1)}_{N_3^{(1)}} \Big(\sqrt{N_3^{(1)}+1}\, b^{(1)}_{N_3^{(1)}+1} + \sqrt{N_3^{(1)}}\, b^{(1)}_{N_3^{(1)}-1} \Big) \sum_n u_n \Big(u_{n+1} + u_{n-1} \Big) \\
& - V_{12}^{(2)} \sqrt{n_0} \sqrt{N_1^{(2)}} \sum_{N_2^{(2)}} a^{(2)}_{N_2^{(2)}} \Big(\sqrt{N_2^{(2)}+1}\, a^{(2)}_{N_2^{(2)}+1} + \sqrt{N_2^{(2)}}\, a^{(2)}_{N_2^{(2)}-1} \Big) \sum_n u_n \Big(u_{n+1} + u_{n-1} \Big) \\
& - V_{13}^{(2)} \sqrt{n_0} \sqrt{N_1^{(2)}} \sum_{N_3^{(2)}} b^{(2)}_{N_3^{(2)}} \Big(\sqrt{N_3^{(2)}+1}\, b^{(2)}_{N_3^{(2)}+1} + \sqrt{N_3^{(2)}}\, b^{(2)}_{N_3^{(2)}-1} \Big) \sum_n u_n \Big(u_{n+1} + u_{n-1} \Big)
\end{aligned}
\tag{53}
$$

subject to

$$
\sum_{N_2^{(1)}} [a^{(1)}_{N_2^{(1)}}]^2 \;=\; 1, \qquad \sum_{N_3^{(1)}} [b^{(1)}_{N_3^{(1)}}]^2 \;=\; 1, \tag{54}
$$

$$\sum_{N_2^{(2)}} [a^{(2)}_{N_2^{(2)}}]^2 \;=\; 1, \qquad \sum_{N_3^{(2)}} [b^{(2)}_{N_3^{(2)}}]^2 \;=\; 1, \tag{55}$$

$$\sum_n u_n^2 \;=\; 1. \tag{56}$$

5.6. Optimization of the product wavefunction

We use the variational principle to optimize the approximate product wavefunction, and we obtain constraints of the form

$$\lambda_a a_{N_2} \;=\; E_2 a_{N_2} - V_{12}\sqrt{n_0}\sqrt{N_1}\left[\sum_n u_n(u_{n+1}+u_{n-1})\right]\left[\sqrt{N_2+1}a_{N_2+1} + \sqrt{N_2}a_{N_2-1}\right], \tag{57}$$

$$\lambda_b b_{N_3} \;=\; E_3 b_{N_3} - V_{13}\sqrt{n_0}\sqrt{N_1}\left[\sum_n u_n(u_{n+1}+u_{n-1})\right]\left[\sqrt{N_3+1}b_{N_3+1} + \sqrt{N_3}b_{N_3-1}\right], \tag{58}$$

where there are one of each constraint for the two different sets of three-level systems. In addition, we end up with a constraint for u_n of the form

$$\begin{aligned}
\lambda_u u_n \;=\; \hbar\omega_0 u_n - \Bigg[& V^{(1)}_{12}\sqrt{n_0}\sqrt{N_1^{(1)}} \sum_{N_2^{(1)}} a^{(1)}_{N_2^{(1)}} \left(\sqrt{N_2^{(1)}+1}\,a^{(1)}_{N_2^{(1)}+1} + \sqrt{N_2^{(1)}}\,a^{(1)}_{N_2^{(1)}-1}\right) \\
& + V^{(1)}_{13}\sqrt{n_0}\sqrt{N_1^{(1)}} \sum_{N_3^{(1)}} b^{(1)}_{N_3^{(1)}} \left(\sqrt{N_3^{(1)}+1}\,b^{(1)}_{N_3^{(1)}+1} + \sqrt{N_3^{(1)}}\,b^{(1)}_{N_3^{(1)}-1}\right) \\
& + V^{(2)}_{12}\sqrt{n_0}\sqrt{N_1^{(2)}} \sum_{N_2^{(2)}} a^{(2)}_{N_2^{(2)}} \left(\sqrt{N_2^{(2)}+1}\,a^{(2)}_{N_2^{(2)}+1} + \sqrt{N_2^{(2)}}\,a^{(2)}_{N_2^{(2)}-1}\right) \\
& + V^{(2)}_{13}\sqrt{n_0}\sqrt{N_1^{(2)}} \sum_{N_3^{(2)}} b^{(2)}_{N_3^{(2)}} \left(\sqrt{N_3^{(2)}+1}\,b^{(2)}_{N_3^{(2)}+1} + \sqrt{N_3^{(2)}}\,b^{(2)}_{N_3^{(2)}-1}\right)\Bigg](u_{n+1}+u_{n-1}).
\end{aligned} \tag{59}$$

We can implement the loss model in this case by omitting u_n for $n < 0$, and adopting the boundary condition

$$u_0 \;=\; 0. \tag{60}$$

5.7. Discussion

Although we started out with a rather complicated model, within the framework of the product wavefunction approximation we have obtained a set of constraints that are closely connected with what we obtained above for the two-level system version of the problem. In connection with each excited state we end up with a constraint of the form

$$\lambda_a a_N \;=\; \Delta E a_N - V\sqrt{n_0}\sqrt{N_1}\Big[\sum_n u_n(u_{n+1}+u_{n-1})\Big]\Big[\sqrt{N+1}a_{N+1}+\sqrt{N}a_{N-1}\Big]. \tag{61}$$

We expect this to be true even for systems more complicated than three-level systems, and also if there are more than two different sets.

In connection with the oscillator, we obtain a constraint that we might write as

$$\lambda_u u_n \;=\; \hbar\omega_0 u_n - \Bigg[\sum_\beta \sqrt{N_1^{(\beta)} n_0}\;\sum_\kappa V_{1\kappa}^{(\beta)} \sum_{N_\kappa^{(\beta)}} a^{(\beta)}_{N_\kappa^{(\beta)}}\Big(\sqrt{N_\kappa^{(\beta)}+1}\;a^{(\beta)}_{N_\kappa^{(\beta)}+1}+\sqrt{N_\kappa^{(\beta)}}\;a^{(\beta)}_{N_\kappa^{(\beta)}-1}\Big)\Bigg](u_{n+1}+u_{n-1}). \tag{62}$$

The spreading of the oscillator distribution in this model is determined by contributions from all of the different isotopes (denoted by β), with individual contributions over the different excited states of each isotope (denoted by κ). To obtain the contributions in each case, we need to sum over the appropriate excited state distribution (denoted by $N_\kappa^{(\beta)}$).

6. Approximation for the Oscillator Distribution

In the applications of the model that will follow, we will be most interested in estimates for the oscillator distribution given a particular set of nuclei and a specific excitation of the oscillator (in terms of n_0). From the discussion of the previous section we can solve self-consistently for the excited state distributions and oscillator distribution, although it requires some effort to do so.

It would be useful to develop simpler analytic estimates in connection with the product solution above in order to gain a better understanding of how the contributions of the different transitions in the various isotopes spread the oscillator distribution. We recognize two features of the constraints associated with the product model in the strong coupling limit that can lead to a simplification. In the strong coupling regime the oscillator distribution is slowly varying, and we can use this to isolate the different constraints that pertain to the excited state distribution. Additionally, we recognize that we do not actually need explicit solutions for the excited state distributions; instead we only need an estimate for the average off-diagonal transition matrix element. We can use these to develop a specific solution for the oscillator distribution directly from a knowledge of the transition parameters. We will pursue these ideas in what follows.

6.1. Isolation of the excited state distributions

In the strong coupling regime the oscillator distribution will be spread out over a great many oscillator states, and from earlier work we know that when a product wavefunction is used the u_n distribution will be slowly varying so that

$$u_{n\pm1} \;\approx\; u_n. \tag{63}$$

In this case we can write

$$\sum_n u_n(u_{n+1}+u_{n-1}) \;=\; 2\sum_n u_n^2 \;=\; 2. \tag{64}$$

Each constraint associated with the excited state distributions in this case can then be dealt with separately, and is described through

$$\lambda_a a_N \;=\; \Delta E a_N - 2V\sqrt{n_0}\sqrt{N_1}\Big[\sqrt{N+1}\,a_{N+1} + \sqrt{N}\,a_{N-1}\Big]. \tag{65}$$

This is potentially interesting, since the distribution ultimately depends on a single parameter; we can recast this constraint in the form

$$\lambda'_a a_N \;=\; a_N - 2g_a\Big[\sqrt{N+1}\,a_{N+1} + \sqrt{N}\,a_{N-1}\Big] \tag{66}$$

with $\lambda'_a = \lambda_a/\Delta E$, and where g_a is defined as

$$g_a \;=\; \frac{V\sqrt{n_0}\sqrt{N_1}}{\Delta E}. \tag{67}$$

6.2. Estimate for the contribution of each excited state

As a practical matter, we don't require the excited state distributions in order to solve for the oscillator distribution; instead, we require the sum

$$f(g_a) \;=\; \sum_N a_N\Big(\sqrt{N+1}\,a_{N+1} + \sqrt{N}\,a_{N-1}\Big). \tag{68}$$

This can be evaluated directly from a numerical solution of the constraint equation; we find

$$f(g_a) \;=\; 4g_a. \tag{69}$$

We can use this to write for the oscillator distribution

$$\lambda_u u_n \;=\; \hbar\omega_0 u_n - \Big[\sum_\beta \sum_\kappa \frac{4[V_{1\kappa}^{(\beta)}]^2 n_0 N_1^{(\beta)}}{E_\kappa^{(\beta)}}\Big](u_{n+1} + u_{n-1}). \tag{70}$$

We see that the oscillator distribution in this model depends only on a single parameter; we may write

$$\lambda'_u u_n \;=\; u_n - 2g_u(u_{n+1} + u_{n-1}), \tag{71}$$

where $\lambda'_u = \lambda_u/\hbar\omega_0$, and where the dimensionless coupling strength appropriate to the oscillator distribution is

$$g_u \;=\; \sum_\beta \sum_\kappa \frac{2[V_{1\kappa}^{(\beta)}]^2 n_0 N_1^{(\beta)}}{\hbar\omega_0 E_\kappa^{(\beta)}}. \tag{72}$$

In this summation β indicates the isotope and κ indicates the transition within the isotope.

6.3. Continuum approximation

This model will be most interesting to us in connection with coherent energy exchange under conditions that a great many oscillator quanta are exchanged. In this case the spread in the oscillator distribution will be very large, and this motivates us to pursue a continuum approximation. We can adopt a continuum approximation using

$$\text{discrete } n \;\rightarrow\; \text{continuous } n, \tag{73}$$

$$u_n \;\rightarrow\; u(n). \tag{74}$$

We can use this to write

$$u_{n+1} + u_{n-1} \;\rightarrow\; u(n+1) + u(n-1) \;=\; 2u(n) + \frac{\mathrm{d}^2}{\mathrm{d}n^2}u(n) + \cdots \tag{75}$$

The continuous version of the eigenvalue equation becomes

$$\lambda' u(n) \;=\; nu(n) - 4g_u u(n) - 2g_u \frac{\mathrm{d}^2}{\mathrm{d}n^2}u(n). \tag{76}$$

We can solve this analytically to obtain an unnormalized oscillator wavefunction

$$u(n) \;=\; \mathrm{Ai}\left(\frac{n}{(2g_u)^{\frac{1}{3}}} - 2.33810\right) \quad \text{for } n \geq 0, \tag{77}$$

$$\lambda' \;=\; -4g_u. \tag{78}$$

The constant offset 2.33810 here is intended to make the Airy function be zero for incremental $n = 0$. For $n < 0$ the oscillator states in this approximation are omitted.

7. Donor and Receiver Model with Unstable Receiver States

The reviewer noted that it was unclear from the discussion presented so far how the model connects with earlier work, and what impact it might have on cold fusion models. In our view the impact is enormous; however, it will take some further discussion beyond what we can do in this paper to make clear quite how important the result is. However, one thing that can be done, given the present result, is to consider the impact of the new model on the donor and receiver model presented previously [9].

7.1. Brief review of the donor and receiver model

The first indication that a large quantum could be fractionated with a substantial associated rate for coherent energy exchange came with the introduction of the lossy spin–boson model. With strong coupling between a set of two-level systems and an oscillator, and with loss in the vicinity of the two-level transition energy, the lossy spin–boson model predicts coherent energy exchange between the two systems under conditions of resonance. The absence of energetic particle emission commensurate with the excess energy produced in the Fleischmann–Pons experiment underscores the

need for such a mechanism, and we have been optimistic now for more than a decade that lossy spin–boson models could lead to a fundamental understanding of the new physical mechanism.

However, the experiments seem to point to ^{4}He as a product, perhaps with 24 MeV energy release per atom, which seems consistent with the mass difference between two deuterons and the ^{4}He nucleus. Because of Coulomb repulsion between the two deuterons, we would expect the phonon exchange matrix element for the $D_2/^4$He transition to be very small under any reasonable set of assumptions. We could not make use of the lossy spin–boson model directly for a D_2 to ^{4}He transition. This motivated us to introduce the donor and receiver generalization of the lossy spin–boson model.

In the donor and receiver model, the donor two-level systems are assumed to be weakly coupled to the oscillator (consistent with the $D_2/^4$He transition), and the receiver two-level systems are strongly coupled with the oscillator in order to accomplish the fractionation of the large quantum as a lossy spin–boson model. The associated Hamiltonian is [9]

$$\hat{H} \;=\; \Delta E_1 \frac{\hat{S}_z^{(1)}}{\hbar} + \Delta E_2 \frac{\hat{S}_z^{(2)}}{\hbar} + \hbar\omega_0 \hat{a}^\dagger \hat{a} + V_1 e^{-G}(\hat{a}^\dagger + \hat{a}) \frac{2\hat{S}_x^{(1)}}{\hbar} + V_2(\hat{a}^\dagger + \hat{a}) \frac{2\hat{S}_x^{(2)}}{\hbar} - i\frac{\hbar}{2}\hat{\Gamma}(E). \tag{79}$$

The analysis of the model was based on the fact that the donor coupling is very weak, as indicated by the e^{-G} Gamow factor in association with the donor coupling term in the model. As a result, we worked with basis states of the coupled receiver and oscillator model, which were available from the earlier analysis of the lossy spin–boson model. The donor coupling could then be treated simply using perturbation theory, relying on transitions between the different lossy spin–boson states of the coupled receiver and oscillator system to describe the coherent energy exchange associated with sequential resonant donor transitions.

The dynamics of the donor system that results can be described in the classical limit by

$$\frac{\mathrm{d}^2}{\mathrm{d}t^2} m_1(t) \;=\; \frac{2}{\hbar^2} \frac{\mathrm{d}}{\mathrm{d}m_1} [V_1^{\mathrm{eff}}]^2, \tag{80}$$

where m_1 describes the donor excitation, and where V_1^{eff} is the indirect coupling matrix element for a resonant donor transition, where the coupled oscillator and receiver transition take up the donor energy. This indirect coupling matrix element was found to be

$$V_1^{\mathrm{eff}} \;=\; 2V_1\sqrt{n}\,\mathrm{e}^{-G} |\langle v_n(\phi_2) | v_{n+\Delta n_1}(\phi_2)\rangle| \sqrt{S_1^2 - m_1^2}. \tag{81}$$

Significant in this equation is that the indirect coupling matrix element is proportional to the magnitude of the overlap matrix element between two lossy spin–boson states (which is a weak function of the phase angle ϕ_2).

7.2. Subdivision in the donor and receiver model

Since some time has passed since the donor and receiver model was published, it seems helpful to update the discussion to take advantage of the pulse and amplitude approximation for the lossy spin–boson model [21]. As was noted in [9] the donor and receiver model describes a subdivision effect, so that we can think of the donor transition energy ΔE_1 as being split among many receiver transitions, each with an energy of ΔE_2, plus an offset energy that accounts for the mismatch. For this we may write

$$\Delta E_1 \;=\; \Delta N \Delta E_2 + \delta E, \tag{82}$$

where ΔN receiver excitations can be associated with a donor transition. For this case, we can make use of the pulse and amplitude approximation to estimate

$$|\langle v_n(\phi_2)|v_{n+\Delta n_1}(\phi_2)\rangle| \;=\; f\left(\frac{\delta E}{(2g_u)^{1/3}\hbar\omega_0}\right) f\left(\frac{\Delta N}{(2g_a)^{1/3}}\right), \tag{83}$$

where for the lossy spin–boson model with stable upper states for the receiver the two dimensionless coupling constants are

$$g_u \;=\; \left(\frac{V_2\sqrt{n}}{\hbar\omega_0}\right)\sqrt{S_2^2-m_2^2} \qquad \text{(stable)}, \tag{84}$$

$$g_a \;=\; \left(\frac{V_2\sqrt{n}}{\Delta E_2}\right)\sqrt{S_2^2-m_2^2} \qquad \text{(stable)}, \tag{85}$$

where we have indicated that these pulse and amplitude approximation parameters are for the lossy spin–boson model with stable upper states. The hindrance factor $f(y)$ is defined by

$$f(y) \;=\; \frac{\displaystyle\int_{-2.33810}^{\infty} \mathrm{Ai}(x)\mathrm{Ai}(x+y)\mathrm{d}x}{\displaystyle\int_{-2.33810}^{\infty} \mathrm{Ai}^2(x)\mathrm{d}x}. \tag{86}$$

This function is illustrated in Fig. 6.

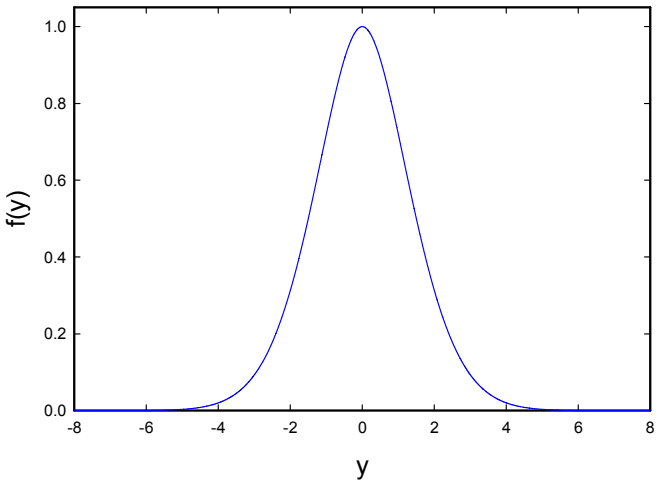

Figure 6. Plot of $f(y)$ as a function of y.

7.3. Donor and receiver model, lossy upper states

In light of the discussion of the previous sections of this paper, we are motivated to consider how the donor and receiver model would be modified were we to use receiver transitions with unstable upper states. In this case we might write the model as

$$\begin{aligned}\hat{H} \;=\; & \left(\Delta E_1 \frac{\hat{S}_z^{(1)}}{\hbar}\right)_{\rm stable} + \left(\Delta E_2 \frac{\hat{S}_z^{(2)}}{\hbar}\right)_{\rm unstable} + \hbar\omega_0 \hat{a}^\dagger \hat{a} \\ & + V_1 {\rm e}^{-G}(\hat{a}^\dagger + \hat{a}) \frac{2\hat{S}_x^{(1)}}{\hbar} + V_2(\hat{a}^\dagger + \hat{a}) \frac{2\hat{S}_x^{(2)}}{\hbar} - i\frac{\hbar}{2}\hat{\Gamma}(E)\end{aligned} \tag{87}$$

to make clear that the upper state of the donor transition is stable, and the upper state of the receiver transition is unstable. Otherwise, the analysis of the model would be very similar. Since the coupling with the donor is very weak, we would compute the states of the coupled unstable receiver and oscillator model

$$E_n \Phi_n \;=\; \left\{\left(\Delta E_2 \frac{\hat{S}_z^{(2)}}{\hbar}\right)_{\rm unstable} + \hbar\omega_0 \hat{a}^\dagger \hat{a} + V_2(\hat{a}^\dagger + \hat{a}) \frac{2\hat{S}_x^{(2)}}{\hbar} - i\frac{\hbar}{2}\hat{\Gamma}(E)\right\}\Phi_n. \tag{88}$$

Then we would make use of perturbation theory to develop an approximation for the indirect coupling matrix element. In the end, we obtain

$$V_1^{\rm eff} \;=\; 2V_1\sqrt{n}\;{\rm e}^{-G} |\langle \Phi_n | \Phi_{n+\Delta n_1}\rangle| \sqrt{S_1^2 - m_1^2}. \tag{89}$$

We can make use of the pulse and amplitude approximation for the unstable case for the approximation

$$|\langle \Phi_n | \Phi_{n+\Delta n_1}\rangle| \;=\; f\left(\frac{\Delta n_1}{(2g_u)^{1/3}}\right). \tag{90}$$

In this case there is no subdivision or offset energy; the receiver transition with the unstable upper state has to accept all of the donor energy, or else no transition occurs. In this case we may write

$$g_u \;=\; \left(\frac{2V_2^2 n}{\hbar\omega_0 \Delta E_2}\right)(2S_2) \qquad ({\rm unstable,\ two-level}). \tag{91}$$

7.4. Further generalization of the model

In the event that we have more complicated receiver systems that are not described by simple two-level systems, with many transitions in each isotope, with many different isotopes, and perhaps with different spin states of the different isotopes, then we can make use of the results in the earlier sections to write

$$|\langle \Phi_n | \Phi_{n+\Delta n_1}\rangle| \;=\; f\left(\frac{\Delta n_1}{(2g_u)^{1/3}}\right) \tag{92}$$

with

$$g_u = \sum_\beta \sum_\kappa \frac{2[V_{1\kappa}^{(\beta)}]^2 n_0 N_1^{(\beta)}}{\hbar\omega_0 E_\kappa^{(\beta)}} \qquad \text{(general unstable case)}. \tag{93}$$

In this case the sum is over all receiver nuclei (κ) and all receiver transitions in each nucleus (β).

7.5. Discussion

When we found the new relativistic coupling mechanism presented in [13] our initial response was to assume that every transition in every nucleus in the lattice would contribute to the fractionation in the way described by the models outlined in this section. Since most of the coupling strength occurs for transitions with unstable upper states, the total amount of excitation is small, so the analytic approximation described in Section 6 will be applicable. In a sense this appeared to provide a simple and perhaps elegant extension of the donor and receiver model that could be adapted for the coupling of the physical system.

After we worked out the calculations outlined above, we used realistic estimates for the coupling matrix elements to estimate fractionation within the model; unfortunately, we found that essentially no fractionation occurs in this model. At first this seemed to be a crushing blow, as we had been very optimistic about the model, and it did not seem obvious what could be done to salvage the model. As we have noted at various conferences, we have analyzed a very large number of models and variants, in each case so far coming to the conclusion that the model was not consistent with experiment; consequently, it is not a rare occurrence to prove that a given model isn't right in this sense.

As mentioned in the Introduction, these negative results motivated us to seek a modification of the approach which might breathe life back into the models, which was done under the gun in preparing for ICCF17. The result of this effort was the development of a new kind of model which takes advantage of both unstable and stable transitions, and which appears to give results that have a nontrivial connection with experiment [14,15]. The new model is closely related to those under discussion in this section. We will described the new model and results obtained with it in more detail in following publications.

8. Discussion and Conclusions

We have analyzed an extension of the lossy spin–boson model where the upper state of the two-level system is unstable, assuming as before that the loss where important is taken to be infinite. The unstable upper states are taken into account in this model by restricting the available oscillator states to include only basis states above a fixed threshold, in order to prevent energy exchange from the oscillator to cause any real excitation of the two-level systems.

A key feature of the earlier lossy spin–boson model was that coherent energy exchange between the two-level systems and oscillator could occur at a rate orders of magnitude greater than expected for the (lossless) spin–boson model. Since the upper states are unstable in this model, there is no equivalent coherent energy exchange leading to real (as opposed to virtual) excitation of the two-level systems. Instead we find a simpler mixing of the degrees of freedom, and our focus has been on the ground state of the coupled system which we expect to be produced during the (adiabatic) evolution of the system as an increase in oscillator excitation results in stronger coupling between the two degrees of freedom.

In physical systems that motivate our interest in this kind of model there are present different isotopes, different spin states for the ground state of a given isotope, and in general many excited states which can be coupled to with phonon exchange. As a result we considered a generalization of the model suitable for analyzing these more complicated, but more relevant, physical systems. When many such identical nuclei are present, we find from the associated Dicke factors that the strongest transitions couple to and from ground states, which greatly simplifies the problem. We used a product

solution approximation for this model, which allowed us to determine constraints for the excited state distributions and for the distribution of oscillator states. We are able to develop a useful analytic continuum model for the oscillator distribution based on this approach.

Stimulated by reviewer comments, we considered how the donor and receiver model is changed when the receiver transition has an unstable upper state. In the original donor and receiver model it was possible to subdivide the large donor quantum into many donor excitations, with an offset energy to be fractionated by the receiver; in the new version of the model subdivision is no longer since there can be no real excitation of the receiver transitions. We summarized results in terms of the equivalent classical evolution of the donor system, which depends on the strength of the receiver coupling in order to make transitions.

As discussed above a major motivation of this modeling effort has been to identify receiver transitions within the context of the donor and receiver model with sufficiently strong coupling to be able to fractionate a 24 MeV quantum in connection with the Fleischmann–Pons experiment. We had hoped that the new relativistic interaction described in [13] would lead to a large enough coupling to do the job. Since the strongest coupling with this interaction occurs for transitions with very highly excited nuclear states that are very unstable, we were motivated to carry out the analysis of the model described in this paper. However, using this new model for the receiver in the donor and receiver model does not solve the problem. There are no transitions with sufficiently strong coupling that can fractionate the 24 MeV (under conditions relevant to experiment) required to make a connection with the Fleischmann–Pons experiment. As a result, we end up with the conclusion that the basic donor and receiver model does not describe the excess heat effect in these experiments; we need a stronger model to account for the experimental results. Fortunately, such a model has been found recently [14,15], and will be discussed further in a following paper.

Appendix A. Loss Models

A reviewer has expressed concern that the inclusion of loss in the Hamiltonian has the potential to lead to difficulties, and that there exist other loss models in the literature (such as the Caldirola–Kanai model [23,24]) that might be used instead. This in our view is an important comment, and it seems appropriate to take the opportunity in this Appendix to discuss oscillator loss models briefly, and to consider loss models we are interested in.

Appendix A.1. Approaches to oscillator loss in the literature

Since the lossy oscillator constitutes the prototypical example of a dissipative system, it is no surprise that there appear a great many papers addressed to the problem. Within the general area, there are a number of specific topics that focus on aspects of the problem: such as how one quantizes a dissipative system [23,24]; simple models that are useful for analytic calculations [25,26]; general models used for modeling specific physical systems [27,28]; and advanced mathematical approaches available for analyzing such problems [29]. Our focus in the discussion here will be on the simple and more general loss models, since the other topics are not relevant to what we have presented in this paper, or in earlier papers.

Appendix A.2. Standard loss models

One can find models in the literature in which loss is taken into account coupling to a bath of oscillators; in the case of a lossy oscillator we might adopt a Hamiltonian of the form [30]

$$\hat{H} \;=\; \hbar\omega_0\hat{a}^\dagger\hat{a} + \sum_j \hbar\omega_j\hat{b}_j^\dagger\hat{b}_j + \sum_j K_j(\hat{a}+\hat{a}^\dagger)(\hat{b}_j+\hat{b}_j^\dagger). \tag{A.1}$$

The reference oscillator in this case has frequency ω_0 and creation and annihilation operators $\hat{a}^\dagger$ and $\hat{a}$; the oscillators that make up the bath would have frequencies ω_j in the vicinity of ω_0, and we have used $\hat{b}_j^\dagger$ and $\hat{b}_j$ for the associated creation and annihilation operators. This model relies on linear coupling between the reference and bath oscillators to provide loss. A related model based on a two-level system coupled to a bath of oscillators is considered in [31].

Used less often are models where a bath of two-level systems is adopted rather than a bath of oscillators. In this case we might consider a Hamiltonian based on

$$\hat{H} \;=\; \hbar\omega_0\hat{a}^\dagger\hat{a} + \sum_j \Delta E_j \left(\frac{\hat{s}_z}{\hbar}\right)_j + \sum_j K_j(\hat{a}+\hat{a}^\dagger)\left(\frac{2\hat{s}_x}{\hbar}\right)_j . \tag{A.2}$$

Here the bath is described using many site-dependent pseudo-spin operators $\hat{s}_x$ and $\hat{s}_z$. Note that in both cases, the basic model is explicitly Hermitian. Loss comes about from the interaction of the reference oscillator with a bath of oscillators or two-level systems that have a frequency distribution which can be chosen to match any physical loss process of interest.

The basic idea in such models is that the oscillator that is being focused on can lose energy by phonon exchange with a bath, one quantum at a time, eventually reaching thermal equilibrium with the bath. The problem simplifies if the bath is taken to be at zero temperature, in which case the oscillator eventually decays to the ground state.

Appendix A.3. Caldirola–Kanai model

The Caldirola–Kanai model is a much simpler model based on an oscillator with a dynamical mass, such as

$$\hat{H} \;=\; \frac{\hat{p}^2}{2m(t)} + \frac{1}{2}m(t)\omega_0^2x^2 \;=\; \mathrm{e}^{-\gamma t}\frac{\hat{p}^2}{2m} + \mathrm{e}^{\gamma t}\frac{1}{2}m\omega_0^2x^2. \tag{A.3}$$

The increasing mass in this case causes a reduction in velocity, which mimics dissipative loss in the sense that the expectation value of position satisfies

$$\frac{\mathrm{d}^2}{\mathrm{d}t^2}\langle x\rangle + \gamma\frac{\mathrm{d}}{\mathrm{d}t}\langle x\rangle \;=\; -m\omega_0^2\langle x\rangle. \tag{A.4}$$

A nice feature of the model is that one can develop generalized classical states for it analytically, which makes it convenient for analyzing forced lossy oscillator models approximately. This model is widely used in the literature. There are technical issues associated with the model, as the "loss" is due to a mass increase rather than dissipation so that the uncertainty relation is not obeyed as time goes to infinity [32].

One could imagine making use of such a simple model to account for conventional oscillator loss in the models that we have studied (and based on the reviewer's comment, this may be a project to pursue in the future). Unfortunately, we would not expect it to be relevant to the loss which is responsible for the enhanced coherent energy exchange effect in the many-quantum regime that we have focused our efforts on, since it relies on a dynamical mass to mimic loss rather than modeling higher-energy loss processes (as we will discuss further below).

Appendix A.4. Spin–boson model without loss

To discuss loss in our lossy-spin boson models, the best place to start is with a spin–boson model first without loss; we write

$$\hat{H} \;=\; \hbar\omega_0\hat{a}^\dagger\hat{a} + \Delta E\frac{\hat{S}_z}{\hbar} + V\frac{2\hat{S}_x}{\hbar}(\hat{a}^\dagger + \hat{a}). \tag{A.5}$$

In the absence of coupling ($V = 0$), then the resulting states will be pure oscillator and two level system states of the form

$$\Psi \;=\; |S, m\rangle|n\rangle. \tag{A.6}$$

When we begin to turn on the interaction, so that V is small but finite, then we would expect that the pure eigenstate will develop a small admixture of nearby states. In this case we would write approximately

$$\begin{aligned}\Psi \;=\; & c_0|S, m\rangle|n\rangle \\ & + c_1|S, m-1\rangle|n-1\rangle + c_2|S, m-1\rangle|n+1\rangle + c_3|S, m+1\rangle|n-1\rangle + c_4|S, m+1\rangle|n+1\rangle.\end{aligned} \tag{A.7}$$

We see that the pure $|S, m\rangle|n\rangle$ state now will have a small admixture of states with $m \pm 1$. We would expect the state energy to be near the pure state energy

$$E_{m,n} \;=\; m\Delta E + n\hbar\omega_0. \tag{A.8}$$

For the admixed states with $m - 1$, the basis state energies are much lower than E since we assume that

$$\Delta E \;\gg\; \hbar\omega_0. \tag{A.9}$$

In the absence of loss channels this superposition presents no problem, and we view the admixed states simply as providing an off-resonant (virtual) contribution.

Appendix A.5. Spin–boson model with loss

However, things change dramatically when we augment the model with loss. Suppose we augment the spin–boson model with a bath of oscillators, consistent with

$$\hat{H} \;=\; \hbar\omega_0\hat{a}^\dagger\hat{a} + \Delta E\frac{\hat{S}_z}{\hbar} + V\frac{2\hat{S}_x}{\hbar}(\hat{a}^\dagger + \hat{a}) + \sum_j \hbar\omega_j\hat{b}_j^\dagger\hat{b}_j + \sum_j K_j(\hat{a}^\dagger + \hat{a})(\hat{b}^\dagger + \hat{b}). \tag{A.10}$$

The idea here is that $\hat{a}$ and $\hat{a}^\dagger$ refer to the highly excited oscillator, while the oscillators described by $\hat{b}_j$ and $\hat{b}_j^\dagger$ constitute the bath.

Now, it is true that the coupling of the bath will produce oscillator loss, leading ultimately to the thermalization of the oscillator as before. But from our perspective, this isn't the most important thing that happens; more important in connection with energy exchange is the decay of the admixed states with $m - 1$. Now these admixed states have allowed coupling to decay channels in which the primary oscillator gains or loses a single additional quantum, but where a bath oscillator with energy $\hbar\omega_j$ near ΔE is excited.

Perhaps it is useful to spell this out in the case of a bath at zero temperature. If we first assume that V is small, and $K_j = 0$, then we might write the admixture above as

$$\begin{aligned}\Psi &= c_0|S,m\rangle|n\rangle|\Phi_0\rangle + c_1|S,m-1\rangle|n-1\rangle|\Phi_0\rangle + c_2|S,m-1\rangle|n+1\rangle|\Phi_0\rangle \\ &\quad + c_3|S,m+1\rangle|n-1\rangle|\Phi_0\rangle + c_4|S,m+1\rangle|n+1\rangle|\Phi_0\rangle, \end{aligned} \tag{A.11}$$

where $|\Phi_0\rangle$ is the ground state of the bath oscillators.

If next we allow for loss, so that $K_j \neq 0$, the relevant admixture will be

$$\begin{aligned}\Psi &= c_0|S,m\rangle|n\rangle|\Phi_0\rangle + c_1|S,m-1\rangle|n-1\rangle|\Phi_0\rangle + c_2|S,m-1\rangle|n+1\rangle|\Phi_0\rangle \\ &\quad + c_3|S,m+1\rangle|n-1\rangle|\Phi_0\rangle + c_4|S,m+1\rangle|n+1\rangle|\Phi_0\rangle \\ &\quad + \sum_j d_{0,j}|S,m\rangle|n+1\rangle\,\hat{b}^\dagger|\Phi_0\rangle + \sum_j e_{0,j}|S,m\rangle|n-1\rangle\,\hat{b}^\dagger|\Phi_0\rangle \\ &\quad + \sum_j d_{1,j}|S,m-1\rangle|n\rangle\,\hat{b}^\dagger|\Phi_0\rangle + \sum_j e_{1,j}|S,m-1\rangle|n-2\rangle\,\hat{b}^\dagger|\Phi_0\rangle \\ &\quad + \sum_j d_{2,j}|S,m-1\rangle|n+2\rangle\,\hat{b}^\dagger|\Phi_0\rangle + \sum_j e_{2,j}|S,m-1\rangle|n\rangle\,\hat{b}^\dagger|\Phi_0\rangle \\ &\quad + \sum_j d_{3,j}|S,m+1\rangle|n\rangle\,\hat{b}^\dagger|\Phi_0\rangle + \sum_j e_{3,j}|S,m+1\rangle|n-2\rangle\,\hat{b}^\dagger|\Phi_0\rangle \\ &\quad + \sum_j d_{4,j}|S,m+1\rangle|n+2\rangle\,\hat{b}^\dagger|\Phi_0\rangle + \sum_j e_{4,j}|S,m+1\rangle|n\rangle\,\hat{b}^\dagger|\Phi_0\rangle. \end{aligned} \tag{A.12}$$

The admixed states with $d_{0,j}$ and $e_{0,j}$ coefficients are involved with conventional oscillator loss. The associated process is consistent with normal thermalization of the oscillator (in this case to zero temperature ultimately), and consistent with oscillator loss models in which there are no two-level systems.

However, the admixed states with $d_{1,j}$ and $e_{1,j}$ coefficients, and also with $d_{2,j}$ and $e_{2,j}$ coefficients, are new and special. The reason for this is that the system has now coupled to states in which the two-level system energy ΔE is given to the bath, under conditions where the bath has resonant states with energy $\hbar\omega_j = \Delta E$ and $\hbar\omega_j = \Delta E \pm 2\hbar\omega_0$. Because of the mixing with these states, we might expect incoherent decay process to occur, which we could evaluate using the Golden Rule decay formula.

The same is not true for the admixed states with $d_{3,j}$ and $e_{3,j}$ coefficients, and also with $d_{4,j}$ and $e_{4,j}$ coefficients. Although they appear in the admixture, there are now no resonant states in the bath because we have $m+1$ states with an extra two-level system excited. The resonance conditions would have to be $\hbar\omega_j = -\Delta E$ and $\hbar\omega_j = -\Delta E \pm 2\hbar\omega_0$, which is impossible since the bath oscillator frequencies are positive.

The enhancement of the coherent energy exchange rate in the multi-quantum regime comes about because loss channels are present generally for basis states with energies below E, and restricted for basis states with energies above E. This breaks the interference effect in which contributions from the two groups of states destructively interfere in connection with coherent energy exchange in the multi-quantum regime.

Note that in this kind of model we are making use of oscillator models to account for energetic transitions that may have nothing to do with any oscillator. For example, such an energetic loss process might involve atom ejection, electron ejection, or a nuclear decay. However, since loss impacts these models in essentially the same way independent of the particular loss channel, we would expect that any bath model which describes loss channels in the relevant energy regime will behave similarly.

Appendix A.6. Sectors

Loss can be analyzed by making use of sectors in connection with infinite-order Brillouin–Wigner theory; although the approach is not so widely used in condensed matter problems these days. It is possible to make clear how this works within the context of our modeling effort. For simplicity it will be convenient to assume that the bath starts in the ground state. In this case it will be useful to make use of two sectors: one in which the bath remains in the ground state; and one in which the bath has at least one excitation. We can divide the wavefunction into two sector wavefunctions

$$\Psi \;=\; \Psi_A + \Psi_B, \tag{A.13}$$

where Ψ_A will denote the sector with the zero-temperature bath, and Ψ_B will contain all states with an excited bath. We might denote time independent Schrödinger equation for Ψ as

$$E\Psi \;=\; \hat{H}\Psi. \tag{A.14}$$

This can be rewritten in terms of the two different sectors as

$$E\Psi_A + E\Psi_B \;=\; \hat{H}_{AA}\Psi_A + \hat{H}_{AB}\Psi_B + \hat{H}_{BA}\Psi_A + \hat{H}_{BB}\Psi_B, \tag{A.15}$$

where the Hamiltonian is split into pieces which preserve sector, and which change sector. It is possible to separate this into two sector equations

$$\begin{aligned} E\Psi_A \;&=\; \hat{H}_{AA}\Psi_A + \hat{H}_{AB}\Psi_B, \\ E\Psi_B \;&=\; \hat{H}_{BA}\Psi_A + \hat{H}_{BB}\Psi_B. \end{aligned} \tag{A.16}$$

The overall problem is still explicitly Hermitian.

If we were to focus only on sector A, then $\hat{H}_{AA}$ would appear to us to be Hermitian relative to that sector, but $\hat{H}_{AB}$ would seem to us not to be Hermitian since it couples to a different sector. So, within the context of an explicitly Hermitian formulation, we can have a situation in which part of a Hermitian Hamiltonian is going to act as if it is not Hermitian within sector A.

In the infinite-order Brillouin–Wigner formulation, we can write the sector B wavefunction in terms of the source from sector A as

$$\Psi_B \;=\; \left(E - \hat{H}_{BB}\right)^{-1} \hat{H}_{BA}\Psi_A. \tag{A.17}$$

This can be used to write the sector A part of the eigenvalue equation as

$$E\Psi_A \;=\; \hat{H}_{AA}\Psi_A + \hat{H}_{AB}\left(E - \hat{H}_{BB}\right)^{-1} \hat{H}_{BA}\Psi_A. \tag{A.18}$$

Even at this point the problem remains Hermitian, but in this form it is written so that we have isolated sector A, and taken into account the effect of sector B in a complicated infinite-order Brillouin–Wigner operator. Using this approach, we might think of the sector A wavefunction as being governed by a complicated second-order Hamiltonian of the form

$$\hat{H}_A \;=\; \hat{H}_{AA} + \hat{H}_{AB}\left(E - \hat{H}_{BB}\right)^{-1}\hat{H}_{BA}. \tag{A.19}$$

Such a model is still Hermitian, since it has not discarded any part of the original Hermitian problem, and the original eigenvalues can in principle be recovered (although there are technical issues in doing so).

When the decay is exponential, this infinite-order Brillouin–Wigner formulation can be used to obtain a Golden Rule estimate for the decay rate directly

$$\gamma \;=\; -\frac{2}{\hbar}\mathrm{Im}\left\{\hat{H}_{AB}\left(E - \hat{H}_{BB}\right)^{-1}\hat{H}_{BA}\right\}. \tag{A.20}$$

It is possible to take advantage of this to write for the sector A Hamiltonian

$$\hat{H}_A \;\rightarrow\; \hat{H}_{AA} - \frac{i\hbar\hat{\Gamma}(E)}{2}. \tag{A.21}$$

One could argue at this point that the resulting model is now not Hermitian, and then argue that all results obtained from such a model are suspect. Another might argue that since sector A experiences loss which goes to sector B, no loss of probability appears in the overall model so the overall problem remains Hermitian. For some applications having an explicit loss operator capable of giving an accurate estimate for the sector loss might be considered to be an advantage.

Since the enhanced coherent energy exchange rate in the lossy spin–boson model comes about by eliminating the destructive interference associated with the different virtual states (as described above), there are only minor differences between the results if an accurate loss model is used compared to simply making the loss infinite whenever a loss channel is open. When the decay rate for a state becomes infinitely fast, then it accumulates no occupation probability, so it is the same as if the state were not included in the first place. We have found it convenient to model loss then by assuming infinitely fast decay, and eliminating the associated states. The exclusion of states done in this way leads to a sector A Hamiltonian that is Hermitian, since there is no net decay from the sector if all loss channels are infinitely fast (as long as some accessible stable states remain).

Appendix A.7. Discussion

In view of the discussion above, we conclude that there are two distinct oscillator loss mechanisms which are important in the lossy spin–boson models. One loss mechanism is conventional, in which the oscillator couples a single oscillator energy quantum $\hbar\omega_0$ at a time to roughly resonant bath modes. This loss is connected to the fast thermalization of high frequency oscillator modes that is observed experimentally, and is modeled in the literature using standard approaches. It would be possible to imagine making use of the Caldirola–Kanai model (or some other simple model) in connection with this basic type of oscillator loss.

The other loss mechanism is unconventional, in which the oscillator couples an energetic quantum with energy near the two-level system transition energy ΔE to energetic modes in the bath via single phonon exchange. In this case, it is perhaps more useful to think about the two-level systems and oscillator as a coupled system which couples the bath (instead of the oscillator alone coupling to the bath). With such a view, it is natural to expect the coupling to involve energy exchange $\hbar\omega_0$ and also ΔE, since the coupled two-level system and oscillator has excitations in the vicinity of both energies. It is this phonon loss mechanism that is responsible for the enhancement in the coherent multiphonon energy exchange which is the hallmark of the lossy spin–boson models that we have studied. We would not expect

the Caldirola–Kanai model, or other simple oscillator loss models, to result in an enhancement of the coherent energy exchange rate.

The underlying model for our work is one in which the physical loss mechanisms can be thought of as represented by a bath of oscillators over a large energy range. Then, within the framework of the infinite-order Brillouin–Wigner formalism, the energetic decay processes responsible for the elimination of destructive interference effects are replaced formally by a loss operator (resulting in a sector Hamiltonian that as written is non-Hermitian). Finally, for quantitative estimates we take the limit of infinitely fast loss, which is equivalent to the exclusion of the states which experience the loss. In the end, the sector model is Hermitian, since there is no net decay from the excluded states.

For more accurate modeling in the future where quantitative estimates for state distributions and loss rates in the presence of finite loss will be important, then we will have to work with a explicitly non-Hermitian sector Hamiltonian if we retain an infinite-order Brillouin–Wigner formalism. At that time some effort would be required to be sure that the results are reliable. But for the detailed calculations so far Hermitian sector Hamiltonians have been used for all results over the past several years.

References

[1] P.L. Hagelstein and I.U. Chaudhary, Energy exchange in the lossy spin-boson model, *J. Condensed Matter Nucl. Sci.* **5** (2011) 52.

[2] P.L. Hagelstein and I.U. Chaudhary, Second-order formulation and scaling in the lossy spin-boson model, *J. Condensed Matter Nucl. Sci.* **5** (2011) 87.

[3] P.L. Hagelstein and I.U. Chaudhary, Local approximation for the lossy spin–boson model, *J. Condensed Matter Nucl. Sci.* **5** (2011) 102.

[4] P.L. Hagelstein and I.U. Chaudhary, Coherent energy exchange in the strong coupling limit of the lossy spin-boson model, *J. Condensed Matter Nucl. Sci.* **5** (2011) 116.

[5] M. Fleischmann, S. Pons and M. Hawkins, *J. Electroanal. Chem.* **201** (1989) 301; errata **263** (1990) 187.

[6] M. Fleischmann, S. Pons, M.W. Anderson, L.J. Li and M. Hawkins, *J. Electroanal. Chem.* **287** (1990) 293.

[7] P.L. Hagelstein, M. C. H. McKubre, D. J. Nagel, T. A. Chubb and R. J. Hekman, *Proc. ICCF11* (2004) 23.

[8] P.L. Hagelstein, *Naturwissenschaften* **97** (2010) 345.

[9] P.L. Hagelstein and I.U. Chaudhary, Generalization of the lossy spin-boson model to donor and receiver systems, *J. Condensed Matter Nucl. Sci.* **5** (2011) 140.

[10] P.L. Hagelstein, Bird's eye view of phonon models for excess heat in the Fleischmann–Pons experiment, *J. Condensed Matter Nucl. Sci.* **6** (2011) 169.

[11] D. Letts, D. Cravens and P.L. Hagelstein, Dual laser stimulation and optical phonons in palladium deuteride, *Low-Energy Nuclear Reactions and New Energy Technologies Sourcebook*, American Chemical Society, Washington DC, Volume 2, 2009, p. 81.

[12] P.L. Hagelstein, D. Letts and D. Cravens, *J. Condensed Matter Nucl. Sci.* **3** (2010) 59.

[13] P.L. Hagelstein and I.U. Chaudhary, Including nuclear degrees of freedom in a lattice Hamiltonian, *J. Condensed Matter Nucl. Sci.* **7** (2012) 35.

[14] P.L. Hagelstein and I.U. Chaudhary, A model for collimated X-ray emission in the Karabut experiment, *Proc. ICCF17 J. Condensed Matter Nucl. Sci.* **6** (2012) 217.

[15] P.L. Hagelstein and I.U. Chaudhary, Models for excess heat in PdD and NiH, *Proc. ICCF17* (in press).

[16] F. Bloch and A. Siegert, *Phys. Rev.* **57** (1940) 522.

[17] J. Shirley, *Phys. Rev.* **138** (1965) B979.

[18] C. Cohen-Tannoudji, J. Dupont-Roc and C. Fabre, *J. Phys. B: Atomic Mol. Phys.* **6** (1973) L214.

[19] P.L. Hagelstein and I.U. Chaudhary, Dynamics in the case of coupled degenerate states, *J. Condensed Matter Nucl. Sci.* **5** (2011) 72.

[20] P.L. Hagelstein and I.U. Chaudhary, *J. Phys. B: Atomic Mol. Phys.* **41** (2008) 035601.

[21] P.L. Hagelstein and I.U. Chaudhary, Pulse and amplitude approximation for the lossy spin–boson model, *J. Condensed Matter Nucl. Sci.* **9** (2012) 30.
[22] P.L. Hagelstein and I.U. Chaudhary, Coupling between a deuteron and a lattice, *J. Condensed Matter Nucl. Sci.* **9** (2012) 50.
[23] P. Caldirola, Forze non conservative nella meccanica quantistica, *Il Nuovo Cimento* **18** (1941) 393.
[24] E. Kanai, On the quantization of the dissipative systems, *Prog. Theoret. Phys.* **3** (1948) 440.
[25] V.V. Dodonov and V.I. Man'ko, Coherent states and the resonance of a quantum damped oscillator, *Phys. Rev. A* **20** (1979) 550.
[26] F. Riew, Mechanics with fractional derivatives, *Phys. Rev. E* **55** (1997) 3581.
[27] P.S. Riseborough, P.Hänggi and U. Weiss, Exact results for a damped quantum-mechanical oscillator, *Phys. Rev. A* **31** (1985) 471.
[28] M. Thorwart and P. Hänggi, Decoherence and dissapation during a quantum XOR operation, *Phys. Rev. A* **65** (2001) 012309.
[29] M. Blasone and P. Jizba, Quantum mechanics of the damped harmonic oscillator, *Can. J. Phys.* **80** (2002) 645.
[30] K. Lindenberg and B.J. West, Statistical properties of quantum systems: the linear oscillator, *Phys. Rev. A* **30** (1984) 568.
[31] R. Silbey and R.A. Harris, Variational calculation of the dynamics of a two level system interacting with a bath, *J. Chem. Phys.* **80** (1984) 2615.
[32] C.-I. Um, K.-H. Yeon and T.F. George, The quantum damped harmonic oscillator, *Physics Reports* **362** (2002) 63.

J. Condensed Matter Nucl. Sci. 11 (2013) 93–100

Research Article

Evaluation of Uncertainties in Measurement of Isotopic Abundance by Semi-quantitative Analysis with TOF-SIMS

S. Narita *

Department of Electrical Engineering and Computer Science, Iwate University, Morioka 020-8551, Japan

K. Neichi †

Department of Business Administration, Tohoku Gakuin University, Sendai 980-8511, Japan

T. Matsumoto ‡

Department of Nutrition, Kurashiki Sakuyo University Kurashiki, 710-0292, Japan

Abstract

In *Condensed Matter Nuclear Science*, an anomaly in isotopic abundances of the sample components is often considered as an evidence of a nuclear transmutation. TOF-SIMS is one of the popular tools to investigate the isotopic composition in the research, and it is known that a measured abundance possibly has a certain uncertainty due to unique effects of the device. In this study, we measured isotopic abundances for some types of metal foil samples with various surface conditions by a semi-quantitative analysis with TOF-SIMS, and evaluated the uncertainties.
© 2013 ISCMNS. All rights reserved. ISSN 2227-3123

Keywords: Isotopic abundance, Metal deuteride, Surface morphology, TOF-SIMS, Transmutation

1. Introduction

In *Condensed Matter Nuclear Science* (CMNS), an anomaly in the isotopic abundances on the sample components is often referred as an evidence of a low-energy nuclear transmutation. Iwamura et al. performed a deuterium permeation experiment and they found that the ratios of signals on the masses corresponding to Mo isotopes were quite similar to natural abundances of Sr isotopes, which were deposited onto the sample surface [1]. This result was considered to be an evidence of the selective transmutation from Sr to Mo. Omori et al. found that the abundance of Pd isotopes on the

*E-mail: narita@iwate-u.ac.jp
†E-mail: neichi@tscc.tohoku-gakuin.ac.jp
‡E-mail: matsu@ksu.ac.jp

© 2013 ISCMNS. All rights reserved. ISSN 2227-3123

surface layers of the Pd cathode can change from natural abundance in light water critical electrolysis [2]. They also found an isotopic anomaly of potassium in plasma electrolysis in K_2CO_3/H_2O and K_2CO_3/D_2O solutions [3]. These results suggested an occurrence of a nuclear transmutation. In these experiments, Time-of-flight secondary ion mass spectrometry (TOF-SIMS) was used to analyze the isotope compositions.

The TOF-SIMS is capable of analyzing all the elements including their isotopes as well as good sensitivity for detecting a small amount of elements on a sample with high mass resolution, and it is widely used in various fields such as physics, chemistry, biology, and medical researches [4–6]. In CMNS experiments, it is used as one of the most popular tools to identify a small amount of nuclear products on the sample. In addition, it provides us information on isotopic composition to discuss an occurrence of a nuclear transmutation. Once a significant difference between the measured and natural isotopic abundances, it is referred as a strong evidence of an occurrence of a nuclear transmutation. However, a signal intensity of existing elements/isotopes depends on various effects such as surface sputtering, surface scattering, thermo-diffusion by external source, and so on [7,8]. Then, appreciable changes from the natural isotopic composition can happen for an element at near-surface layer even for a sample not subjected to an experiment. Therefore, it is really important to make out the uncertainty for the signal intensity in the TOF-SIMS measurement to justify the results of a low energy nuclear transmutation if we discuss an anomaly in the isotopic abundance.

In this study, we measured isotopic abundances for some types of metal foil with various surface conditions by a semi-quantitative analysis with TOF-SIMS. Then, the varieties of the isotopic abundances were evaluated for those samples and the uncertainties in the measurements were discussed quantitatively.

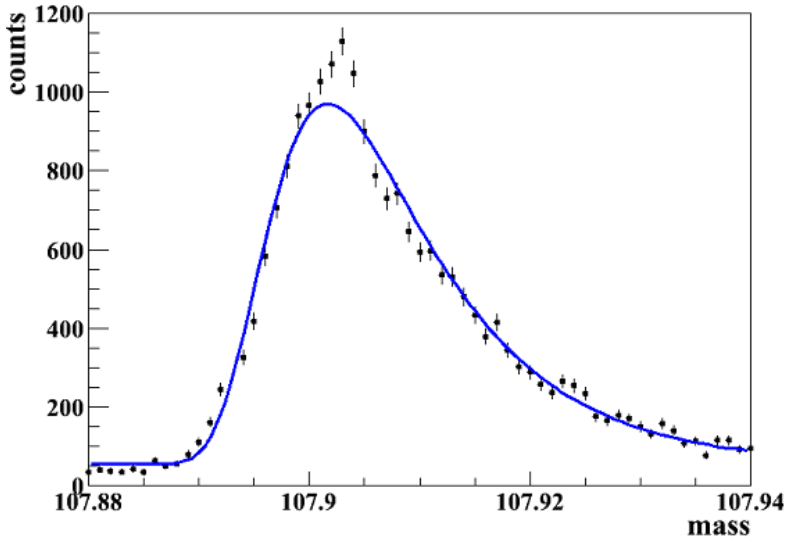

Figure 1. Signal of ^{108}Pd in TOF-SIMS mass spectrum with a fitted function; $f(x) = 54.79 + 1508.47 \times \exp\left[-\frac{1}{2}\left\{\frac{x-107.90}{0.0050} + \exp\left(-\frac{x-107.90}{0.0050}\right)\right\}\right]$.

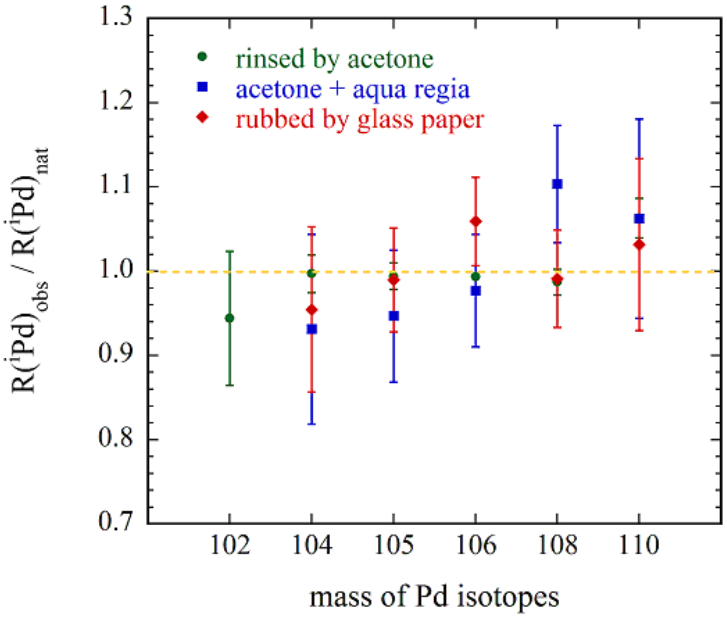

Figure 2. Ratio of measured and natural abundances of Pd isotopes for surface processed Pd foils.

2. Experiment

2.1. Sample preparation

In the experiments for CMNS study, a metal sample is often used as a host material for inducing a nuclear reaction. The metal sample is usually rinsed with acetone and soaked into acid to remove possible impurities in the preparation process, so that the surface condition of the metal can be affected [1,9]. Considering the treatments in the experiment, we prepared Pd, Ni, and Cu foil samples subjected to rinsing by acetone and soaking into aqua regia, and investigated how much the isotopic abundance changed by TOF-SIMS analysis. We also prepared samples rubbed with a glass paper (No. 1000) for making the surface much more rough to examine the effects. Moreover, a metal sample is exposed to hydrogen isotope in most of CMNS experiments, so that a condition of the sample surface can change by sorption of hydrogen atoms. So, we prepared a Pd foil exposed to 5 atm deuterium gases for 23 h, and analyzed the surface of the deuterium loaded Pd.

The surface morphology of these samples was analyzed by AFM to investigate the surface condition, and roughness was found to be 0.05–1 μm for the sample processed by aqua regia and 0.5–1.5 μm for the sample rubbed with a glass paper, typically. Even in the case of showing almost same roughness values, the morphology is indeed different in sample by sample. For example, the mesh pattern on the surface of the sample rubbed with a glass paper is finer and shallower in comparison with that of the sample processed with aqua regia.

2.2. TOF-SIMS measurement

The TRIFT V nano-ToF (ULVAC Phi) equipped with Bi liquid metal ion source was employed in this study. The primary ion beam was 30 keV Bi^+ with a 8400 Hz repetition rate and a pulse width of 10 ns. The current on the target

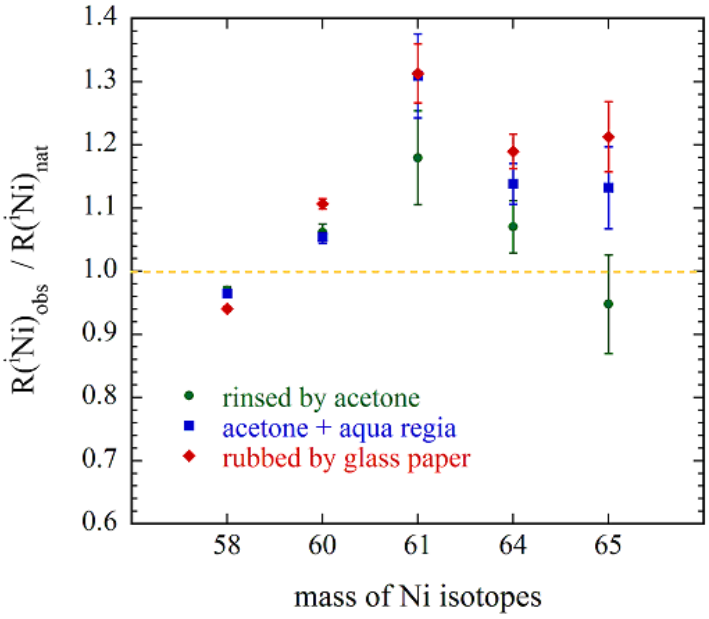

Figure 3. Ratio of measured and natural abundances of Ni isotopes for surface processed Ni foils.

surface was 1–2 nA. The raster size was set to be 40 μm × 40 μm. The mass resolution, $m/\Delta m$, was typically ~5000 at m/z = 27. These conditions are the same in our typical analysis for CMNS study [10]. The depth profile of the abundance was obtained by sputtering with DC Bi^+ for 30, 60, 180, 300 s. The raster size of the DC beam was 200 μm x 200 μm which covers wholly the analysis area. In our typical measurements, no significant variation could be seen in the measured mass spectra for different areas on a sample, so far. Then, we only analyzed an area selected randomly for each sample in this study.

3. Results and Discussion

In order to obtain the intensity of a specific signal, we fitted a function to the corresponding peak on the mass spectrum. Since a secondary ion sputtered by a primary ion has a variety of the initial kinetic energy, especially for metal elements, the signal in the mass spectrum shows a tail [11,12]. In order to determine the signal intensity for an objective isotope, the Moyal function was fitted to the signal distribution with parameters, p_1, p_2, p_3, and p_4 [13],

$$f(x) = p_1 + p_2 \times \exp\left[-\frac{1}{2}\left\{\frac{x-p_3}{p_4} + \exp\left(-\frac{x-p_3}{p_4}\right)\right\}\right].$$

Then, we obtained the number of contained events by integral of the fitted function. Figure 1 shows the signal of ^{108}Pd isotope for the Pd foil rinsed by acetone. A fitted function was also shown in the figure.

Table 1. Natural isotopic abundance of Pd, Ni, and Cu.

Pd	Mass	102	104	105	106	108	110
	Abundance (%)	1.0	11.1	22.3	27.3	26.5	11.7
Ni	Mass	58	60	61	62	64	
	Abundance (%)	68.1	26.2	1.1	3.6	0.9	
Cu	Mass	63	65				
	Abundance (%)	69.2	30.8				

In evaluation of the change in the abundance, we took into account for the ratio of observed abundance to natural one with the following equation,

$$\frac{\left(N_{M_i} / \sum N_{M_i}\right)_{\text{observed}}}{\left(N_{M_i} / \sum N_{M_i}\right)_{\text{natural}}} = \frac{R(M_i)_{\text{obs}}}{R(M_i)_{\text{nat}}}.$$

Here, N_{Mi} is the intensity of the TOF-SIMS on the mass of i-th isotope of metal M. Sets of natural abundances for the metals investigated in this study are shown in Table 1 [14].

Figure 2 shows the ratios of measured and natural abundances of the Pd isotopes for the samples rinsed by acetone, soaked in aqua regia, and rubbed with a glass paper. These data were taken after 30 s surface sputtering in the TOF-SIMS measurement. Since the yields of secondary ions for Pd isotopes are relatively low, the statistic errors were large. The measured abundances show reasonably good agreement with the natural ones within the errors for every sample

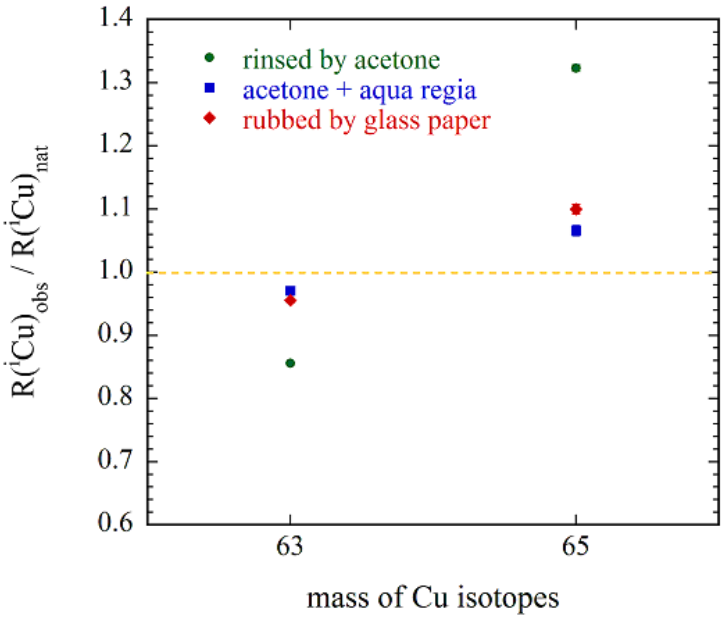

Figure 4. Ratio of measured and natural abundances of Cu isotopes for surface processed Cu foils..

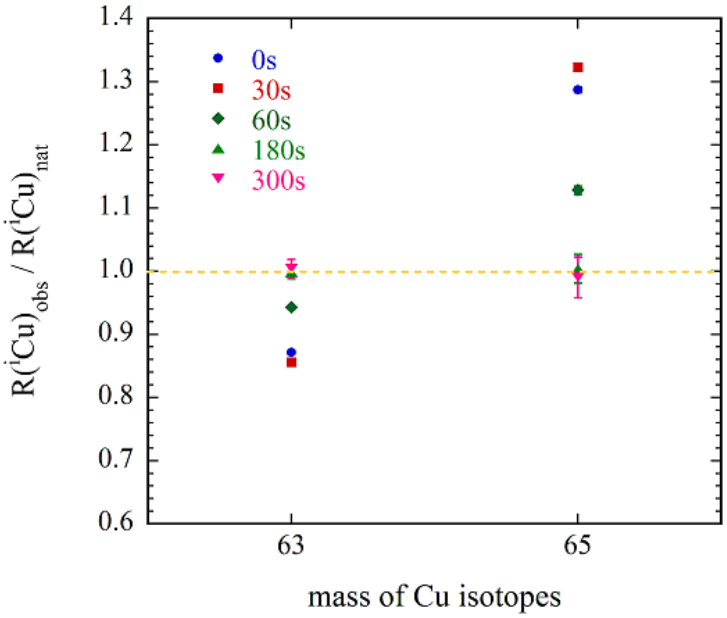

Figure 5. Ratio of measured and natural abundances of Cu isotopes for the sample washed by acetone, for each etching time.

condition except for the isotope ^{102}Pd, which has a small natural abundance. The abundance of an isotope with a small number of counts may have a large fluctuation.

Figure 3 shows the ratios of measured and natural abundances of the Ni samples with the same conditions as the Pd ones. We found up to 20 % discrepancies between measured and natural abundances. They seem to be larger for an isotope with a small abundance, as observed for Pd isotopes. In addition, we found larger differences for the surface processed samples.

Figure 4 shows the results for the Cu samples. Even for the sample just rinsed by acetone, the measured abundance is more than 20% different from natural one. In principle, relative yield of a light isotope in comparison to a heavy one is likely to become larger than natural isotopic ratio because a lighter atom is easy to be sputtered by an incident primary ion. However, our result showed a larger ratio in the heavier isotope. This shift is not due to such a mass effect, but supposed to be a kind of systematic uncertainty in our analysis conditions. Figure 5 shows a comparison for the data taken with a different sputtering time for the sample rinsed by acetone. We found that the abundances get close to natural ones increasing the sputtering time. Since there is more contaminant on the layer such as molecular ion of hydro-carbon so that the secondary ion signal may overlap the original signal and its intensity becomes larger. We should take really care for this effect in estimating isotopic abundances.

Figure 6 shows the results for the Pd sample before and after exposing to deuterium gas. The sample surface condition was apparently different between before and after exposing deuterium according to the AFM images. We observed formation of many small protrusions and change in the surface pattern for the sample after exposing deuterium, as shown in Fig. 7. These changes are supposed to be due to hydrogen embrittlement. However, we did not observe a significant change in the isotopic abundances and the difference of abundance in each isotope was less than 10%. In the case of analyzing the metal sample (X) exposed to the hydrogen isotopes, we should be careful about the interference of the molecular ion of X+H/D. The signal of the molecular ion can overlap the signal for an isotope with corresponding

$$\text{Mass 102:} \quad N(^{102}\text{Pd}) - N(\text{PdD}) \times R(^{102}\text{Pd}),$$

$$\textit{Mass } 104\text{:} \quad N(^{104}\text{Pd}) - N(\text{PdD}) \times \left\{R(^{104}\text{Pd}) - R(^{102}\text{Pd})\right\},$$

$$\text{Mass 105:} \quad N(^{105}\text{Pd}) - N(\text{PdD}) \times R(^{105}\text{Pd}),$$

$$\text{Mass 106:} \quad N(^{106}\text{Pd}) - N(\text{PdD}) \times \left\{R(^{106}\text{Pd}) - R(^{104}\text{Pd})\right\},$$

$$\text{Mass 108:} \quad N(^{108}\text{Pd}) - N(\text{PdD}) \times \left\{R(^{108}\text{Pd}) - R(^{106}\text{Pd})\right\},$$

$$\text{Mass 110:} \quad N(^{110}\text{Pd}) - N(\text{PdD}) \times \left\{R(^{110}\text{Pd}) - R(^{108}\text{Pd})\right\},$$

mass, and we cannot distinguish them usually because their masses are very close. Now, we considered the effect of formation of PdD for an identified signal. Assuming that the probabilities of the formation of PdD molecule for every Pd isotopes are same, the signal intensity of the mass corresponding to the Pd isotopes can be expressed as follows;

where $N(^{i}\text{Pd})$ and $N(\text{PdD})$ are the number of the ^{i}Pd isotopes and the Pd+D compound, respectively, and $R(^{i}\text{Pd})$ is the natural abundance of ^{i}Pd isotope. Substituting the values of the natural abundance (Table 2) into the equations above, the abundances of ^{102}Pd, ^{104}Pd and ^{105}Pd should get smaller, while the abundances of ^{106}Pd, ^{108}Pd and ^{110}Pd

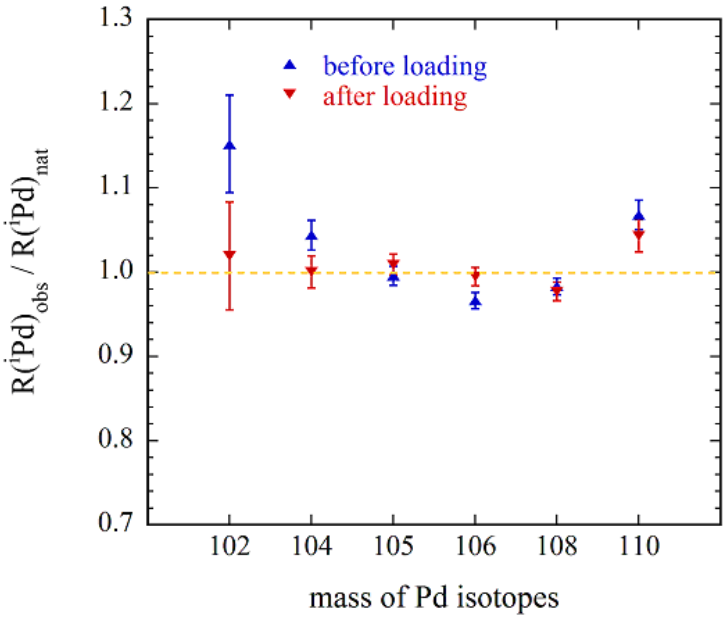

Figure 6. Ratio of measured and natural abundances of Pd before and after exposing high pressure deuterium gas.

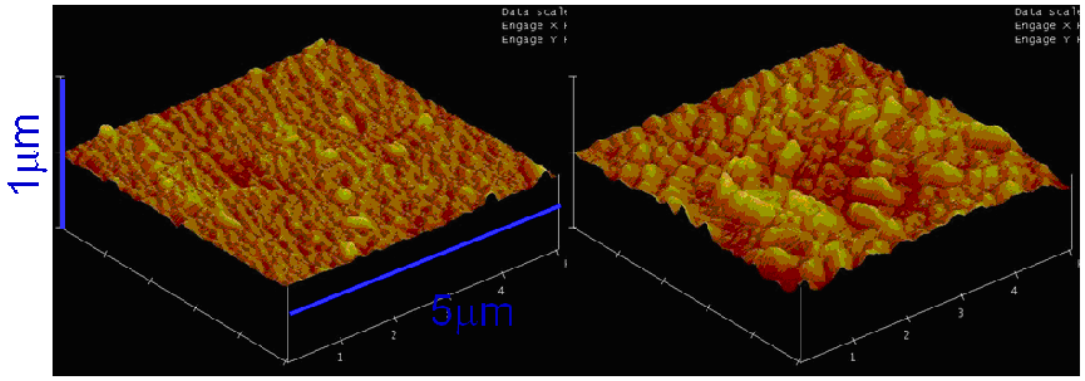

Figure 7. AFM images of Pd surface before (*left*) and after (*right*) exposing to deuterium.

should get larger. We have not seen such a tendency clearly in our results. Thus, the effect of the PdD compound is smaller than that of other effects.

4. Conclusion

We measured the isotopic abundance for the samples with various surface conditions by the semi-quantitative analysis with TOF-SIMS. We found uncertainties in determining the abundance is a range of 10– 30%. No clear dependence on the surface morphology but the sample material. We also found that the abundance of the isotope with small intensity is likely to shift from natural one. We should consider these results when we discuss the anomaly in isotopic abundance in the CMNS study.

References

[1] Y. Iwamura, M. Sakano and T. Itoh, *Jpn. J. Appl. Phys.* **41** (2002) 4642.
[2] T. Ohmori, T. Mizuno, H. Yamada and S. Narita, *Proc. JCF5* 36 (2004).
[3] T. Ohmori, H. Yamada, S. Narita, T. Mizuno and A. Aoki, *J. Appl. Electrochem.* **33** (2003) 643.
[4] A. Palmquist, L. Emanuelsson and P. Sjovall, *Appl. Surf. Sci.* **258** (2012) 6485.
[5] E. Lanni, S. Rubakhin and J. Sweedler, *J. Proteomics* **75** (2012) 5036.
[6] S.K. Singhal, R. Pasricha, M. Jangra, R. Chahal. S. Teotia and R.B. Mathur, *Powder Technol.* **215–216** (2012) 254.
[7] N.N. Nikitenkov, D.Yu. Kolokolov, I.P. Cherenov and Yu.I. Tyurin, *Vacuum* **81** (2006) 202.
[8] T. Nakanaga, H. Nagai, N. Saito, Y. Fujiwara and H. Nonaka, *Int. J. Mass Spec.* **311** (2012) 24.
[9] H. Sasaki, T. Murakami, H. Ougida, S. Narita and H. Yamada, *Proc. JCF10* **31** (2010).
[10] H. Ougida, H. Sasaki, A. Tamura, S. Narita and H. Yamada, *Proc. JCF11* **23** (2011).
[11] G. Betz and K. Wien, *Int. J. Mass Spec. and Ion Processes* **140** (1994) 1.
[12] A. Delcorte and P. Bertrand, *Surface Sci.* **412/413** (1998) 97.
[13] J.E. Moyal, *Phil. Mag. Ser.* **46** (1955) 263.
[14] K.J.R. Rosman and P.D.P. Taylor, *Pure and Appl. Chem.* **70** (1998) 217.

J. Condensed Matter Nucl. Sci. 11 (2013) 101–122

Research Article

Compatibility of Hydrino States and Quantum Mechanics

Burke Ritchie *

Lawrence Livermore National Laboratory, Livermore, CA 94550, USA

Abstract

Rathke's assertion [*New J. Phys.* **7** (2005) 127] that states with binding energy and size below those of known literature values are incompatible with quantum mechanics is corrected by reviewing the analytically known Coulomb solution of the Klein–Gordon equation with binding energy of order mc^2 and size of order of the Compton wavelength. This is an example of a quantum state, which is mathematically acceptable in the sense of being square integrable and having a finite binding energy but yet is rejected as unphysical due in part to the point-nucleus nature of the model. Then the Dirac equation is studied for the existence of states which are similarly mathematically acceptable but whose physical acceptability requires physical judgment. States of Landau symmetry are found which meet these criteria. The existence of states of ambiguous physical interpretation for both the Klein–Gordon and Dirac equations depends on using a point-nucleus versus a finite-nucleus potential model. On using a realistic model for the charge distribution of the proton, a Klein–Gordon state is found in the binding range of 5 keV, but no state is found for the Dirac equation.
© 2013 ISCMNS. All rights reserved. ISSN 2227-3123

Keywords: Dirac equation, Hydrino states, Klein–Gordon equation

1. Introduction

Rathke [1] has presented a critical analysis of the hydrino model [2,3], which has been invoked to interpret experimental results which have appeared in respectable physics journals [4–7]. He also reviews the incompatibility of hydrino states with quantum mechanics. It is this last area which is the focus of the present paper. What I mean by a hydrino state, in a generic sense, is any quantum state with binding in a Coulomb potential characterized by a binding energy and size below those of the known states of the Schrödinger, Klein–Gordon, or Dirac equations. This point has arisen historically whenever experimental results appear to be uninterpretable using standard theory. The earliest example following the discovery of the neutron was likely the proposal that the neutron might be a small hydrogen atom. Margenau examined this question and concluded in his 1934 paper [8] that the Schrödinger or Dirac equations could not support such states unless the potential is modified at small distances from the origin. As a more recent example Evans [9] has studied an unconventional form of Dirac theory, called 4-space Dirac theory, in which the three spatial variables and the scaled time, ct, are treated on an equal footing to avoid any suggestion of a preferred reference frame. Evans' motivation was to find possible theoretical support for low-energy nuclear reactions (LENR), a field which is known pejoratively as

*E-mail: ritchie@lstc.com

© 2013 ISCMNS. All rights reserved. ISSN 2227-3123

"cold fusion." Hence, this subject is regarded as closed by many theorists, and Rathke's blanket assertion that hydrino states are incompatible with quantum mechanics, by which he seems to mean nonrelativistic quantum mechanics (although "quantum mechanics" certainly includes relativistic quantum mechanics), follows in this tradition. In any event the Rathke-hydrino controversy provides a sound opportunity to clarify much of the confusion which exists in the literature on this subject.

For example there is at least one known exception to Rathke's conclusion which, although it appeared in the third edition of Schiff's text on quantum mechanics [10], seems to be little known in the physics community. The Klein–Gordon equation has an analytically known state with binding energy of order mc^2 and Compton wavelength size. It is this state which is irregular at the origin in Schroedinger theory (or more precisely in the Schroedinger limit of Klein–Gordon theory obtained by neglecting terms scaling as α^2, where $\alpha = e^2/\hbar c$ is fine structure constant) and which is therefore unambiguously rejected as unphysical. In Klein–Gordon theory, however, the state is mathematically acceptable in the sense of being square integrable and having a finite binding energy. The state is rejected as unphysical by Schiff for two reasons. First he points out that the particle described by the Klein–Gordon equation has no spin and therefore cannot be an electron. The particle described by Schrödinger's equation also has no spin and yet its electronic properties in the nonrelativistic regime are described with stunning success. To be fair the Klein–Gordon equation fails to account for the observed magnetic fine structure of the atom, which depends on the electron's spin. Second Schiff rejects the Klein–Gordon state as unphysical because it is calculated using a point-nucleus model and therefore fails to account for the finite size of the proton. Nevertheless the Klein–Gordon point-nucleus result illustrates a principle of binding which is unknown in standard quantum theory, namely that an electromagnetic potential, even one of unit strength, can support binding with binding energy of order mc^2 without any modification of the potential at small distances from the center of attraction, as suggested by Margenau [8]. This principle appears to be unrecognized in the physics community, probably owing to arguments that the state is not physically realizable and that the Klein–Gordon equation is inapplicable to the electron. The principle depends on the nature of the relativistic motion and not on the strength of the potential, the latter of which derives purely from Schrödinger theory and is the basis for the wisdom, in beta decay for example, that an electron cannot reside initially inside the small volume of a nucleus because the uncertainty principle for momentum and position, $\Delta p\,\Delta r \geq \hbar$, would be violated for a Δr of nuclear size unless a potential of sufficient strength exists to produce a very largeΔp.

This proof-of-principle binding by the Klein–Gordon equation is reviewed in Section 2. Then in Section 3 the Dirac equation is examined from a new perspective. The general acceptability of Dirac's equation as the equation of motion for the electron rests fundamentally on its success in accounting for the observed magnetic fine structure of the atom and for the anomalous Zeeman effect, which was first successfully described by Pauli's equation, which is an *ad hoc* modification of Schrödinger's equation to account for the observed splitting of a *zero orbital angular momentum* state in the presence of a magnetic field. Pauli's spin vector, $\vec{\sigma}$, in Pauli's or in Dirac's equations occurs diagonally along the z-axis and is therefore compatible with the orbital angular momentum operator, $\vec{\ell}$, which is also is an Eigen operator along the z-axis. This magnetic-axis preference in Dirac's equation suggests that it may be possible for states having Landau symmetry to exist even in absence of a magnetic field. (Landau states [11,12] are states which are bound transversely to a uniform magnetic field along the quantization- or z-axis.) A suggestion that Landau states may exist is found in the non-diagonal nature of all four components of Dirac's wave function simultaneously when each of the large and small components (more in Section 3) is written in the standard way as a product of a radial function, the large or small component, and a two-component spinor, $\chi_{\kappa\mu}(\theta, \phi)$, where κ and μ are the "good"quantum numbers in the $\vec{j} = \vec{\ell} + \frac{1}{2}\vec{\sigma}$ or total angular-momentum representation. The spinors belonging to the large and small components have equal and opposite values of the κ quantum number. The series expansion in which all four components of Dirac's vector wave function can be brought into diagonal form comprises basis members having the Laudau symmetry, as we discuss in Section 3.

In view of the emergence of experiments by Mills and others whose interpretation suggests the existence of quantum

states, which are unknown in the literature, it is imperative to investigate quantum states whose elimination as unphysical on the application of boundary conditions may be ambiguous and may rest on physical judgment alone. In this paper I study the Dirac equation from this viewpoint. It is critical, as pointed out by Rathke, to use a Lorentz-invariant theory. Schrödinger theory is not Lorentz invariant and will yield nothing further on this subject. The Klein–Gordon equation is Lorentz invariant, but it is inapplicable to the electron. The Dirac equation is Lorentz invariant, and it is applicable to the electron.

Finally, I wish to emphasize that the approach in this paper is not based on the concepts or methodology of quantum electrodynamics (QED).

2. Klein–Gordon Equation. Regularization of Schrödinger Irregular States

Readers should recall that a criterion for an acceptable relativistic quantum EOM is that it is invariant to a Lorentz transformation. The scalar product of 4-vectors is always Lorentz invariant [13], and the Klein–Gordon equation follows from the scalar product of the covariant and contra variant 4-momentum,

$$(\gamma mc,\ -\gamma m\overrightarrow{v}) = \left(\frac{E}{c} - \frac{V}{c},\ i\hbar\overrightarrow{\nabla} + \frac{e}{c}\overrightarrow{A}\right),$$

operating on a scalar wave function equal to the Lorentz-constant *mc* times the wave function,

$$\left(\frac{1}{c}(E-V),\ i\hbar\vec{\nabla} + \frac{e}{c}\vec{A}\right)\cdot\left(\frac{1}{c}(E-V), -i\hbar\vec{\nabla} - \frac{e}{c}\vec{A}\right)\psi = \left[\frac{1}{c^2}(E-V)^2 - (i\hbar\vec{\nabla} + \frac{e}{c}\vec{A})^2\right]\psi = mc\psi, \qquad (1)$$

where

$$E = \gamma mc^2 + V, \quad \gamma m\overrightarrow{v} = \overrightarrow{p} = \overrightarrow{P} - \frac{e}{c}\overrightarrow{A}, \quad \overrightarrow{P} \to i\hbar\vec{\nabla}$$

have been used where γ is the Lorentz factor and $\vec{P}$ is the generalized or canonical momentum. Let us look at the small-r equation for $V = -Ze^2/r$ and $\vec{A} = 0$, restricting ourselves to zero-angular-momentum states and keeping only dominant terms,

$$\left(\frac{\mathrm{d}^2}{\mathrm{d}r^2} + \frac{2}{r}\frac{\mathrm{d}}{\mathrm{d}r} + \frac{\beta^2}{r^2}\right)g = 0, \qquad (2)$$

for $\beta = Ze^2/\hbar c$. Using $g = r^s$ in Eq. (2) the indicial equation for s is found by setting the coefficient of r^{s-2} equal to zero, $s(s-1) + 2s + \beta^2 = 0$, whose solutions are given by

$$s = -\frac{1}{2} \pm \frac{1}{2}\sqrt{1 - 4\beta^2} \simeq -\beta^2,\ -1 + \beta^2$$

for the upper and lower signs, respectively. The upper sign is retained in the standard set of solutions in the literature. Notice that $\beta = 0$ for the Schrödinger equation such that the lower-sign solution can be unambiguously rejected as irregular at the origin and therefore as unphysical. (Although the irregular Schrödinger solution is square integrable and therefore normalizable, its expectation value of V diverges logarithmically such that the second criterion of an acceptable solution, a finite binding energy, is not satisfied.) Proceeding heuristically I propose a variational trial

solution over all r having the form, $\psi = Nr^{\beta^2-1}\mathrm{e}^{-wr}$, where the normalization constant is given by

$$N = \left(\int_0^\infty \mathrm{d}r\, r^2 r^{2\beta^2-2}\mathrm{e}^{-2wr}\right)^{-1/2} \cong (2w)^{1/2}, \tag{3}$$

and where w is a parameter chosen to minimize the energy, which is found from Eq. (1),

$$E^2 + 2EZe^2\langle\psi|o|\psi\rangle - m^2c^4 + \hbar^2c^2\left\{w^2 - w\left[2(\beta^2-1)+2\right]\langle\psi|o|\psi\rangle\right]\right\} = 0, \tag{4}$$

where

$$\langle\psi|o|\psi\rangle = 2w\int_0^\infty \mathrm{d}r\, r^{2\beta^2-1}\mathrm{e}^{-2wr} = \frac{wr^{2\beta^2}\mathrm{e}^{-wr}}{\beta^2}|_0^\infty + \frac{2w^2}{\beta^2}\int_0^\infty \mathrm{d}r\, r^{2\beta^2}\mathrm{e}^{-2wr} \simeq \frac{w}{\beta^2}. \tag{5}$$

The approximately equals sign is used whenever $r^{2\beta^2} \simeq 1$, which it cannot be in the first term on the right-hand side of Eq. (5) after the second equality sign, since the limit of $r = 0$ is taken for finite β, but which it can be in the second term and in Eq. (3) since the contribution of $r^{2\beta^2}$ to the integral is negligible. Notice the cancellation of terms in the curly bracket in Eq. (4), including the cancellation of β^2. This is responsible for the binding since otherwise the kinetic energy would exceed the potential energy making binding impossible.

The energy is given by the quadratic-root formula,

$$E = -\frac{wZe^2}{\beta^2} \pm \sqrt{\left(\frac{wZe^2}{\beta^2}\right)^2 + m^2c^4 + \hbar^2c^2w^2}, \tag{6}$$

where the upper sign is taken to be the physical root. Minimizing E with respect to w, $w \simeq mc/\hbar$ and $E \simeq mcZe^2/\hbar$, which is identical to the leading term of the exact analytic energy given by Schiff's formula 51.16 [10],

$$E = mc^2\left(1 + \frac{\beta^2}{\lambda^2}\right)^{-1/2} = mc^2\beta(1+\beta^2)^{-1/2} \simeq \frac{mcZe^2}{\hbar}$$

using his formula 51.17 for $\lambda = s + 1 \simeq \beta^2$. Equation (6) is plotted in Fig. 1 versus w.

The binding energy is given by $E_\mathrm{b} = mc^2 - E$. Notice that Schiff asserts that s is the nonnegative solution of the indicial equation, his formula 51.18, in anticipation of his argument, which follows immediately, that when the finite size of the proton is considered then negative values of s are ruled out in the limit of a point-Coulomb source for a *finite* wave function at $r = 0$. But a finite wave function calculated for a finite-source model will of course have the limit of the positive-s point-source solution when the radius of the finite-source model is taken to zero. Schiff's exercise does not really lift the ambiguity of the positive-s, negative-s, point-source solutions in the sense that both solutions are normalizable with finite binding energies. Point Coulomb sources really do exist in nature, an electron–positron pair for example.

As pointed out earlier, we are concerned in this study with point center-of-force solutions which satisfy two criteria – normalizable with finite binding energy – in order to understand binding of order mc^2 which is due not to the strength of the potential, as in Schrödinger theory, but to the relativistic nature of the motion. Although the probability density is infinite as $r^{2\beta^2-2}$ at $r = 0$, the radial distribution is nevertheless finite. Notice that the size of the negative-s solution is comparable to the Compton wavelength and thus is still much larger than the size of the proton.

Finally, we comment on the double energy-root nature of the Klein–Gordon equation. This also occurs of course in Dirac's equation, and Dirac lifted the ambiguity by filling up the negative-energy levels with electrons such that

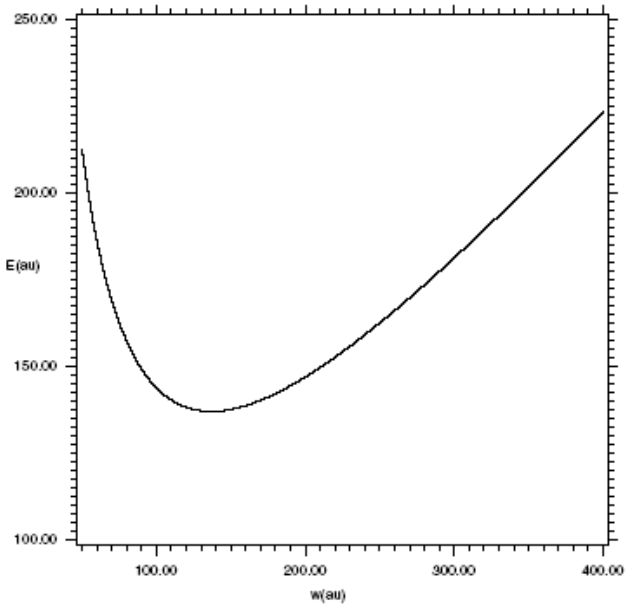

Figure 1. Energy versus variational parameter, w, for the negative-s state of the Klein–Gordon equation. The binding energy is $mc^2 - E$.

positive-energy electrons are forbidden from occupying negative-energy states, which averts the instability of the atom against spontaneous radiative transitions from positive-energy to negative-energy states. The Klein–Gordon equation is criticized on the basis that Dirac's interpretation of the negative-energy states for his own equation would not apply to the Klein–Gordon equation due to the absence of spin such that Pauli's exclusion principle is not obeyed. But the same criticism can be applied to Schrödinger's equation with respect to the positive-energy states. The shell structure of the atom depends entirely on an *ad hoc* antisymmetrization of a product of Schrödinger orbitals augmented by up or down spin states in order to satisfy the Pauli principle. This procedure is totally phenomenological and does not identify spin as a relativistic property of the electron, even though it derives in an *ab initio* sense from Dirac's equation, or explain how the spin of an individual electron is responsible in a causal sense for Fermi–Dirac statistics for an aggregate of many electrons.

Finally, having just mentioned the role of the negative-energy states and Dirac's interpretation of them as antimatter states, I will henceforth limit the investigations of this paper to positive-energy states, as in the Klein–Gordon example above.

3. Dirac Equation

Pauli modified Schrödinger's equation to account for the observed anomalous Zeeman effect, which is the splitting of states of zero orbital angular momentum ($\ell = 0$) in a magnetic field. He introduced the spin vector $\vec{\sigma}$ in an *ad hoc* sense, whose properties were such that

$$\frac{1}{2m}\left[\vec{\sigma}\cdot(i\hbar\vec{\nabla}+\frac{e}{c}\vec{A})\right]^2 = -\frac{\hbar^2}{2m}\nabla^2 + \frac{ie\hbar}{mc}\vec{A}\cdot\vec{\nabla} + \frac{e^2}{2mc^2}A^2 - \frac{e\hbar}{2mc}\vec{\sigma}\cdot(\vec{\nabla}\times\vec{A}), \tag{7}$$

where

$$\overrightarrow{\sigma} = \hat{\imath} \begin{pmatrix} 0 & 1 \\ 1 & 0 \end{pmatrix} + \hat{\jmath} \begin{pmatrix} 0 & -i \\ i & 0 \end{pmatrix} + \hat{k} \begin{pmatrix} 1 & 0 \\ 0 & -1 \end{pmatrix} \tag{8}$$

and the vector identity,

$$(\vec{\sigma} \cdot \vec{C})(\vec{\sigma} \cdot \vec{D}) = \vec{C} \cdot \vec{D} + i\vec{\sigma} \cdot (\vec{C} \times \vec{D}), \tag{9}$$

has been used. In a spatially uniform magnetic field, $\vec{H}$,$\vec{A} = (1/2)\vec{H} \times \vec{r}$ such that the last three terms on the right-hand side of Eq. (7) are

$$V_m = -\frac{e\hbar}{2mc}(\ell_z + \sigma_z)H_z + \frac{e^2}{8mc^2}\rho^2 H_z^2 \tag{10}$$

for a field in the z-direction, where $\rho = \sqrt{x^2 + y^2}$. Notice that even in absence of V, the Coulomb potential, an electron can be bound harmonically in the transverse direction to z, in which direction the electron is free but whose states are split into magnetic sublevels. These are Landau states [11,12]. This point will be revisited when we analyze Dirac's equation for the possibility of the existence of states of Landau symmetry in the presence of V but absence of H_z owing to the diagonal nature of $\vec{\sigma}$ along the z-axis, as given by Eq. (8).

Dirac's equation is usually written as the Lorentz invariant found from the scalar product of the Dirac 4-γ matrix, $(\gamma_0, \vec{\gamma})$, and the electron's 4-momentum operating on a 4-component wave function to give the Lorentz constant mc times the wave function, thus,

$$\left[(\gamma_0, \vec{\gamma}) \cdot \left(i\hbar\frac{\partial}{c\partial t} - \frac{V}{c}, i\hbar\vec{\nabla} + \frac{e}{c}\vec{A}\right)\right]\psi_{\mathrm{D}} = \left[\gamma_0\left(i\hbar\frac{\partial}{c\partial t} - \frac{V}{c}\right) + \vec{\gamma} \cdot \left(i\hbar\vec{\nabla} + \frac{e}{c}\vec{A}\right)\right]\psi_{\mathrm{D}} = mc\psi_{\mathrm{D}}, \tag{11}$$

where the time-dependent operator form of E, $E \to i\hbar(\partial/\partial t)$, has been used and where $\gamma_0 = \beta$ and $\vec{\gamma} = \beta\vec{\alpha}$ on using Dirac's own $\vec{\alpha}$ and β matrices from his original derivation [14],

$$\beta = \begin{pmatrix} I & 0 \\ 0 & -I \end{pmatrix}, \qquad \overrightarrow{\alpha} = \begin{pmatrix} 0 & \overrightarrow{\sigma} \\ \overrightarrow{\sigma} & 0 \end{pmatrix}, \tag{12}$$

where I is the identity matrix. The γ matrices form a Clifford algebra [15], which has been in the mathematics literature for some time. A separate step is then required to prove the Lorentz invariance of the wave equation itself [14].

Recalling that the scalar product of 4-vectors is always Lorentz invariant, Dirac's equation can be derived by further elucidating the close relationship between Dirac's equation and the spinorial form of Maxwell's equation, which has been studied continuously since 1928 [16–19]. Dirac's equation can be inferred from the scalar product of the electron's 4-momentum and an electromagnetic 4-potential, $(\Psi, \vec{\mathrm{X}})$, posited for the electron as follows,

$$\left(i\hbar\frac{\partial}{c\partial t} - \frac{V}{c}, i\hbar\vec{\nabla} + \frac{e}{c}\vec{A}\right)(\Psi, \overrightarrow{X}) = \left(i\hbar\frac{\partial}{c\partial t} - \frac{V}{c}\right)\Psi + \left(i\hbar\vec{\nabla} + \frac{e}{c}\vec{A}\right) \cdot \overrightarrow{X} = 0. \tag{13}$$

Using a carrier-wave expansions for $(\Psi, \vec{\mathrm{X}})$ in order to isolate a dominant frequency component of the 4-potential we obtain,

$$\Psi = \Psi_-(\vec{r}, t)\mathrm{e}^{-i\omega t} + \Psi_+(\vec{r}, t)\,\mathrm{e}^{i\omega t}, \tag{14}$$

$$\vec{\mathrm{X}} = \vec{\mathrm{X}}_-(\vec{r}, t)\,\mathrm{e}^{-i\omega t} + \vec{\mathrm{X}}_+(\vec{r}, t)\,\mathrm{e}^{i\omega t}. \tag{15}$$

On substituting Eqs. (14) and (15) into Eq. (13) and separately setting the coefficients of the exponential factors equal to zero, we obtain,

$$\left(i\hbar\frac{\partial}{\partial t} - V - \hbar\omega\right)\Psi_+ + (i\hbar c\vec{\nabla} + e\vec{A})\cdot\vec{\mathrm{X}}_+ = 0, \tag{16}$$

$$\left(i\hbar\frac{\partial}{\partial t} - V + \hbar\omega\right)\Psi_- + (i\hbar c\vec{\nabla} + e\vec{A})\cdot\vec{\mathrm{X}}_- = 0. \tag{17}$$

Dirac's equation ,

$$\left(i\hbar\frac{\partial}{\partial t} - V - mc^2\right)\psi + c\vec{\sigma}\cdot(i\hbar\vec{\nabla} + e\vec{A})\xi = 0 \tag{18}$$

$$\left(i\hbar\frac{\partial}{\partial t} - V + mc^2)\xi + c\vec{\sigma}\cdot(i\hbar\vec{\nabla} + e\vec{A}\right)\psi = 0, \tag{19}$$

follows immediately on setting $\hbar\omega = mc^2$, $\vec{\mathrm{X}}_+ = \vec{\sigma}\vec{\Psi}_-$, $\vec{\mathrm{X}}_- = \vec{\sigma}\vec{\Psi}_+$, $\Psi_+ = \psi$, $\Psi_- = \xi$. The reader may verify that Eqs. (18), (19) and (11) are identical on carrying out the matrix operations in Eq. (11) using

$$\psi_{\mathrm{D}} = \begin{pmatrix}\psi\\ \xi\end{pmatrix}$$

where ξ and ψ are known in the literature as the large and small components of the Dirac solution. Notice that the electron's spin can be interpreted as the polarization of the vector component of its posited 4-potential. The derivation suggests that the distinction between the material and electromagnetic properties of the electron, which I examined in a previous paper [20], may be an artificial one due to conceptual and practical limitations of theory but manifestly present in observations such as the Lamb shift or the electron's anomalous magnetic moment. Notice that no further proof of the Lorentz invariance of the wave equation itself is required since Eqs. (18) and (19) have been inferred directly from a scalar product of 4-vectors.

The standard 4-component solutions are separated into products of radial and angular solutions, thus,

$$\psi_{\mathrm{D}}(r,\theta,\phi) = \begin{pmatrix}\psi(r,\theta,\phi)\\ \xi\,(r,\theta,\phi)\end{pmatrix} = \begin{pmatrix} g_\kappa(r)\chi_{\kappa\mu}(\theta,\phi)\\ if_\kappa(r)\chi_{-\kappa\mu}(\theta,\phi)\end{pmatrix}, \tag{20}$$

where the relative phases are chosen so that the radial functions are real. The two-component spinors, $\chi_{\kappa\mu}(\theta,\phi)$, have equal and opposite quantum numbers forκ and$-\kappa$ due to the properties of the operator,

$$\vec{\sigma}\cdot\vec{\nabla} = \sigma\cdot\hat{r}\left(\frac{\partial}{\partial r} - \frac{1}{r}\vec{\sigma}\cdot\vec{\ell}\right),$$

where $\vec{\sigma}\cdot\vec{\ell}\chi_{\kappa\mu}(\theta,\phi) = -(\kappa+1)\chi_{\kappa\mu}(\theta,\phi)$ and $\vec{\sigma}\cdot\hat{r}\chi_{\kappa\mu}(\theta,\phi) = -\chi_{-\kappa\mu}(\theta,\phi)$. The spinors are eigen functions of the operators j^2, j_z, ℓ^2, and s^2, where$\vec{j}$ is the total angular momentum operator, $\vec{j} = \vec{\ell} + \vec{s}$, and therefore of $\vec{\sigma}\cdot\vec{\ell} = 2\vec{\ell}\cdot\vec{s} = j^2 - \ell^2 - s^2$ where the eigen values of j^2, ℓ^2, and s^2 are j (j+1), $\ell(\ell+1)$, and $\frac{1}{2}(\frac{1}{2}+1)$, respectively, such that the κ quantum number has values κ=-1, -2… for $j = \ell + \frac{1}{2}$ and κ =1, 2… for $j = |\ell - \frac{1}{2}|$.

The key point here is that the spinors are eigen functions of the angular-momentum operators listed above but not of $\vec{\sigma}\cdot\vec{\nabla}$ due to the diagonal nature of this operator in the z-coordinate , the axis along which the permanent magnetic moment due to the electron's spin is measured. Let us look at this operator in z, ρ, ϕ coordinates,

$$\vec{\sigma}\cdot\vec{\nabla} = \begin{pmatrix} \frac{\partial}{\partial z} & \mathrm{e}^{-i\phi}(\frac{\partial}{\partial\rho} - \frac{i}{\rho}\frac{\partial}{\partial\phi})\\ \mathrm{e}^{i\phi}(\frac{\partial}{\partial\rho} + \frac{i}{\rho}\frac{\partial}{\partial\phi}) & -\frac{\partial}{\partial z}\end{pmatrix} \tag{21}$$

The diagonal nature of $\vec{\sigma}\cdot\vec{\nabla}$ along z suggests that it may be possible for bound states having the Landau form to exist. Of course the standard set of states in r, θ, ϕ coordinates known in the literature must also be recoverable in z, ρ, ϕ coordinates using *the same set of physical boundary conditions* as used in the standard set of states. One would expect however for Landau-type states to have a different set of boundary conditions from the standard solutions in analogy to the different boundary conditions used in Section 2 for the small-size, low-energy states of the Klein–Gordon equation.

4. Dirac-equation States with Landau Symmetry

Dirac's equation should be cast in exact second-order form [21] for ease of analysis by elimination of Eq. (19) in favor of Eq. (18),

$$\left[(E-V)^2 - m^2c^4 + \hbar^2c^2\left(\nabla^2 + \frac{(\vec{\sigma}\cdot\vec{\nabla}V)(\vec{\sigma}\cdot\vec{\nabla})}{E-V+mc^2}\right)\right]\psi = 0, \tag{22}$$

where we return once again to the time-independent equation. First, let us analyze the equation in r, θ, ϕ coordinates where, using Eq. (9),

$$(\vec{\sigma}\cdot\vec{\nabla}V)(\vec{\sigma}\cdot\vec{\nabla}) = \vec{\nabla}V\cdot\nabla + i\vec{\sigma}\cdot(\vec{\nabla}V\times\vec{\nabla}) = V'\left(\frac{\mathrm{d}}{\mathrm{d}r} - \frac{\vec{\sigma}\cdot\vec{\ell}}{r}\right), \tag{23}$$

where the V' denotes the radial derivative of V. Specializing to $\ell = 0$ ($\kappa = -1$) states the last term on the right-hand side of Eq. (23) gives zero contribution. Neglecting $E+mc^2$compared to -V in Eq. (22) the small-r equation is

$$\left(\frac{\mathrm{d}^2}{\mathrm{d}r^2} + \frac{3}{r}\frac{\mathrm{d}}{\mathrm{d}r} + \frac{\beta^2}{r^2}\right)g = 0, \tag{24}$$

which may be compared with Eq. (2) and whose indicial equation is $s(s-1)+3s+\beta^2 = 0$ with solutions

$$s = -1 \pm \sqrt{1-\beta^2} \simeq -\frac{1}{2}\beta^2, -2 + \frac{1}{2}\beta^2$$

for upper and lower signs, respectively. Notice that the lower-sign solution, in contrast to that of the Klein–Gordon equation, is unambiguously irregular at the origin and must be rejected as unphysical. The $V'(\mathrm{d}/\mathrm{d}r)$ term in Eq. (23) increases the kinetic energy near $r = 0$ beyond the physical bounds encompassed by a normalizable wave function. In contrast the Klein–Gordon wave function is infinite at $r = 0$, but it is still normalizable and therefore has a chance of being physically realizable in a realistic point-source situation.

Compared to the Schrödinger and Klein–Gordon equations it may seem fishy to the reader to have a V' or radial-force contribution to the kinetic energy, but that is the nature of the spin–orbit interaction. It may be possible, however, for a wave function to exist whose probability distribution is not radially concentrated at a single point in space but is cylindrically distributed along z in a cigar shape, which is the shape of the electronic distribution for an atom in a strong magnetic field [12]. Returning to Eq. (22) the numerator of the spin–orbit term in z, ρ, ϕ coordinates is

$$(\vec{\sigma}\cdot\vec{\nabla}V)(\vec{\sigma}\cdot\vec{\nabla}) = \begin{pmatrix} V_z\frac{\partial}{\partial z} + V_\rho\left(\frac{\partial}{\partial\rho} + \frac{i}{\rho}\frac{\partial}{\partial\phi}\right) & \mathrm{e}^{-i\phi}\left[V_z\left(\frac{\partial}{\partial\rho} - \frac{i}{\rho}\frac{\partial}{\partial\phi}\right) - V_\rho\frac{\partial}{\partial z}\right] \\ -\mathrm{e}^{i\phi}\left[V_z\left(\frac{\partial}{\partial\rho} + \frac{i}{\rho}\frac{\partial}{\partial\phi}\right) - V_\rho\frac{\partial}{\partial z}\right] & V_z\frac{\partial}{\partial z} + V_\rho\left(\frac{\partial}{\partial\rho} - \frac{i}{\rho}\frac{\partial}{\partial\phi}\right) \end{pmatrix} \tag{25}$$

where the subscripts on V denote first-order derivatives with respect to z or ρ. This operator can be represented by expanding the wave function in a basis set, $\{\psi_\nu(z, \rho, \phi)\}$, whose members comprise products of magnetic sub-states,

$$\psi_\nu(z, \rho, \phi) = \psi_{\alpha,m_z}(z, \rho)\,\mathrm{e}^{im_z\phi}\alpha + \psi_{\beta,m_z+1}(z, \rho)\,\mathrm{e}^{i(m_z+1)\phi}\beta, \tag{26}$$

where α, β are spin-up, spin-down spin states and $\nu = 1/2$ for $m_z = 0$, $\nu = 3/2$ for $m_z = 1$ and so on. We will examine only the azimuthally symmetric component, $\psi_{\alpha,0}$, here.

Again proceeding heuristically I propose a variational trial solution having the form $\psi_{\alpha,0} = N(\rho^s \pm az)^{-1}\mathrm{e}^{-w\rho^2}$ in the positive, negative domain of z for the upper, lower sign, where $a > 0$ to insure that the wave function is bounded in the z direction and $s < 1$ to insure that integrals with integrands which are singular as ρ^{-2s+1}, which occur in the expectation value of the potential, do not diverge logarithmically. Notice that these Landau-type states are bound in an elongated sense along the z direction and are bound radially in the standard exponentially decaying manner. Hence, these are bound states which are stabilized by spreading out the kinetic energy in an elongated, cigar shape rather than concentrating it at a single point, as for the Dirac solution in r, θ, ϕ coordinates.

The a parameter is determined from a generalized indicial equation to be given shortly. The s parameter is written $s = 1 - b$ where $b \ll 1$ and, along with w, is determined by minimizing the energy. The trial wave function is obviously square integrable,

$$N^2 \int_0^\infty \mathrm{d}\rho\, \rho\, \mathrm{e}^{-2w\rho^2} 2 \int_0^\infty \mathrm{d}z\, (\rho^s + az)^{-2} = 1, \tag{27}$$

where the z integral, along with all of the z integrals except one, are evaluated analytically. In Eq. (27) the z integral is equal to$\rho^{-s}a^{-1}$. The Gaussian form, $\mathrm{e}^{-w\rho^2}$, is used rather than the Slater form, $\mathrm{e}^{-w\rho}$, because the latter boosts the kinetic energy to an extent that binding is impossible.

The small z, smallρ equation for $\psi_{\alpha 0}$ from Eq. (22) is

$$\left(\frac{\partial^2}{\partial z^2} + \frac{\partial^2}{\partial \rho^2} + \frac{1}{\rho}\frac{\partial}{\partial \rho} + \frac{1}{\rho^2 + z^2}\left(z\frac{\partial}{\partial z} + \rho\frac{\partial}{\partial \rho}\right) + \beta^2 \frac{1}{\rho^2 + z^2}\right) g = 0, \tag{28}$$

where again $E + mc^2$ is neglected compared to $-V$. Substituting $g = (\rho^s \pm az)^{-1}$ into Eq. (28), carrying out the operations, multiplying the result by g, and finally integrating over z, an indicial equation is given by

$$\rho^{-3}\left\{\frac{1}{6a} + \frac{2a}{3} + (\beta^2 - 1)a(1 + a^2)^{-1}\left[1 + (1 + a^2)^{-1}\left[\ln a^2 + a^{-1}(1 - a^2)(\tan^{-1} a + \tan^{-1} a^{-1})\right]\right]\right\} = 0, \tag{29}$$

where without loss of accuracy b has been set equal to zero, which choice makes the factorization of ρ^{-3}possible, as shown in Eq. (29). Two values of a are found to satisfy Eq. (29), $a \simeq 0.19$ and $a \simeq 0.565$, for which values the energy is plotted versus w in Fig. 2.

The energy is found from Eq. (22),

$$E^2 + 2EZe^2\langle\psi|o_1|\psi\rangle - m^2c^4 + \hbar^2c^2(\langle\psi|(o_2 + o_3 + o_4 + o_5)|\psi\rangle) = 0, \tag{30}$$

with roots,

$$E = -Ze^2\langle\psi|o_1|\psi\rangle \pm \sqrt{(Ze^2\langle\psi|o_1|\psi\rangle)^2 + m^2c^4 - \hbar^2c^2(\langle\psi|o_2 + o_3 + o_4 + o_5|\psi\rangle)}, \tag{31}$$

where the potential-energy expectation value is

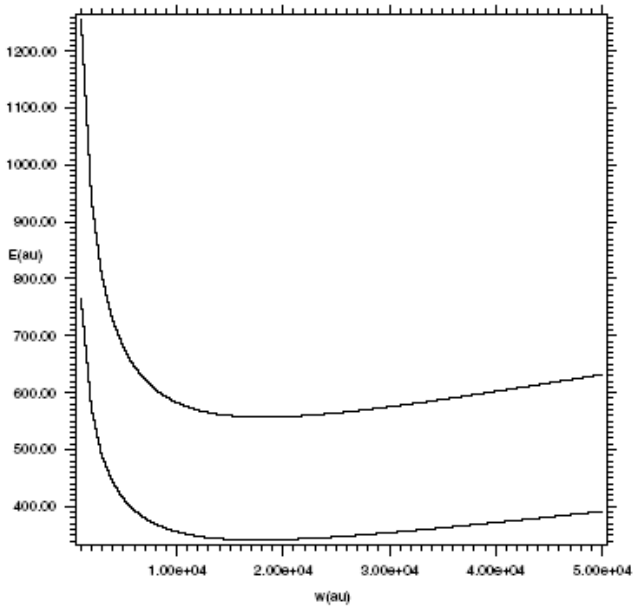

Figure 2. Energy versus variational parameter, w, for two Landau-type states of the Dirac equation for $b = \alpha^2$. Upper: $a = 0.19$. Lower: $a = 0.565$. The binding energy is $mc^2 - E$.

$$\begin{aligned}\langle\psi|o_1|\psi\rangle &= 2N^2 \int_0^\infty \mathrm{d}\rho\, \rho\, \mathrm{e}^{-2w\rho^2} \int_0^\infty \mathrm{d}z\, (\rho^s + az)^{-2}(\rho^2 + z^2)^{-1/2} \\ &\simeq 2N^2 c_p \int_0^\infty \mathrm{d}\rho\, \rho^{2b-1}\mathrm{e}^{-2w\rho^2} \\ &= \frac{N^2 c_p \rho^{2b}\mathrm{e}^{-w\rho^2}}{b}\bigg|_0^\infty + \frac{4N^2 c_p w}{b} \int_0^\infty \mathrm{d}\rho\, \rho^{2b+1}\mathrm{e}^{-2w\rho^2} \end{aligned} \tag{32}$$

$$c_\mathrm{p} = \frac{a-1}{1+a^2} + \frac{1}{(1+a^2)^{3/2}} \ln \frac{a\left[(1+a^2)^{1/2} + a\right]}{(1+a^2)^{1/2} - 1}. \tag{33}$$

The kinetic-energy expectation values are

$$\langle\psi|o_2|\psi\rangle = 2N^2 \int_0^\infty \mathrm{d}\rho\, \rho \left[(2w\rho)^2 - 2w\right] \mathrm{e}^{-2w\rho^2} \int_0^\infty \mathrm{d}z\, (\rho^s + az)^{-2} = 2N^2 a^{-1} \int_0^\infty \mathrm{d}\rho\, \rho^b \left[(2w\rho)^2 - 2w\right] \mathrm{e}^{-2w\rho^2} \tag{34}$$

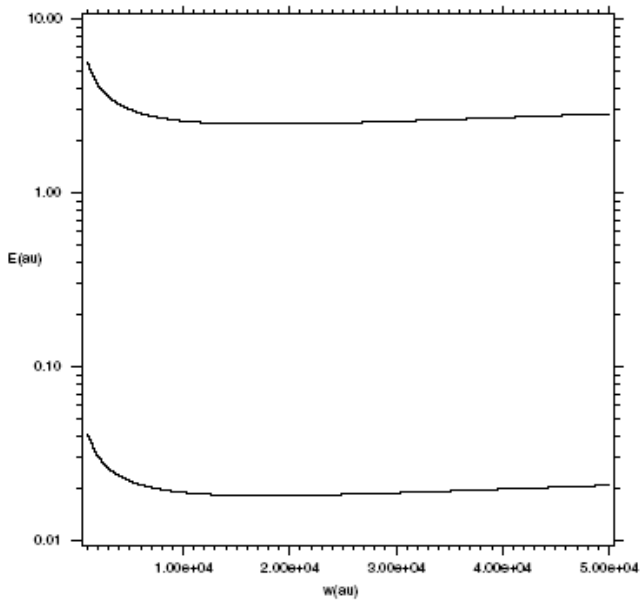

Figure 3. Energy versus variational parameter, w, for two Landau-type states of the Dirac equation for $a = 0.565$. Upper: $b = \alpha^3$. Lower: $b = \alpha^4$. The binding energy is $mc^2 - E$.

$$\langle\psi|o_3|\psi\rangle = 4N^2 w \int_0^\infty \mathrm{d}\rho\, \rho^2 \mathrm{e}^{-2w\rho^2} \int_0^\infty \mathrm{d}z\, (\rho^s + az)^{-3} = 2N^2 a^{-1} w \int_0^\infty \mathrm{d}\rho\, \rho^{2b} \mathrm{e}^{-2w\rho^2}, \tag{35}$$

$$\langle\psi|o_4|\psi\rangle = -4N^2 w \int_0^\infty \mathrm{d}\rho\, \rho\, \mathrm{e}^{-2w\rho^2} \int_0^\infty \mathrm{d}z\, (\rho^s + az)^{-2} = -2N^2 a^{-1} w \int_0^\infty \mathrm{d}\rho\, \rho^{b} \mathrm{e}^{-2w\rho^2}, \tag{36}$$

$$\langle\psi|o_5|\psi\rangle = -4N^2 wZe^2 \int_0^\infty \mathrm{d}\rho\, \rho^3 \mathrm{e}^{-2w\rho^2} \int_0^\infty \mathrm{d}z \frac{1}{(\rho^s + az)^2(\rho^2 + z^2)(Ze^2 + mc^2\sqrt{\rho^2 + z^2})}. \tag{37}$$

The integral over z in Eq. (36) is evaluated numerically. All integrals over ρ are evaluated numerically. Notice that $\langle\psi|o_3|\psi\rangle \simeq -\langle\psi|o_4|\psi\rangle$, such that these contributions to the kinetic energy nearly cancel. As in the case of the Klein–Gordon equation the binding energy is of order mc^2. Our solution of the Dirac equation requires two variational parameters, w and b, and Figs. 2 and 3 show that E has a minimum versus w for different values of b, while the energy approaches zero – binding energy of mc^2 – as b approaches zero. This behavior merely reflects the logarithmic divergence of the potential-energy expectation value for $b = 0$. But the rule for evaluating the integral in Eq. (32) is the take the limit as$\rho \to 0$ for finite b. For example using L'Hopital's rule for the opposite limit, $b \to 0$ for finite ρ,

$$\frac{\rho^{2b}}{b} = \frac{\mathrm{e}^{2b\ln\rho}}{b} \to 2\ln\rho.$$

This means that any physical problem for which the present theory is suitable must truly involve a point-Coulomb source such as an electron or positron. In the case of experiments whose interpretation appears to require the existence of quantum states whose energies are lower than those of the known states in the literature, to which I have given the generic name "hydrino states," this work is intended to establish that no general rule exists by which such states can be said to be incompatible with quantum mechanics. In the original hydrino-state work [1–7] no distinction was made between a point-nucleus and a finite-nucleus model of the hydrogen atom, although, as we now understand from the present analysis, this distinction is of critical importance.

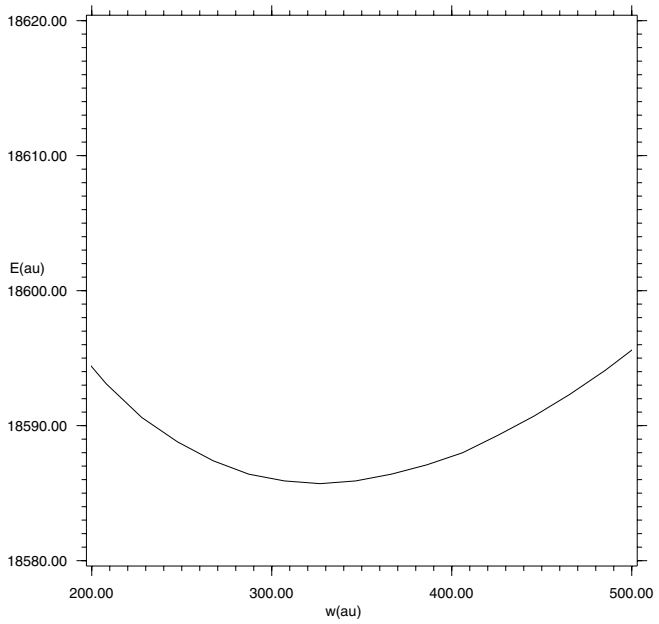

Figure 4. Energy versus variational parameter, w, for the negative-s state of the Klein–Gordon equation using a finite-proton potential model. The binding energy is $mc^2 - E$.

5. Finite-nucleus Potential Model

The interpretation of experimental data requires the use of finite-nucleus potential models in which the nuclear charge-distribution from the origin to the surface of the nucleus is represented. A well-studied model [22] is used, in which

$$V = \frac{-Ze^2}{2r_0}\left[3 - (r/r_0)^2\right] \quad \text{for} \quad r < r_0 \quad \text{and} \quad V = \frac{-Ze^2}{r} \quad \text{for} \quad r > r_0 \,,$$

where r_0 is the nuclear radius; for a proton $r_0 = 1.044 \times 10^{-13}$cm or 1.974×10^{-5}Å. No bound states were found for Dirac's equation using this model. The trial function $\psi_{\alpha,0} = N(\rho^s \pm az)^{-p}\mathrm{e}^{-w\rho^2}$ was used, where $\frac{1}{2} < p \leq 1$. For $p = 1$, which was used in the point-nucleus model in Section 4, the indicial equation appropriate for a finite proton did not have a solution for any value of a. A solution of the indicial equation for $p = 0.8$ was found for $a = 0.65$, but this solution had no bound states. With reference to Eq. (31) the reason appeared to be the lack of cancellation of $\langle\psi|o_3|\psi\rangle$ and $\langle\psi|o_4|\psi\rangle$ for $p = 0.8$, giving a kinetic energy which exceeds the potential energy.

The Klein–Gordon equation was revisited using the finite-proton model, and the trial function $\psi = Nr^{-1}\mathrm{e}^{-wr}$ (first trial function) was used, for which the kinetic energy was negative and therefore unphysical. Then the trial function $\psi = Nr^{-1}\mathrm{e}^{-wr^2}$ (second trial function) was used, for which a bound state was found whose energy is plotted versus w in Fig. 4. The binding energy at the minimum is in the 5 keV range. Notice that the Schrödinger irregular form r^{-1} may be used since the potential is now finite at $r = 0$. With reference to Eq. (4), the kinetic energy is negative for the first trial function due to the exact cancellation of the $2\frac{\mathrm{d}}{\mathrm{d}r}r^{-1}\frac{\mathrm{d}}{\mathrm{d}r}\mathrm{e}^{-wr}$ and $\frac{2}{r^2}\frac{\mathrm{d}}{\mathrm{d}r}\mathrm{e}^{-wr}$ contributions to the kinetic energy. This cancellation also occurs using the second trial function, but the term $r^{-1}\frac{\mathrm{d}^2}{\mathrm{d}r^2}\mathrm{e}^{-wr^2}$ sufficiently boosts the kinetic energy to avert total cancellation of the m^2c^4 term. The latter situation leads to the dominance of the matrix element of V^2, which is negative. Recall that V^2 is removed in the indicial equation in the point-nucleus model. The magnitude of the energy in Fig. 4 is large owing to the smallness of matrix elements of V in the finite-proton model.

6. Conclusions

In summary, the hydrino states exist for both the Klein–Gordon and the Dirac equations, but they are sensitive to using a point-nucleus versus a finite-nucleus model, critically so in Dirac's equation and less so in the Klein–Gordon equation. Since the Klein–Gordon equation cannot sensibly be proposed as an EOM for the electron, the negative result for Dirac's equation suggests that evidence of excess energy production in experiments likely cannot be explained as due to the existence of an unusual quantum state.

What might be considered for further investigation using Dirac-equation anomalous quantum states is the nature of the positron-electron state as a real two-fermion state rather than as a two-fermion-state concept in order to interpret Dirac's equation. The latter concept encompasses the standard interpretation of Dirac's equation, not as an equation for a single particle, but as an equation for an infinite number of particles, providing a practical calculational tool possibly at the cost of providing an idealization of physical reality. The Bethe–Salpeter equation [23] for two fermions was a move in the direction of an actual many-fermion theory, but its mathematical complexity appears to put it beyond the reach of realistic practical calculations. A recent quantum-dynamical approach [24] proposed by the present author might be worth pursuing since the two-fermion Coulomb interaction can be represented, as discussed there, without loss of Lorentz invariance.

Appendix A. Reviewer Comments

It is proposed that Ritchie's paper be published. However, since there remain issues, it seems appropriate to develop a brief set of reviewer's comments to be made available for the benefit of those reading the paper. I will summarize some

of these issues in what follows.

Appendix A.1. Lorentz invariance

Ritchie has included some discussion about using a Lorentz-invariant model to address the associated problems. One approach to this would be to include the nucleus in the calculation in the framework of a relativistic two-body problem, making use of a Bethe–Salpeter or related type of model. The resulting model would be explicitly Lorentz-invariant. Relativistic field theory was constructed to allow for such problems to be analyzed systematically. An electron in a fixed central field potential would generally not be regarded as a Lorentz- invariant model.

Appendix A.2. Coulomb point source model

Ritchie argues that the problem of an electron and positron would provide an example of a system involving two point source charges, since the nuclear charge is spread out on the Fermi scale. I note that vacuum polarization effects lead to a spreading out of the effective charge of electrons and positrons, also on the Fermi scale, so that in the end there is no qualitative difference between the problems.

Appendix A.3. Occupation of negative energy states

Ritchie reminds us of the (somewhat anachronistic) view that negative energy Dirac states are occupied, which was put forth (about 80 years ago) by analogy with electrons and holes in semiconductors. In more modern times, the positive energy solutions are adopted to describe electrons, and the negative energy states are used to describe positrons; as in the construction of QED. Within such a picture there cannot be real electron occupation of a negative energy Dirac state, so the issue of transitions to such states does not arise.

Appendix A.4. Use of the variational principle

Ritchie has made use of a variational calculation under conditions where there is not a lowest energy state. Although under some conditions reasonable results can be obtained, in general one does not have confidence in the result of such a computation. It would have been better to make use of a modified variational method, perhaps based the minimization of $I\,[\psi] = \langle\psi|(H - E_{\rm off})^2|\psi\rangle/\langle\psi|\psi\rangle$ where $E_{\mathbf{off}}$ is selected to be close to the target state energy.

Appendix A.5. Use of the mixed symmetry states

In the case of the Dirac equation, Ritchie uses a variational wave function with mixed symmetry. In a central potential one would expect states with pure (or unmixed) symmetry to be Eigen functions. It would have been better to focus on a single channel with fixed symmetry.

Appendix A.6. Localized $S_{1/2}$ state

I provided Ritchie with an analytic result for a localized $S_{1/2}$ state in the case of the Dirac equation. If one starts with $E\psi = \beta mc^2 + \alpha \cdot c_{\rm p} + V(r)\psi$ and works with states of the form

$$\psi = \begin{pmatrix} \frac{P(r)}{r}\chi_{k,m}(\theta,\phi) \\ \\ i\,\frac{Q(r)}{r}\chi_{-k,m}(\theta,\phi) \end{pmatrix}$$

then the Dirac equation for large and small components in the case of a point Coulomb model reduces to

$$E_P = mc^2 P - \hbar c \left(\frac{\mathrm{d}}{\mathrm{d}r} - \frac{k}{r}\right) Q - \frac{e^2}{r} P,$$

$$E_Q = -mc^2 Q + \hbar c \left(\frac{\mathrm{d}}{\mathrm{d}r} + \frac{k}{r}\right) P - \frac{e^2}{r} Q$$

It is possible to develop exact solutions based on the ansatz

$$P(r) = r^s \mathrm{e}^{-\beta r} \quad \text{and} \quad Q(r) = A r^s \mathrm{e}^{-\beta r}.$$

After plugging in, we get two $S1/2$ state solutions. In the case of the ground state $1S_{1/2}$ state, we end up with

$$s = \sqrt{1-\alpha^2}$$

$$P(r) = r^{\sqrt{1-\alpha^2}} \mathrm{e}^{-r/a_0} \quad \text{and} \quad Q(r) = A r^{\sqrt{1-\alpha^2}} \mathrm{e}^{-r/a_0},$$

$$E = mc^2 + \frac{\hbar c}{\alpha a_0}(s+k) = mc^2 + 2I_H \frac{s+k}{\alpha^2} \approx mc^2 - I_H$$

We also get a localized state with

$$s = -\sqrt{1-\alpha^2}$$

$$P(r) = r^{-\sqrt{1-\alpha^2}} \mathrm{e}^{-r/a_0} \quad \text{and} \quad Q(r) = A r^{-\sqrt{1-\alpha^2}} \mathrm{e}^{-r/a_0},$$

$$E = mc^2 + \frac{\hbar c}{\alpha a_0}(s+k) = mc^2 + 2I_H \frac{s+k}{\alpha^2} \approx -mc^2$$

We have found a localized $\mathrm{S}_{1/2}$state in the case of a point Coulomb potential. We recognize this as a negative energy state.

Appendix A.7. Acceptance of QED

Quantum electrodynamics (QED) was constructed as a relativistic quantum theory capable of addressing problems involving electrons, positrons, and photons. Extensions of QED that treat protons as Dirac particles have been used for high-precision calculations for atomic hydrogen. As a theory QED by now has achieved many striking successes, and is sometimes called the most accurate physical theory.

Due to the close connection between the positive energy Dirac states and the spectrum of states predicted in QED, we would not expect electrons in localized (negative energy) states around a proton. We would also not expect an electron to be able to make a transition to a negative energy Dirac orbital since these are not part of the state space available to electrons in the theory.

There are a number of proposals for localized electronic states under discussion in the literature. In light of the comments here, almost all such models would then be immediately at variance with QED. The electron orbitals might be derived from a Klein–Gordon equation, or from some other model, which at the outset would not be consistent with QED. Alternatively, the orbital might come from a localized solution of the Dirac equation; which if made up of positive energy states must have a large positive kinetic energy; and if made up of negative energy states is excluded in QED.

It would seem that a model which seeks to account for cold fusion effects based on electronic transitions to negative energy Dirac states, to states predicted by the Klein–Gordon equation, or to other states inconsistent with QED, ultimately implies that either QED is deficient in some way (that one is proposing to improve QED itself in a fundamental way). I will point out that if one thinks that the road is hard dealing with anomalies connected with the Fleischmann–Pons experiment, the road associated with arguing that QED as a theory is wrong in some fundamental way will be a thousand times hard

Author's Response: General Considerations

I wish to emphasize that the approach in this paper is not based on the methodology of standard quantum electrodynamics (QED). A considerable literature exists on different electro-dynamical theories proposed for the calculation of the radiative properties of matter, for which, in order better to orient the reader to the subject matter of this paper, I give a brief review as follows. The quantization of the classical electromagnetic field was carried out by Dirac in 1927 [25]. A review of the quantized radiation field (QRF), as it is called, and its use in the calculation of radiative spontaneous emission and the Lamb shift is given by Louisell [26]. The QRF may be criticized in the sense that its distribution of frequencies is unrelated to the electron's own distribution of frequencies and is therefore unbounded such that its use in the radiation-matter interaction Hamiltonian for the electron leads to an energy shift – Lamb shift – which diverges linearly in the photon frequency, ω. As explained in [26] and elsewhere the linear divergence is interpreted as a permanent radiant property of a free electron such that, when it is included or "added back" to the calculation for a bound electron which is "bare" or undressed by the radiation field in the original calculation, the linear divergence is exactly canceled. This procedure is known as mass renormalization. Although a logarithmic divergence in the photon frequency remains, use of a suitable cut off leads to results, which agree quantitatively with experiment [27,28]. Notice that the linearly divergent mass of a free electron appears to be irremovable.

In order to gain a more satisfactory physical picture of the radiant aspect of the electron, pioneers have presented formulations – the neoclassical theory of Edwin Jaynes and coworkers [28] and self-field quantum electrodynamics of Asim Barut and coworkers [29] – in which the electromagnetic vector potential is calculated from the electron's current. These theories were problematic either in a quantitative sense in Jaynes' case or in the sense of possible flaws in the use of Schrödinger theory to calculate the electron's current in Barut's case [30,31].

The quantization condition for the photon and electron [25,26] requires that an initial higher-energy state of the electron has zero photons and that a final lower-energy state of the electron has one photon. The radiative emission rate converges because it vanishes by destructive interference of the out-of-phase electron wave functions of the initial and final states unless $\hbar\omega = \Delta E_{fi}$, where ΔE_{fi} is the energy gap between the two states and $\hbar\omega$ is the photon energy. On the other hand emission of a photon from the ground state means that the photon must be re-absorbed by the same state leading to a closed photon loop in which the electron energy shift diverges as ω. Dirac's relativistic-electron equation [32] leads to further complications in interpretation since a set of negative-energy states lies below the nominal ground state such that radiative spontaneous emission from the ground state to a negative-energy state lying below it would occur, which is unobserved in nature. Dirac's hole interpretation that the negative-energy states are filled with electrons in which an absent electron or hole represents a positron avoids the unphysical prediction since a positive-energy electron is forbidden by Pauli's exclusion principle from falling into a negative-energy state. But Dirac's hole theory also rules out the existence of Zitterbewegung, which arises from the interference between positive-energy and negative-energy states in observables in which an electron simultaneously occupies a superposition of positive-energy and negative-energy states. The recent observation of Zitterbewegung in a simulated electron experiment using a trapped-ion [33] suggests that hole theory, for all its success in positron physics, should be reexamined from the point of view of its possible reconciliation with Zitterbewegung. What is the ground state? A body of theory exists known as 4-space Dirac theory [34,35] in which the positive-energy spectrum of states is identical to that of standard Dirac theory but in which the wave function comprises contributions from both electrons and positrons, which one may surmise is just a bound-state form of Zitterbewegung, although not identified as such likely owing to the fact that the original prediction

of Zitterbewegung [36] was for a free electron. Following Barut and coworkers [29,37] and others, it is necessary here to pursue a first-quantization approach in order to understand phenomena usually treated within second quantization.

Recent work [34] suggests that the negative-energy states do not lie empty below the ground state but rather actively participate with it to form a two-component ground-state configuration. If the negative-energy states do not lie empty below the positive-energy states, then the quantization rules for radiative spontaneous emission do not physically apply. In [34, 35] the positive-energy spectrum is identical to that of standard Dirac theory, but the wave function exhibits Zitterbewegung (or comprises contributions from both electrons and positrons in the post-hole language of [35]). But the original motivation and experimental confirmation of Dirac theory was the spectroscopic observation of atomic fine structure. *Thus standard Dirac theory and 4-space Dirac theory* [34,35] *are therefore both confirmed by spectroscopic experiments, such that the confirmation of wave-function Zitterbewegung predicted by 4-space theory requires experiments designed to probe the wave function and not the energy spectrum*. In short Dirac hole theory is incompatible with the experimental observation of Zitterbewegung, which exists if indeed the negative-energy states do not lie empty below the positive-energy states such that radiative spontaneous emission from the *nominally* positive-energy ground state cannot exist and therefore does not need to be blocked by the artifice of filling up the negative-energy levels with electrons.

It seems clear from the above discussion that, while the QRF is physically correct for radiative spontaneous emission, it has unphysical consequences for the radiative shift of energy levels, which is corrected in practical applications by using the physical argument of mass renormalization. Indeed in his original paper [25] Dirac *limits* the use of the QRF to the emission and absorption of radiation and the derivation of the Einstein A and B coefficients. But one can use the renormalization concept that an electron permanently has radiant properties, which are therefore always present, such that the concept of a bare electron loses meaning. In standard QED this concept takes the form of continuously emitted and reabsorbed photons by the quantum state of a free electron, whose mathematical implementation, as stated above, leads to the divergent shift linear in ω for a free electron – the divergence which, when included in the bound-electron calculation, cancels the divergent shift linear in ω for the bound electron. One may postulate that this concept can be realized by finding a first-quantized Lorentz-invariant relativisitic equation of motion which accounts for the radiant properties of the electron in the same way that Dirac's equation accounts for the material properties of the electron. A small literature using the concept of a photon EOM already exists [26], but its applications appear to be confined to experiments in which the radiation-matter interaction is unimportant.

The shift of an atomic energy level relative to its position as predicted by radiation-free quantum mechanics and as observed experimentally, suggests that radiation is a permanent component of atomic structure. But existing theory, which comprises a quantum theory of matter, a quantum theory of radiation, and a quantum theory of radiation-matter interaction, perversely forces one to discard this conclusion in favor of a quantum-field-theoretic picture in which photons are created and destroyed relative to a quantum vacuum state [25,26]. Second, quantization extends this picture to particle fields, but in this paper we will be concerned only with first quantization for electron states. We can propose as well a first quantization picture for the quantum states of radiation. This is a departure from the approach outlined in [38], which used quantum field theory to propose a photon EOM. Our motivation is clear. The quantization of the radiation field by Dirac [25] to describe the emission and absorption of radiation fails to describe radiative energy shifts in absence of the use of renormalization theory to remove infinite contributions. The concept of radiation as a permanent part of the quantum states of the electron is actually introduced in renormalization theory, as discussed above. But again the inexorable field-theoretic logic of the continuous emission and absorption of virtual photons by the *same quantum state in a closed photon loop* leads to a radiative correction to the electron's mass which diverges as ω [26]. The missing concept whose mathematical implementation would avoid this failure uses the logic that the quantum states of matter *exist simultaneously and permanently with the quantum states of radiation* such that the artificial boundary-value setup of virtual-photon emission and absorption is avoided. Since the quantum states of matter are given by Dirac's equation, we require a supplemental wave equation to give the quantum states of radiation associated with the electron.

While Dirac's equation accounts for the material properties of the electron, the supplemental radiation wave equation may be considered to account for the radiant properties of the electron, as observed experimentally in the Lamb shift and the electron's anomalous magnetic moment.

It is easy to propose a radiant equation of motion (REOM) for the electron once it is recognized that the electron's material equation of motion (MEOM), which is Dirac's equation, can be inferred from the scalar product of the electron's 4-momentum and a material 4-potential posited for the electron. This understanding of Dirac's equation suggests that a REOM can be inferred from the photon's 4-momentum and an electromagnetic 4-potential posited for the electron.Recalling that the scalar product of 4-vectors is always Lorentz invariant [39], Dirac's equation can be derived by further elucidating the close relationship between Dirac's equation and the spinorial form of Maxwell's equation, which has been studied continuously since 1928 [40–43]. Dirac's equation can be inferred from the scalar product of the electron's 4-momentum and a material 4-potential, $(\Psi, \vec{X})$, posited for the electron as follows,

$$\left(i\hbar\frac{\partial}{c\partial t} - \frac{V}{c}, i\hbar\vec{\nabla} + \frac{e}{c}\vec{A}\right)(\Psi, \vec{X}) = \left(i\hbar\frac{\partial}{c\partial t} - \frac{V}{c}\right)\Psi + \left(i\hbar\vec{\nabla} + \frac{e}{c}\vec{A}\right)\vec{X}) = 0. \tag{A.1}$$

Using a carrier-wave expansions for $(\Psi, \vec{\mathrm{X}})$ in order to isolate a dominant frequency component of the 4-potential we obtain,

$$\Psi = \Psi_{-}(\vec{r}, t)\,\mathrm{e}^{-i\omega t} + \Psi_{+}(\vec{r}, t)\,\mathrm{e}^{i\omega t} \tag{A.2}$$

$$\vec{\mathrm{X}} = \vec{\mathrm{X}}_{-}(\vec{r}, t)\,e^{-i\omega t} + \vec{\mathrm{X}}_{+}(\vec{r}, t)\,\mathrm{e}^{i\omega t}. \tag{A.3}$$

On substituting Eqs. (A.2) and (A.3) into Eq. (A.1) and separately setting the coefficients of the exponential factors equal to zero, I obtain,

$$\left(i\hbar\frac{\partial}{\partial t} - V - \hbar\omega\right)\Psi + c\vec{\sigma}\cdot(i\hbar c\vec{\nabla} + e\vec{A})\xi = 0, \tag{A.4}$$

$$\left(i\hbar\frac{\partial}{\partial t} - V + \hbar\omega\right)\xi + c\vec{\sigma}\cdot(i\hbar c\vec{\nabla} + e\vec{A})\psi = 0. \tag{A.5}$$

Dirac's equation,

$$\left(i\hbar\frac{\partial}{\partial t} - V - mc^2)\psi + c\vec{\sigma}\cdot(i\hbar\vec{\nabla} + e\vec{A}\right)\xi = 0 \tag{A.6}$$

$$\left(i\hbar\frac{\partial}{\partial t} - V + mc^2)\xi + c\vec{\sigma}\cdot(i\hbar\vec{\nabla} + e\vec{A}\right)\psi = 0 \tag{A.7}$$

follows immediately on setting $\hbar\omega = mc^2,\ \vec{X}_{+} = \vec{\sigma}\,\Psi_{-},\ \vec{X}_{-} = \sigma\,\Psi_{+},\ \Psi_{+} = \psi,\ \Psi_{-} = \xi$. The reader may verify that Eqs. (A.6) and (A.7) are indeed Dirac's equation in coupled first-order form where ψ and ξ are known in the literature as the large and small components of the Dirac solution, respectively. Notice that the electron's spin can be interpreted as the polarization of the vector component of its posited material 4-potential. Notice that no further proof of the Lorentz invariance of the wave equation itself is required since Eqs. (A.6) and (A.7) have been inferred directly from a

scalar product of 4-vectors, which is always a Lorentz invariant [39]. As an example Dirac's equation for a hydrogen-like ion [44] is manifestly Lorentz invariant, but a fully relativistic Lorentz-invariant theory for two fermions is given by the Bethe–Salpeter equation [45]. As a further complication Coulomb's law for the interelectronic interaction is incompatible with Lorentz invariance such that it is represented field-theoretically by the exchange of virtual photons. If indeed future experiments show that Zitterbewegung is a real physical effect arising from the simultaneous occupancy of both positive-energy and negative-energy states by an electron, then the Bethe–Salpeter equation describing a positron and electron should be appealed to for a proper description of annihilation and pair creation.

While Eqs. (A.6) and (A.7) account for atomic fine structure and the anomalous Zeeman effect, whose spectroscopic observation was the motivation for Dirac's equation and its experimental confirmation, radiant properties of the electron also exist which are observed as a quantum electro-dynamical shift of atomic energy levels and the electron's anomalous magnetic moment. It is assumed that an electromagnetic 4-potential exists for the electron such that a REOM can be inferred from the Lorentz invariant found from the scalar product of the photon's 4-momentum and the electron's posited electromagnetic 4-potential thus,

$$\left(\frac{\hbar}{c}\frac{\partial}{\partial t}, \hbar\vec{\nabla} - \frac{e\hbar}{mc^2}\vec{E}, \vec{H}\right)\cdot(\Phi_v, \vec{A}_v) = \frac{\hbar}{c}\frac{\partial}{\partial t}\Phi_e + \left(\hbar\vec{\nabla} - \frac{e\hbar}{mc^2}\vec{E}, \vec{H}\right)\cdot\vec{A}_v = 0, \tag{A.8}$$

for either electric or magnetic fields $\vec{E}, \vec{H}$. The photon four-momentum is found from $\hbar$times a 4-gradient,

$$\left(\frac{\partial}{c\partial t}, \vec{\nabla} - \frac{e}{mc^2}\vec{E}, \vec{H}\right),$$

whose scalar product with the electromagnetic 4-current,

$$c\left(u + \int_0^t \mathrm{d}t'\vec{j}\cdot\vec{E}\right), \vec{S},$$

where

$$u = \frac{1}{8\pi}(\vec{E}\cdot\vec{D} + \vec{H}\cdot\vec{B})$$

is the electromagnetic energy density and

$$\vec{S} = \frac{c}{4\pi}\vec{E}\times\vec{H}$$

is the electromagnetic 3-current, gives the Lorentz-invariant electromagnetic continuity equation,

$$\frac{\partial u}{\partial t} + \vec{\nabla}\cdot\vec{S} + \vec{j}\cdot\vec{E} = 0. \tag{A.9}$$

This is simply the electromagnetic analog of writing the Lorentz-invariant material continuity equation,

$$\frac{\partial\rho}{\partial t} + \vec{\nabla}\cdot\vec{j} = 0, \tag{A.10}$$

as the scalar product of the known 4-gradient,

$$\left(\frac{\partial}{c\partial t}, \vec{\nabla}\right),$$

and the known material 4-current, $(c\rho, \vec{j})$. Notice that in the radiant-electron theory developed above the known 4-gradient is simply renormalized by the replacement

$$\vec{\nabla} \to \vec{\nabla} - \frac{e}{mc^2}\vec{E}, \vec{H},$$

which gives a Lorentz-invariant electromagnetic continuity equation since the scalar product of $\vec{E}$ or $\vec{H}$ with the electromagnetic 3-current, $\vec{S}$, vanishes. It is remarkable that a photon 4-momentum seems not to have been previously proposed in the literature.

As with the electron the photon scalar and vector potentials can be written in the form of carrier-wave expansions,

$$\Phi_\nu = \Phi_{\nu-}\mathrm{e}^{-i\omega_\nu t} + \Phi_{\nu+}\mathrm{e}^{i\omega_\nu t} \tag{A.11}$$

$$\vec{A}_\nu = \vec{A}_{\nu-}\mathrm{e}^{-i\omega_\nu t} + \vec{A}_{\nu+}\mathrm{e}^{i\omega_\nu t}, \tag{A.12}$$

from which on substituting Eqs. (A.11) and (A.12) into Eq. (A.8) and separately setting the coefficients of the exponential factors equal to zero, we obtain,

$$\left(\frac{1}{c}\frac{\partial}{\partial t} + i\frac{\omega_\nu}{c}\right)\Phi_{\nu+} + \left(\vec{\nabla} - \frac{e}{mc^2}\vec{E}, \vec{H}\right)\cdot\vec{A}_{\nu+} = 0, \tag{A.13}$$

$$\left(\frac{1}{c}\frac{\partial}{\partial t} - i\frac{\omega_\nu}{c}\right)\Phi_{\nu-} + \left(\vec{\nabla} - \frac{e}{mc^2}\vec{E}, \vec{H}\right)\cdot\vec{A}_{\nu-} = 0. \tag{A.14}$$

On setting

$$\Phi_{\nu+} = \xi_{E,H}, \quad \vec{A}_{\nu+} = \vec{\sigma}\zeta_{E,H}, \quad \Phi_{\nu-} = \zeta_{E,H}, \quad \vec{A}_{\nu-} = \vec{\sigma}\xi_{E,H}$$

we obtain the

Dirac form for the REOM,

$$\frac{\partial\xi_{E,H}}{c\partial t} + i\frac{\omega_\nu}{c}\xi_{E,H} + \vec{\sigma}\cdot\left(\vec{\nabla} - \frac{e}{mc^2}\vec{E}, \vec{H}\right)\zeta_{E,H} = 0 \tag{A.15}$$

$$\frac{\partial\zeta_{E,H}}{c\partial t} - i\frac{\omega_\nu}{c}\zeta_{E,H} + \vec{\sigma}\cdot\left(\vec{\nabla} - \frac{e}{mc^2}\vec{E}, \vec{H}\right)\xi_{E,H} = 0. \tag{A.16}$$

Writing

$$\xi_{E,H} = \mathrm{e}^{-i\omega t}\psi_{E,H} \quad \text{and} \quad \zeta_{E,H} = \mathrm{e}^{-i\omega t}\chi_{E,H}$$

in Eqs. (A.15) and (A.16) we derive stationary equations for $\psi_{E,H}$ and $\chi_{E,H}$; then we eliminate the equation for $\chi_{E,H}$ in favor of a second-order equation for $\psi_{E,H}$, obtaining equations for the electric and magnetic photon wave functions which have the Helmholtz form,

$$\left\{\nabla^2 + \frac{\omega^2 - \omega_\nu^2}{c^2} - \frac{e}{mc^2}\left[\vec{\nabla}\cdot\vec{E} + 2\vec{E}\cdot\vec{\nabla} + i\vec{\sigma}\cdot(\vec{\nabla}\times\vec{E}) - \frac{e}{mc^2}E^2\right]\right\}\psi_E = 0, \tag{A.17}$$

$$\left\{\nabla^2 + \frac{\omega^2 - \omega_\nu^2}{c^2} - \frac{e}{mc^2}\left[\vec{\nabla}\cdot\vec{H} + 2\vec{H}\cdot\vec{\nabla} + i\vec{\sigma}\cdot(\vec{\nabla}\times\vec{H}) - \frac{e}{mc^2}H^2\right]\right\}\psi_H = 0, \tag{A.18}$$

where we have used the identity,

$$(\vec{\sigma}\cdot\vec{A})(\vec{\sigma}\cdot\vec{B}) = \vec{A}\cdot\vec{B} + i\vec{\sigma}\cdot(\vec{A}\times\vec{B}).$$

Equation (A.18), for $\hbar\omega_\nu = 0$, was used in physical applications to calculate a *divergence-free* Lamb shift [46] and electron's anomalous magnetic moment [47].

Notice that all four of Maxwell's equations appear in Eqs. (A.17) and (18) as radiation-matter interaction terms and that the electromagnetic fields themselves and not the electromagnetic potentials occur such there is no question of a gauge dependence of matter-light interactions in the electron's REOM. The success of the use of Eqs. (A.17) and (18) to calculate divergence-free radiative properties of matter [46,47] suggests that the concept of radiation as a permanent part of the structure of matter is a valid one. Recall that this is identically the concept of mass renormalization used in standard QED used to remove infinite contributions to the electron's energy arising from unphysical logic that *first-quantized* states of matter exist which are totally free of radiation. As I have shown here it is possible to present a theory in which the electron does not exist in a bare or radiation-free state and whose material and radiant properties are described by a pair of relativistic, Lorentz-invariant first-quantized material and radiant EOM's respectively.

Acknowledgements

The author is grateful to T. Scott Carman for supporting this work. This work was performed under the auspices of the Lawrence Livermore National Security, LLC, (LLNS) under Contract No. DE-AC52-07NA27344.

References

[1] A. Rathke, *New J. Phys.* **7** (2005) 127.
[2] R.L. Mills, *J. Hydrogen Energy* **27** (2002) 565.
[3] R.L. Mills, *J. Hydrogen Energy* **26** (2001) 1059.
[4] R.L. Mills, M. Nansteel and P.C. Ray, *New J. Phys.* **4** (2002) 70.
[5] R.L. Mills and P.C. Ray, *New J. Phys.* **4** (2002) 22.
[6] R.L. Mills, P.C. Ray, B. Dandapani, R. M. Mayo and J. He, *J. Appl. Phys.* **92** (2002) 7008.
[7] Phillips, R.L. Mills and X. Chen, *J. Appl. Phys.* **96** (2004) 3095.
[8] H. Margenau, *Phys. Rev.* **46** (1934) 107.
[9] A.B. Evans, *J. Condensed Matter Nucl. Sci.* **2** (2009) 7.
[10] L. Schiff, *Quantum Mechanics,* 3^{rd} Edn. (Wiley, New York, 1968), pp. 470–471.
[11] L.D. Landau and L.M. Lifshitz, *Quantum Mechanics,* 3^{rd} Edn. (Pergamon Press, New York, 1977).
[12] B. Ritchie, *Phys. Rev.* A **59** (1999) 4571 and references therein.
[13] P. Morse and H. Feshbach, *Methods of Theoretical Physics* (McGraw-Hill, New York, 1953), p. 208.
[14] J.D. Bjorken and S.D. Drell, *Relativistic Quantum Mechanics* (McGraw-Hill, New York, 1964).
[15] W.K. Clifford, *Mathematical Papers,* R. Tucker (Ed.) (Macmillan, London, 1882).
[16] C.G. Darwin, *Proc. Roy. Soc.* **118** (1928) 654–680.
[17] O. Laporte and G, Uhlenbeck, *Phys. Rev.* **37** (1931) 1380–1397.
[18] R. Armour, Jr., *Found. Phys.* **34** (2004) 815–842 and references therein.
[19] B. Ritchie, *Optics Communications* **262** (2006) 229–233.
[20] B. Ritchie, *J. Mod. Optics* **55** (2008) 2003.

[21] M.E. Rose, *Relativistic Electron Theory* (Wiley, New York, 1961).
[22] W.R. Johnson and G. Soff, *Atomic and Nuclear Data Tables* **33** (1985) 405.
[23] H. A. Bethe and E.E. Salpeter, *Quantum Mechanics of One- and Two-Electron Atoms* (Dover, New York, 2008), pp. 195–196.
[24] B. Ritchie, *Int. J. Quantum Chem*. **111** (2011) 1.
[25] P.A.M. Dirac, *Proc. Roy. Soc.* (London) **A 114** (1927) 243.
[26] W. Louisell, Quantum Statistical Properties of Radiation (Wiley, New York, 1973).
[27] W.R. Johnson and G. Soff, Ato*mic and Nuclear Data Tables* **33** (1985) 405.
[28] M.D. Crisp and E.T. Jaynes, Phy*s. Rev*. **179** (1969) 1253.
[29] A.O. Barut and J.F. van Huele, *Phys. Rev*. A **32** (1985) 3187.
[30] I. Bialynicki-Birula, *Phys. Rev*. A **34** (1986) 3500.
[31] A.O. Barut, *Phys. Rev.* A **34** (1986) 3502.
[32] P.A. M. Dirac, *Proc. Roy. Soc.* (London) **A 117** (1928) 610.
[33] R. Gerritsma, G. Kirchmair, F. Zaehringer, E. Solano, R. Blatt and C. Roos, *Nature* **463** (2010) 68.
[34] B. Ritchie and C. Weatherford, *Int. J. Quantum Chem*. (2012), DOI: 10.1002/qua.24156.
[35] A. B. Evans, *J. Condensed Matter Nucl. Sci*. **2** (2009) 7; *Found. Phys.* **28** (1998) 291; **21** (1991) 633; **20** (1990) 309; references therein. This author uses the proper time from classical relativity to implement time-dependent Dirac theory as a 4-space theory. It is found in [10] that a geometric space-time or 4-space solution evolves naturally on solving the time-dependent Dirac equation in 3-space and the scaled time, *ct*. The electronic density is positive definite in our theory.
[36] E. Schroedinger, *Sitzungb. Preuss. Akad. Wiss. Ohys.-Math* Kl, **24** (1930) 418.
[37] A.O. Barut and J. Kraus, *Found. Phys.* **13** (1983) 189; A.O. Barut and J.P. *Dowling Phys. Rev* A **36** (1987) 649; **36** (1987) 2550; A.O. Barut, *Found. Phys.* **18** (1988) 95.
[38] Brian J. Smith and M.G. Raymer, *New J. Phys.* **9** (2007) 414 and references therein.
[39] P. Morse and H. Feshbach, *Methods of Theoretical Physics* (McGraw-Hill, New York, 1953), p. 208.
[40] C.G. Darwin, *Proc. Roy. Soc*. **118** (1928) 654–680.
[41] O. Laporte and G, Uhlenbeck, *Phys. Rev*. **37** (1931) 1380–1397.
[42] R. Armour, Jr., *Found. Phys*. **34** (2004) 815–842 and references therein.
[43] B. Ritchie, *Optics Communications* **262** (2006) 229–233.
[44] J.D. Bjorken and S.D. Drell, *Relativistic Quantum Mechanics* (McGraw-Hill, New York, 1964).
[45] H.A. Bethe and E.E. Salpeter, Quantum Mechanics of One- and Two-Electron Atoms (Dover, New York, 2008), pp. 195–196.
[46] B. Ritchie, *Optics Communications* **280** (2007) 126; *Int. J. Quantum Chem*. **112** (2012) 2632.
[47] B. Ritchie, *Optics Communications* **281** (2008) 3492.

J. Condensed Matter Nucl. Sci. 11 (2013) 123–141

Research Article

The Role of Voids as the Location of LENR

Edmund Storms *

KivaLabs, Santa Fe, NM, USA

Abstract

A proposed model explaining the low-energy nuclear reaction (LENR) process is described. The process occurs in voids of a critical size and involves a string of resonating hydrons, each of which is separated by an electron. This unique structure, called a "hydroton", is proposed to make LENR possible and provides a process that can explain all reported observations and predict several new behaviors while using only three basic assumptions.
© 2013 ISCMNS. All rights reserved. ISSN 2227-3123

Keywords: Cold fusion, Crack structure, Energy

1. Introduction

The phenomenon labeled low-energy nuclear reaction (LENR) or cold fusion [1] has now emerged from the shadows of rejection to become a demonstrated phenomenon [2]. Over the last 22 years, numerous attempts were made to explain how this novel effect functioned, but without any theory gaining wide acceptance. This failure resulted partly because insufficient information was available and basic laws of nature were frequently ignored.

The following basic information is now known. The effect does not to follow the rules used to describe hot-fusion, its close relative; the main nuclear products are at least helium and tritium without significant energetic particle emission; the process functions when either deuterium or ordinary hydrogen is used; the effect is very difficult to produce; and it does not require application of high energy as is needed to initiate hot-fusion. These features all need to be explained without violating basic laws and experience. The first problem is to identify where in the active material the LENR process occurs, because it obviously does not happen throughout the sample. This environment must be identified because its characteristics will limit any proposed process to only a few possibilities. For the sake of discussion, I call this active region the nuclear-active-environment (NAE) [3]. This paper proposes a location for the NAE and a process causing LENR within the NAE.

This is the third in a series of papers [4,5] justifying the role of voids (cracks) as the NAE [3]. The previous papers show why the LENR process does not occur in a chemical environment, as is commonly assumed, but instead requires a special structure that is independent of chemical restrictions. Several authors in the past have suggested cracks, a form

*E-mail: storms2@ix.netcom.com

© 2013 ISCMNS. All rights reserved. ISSN 2227-3123

of void or gap, as the location of the LENR process, as discussed in Section 3.1. These ideas are not useful because the exact characteristics of the crack were not identified and the proposed mechanism did not fully account for observed behavior. This paper attempts to address these deficiencies. Once the need for a void-like structure is accepted, a mechanism must be proposed that can operate in such an environment while delivering the observed reaction products. This paper will suggest such a mechanism. All previous models have either focused on concentrating enough energy to tunnel through the Coulomb barrier or by forming a structure, such as a neutron [6] or a Bose–Einstein Concentrate (BEC) [7] that ignores the barrier. The model proposed here takes an entirely new approach.

The word "void" includes many different structures having one thing in common – a space in which atoms making up the surrounding material are absent, i.e. a gap. The word "void" will be used in this paper to identify this general condition. These voids can take the form of typical cracks with parallel walls, as tubes grown in or formed by a material, or with a cage-like structure. The carbon nano-tube is a common example [8] of a tube-like structure, although similar structures can be formed by many other materials [9]. Zeolite [10] is an example of a cage-like structure. Regardless of the shape, the main feature important to the LENR mechanism described in this paper is the distance between the walls and local symmetry. It is essential that the maximum distance be no more than a few atomic diameters. Otherwise, the hydron molecule can form, which is known not to allow fusion. Most voids form with too great a distance between the walls to support the LENR process. The proposed mechanism also requires the void to have a length sufficient to hold a string of hydrons.[a]

In summary, LENR has no relationship to the hot-fusion process, does not occur in or on a chemical structure, and requires a void of a critical size and shape with nano-dimensions to function. These voids are apparently formed occasionally by random chance during attempts to initiate the LENR process, thereby accounting for the difficulty in replicating the claims. The first step is to identify how the voids might be created by chance.

2. Void Formation and its Characteristics

Voids form in solid materials as a consequence of stress and its release. This stress can result from applied external forces, as a result of concentration or temperatures gradients within the material, or changes in crystal structure. Several examples of this process are provided in the following figures, but any nuclear-active voids would be too small to detect at the resolution used. In most cases, a range of void sizes is present, with only the largest being visible. The depth of the void can also be variable, with only its penetration of the surface being visible.

Figures 1–3 show several different kinds of voids that have been associated with LENR. Figure 1 shows cracks that form as hydrogen is lost after beta-PdH is plated on copper (1.2 μm). Shrinkage of about 12% as the beta phase converts to alpha-Pd creates obvious gaps, but ones too large to support LENR and too unstable to be useful because the width of the crack will change as the hydrogen content of the layer changes. Nevertheless, a 2 μm layer of Pd plated on Pt was found to make excess energy during electrolysis [11]. Reducing the layer thickness reduces the size of the openings and increases crack density, a condition which might be achieved using the Fleischmann–Pons (F–P) [1,12] method.

Figure 2 shows many pits of many sizes formed after Ni and Pd interact on the surface at high temperature followed by exposure to H_2. Such pits are frequently seen after electrolysis of Pd and are sometimes attributed to local melting. Figure 3 shows complex cracking when a thin deposit of Cr delaminated from a surface. Such cracks are not a NAE and can actually stop the process because the hydrons could be too easily lost from any remaining NAE. All of these materials shown in the figures might contain voids small enough to support the proposed mechanism, although the visible voids are much too large.

[a]The word "hydron" identifies the bare nucleus (ion) of any hydrogen isotope.

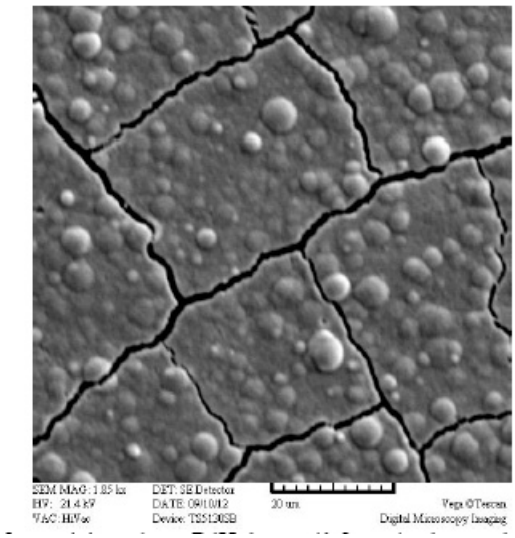

Figure 1. Cracks formed in a beta-PdH layer (1.2 μm) electroplated on copper after the contained hydrogen is removed.

Electrolysis using the F–P method causes an assortment of impurities to deposit on the Pd cathode surface, including Li, Si, and Pt [13–16]. Lithium is present in the electrolyte and silicon comes from the Pyrex. The Li is retained on the surface because it can react with Pd to form various Pd–Li alloys [17] that are stable in the aqueous environment.

Figure 2. SEM image of a surface of Ni plated on Pd on which voids and cracks have formed.

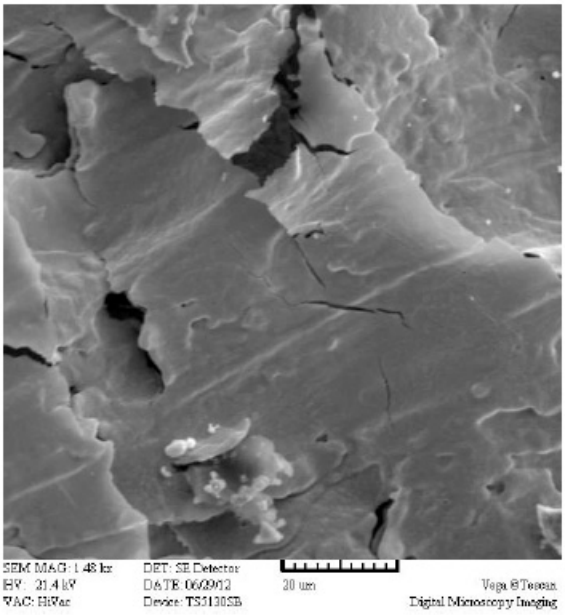

Figure 3. SEM image of surface of Cr on Pd after exposure to H_2.

Formation of such alloys can cause crack formation as the dimension of the surface changes. In addition, absence of care can provide copper from exposed wires and carbonates from the air, both of which can deposit on the cathode. Gradually platinum transfers from the anode and coats the cathode surface. All of these elements can deposit a surface layer in which voids can form. Bockris [18] was the first to attribute the frequently observed long delay in detecting extra energy to slow formation of nano-sized cracks in the surface layer. However, once a crack has grown too wide, it is able to allow loss of deuterium as D_2 from the surface, as shown in Fig. 4, thereby reducing the required high D/Pd ratio [19] and stopping LENR. Consequently, success in initiating LENR by the electrolytic process requires formation of very small cracks rather than a fewer number of large ones. This means, the best palladium for this purpose would have to be specially treated [20] to create many sites where stress can be relieved by crack formation, thereby increasing the number of sufficiently narrow gaps. Indeed, impure Pd in which many potential sites for crack formation would be present has been found to give greater success than pure Pd [21]. McKubre et al. [21] take note of a surface layer as an apparent requirement to achieve LENR. In addition, the observed nuclear products (helium and tritium) [22,23] are only observed to occur at the surface because this is the only location where the required cracks might form. Figure 4 shows several cracks large enough to permit escape of D_2 from a Pd cathode held under acetone, but too large to support LENR. Such large cracks form easily in Pd, which makes this metal a less than ideal cathode. The Pd–Ag alloy is less prone to forming large cracks and has been noted for its success in producing LENR [24–29], presumably for this reason. Titanium has been reported to produce excess heat when used a cathode or when plated on Pd. In this case, crack formation is ongoing and extensive, which may supply a steady number of suitable cracks even though they will rapidly grow too large [30–33]. Beta-PdD can be co-deposited to form a complex surface structure [34] that has been found to produce excess energy. A typical morphology is shown in Fig. 5. These clusters would be expected to produce voids between each one as its size changed owing to loss of Hydron or additional deposits of Pd. In summary, many people have noted and explored conditions that would be expected to create cracks or voids using the F–P method

Figure 4. Bubbles of D_2 arising through acetone from cracks in PdD after electrolysis. The bright lines at which bubbles are forming are surface scratches that focused formation of a deeper crack structure.

and these efforts have been frequently successful in producing LENR, but without the success being attributed to void formation.

Clusters are also found to form on cathodes of palladium subjected to gas discharge, as shown in Fig. 6, where cracks are apparent at a few locations. On occasion, voids take the form of pits, shown in Fig. 7, as an alloy forms on a surface.

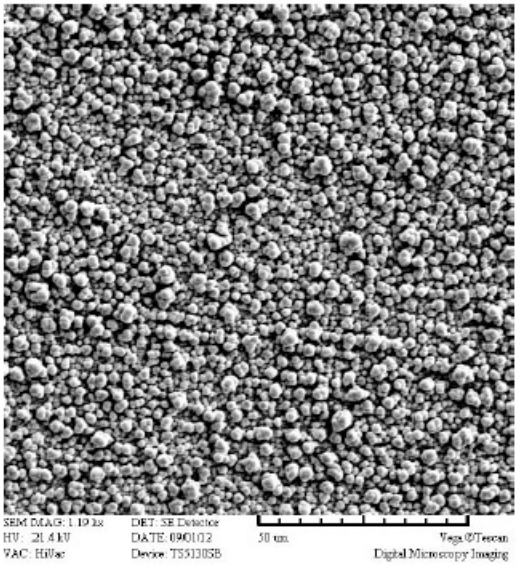

Figure 5. PdH deposited on copper using the slow co-deposition process.

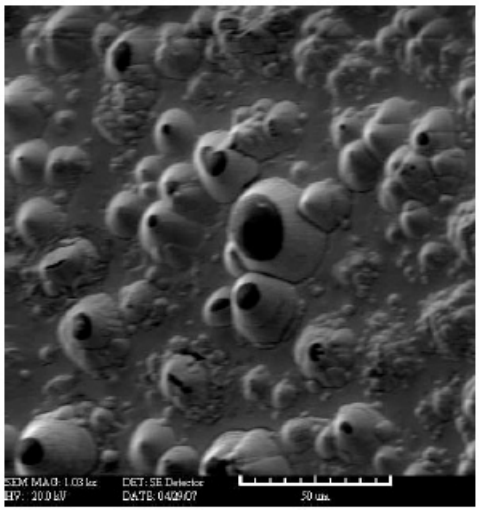

Figure 6. Deposit created by bombardment with D_2 ions. A few local cracks can be seen. Active cracks would not be visible at this magnification (Storms and Scanlan [35]).

3. Proposed Models Based on Voids

3.1. Proposals from the Literature

Although considerable attention has been paid to the surface as a potential site of LENR, crack or void involvement has been largely ignored, with the few exceptions described below.

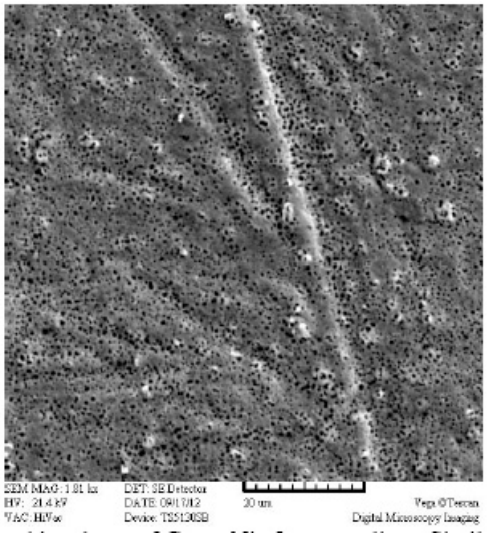

Figure 7. Pits formed in a layer of Cu on Ni after annealing. Similar pits are frequently observed in Pd after electrolysis.

The act of crack formation in many materials generates sufficient charge separation to produce a very brief hot-fusion reaction in the crack. Initially, the role of cracks was attributed to this process, which is called fracto fusion [36–39]. This process has no relationship to LENR.

Bockris [40] noted in 1996 the discrepancy between the short time required to fully react the Pd with deuterium and the long delay before excess power was detected. He proposed this delay allowed cracks to form, which would be influenced by the thickness of the deposited impurity layer, the history of how current was applied [41], and the purity of the Pd metal. High internal pressure within a void was proposed to initiate a nuclear reaction by an undefined mechanism [42,43]. Such a process involving high pressure would not be possible when the gas-loading method is used, which limits application of the process he described.

Frisone [44–49], in a series of papers, calculated the increased rate of what he calls deuteron–plasmon fusion by assuming electron screening can cause tunneling that would be increased by an increased concentration of deuterons in a crack. The model does not address how the resulting energy would be dissipated while conserving momentum and avoiding detection of the resulting energetic radiation.

Godbole [50] using my paper [4] as a starting point, offers an approach best described in his own words; "Unification of the electromagnetic and weak forces at low energy scales. Re-gauging in the lattice to produce attractive EW forces over lattice-constant distances. Periodic Bloch field replacing Higgs field." The proposed model obviously requires a clearer description.

None of these models has shown consistency with observation or has addressed the full range of observed behavior.

3.2. Proposed new mechanism

Having identified where and how voids can form, the next step is to examine the conditions present in a void that might support a fusion reaction.

Electrons populate the void wall, giving it a net average negative charge similar to all clean surfaces. The positive charged hydrons find their way into this negative environment by diffusion from the surrounding material. If the dimension is correct, the hydrons can become suspended in the space at equal distance between the walls. In other words, each wall supplies an equal attractive force that allows the hydrons to be suspended without significant restraint to their movement. A slightly positive energy-well would occur between each positively charge hydron to which an electron would be attracted, thereby creating what appears to be a periodic chemical structure. Up to this point, normal rules of chemistry and physics would apply.

For such a structure to be suitable for the purpose proposed here, the intervening electron must not form a conventional molecular bond, as normally occurs in large cracks. Instead, the electrons on the wall of the gap are proposed to interfere with formation of a conventional molecular structure. As a result, the intervening electrons orbit[b] the virtual (image) charge located between the protons. In addition, the structure is free to vibrate without being constrained by rules governing such behavior in a chemical lattice, such as PdD or NiH. In summary, a linear structure of hydrons separated by electrons having an assumed novel behavior is proposed to form. Figure 8 shows a populated string of hydrons in the gap before resonance starts. The distance between the protons and electrons is controlled by the space between the atoms in the wall, which initially causes the p to be too far apart to allow nuclear interaction.

Once formed, the Hydroton string would vibrate in the normal random, chaotic way as is typical of all atoms. Eventually, local or applied alternating magnetic fields are proposed to cause the vibration to harmonize so that all

[b]Based on the model created by Brian Scanlan, this electron orbits around a virtual (image) charge between the two hydrons. Consequently, its behavior is unique and not determined by rules normally applied when an electron orbits a nucleus. Scanlan is exploring the required rules and expects to publish a paper soon.

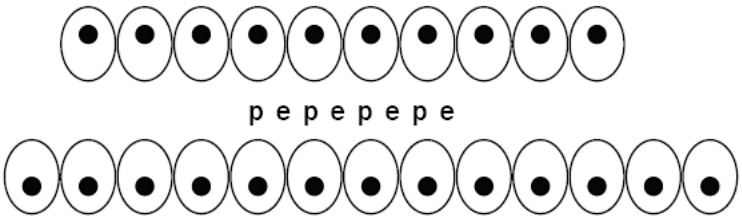

Figure 8. Diagram of a gap within an atomic lattice of metal atoms containing the proposed Hydroton structure. The distorted electron cloud around each metal atom is approximated as an oval. The "p" designates a proton and "e" designates an electron trapped in the potential well between each proton. The alignment between the surrounding atoms and the Hydroton structure is only approximate as drawn. The number of "p" and "e" pairs in the Hydroton structure is arbitrary.

members of the string are vibrating in phase along the line of the components, thereby accounting for the reported effect of applied magnetic fields [51–53].

How can energy be released from such a structure? Normally, energy is released from a chemical structure when it rearranges to a lower energy with emission of photons, called X-rays. In the case of the proposed mechanism, the structure is proposed to rearrange with release of nuclear energy as photons. The process is proposed to start as a resonance within the structure during which its energy becomes greater when the distance between the hydrons is momentarily reduced. This additional energy is released by photon emission. Once this energy is released, the distance between the components in the hydroton is reduced. This process repeats many times until the reduced distance allows direct nuclear interaction, at which point very little energy remains in the structure. In contrast, hot fusion causes the distance to be reduced too rapidly for energy to be released by photon emission. As a result, the nuclear energy must be emitted immediately as kinetic energy, which requires emission of two particles in order to conserve momentum. In contrast, when cold fusion occurs, momentum is dissipated gradually in the form of many photons so that very little momentum or energy remains when the final nuclear product is formed. This process is proposed to explain the lack of energetic radiation, except as photons, when LENR occurs. The small amount of energetic particle radiation occasionally detected is proposed caused by a small amount of hot fusion occurring at the same time. This structure and process are unique and may create a new way to describe nuclear interaction, as revealed by LENR.

The product of the fusion reaction depends on which isotope of hydrogen is present. For example, a string of -d+e+d+e+d+e-[c] etc would condense to form a series of H^4 nuclei, –e+p+e+d+e+p-, etc. would form tritium nuclei, and -p+e+p+e+p-, etc. would form deuterons. The extra electrons not added to the final nucleus would be released from the structure and join the conduction band in the surrounding material. In each case, mass would be lost and energy would be released at each vibration cycle, with two photons being emitted in opposite directions in order to conserve momentum. In addition, weak interaction between the string and the surrounding electrons is expected to transfer some energy into the surrounding atoms as phonons. Because the photons all originate from a common source with the same repetition rate, they would be coherent and have laser-like properties, as first identified by Karabut [54].

This approach is novel and is different from how other models propose fusion takes place. The present approach recognizes that enough energy is already present and only requires a mechanism for its release. In this case, release is gradual as the Coulomb barrier is gradually overcome. In other words, the mechanism acts like a catalyst by providing many small occasions for energy release rather than a single, sudden release as the Coulomb barrier is overcome by a single event during hot-fusion.

[c]Bass [49] proposed a similar vibrating string of -d-e-d- to form within a lattice and concentrate energy by resonance until enough energy is localized to allow the d to tunnel though the barrier. This process would be expected to produce hot fusion products, not cold fusion.

In this model, the photon frequency is determined by the vibration frequency of the string. A string made mostly of d will have a smaller frequency than a string of p, because the mass is greater. The smaller the frequency, the greater the fraction of generated photons will be absorbed by the wall of the apparatus. Consequently, most radiation produced by a deuteron-containing string would not leave the apparatus. On the other hand, a mostly proton-containing string would produce photons of sufficient energy for some to be detected outside of the apparatus. For the same reason, a short string will emit photons with a higher frequency than a long string. As a result, photons produced by a short string of p are expected to have enough energy for many of them to leave the apparatus and be detected. Short strings would be more common when the hydron concentration is low, such as is the case when the material is first exposed to ambient gas. As a result, detected radiation is predicted to be greater when an active sample is first exposed to gas and will gradually drop in intensity as the strings grow longer, as Rossi and Celani have claimed to observe when the material first starts to become active. In addition, the spectrum of measured frequencies will change and become broad as different active voids achieve different sizes for the resonating strings. In other words, easily measured radiation is predicted to occur only when protium is used and then only initially before excess energy is detected. This expectation is consistent with reported experience.

What are the predicted consequences? The LENR process is independent of the material, depends only on the size of voids, and the nuclear product is determined only by which isotope of hydrogen is present. The process is not expected to be unique to Ni–H and Pd–D. In fact, these metal–hydron combinations are not expected to be the best choices. Of all possible combinations of hydrons, pure deuterium will produce the most energy without significant radiation being detected outside of the apparatus, with helium being the only detected nuclear product. A mixture of deuterium and protium will make tritium and have less energy production than the pure d system. Use of pure protium will result in production of deuterium, which will subsequently react with protons to form tritium. This system will produce the least amount of energy, the most radiation, and eventually an inconvenient amount of tritium. Therefore, use of ordinary hydrogen as a practical energy source is not advised, although its use during studies of the process is convenient.

An odd number of protons in an active void will result in neutron emission as the extra electron is occasionally absorbed into the extra proton. Likewise, an odd number of deuterons will result in a dineutron as the odd deuteron absorbs the last electron. These low-energy neutrons and dineutrons can be emitted from the apparatus or combine with surrounding nuclei to produce transmutation. Absence of significant neutron radiation indicates an odd number is much less probable than an even number in the hydroton.

If the number of active voids is small, increased LENR can be obtained by causing the hydrons to move, either as a result of a concentration gradient or by applying an electric field. This flux of moving hydrons will eventually encounter and become available to an active void. In the absence of such a flux, the hydrons must find an active void by random diffusion, which is a slow process. This explanation is consistent with the claims by Liu et al. [55–60] who were able to generate a small amount of power simply by diffusing D_2 through palladium metal. This effect was replicated by Biberian and Armanet [61,62]. The heat reported to result from applying a voltage to a proton conductor ($LaAlO_3$, $SrCeO_3$) containing deuterons is also explained by this process [63-69]. The Cohan-effect proposed by Preparata and Fleischmann [70] and the observations by Celani et al. [71] and McKubre et al. [21] are all consistent with this explanation.

The frequent failure to detect excess energy using normal hydrogen is proposed to result from the great difference on energy produced by the respective fusion reactions. Fusion between two deuterons is observed to produce 25±5 MeV/helium [23] while the same reaction between p-e-p is expected to produce no more than 1.4 MeV/event. Unless a high concentration of NAE is present, the energy resulting from p fusion might be too small to detect. Consequence, the apparent absence of reported power does not necessarily prove that p does not produce energy in the same material as when d is used.

Although the basic predictions are consistent with many seemingly unrelated observations, some aspects of the

proposed processes may seem unlikely and are in conflict with conventional nuclear understanding. Nevertheless, this is the first model to show how all aspects of LENR are logically related and can make predictions not possible using any other model. This fact should encourage acceptance of the less-than plausible suggestions in order to maintain the usefulness of a logically consistent tool. After all, errors and omissions in the model can only be identified by directed research encouraged by the model. A mathematical description of this model will be provided in later papers.

4. Summary

A string of hydrons is proposed to form a novel structure; with each hydron separated from its neighbor by an electron have a novel relationship to the structure. This structure, called a "hydroton", is created by unusual conditions present in a nano-void having critical dimension and shape. Once formed, this structure has the ability to resonate freely and emit photons having a frequency determined by the total mass of the string. As energy is lost from the structure, it collapses into a collection of nuclear products that are determined by the hydon composition of the string. If the string contains only deuterons, the nuclear product is H^4, which immediately decays into He^4 by emission of an electron. When the string contains a mixture of protons and deuterons, a mixture of tritium, deuterium, and He^4 result, with the amount of each determined by the p/d ratio in the string. A string containing only protons will initially produce only deuterium. In the latter case, the photon radiation may have enough energy to be detected outside of the apparatus, especially when the p concentration in the material is small.

This model is based on three basic assumptions:

(1) All LENR products result from the same process in the same NAE.
(2) No basic law of chemistry or physics is violated.
(3) An electron can form a novel relationship to a string of hydrons.

While the assumptions lead to a model that is consistent with all observed behavior of LENR, it predicts two behaviors that are unexpected. The H^4 that results from the process is proposed to decay by prompt beta emission rather than by the expected emission of a neutron. In addition, the role of the electrons in the process does not appear to involve the neutrino as the Standard Model expects. These two important conflicts with expectation should encourage a detailed study of the LENR, aside from it being an important source of ideal energy.

Appendix A. Reviewer Comments

The publication of this paper will likely be controversial, so I thought it might be useful to contribute some reviewer comments to be published following the paper. Ed Storms is of course well known in the field, and has made a great many important contributions over the years. He has published previously many important and relevant experimental papers; on excess heat measurements; on the loading ratio; excess heat versus loading and current density; temperature dependence of excess power; orphan oxygen measurement to estimate the loading in a co-deposited Pd layer; and more recently results on charged particle emission. From my perspective, Storms has more than earned the right to speculate, based on his long record of previous accomplishments.

In the last few years Storms has taken an interest in the theoretical problem as to what is going on microscopically in excess heat experiments. As documented in his book, Storms has over the years accumulated an enormous number of experimental papers; from his own experimental work and his strong interest in experiments generally done in the field, he brings a unique perspective to the theory problem. Consequently, I am interested in his ideas, and in the publication of his thoughts on the problem. At the same time, there are specific issues and details in his paper that I very much do not agree with. The resolution for this is to develop a set of reviewer comments that draw attention to some of these issues. The thought behind this is that some of what Storms proposes goes against what is in the literature, and what

would be expected given physical law; it seems useful here generally to develop some discussion of the associated issues, especially since Storms is not alone in the views presented.

As a reviewer who has recommended for publication of this paper, I have a responsibility to the members of the community on the one hand to help my colleagues get their ideas published (in the hope that the community benefits and the authors get recognition for their work), and also to help make sure that what is published is correct. If I view the Storms paper as speculative, then the question of correctness is not the primary issue, as a speculation can be useful even if incorrect. Since Storms views the paper less as speculative, and more as the way things are, then input from the literature as to how things are is warranted.

The field itself is very much a multi-disciplinary one, and this is reflected in the Storms paper. Part of the discussion concerns voids, and proposed configurations of hydrogen isotopes and electrons within the voids; some of my comments will be specific to this topic. And part of the discussion concerns proposed nuclear mechanisms; some of the comments below will focus on these issues.

Appendix A.1. Proposed p–e–p–e–p–e . . . string

Storms proposes that protons and electrons would alternate forming a p–e–p–e–p–e . . . string inside of a sufficiently small void. Such a structure would not be expected based on what is in the literature. From calculations, and also from experiments, it is known that when molecular H_2 approaches a clean metal surface (such as Pd) that when far away (a few Angstroms) the H_2 molecule is intact [72]. As the molecule gets closer to the surface and the background electron density increases, occupation of anti-bonding orbitals causes the bond length to increase. This starts at an electron density near 3×10^{22} electrons/cm^3, and by the time the electron density has reached about 7×10^{22} electrons/cm^3 the molecule has split apart and the hydrogen atoms individually seek locations where the embedding energy is minimized (which correspond to an electron density near $7 - 8 \times 10^{22}$ electrons/cm^3 [73]).

In a Pd monovacancy in PdD, the electron density at the position of the missing Pd atom reaches its lowest point, and takes on a value of about 2×10^{22} electrons/cm^3 [74]. This is sufficiently low for molecular H_2 to form with a bond length nearly indistinguishable from that of the molecule in vacuum. Storms requires his void to be sufficiently small such that molecular H_2 does not form; this seems to restrict the background electron density to be higher than about $4 - 5 \times 10^{22}$ electrons/cm^3. Since a Pd monovacancy does not satisfy this condition, presumably Storms is thinking of a smaller defect, perhaps a dislocation boundary. In any event, we have a pretty good idea of what hydrogen looks like and how it behaves in the background electron density range from $4 - 5 \times 10^{22}$ electrons/cm^3 and about $7 - 8 \times 10^{22}$ electrons/cm^3 (where the minimum embedding energy occurs). The hydrogen atom under these conditions is reasonably close to the vacuum hydrogen atom (in that it is an atom with slight additional occupation of the 1s orbital), and we would very much not expect to see a bare proton next to a localized electron. The p–e–p–e–p–e . . . string proposed by Storms would cost more than 10 eV per ionized electron to form in this regime.

Appendix A.2. Energy release as X-rays

A key issue associated with the Fleischmann–Pons experiment is the absence of energetic nuclear radiation in amounts that correspond to the energy produced. Any model that seeks to address the excess heat effect must deal with this. Storms proposes x-ray emission in connection with local vibrations of a p–e–p–e–p–e . . . string for this. There are all kinds of problems with this. For example, electrons or protons with keV level energy would quickly leave the structure, so that it is hard to understand why such a structure should remain intact (much less exist at all). Storms connects this with the collimated x-ray emission observed by Karabut, which seems to me to be a different effect. For example, Karabut sees X-ray emission under conditions where no hydrogen or deuterium is present (collimated X-ray emission is shown in his work with a Pd cathode and Kr gas in one example, and with an Al cathode and He in another example); so

one would not expect any p–e–p–e–p–e . . . structure to be present since there is no obvious source of hydrogen isotopes. Moreover, there is no correlation between this collimated x-ray emission and excess heat in Karabut's experiments.

Appendix A.3. Proposed p–e–p reaction mechanisms

The nuclear reactions proposed by Storms in this paper are essentially weak-interaction-based fusion reactions; we consider first

$$\mathrm{p + e + p \rightarrow d + \nu_e + 1.44\ MeV.}$$

A headache with this reaction is that almost all of the reaction energy goes into the neutrino, so it would not be so great for producing excess heat. A second headache is that would expect it to compete with the more probable two-step reaction

$$\mathrm{p + p \rightarrow {}^2He \rightarrow d + e^+ + \nu_e + 0.42\ MeV.}$$

Since this reaction results in positron formation, there would be a very large amount of 511 keV annihilation gammas present (which can be ruled out experimentally). Hence, one would not expect the p–e–p reaction to occur in the absence of the p–p reaction that results in gamma emission.

I note that since the weak interaction is involved, the associated reaction rates once the protons get close enough to interact is extremely slow.

Appendix A.4. Proposed d–e–dreaction mechanisms

Storms describes a d–e–d reaction which he suggests will lead to ^{4}H which he expects to subsequently beta decay to ^{4}He. This reaction again suffers from the headache that for the first step, almost all the reaction energy would go into the neutrino. Next, if ^{4}H were made, there is the question of how it decays. For example, in years past it was thought that ^{4}H might beta decay [75] as proposed by Storms. However, nearly all recent literature (such as [76]) has it decaying kinetically into $^3\mathrm{H} + \mathrm{n}$, which would happen in a very short time (which is to say that the branching ratio for beta decay would be exceedingly small). As was the case above, one would expect competition from the conventional d-d fusion reactions, which should be more likely by roughly twenty orders of magnitude.

Appendix A.5. Tunneling

The reactions proposed by Storms are at the end of the day fusion reactions, so there are issues associated with tunneling as in other theoretical proposals.

Appendix A.6. Discussion

One issue that remains concerns the reconciliation of the experiments with theory more generally. Modern physics has accumulated a stunning array of success in accounting for a wide variety of phenomena, and correspondingly a relatively small number of failures. There are those in the physics community that are of the opinion that pretty much all physics relevant to cold fusion is exceedingly well understood, with the conclusion that cold fusion can be ruled out [77]. On the other hand, those familiar with the experimental results on the Fleischmann–Pons experiment know that the excess heat effect is real. Consequently, there must be something amiss in the physics textbooks, since something very big and very important has been left out (otherwise physics would be able to account for this effect as well).

At issue then is what response might be appropriate in light of this situation? Should we take the position that most of physics is solid, and there is probably some small warranty on a theorem somewhere that needs to be revised so that overall consistency with both the existing experimental set and the Fleischmann–Pons experiment is obtained? Or should we take the position that since physics has gotten it so wrong in the case of the Fleischmann–Pons experiment that we should distrust it in other areas. The answer probably is in the area of philosophy, but it is this issue that seems to make clear the difference between how Storms looks at the theoretical problem in contrast to how this reviewer looks at it.

Appendix B. Response to Reviewer's Comments

I appreciate the comments by the reviewer and the willingness to not only discuss the issues but to encourage publication even though full agreement has not been achieved.

This paper addresses three different assertions. These are:

(1) The LENR phenomenon does not occur in a chemical lattice because to do so would violate basic laws of thermodynamics.
(2) LENR takes place only in cracks having a special dimension.
(3) The fusion process involves creation of a string of hydrons that emit photon energy from a resonance process before the fusion process is finally achieved.

The reviewer has focused only on item (3)

The paper is a preliminary description of a proposed mechanism and a summary of the basic reasons for using this approach. The paper is not a final description or is it intended to answer all questions. Nevertheless, the reviewer has asked some questions I will answer here.

First, I view my description with just as much speculation as, for example, Kim, Takahashi and Hagelstein view their own models. I therefore ask the reviewer to examine my speculations in the same manner he would any other explanation and not assume that I do not believe I'm engaging in speculation. Nevertheless, what would be the purpose of publishing an idea unless its author considered it to be plausible and worth making public?

In contrast to previous models, I am attempting to describe a proposed process in much greater detail than has been done by anyone else while using the model to explain the full range of observed behavior. As expected, the model is in the process of growing in understanding in my own mind and in the detail I have used for its description. Therefore, I would hope a reviewer would provide encouragement to develop the ideas rather than trying to find as many ways possible to reject the basic approach.

The hydron string is basic to the process I am proposing. It is basic because I believe a dynamic mechanism must be proposed that can dissipate energy in the form of low energy photons and phonons before the fusion process is finished. It must operate outside of the lattice and the process must occur rarely to be consistent with well-known laws of chemistry and observed behavior. Other theoreticians have chosen to use different approaches, with each having flaws. In contrast, I am proposing a single universal process involving any isotope of hydrogen during which energy is lost while the observed or expected nuclear products are produced. My approach is well within the accepted style of how theory in this field is reported and developed.

Appendix B.1. Proposed p–e–p–e–p–e . . . string

This concept is not fully understood by the reviewer, and indeed by most readers, because they mistake the diagram I show in the paper as describing the true condition rather than as a cartoon. The true condition requires much more detail

than can be shown in a single figure or was described in this paper, partly because the concept is still being developed.

My present view is that the proposed string of hydrons forms as a large covalent molecule in a gap or crack. Let us start by imagining the situation when the gap is large. The atoms of hydron and the their molecules would be absorbed on each wall in the "normal" manner. This absorption process is known to be exothermic and is spontaneous. Therefore, it satisfies the requirement I discuss in assertion item (1) (above). As the gap is reduced, a distance will eventually be achieved at which the atoms and molecules will be equally absorbed on both walls simultaneously. This is the condition I propose is required for the resonance process to function. To be clear, I use this shrinking description only to make the process easier to understand. The real process starts with the gap being small and growing big enough for the described conditions to form.

Once the required gap dimension is achieved, the contained atoms and molecules can be considered to be suspended at equal distance between the walls. Because the walls are not uniform in charge, they would appear to be "lumpy" because the atomic structure forming the walls is uneven at this scale. Consequently, the hydron atoms will have to move through charge valleys in the process of assembling the proposed structure. This detail in no way distracts from the proposed process.

Formation of the chain requires one additional condition not present in large cracks, on normal surfaces, or within the lattice itself. When the walls are very close together, the spherical form or "cloud", in which an electron orbits the nucleus, is perturbed into a disc shape. In other words, all paths taken by the electrons are forced to align roughly with a plane passing through a line between the photons and parallel to the walls. This shift in position occurs without any change in energy or angular momentum because the distance from the nucleus does not change. Such a structure would be expected to cause the two protons to come closer together because the average negative charge between them would increase as the electrons more often pass through the line between adjacent nuclei. As an example, this reduced distance occurs when H_2 forms under normal conditions for similar reasons. Suppose another proton with an electron in a similarly distorted orbit were to come close. This similar alignment would increase the probability that its electron could be shared in the orbits of the other two atoms by a process of exchange. Addition of more hydrogen atoms would cause this molecular structure to grow in length with the bonding energy being released into the surrounding lattice as heat [d]. Up to this point in the description, the proposal is based on conventional behavior typical of a chemical structure created by covalent bonding. Granted, no such large molecule has been detected or proposed before, but creation of such a structure is not impossible based on any law of Nature, as far as I know. It is the next step that enters uncharted territory.

Appendix B.2. Energy release as X-rays

We know that helium is produced with nearly the expected energy without significant radiation. This means the energy *MUST* be released before fusion occurs in a form that cannot get out of the apparatus. Phonons have this ability but they can carry so little energy that dissipating 23.8 MeV/event seems unreasonable without the environment being disrupted or destroyed. Photons can carry away such energy and, indeed, small fluxes have been detected outside of the apparatus, especially when H_2 is used. The challenge is to identify a process that can generate photons before a fusion reaction is complete and helium, tritium, or deuterium forms. Because the photons would be coherent if they originated from my proposed process, I offer the claims reported by Karabut as an example of what has been observed, not proof that a laser is actually present. Proof will come only after people have an incentive to look for this kind of radiation, which I'm trying to encourage.

[d] Brian Scanlan has a somewhat different view of this process that he will describe in later papers. I am sure that other people can find additional ways to describe the proposed structure. Too little information is known about this stage of the fusion process to make any explanation the final one.

Appendix B.3. Proposed p–e–p reaction mechanisms

The role of the neutrino is complex. First of all, if most energy is lost as photons before the fusion reaction actually occurs, only a small amount of energy would be available to be lost by neutrino emission when the final fusion occurs. The reviewer uses values based on ALL the energy being released at the final moment of fusion, which is not what I propose. The second question is, "Does the neutrino play any role at all during the cold fusion process"? Typically, the neutrino is known to carry energy away when beta emission occurs. Theory must be used to suggest neutrino emission during the proposed fusion process, which might not apply. I suggest a measurement of the energy/D ratio would provide some very important insights into this process. This measurement has not been made. Consequently, the comments by the reviewer are still speculation.

I did not propose direct p + p fusion. This is an idea introduced only by the reviewer.

Appendix B.4. Tunneling

I have no idea how the concept of tunneling applies to the model I am proposing and it was not suggested in the paper

Appendix B.5. Discussion

Yes, I agree, something is a miss in the physics text books. Otherwise, cold fusion cannot be explained. I have proposed a mechanism that has the ability not only to explain more than any other previous explanation but it does not violate known laws. Because many of the comments made by the reviewer were based on a misunderstanding of what I propose, I do not yet know what the reviewer thinks about what I actually propose.

No matter how physics is understood, the behavior *MUST* be explained using the same mechanism regardless of the method used to initiate the effect or the isotopes of hydrogen present, because I do not believe that more than one mechanism can operate to produce such a rare and unusual nuclear process. An attempt to explain all observed behavior has not been attempted before. And yes, I have not applied the model to all observed behavior in this paper. That challenge will come later because this paper is one of a series in which the ideas will be expanded and applied. The purpose is to develop a plausible explanation in stages and use it to guide research from which support might be obtained. What more does the reviewer require of a theory at this early stage?

Acknowledgement

This model was developed while working with Brian Scanlan and would not have resulted without his encouragement and contribution. The Scanlan model describes the novel nature of the hydron-electron bond, which will be described in a future paper.

References

[1] Fleischmann, M., S. Pons, and M. Hawkins, Electrochemically induced nuclear fusion of deuterium. *J. Electroanal. Chem.* **261** (1989) 301–308 and errata in **263** (1989) 187–188.
[2] Storms, E.K., *The Science of Low Energy Nuclear Reaction* (World Scientific, Singapore, 2007), p. 312.
[3] Storms, E.K., The nature of the energy-active state in Pd–D, *Infinite Energy* **5,6** (1995) 77.
[4] Storms, E.K., An explanation of low-energy nuclear reactions (cold fusion), *J. Cond. Matter Nucl. Sci.* **9** (2012) 85–107.
[5] Storms, E.K., Cold fusion from a chemist's point of view, *Infinite Energy* (2013), in press.
[6] Widom, A. and L. Larsen, Ultra low momentum neutron catalyzed nuclear reactions on metallic hydride surfaces, *Eur. Phys. J.* **C46** (2006) 107.
[7] Kim, Y.E., Bose–Einstein condensate theory of deuteron fusion in metal, *J. Cond. Matter Nucl. Sci*. **4** (2011) 188–201.

[8] Harris, P.J.F., *Carbon Nanotube Science* (Cambridge Univ. Press, New York, 2009), p. 301.
[9] Tenne, R., *Inorganic Nanomaterials from Nanotubes to Fullerene-like Nanoparticles* (World Scientific, Singapore, 2012).
[10] Nishimiya, N., et al., Hyperstoichiometric hydrogen occlusion by palladium nanoparticles included in NaY zeolite. *J. Alloys Compounds* **319 (**2001) 312.
[11] Storms, E., Ways to initiate a nuclear reaction in solid environments, *Infinite Energy* **8**(45) (2002) 45.
[12] Fleischmann, M., et al., Calorimetry of the palladium-deuterium-heavy water system. *J. Electroanal. Chem*. **287 (**1990) 293.
[13] Rolison, D.R., et al. Anomalies in the surface analysis of deuterated palladium. in *The First Annual Conference on Cold Fusion*, 1990. University of Utah Research Park, Salt Lake City, Utah, National Cold Fusion Institute, p. 272.
[14] Miyamoto, S., et al. Movement of Li during electrolysis of 0.1M-LiOD/D_2O solution, in *Fourth International Conference on Cold Fusion*, 1993, Lahaina, Maui: Electric Power Research Institute, 3412 Hillview Ave., Palo Alto, CA 94304, p. 28.
[15] Asami, N., et al. Material behaviour of highly deuterium loaded palladium by electrolysis, in *Sixth International Conference on Cold Fusion ,Progress in New Hydrogen Energy,* 1996. Lake Toya, Hokkaido, Japan, New Energy and Industrial Technology Development Organization, Tokyo Institute of Technology, Tokyo, Japan, p. 67.
[16] Dalard, F., et al., Electrochemical incorporation of lithium into palladium from aprotic electrolytes, *J. Electroanal. Chem*. **270** (1989) 445.
[17] Moffatt, W.G., *Pd–Li phase diagram*, in *the Handbook of Binary Alloy Phase Diagrams*(General Electric, Schenectady, NY, 1978).
[18] Bockris, J.O.M., D. Hodko, and Z. Minevski, Fugacity of hydrogen isotopes in metals: degradation, cracking and cold fusion, *Proc. Electrochem. Soc*. **1992 (**1992) 92.
[19] McKubre, M.C.H., et al., Excess power observations in electrochemical studies of the D/Pd system; the influence of loading, in *Third International Conference on Cold Fusion, "Frontiers of Cold Fusion"*, Nagoya, Japan (Universal Academy Press, 1992, Tokyo, Japan), p. 5.
[20] Violante, V., et al., Calorimetric results of ENEA cooperative experiments, in *International Conference on Condensed Matter Nuclear Science, ICCF-13*, 2007, Sochi, Russia: Tsiolkovsky Moscow Technical University, p. 312.
[21] McKubre, M.C.H., et al., New hydrogen energy research at SRI, in *Sixth International Conference on Cold Fusion, Progress in New Hydrogen Energy,* 1996, Lake Toya, Hokkaido, Japan: New Energy and Industrial Technology Development Organization, Tokyo Institute of Technology, Tokyo, Japan, p. 75.
[22] Storms, E.K. and C. Talcott-Storms, *Th*e effect of hydriding on the physical structure of palladium and on the release of contained tritium, *Fusion Technol.* **20 (**1991) 246.
[23] Storms, E.K., The status of cold fusion (2010), *Naturwissenschaften* **97 (**2010) 861.
[24] Bush, R.T. and R.D. Eagleton, Experimental studies supporting the transmission resonance model for cold fusion in light water: II. Correlation of X-Ray emission with excess power, in *Third International Conference on Cold Fusion, "Frontiers of Cold Fusion",* 1992, Nagoya Japan (Universal Academy Press, Tokyo, Japan, 1992), p. 409.
[25] Oyama, N., et al. In situ interferometric microscopy of Pd electrode surfaces and calorimetry during electrolysis of D_2O solution containing sulfur ion, in *Sixth International Conference on Cold Fusion,Progress in New Hydrogen Energy,* 1996, Lake Toya, Hokkaido, Japan: New Energy and Industrial Technology Development Organization, Tokyo Institute of Technology, Tokyo, Japan, p. 234.
[26] Hugo, M. , A home cold fusion experiment, in *Fourth International Conference on Cold Fusion,* 1993, Lahaina, Maui: Electric Power Research Institute 3412 Hill view Ave., Palo Alto, CA 94304. p. 22.
[27] Ota, K., et al., Heat measurement of water electrolysis using Pd cathode and the electrochemistry, in *Fourth International Conference on Cold Fusion,* 1993, Lahaina, Maui: Electric Power Research Institute, 3412 Hill view Ave., Palo Alto, CA 94304, p. 5.
[28] Ota, K., et al., Heat production at the heavy water electrolysis using mechanically treated cathode. in *Third International Conference on Cold Fusion, "Frontiers of Cold Fusion"*, 1992, Nagoya, Japan (Universal Academy Press, Tokyo, Japan, 1992), p. 71.
[29] Gentsch, H., DD-fusion reactions at a PdAg(D) target in a minireactor, *Ber. Bunsenges. Phys. Chem.* **95 (**1991) 1283 (in German).
[30] Dash, J. and J. Solomon, Effect of Recrystallization on Heat Output and Surface Composition of Ti and Pd Cathodes, in *ICCF-17*, Daejeon, Korea, Aug. 12–17, 2012.

[31] . Sun, Y., Q. Zhang, and Q. Gou, The crystal change and "excess heat" production by long time electrolysis of heavy water with titanium cathode due to deuterium atom entering the lattice of titanium, in *The 9th International Conference on Cold Fusion, Condensed Matter Nuclear Science,* Tsinghua Univ., Beijing, China (Tsinghua Univ. Press, 2002), p. 329.
[32] Karabut, A.B. , Production of excess heat, impurity elements and unnatural isotopic ratios in high-current glow discharge experiments, in *Tenth International Conference on Cold Fusion* (World Scientific, Cambridge, MA, 2003), . p. 99.
[33] Zhang, Q., et al*., The relationship of crystal structure transition of Ti-cathode and 'excess heat' on cold fusion*, *Chinese J. Atomic Mol. Phys*. **13**(3) (1996) 257 (in Chinese).
[34] Mosier-Boss, P.A. , It's not Low Energy – But it is Nuclear, in *ICCF-17,* Daejeon, Korea, Aug. 12–17, 2012.
[35] Storms, E.K. and B. Scanlan, Detection of radiation from LENR, in *14th International Conference on Condensed Matter Nuclear Science,* 2008, Washington, DC, www.LENR.org, pp. 261–287.
[36] Golubnichii, P.I., et al., A possible mechanism for cold nuclear fusion, *J. Kratk. Soobshch. Fiz.* **6** (1989) 56 (In Russian).
[37] Lipson, A.G., et al., Neutron generation by mechanical activation of metal surfaces, *Pis'ma Zh. Tekh. Fiz*. **16**(17) (1990) 54 (in Russian).
[38] Bagnulo, L.H., Crack-fusion: A plausible explanation of cold fusion, in *Second Annual Conference on Cold Fusion, "The Science of Cold Fusion"*, 1991, Como, Italy: Societa Italiana di Fisica, Bologna, Italy, p. 267.
[39] Preparata, G. , Fractofusion revisted. in Anomalous Nuclear Effects in Deuterium/Solid Systems, *"AIP Conference Proceedings 228"*, 1990, Brigham Young Univ., Provo, UT, American Institute of Physics, New York, p. 840.
[40] Bockris, J.O.M., The complex conditions needed to obtain nuclear heat from D-Pd systems, *J. New Energy* **1**(3) (1996) 210.
[41] Bockris, J.O.M. and Z. Minevski, The mechansim of the evolution of hydrogen on palladium and associated internal damage phenomena, *J. Hydrogen Energy* **25** (2000) 747.
[42] Bockris, J.O.M. and Z. Minevski, First experimental establishment of high internal pressure of molecular hydrogen developed in palladium during water electrolysis*, J. Hydrogen Energy* **23**(12) (1998) 1079.
[43] Bockris, J.O.M., et al., Cold fusion as a consequence of high fugacity among hydrogen isotopes, *Int. J. Hydrogen Energy* **17** (1992) 445.
[44] Fulvio, F., Deuteron interaction within a microcrack in a lattice at room temperature, *Fusion Technol.* **39** (2 (March)) (2001) 260.
[45] Fulvio, F. , Theoretical model on the relationship between low energies in the probability of deuterium nuclei cold fusion, in *The 9th International Conference on Cold Fusion, Condensed Matter Nuclear Science,* 2002, Tsinghua Univ., Beijing, China (Tsinghua Univ. Press, Beijing, China 2002), p. 101.
[46] Fulvio, F. , Fusion reaction within a microcrack with cubic lattice structure at low energy and study of the nonsemi-classical tunneling, in *Tenth International Conference on Cold Fusion* (World Scientific, Cambridge, MA, 2003), p. 695.
[47] Fulvio, F., Theoretical model of the probability of fusion between deuterons within deformed lattices with microcracks at room temperature, in *11th International Conference on Cold Fusion,* 2004, Marseilles, France (World Scientific, London, 2004), p. 612.
[48] Fulvio, F., Calculation of Deuteron Interactions within microcracks of a D_2 loaded crystalline lattice at room temperature, *J. Cond. Matter Nucl. Sci.* **1** (2007) 41.
[49] Fulvio, F., Theoretical model of the probability of fusion between deuterons within deformed crystalline lattices with microcracks at room temperature. in *15th International Conference on Condensed Matter Nuclear Science,* 2009, Rome, Italy, ENEA, Italy, pp. 312–318.
[50] Godbole, V., Low-energy electroweak (EW) physics (in cavities) in lattices and fluids, in *ICCF-17,* Daejeon, Korea, Aug. 12–17, 2012.
[51] Swartz, M.R., Impact of an applied magnetic field on a high impedance dual anode LANR device, *J. Cond. Matter Nucl. Sci.* **4** (2011) 93–105.
[52] Letts, D. and P.I. Hagelstein, Simulation of optical phonons in deuterated palladium, in *14th International Conference on Condensed Matter Nuclear Science,* 2008, Washington, DC, pp. 333–337.
[53] Szpak, S., P.A. Mosier-Boss, and F. Gordon, Further evidence of nuclear reactions in the Pd/D lattice: emission of charged particles, *Naturwissenschaften* **94** (2009) 515.
[54] Karabut, A.B., X-ray emission in the high-current glow discharge experiments, in *The 9th International Conference on Cold Fusion, Condensed Matter Nuclear Science,* 2002, Tsinghua Univ., Beijing, China (Tsinghua Univ. Press, Beijing, China,

2002), p. 155.
[55] Li, X.Z., et al., Correlation between abnormal deuterium flux and heat flow in a D/Pd system, *J. Phys. D: Appl. Phys.* **36 (**2003) 3095.
[56] Liu, B., et al. ,"Excess heat" induced by deuterium flux in palladium film, in *Condensed Matter Nuclear Science, ICCF-12,* 2005, Yokohama, Japan (World Scientific, Singapore, 2005), p. 75.
[57] Liu, B., et al., "Excess heat" in a gas-loaded D/Pd system with pumping inside palladium tube, in *8th International Workshop on Anomalies in Hydrogen/Deuterium Loaded Metals,* 2007, Catania, Sicily, Italy, The International Society for Condensed Matter Science, p. 204.
[58] Li, X.Z., et al., Wave nature of deuterium flux permeating through palladium thin film with nanometer coating layers – (II) theoretical modeling, in *15th International Conference on Condensed Matter Nuclear Science,* 2009, Rome, Italy, ENEA, Italy, pp. 122–128.
[59] Wu, W., et al., *Anomalous heat effect during permeation of deuterium gas through the palladium tube*. in *The 9th International Conference on Cold Fusion, Condensed Matter Nuclear Science*. 2002. Tsinghua Univ., Beijing, China: Tsinghua Univ. Press. p. 412.
[60] Tian, J., et al. Anomanous heat flow and its correlation with deuterium flux in a gas-loading deuterium-palladium system, in *The 9th International Conference on Cold Fusion, Condensed Matter Nuclear Science,* 2002, Tsinghua Univ., Beijing, China (Tsinghua Univ. Press, Beijing, China, 2002), p. 353.
[61] Biberian, J.-P. and N. Armanet, Excess heat production during diffusion of deuterium through palladium tubes, in *8th International Workshop on Anomalies in Hydrogen/Deuterium Loaded Metals,* 2007, Catania, Sicily, Italy, The International Society for Condensed Matter Science, p. 19.
[62] Biberian, J.-P. and N. Armanet, Excess heat during diffusion of deuterium through palladium. in *International Conference on Condensed Matter Nuclear Science, ICCF-13,* 2007, Sochi, Russia: Tsiolkovsky Moscow Technical University, p. 170.
[63] Granite, E. and J. Jorne, A novel method for studying electrochemically induced cold fusion using a deuteron-conducting solid electrolyte, *J. Electroanal. Chem*. **317 (**1991) 285.
[64] Biberian, J.-P., Excess heat measurements in $AlLaO_3$ doped with deuterium, in *5th International Conference on Cold Fusion,* 1995, Monte-Carlo, Monaco: IMRA Europe, Sophia Antipolis Cedex, France. p. 49.
[65] Mizuno, T., et al., Anomalous heat evolution from $SrCeO_3$-type proton conductors during absorption/desorption in alternate electric field, in *Fourth International Conference on Cold Fusion,* 1993, Lahaina, Maui: Electric Power Research Institute, 3412 Hill view Ave., Palo Alto, CA 94304. p. 14.
[66] Mizuno, T., et al., Anomalous heat evolution from a solid-state electrolyte under alternating current in high-temperature D_2 gas*, Fusion Technol.* **29 (**1996) 385.
[67] Oriani, R.A., An investigation of anomalous thermal power generation from a proton-conducting oxide, *Fusion Technol.* **30 (**1996) 281.
[68] Mizuno, T., et al., Excess heat evolution and analysis of elements for solid state electrolyte in deuterium atmosphere during applied electric field, *J. New Energy* **1**(1) (1996) 79.
[69] Biberian, J.-P., et al., Electrolysis of $LaAlO_3$ single crystals and ceramics in a deuteriated atmosphere, in *The Seventh International Conference on Cold Fusion*, 1998, Vancouver, Canada, ENECO, Salt Lake City, UT, p. 27.
[70] Bartolomeo, C., et al., Alfred Coehn and after: The alpha, beta and gamma of the palladium-hydrogen system, in *Fourth International Conference on Cold Fusion,* 1993, Lahaina, Maui: Electric Power Research Institute, 3412 Hill view Ave., Palo Alto, CA 94304, p. 19.
[71] Celani, F., et al., Deuterium overloading of palladium wires by means of high power microsecond pulsed electrolysis and electromigration: suggestions of a "phase transition" and related excess heat, *Phys. Lett. A* **214 (**1996) 1.
[72] M. Lischka and A. Gross, Hydrogen on palladium: A model system for the interaction of atoms and molecules with a metal surface, *Recent Developments in Vacuum Science and Technology*, J. Dabrowski (Ed.), (2003) pp. 111–132.
[73] F. Besenbacher, S.M. Myers and J.K. Norskov, Interaction of hydrogen with defects in metals, *Nucl. Instr. Methods Phys. Res.* B **7/8** (1985) 55.
[74] V. Rosato and F. Cleri, Deuterium clusters in a strained Pd lattice, *J. Mater. Research* **5** (1990) 2094.
[75] A.I. Baz', V.I. Gol'danskii and Ya.B. Zel'dovich, Systematics of the lightest nuclei, *Sov. Phys. Uspekhi* **8** (1965) 177.

[76] R. Wolski, P. Roussel-Cliomaz, S.I. Sidorchuk and G.M. Ter-Akopian, Search for extremely neutron rich systems, *Nucl. Phys.* A **738** (2004) 431.
[77] J. Maddox, *Nature* **344** (1990) 365.

J. Condensed Matter Nucl. Sci. 11 (2013) 142–156

Research Article

Nature of Energetic Radiation Emitted from a Metal Exposed to H_2

Edmund Storms* and Brian Scanlan

KivaLabs, Santa Fe, NM, USA

Abstract

Layers of metals were applied so as to cause local stress, which is proposed to create voids in which nuclear reactions can be initiated when the material is exposed to H_2. Photon emission having energy sufficient to pass through 3.86 g/cm^2 of absorbing material was detected using a Geiger-Mueller detector. This radiation was observed to last many hours and is not typical of what is called fracto-fusion.
© 2013 ISCMNS. All rights reserved. ISSN 2227-3123

Keywords: Cold fusion, Cracks, Fusion, LENR, Radiation

1. Introduction

Numerous reports have been published [1] describing radiation emitted from a nuclear process called LENR when palladium, nickel, and other materials are exposed to deuterium and normal hydrogen. Because such energetic radiation cannot be mistaken for a prosaic or chemical effect and can only result from a nuclear reaction, these observations are highly anomalous and in conflict with conventional understanding. This radiation, in addition to revealing how nuclear reactions can be initiated in ordinary materials, must be explored to avoid health risks when such systems are studied or used as energy sources.

For this study, samples were made and treated to form the kind of voids proposed by Storms [2–4] to be the location of the LENR process. Three different materials were used, with each showing the same behavior once the active conditions were produced and the materials were exposed to H_2. Radiation, which had the characteristics of photons, was detected using large area Geiger-Muller detectors. The amount of material was too small for the nuclear process to produce detectable energy.

Unusual radiation, both particle and photon, has been found when certain materials are exposed to H_2 or D_2. For example, such radiation has been produced during electrolysis [5,6], gas discharge [7–10], and by exposing specially treated metal to H_2 [11,12] or D_2 gas. Focardi [12] places the photon energy resulting from specially treated Ni being exposed to H_2 at 661 $\pm$ 0.8 keV. This value was corrected to 744 keV by Takahashi [13]. Piantelli et al. [12,11,14] published a detailed description of various kinds of radiation emitted from Ni rods after being heated repeatedly in H_2,

*E-mail: storms2@ix.netcom.com

© 2013 ISCMNS. All rights reserved. ISSN 2227-3123

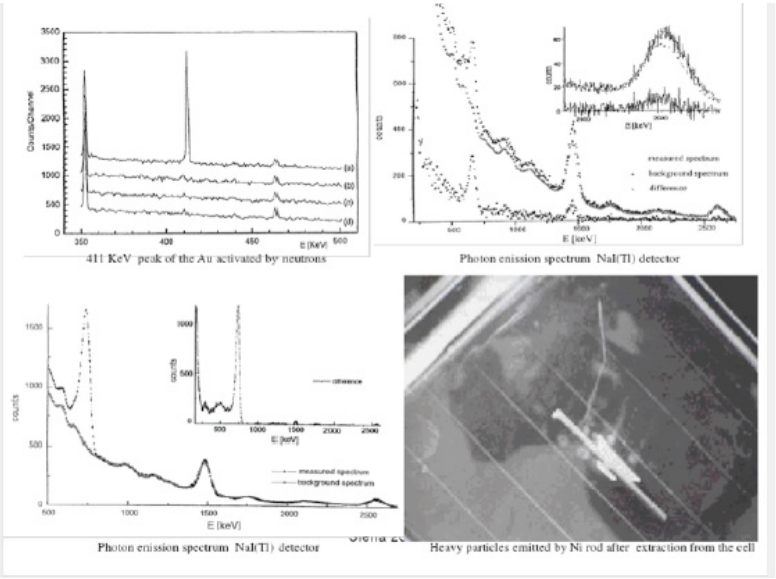

Figure 1. Examples of radiation reported as a result of studies by Piantelli et al. using specially treated Ni exposed to H_2.

after which the metal was found to generate extra energy. Evidence for photon radiation of various frequencies, energetic particles that were visible in a cloud chamber, and neutrons are shown in Fig. 1. Violante et al. [15] electrolyzed a thin layer of Ni that was sputter-deposited on polyethylene. The electrolyte was H_2O–Li_2SO_4 and radiation was detected using a planar HPGe detector after the radiation had passed through the polyethylene cell wall. Figure 2 shows the behavior when a blank cathode was examined and Fig. 3 shows the presence of radiation. Although the amount of radiation leaving the cell as photons is small, radiation is clearly present when none would be expected. Matsumoto[a] [16] detected radiation using X-ray film produced by a nickel cathode in a glass electrolytic cell containing $H_2O + K_2CO_3$. One side of the foil was electrolyzed while the other side was in contact with the film. As a result, any radiation had to pass through 0.1 mm of Ni. Many unusual complex tracks were seen, suggesting secondary nuclear reactions were produced in the film by radiation from the nickel. Bush and Eagleton [17] used a NaI scintillation detector to measure photons from a Ni cathode (fibre x) electrolyzed in H_2O + LiOH. They claimed to find a rough correlation between excess power and the amount of total radiation as shown in Fig. 4. Anecdotal experience has been reported by Rossi [18] and Celani, claiming radiation is detected when heat production is first initiated but is much reduced later while extra energy is being made.

2. Method

2.1. Radiation measurement

Figure 5 shows a cross-section drawing of the sample, cell, vacuum housing, and GM detector (GM No. 1) (LND-7313) and Fig. 6 is a photograph of the system. The radiation had to pass through the absorber material listed in Table 1. As a result, a large fraction of the radiation being emitted by the sample was removed before measurements were made. The

[a]This author has published many papers describing how variations in the cold fusion conditions can generate strange tracks in film.

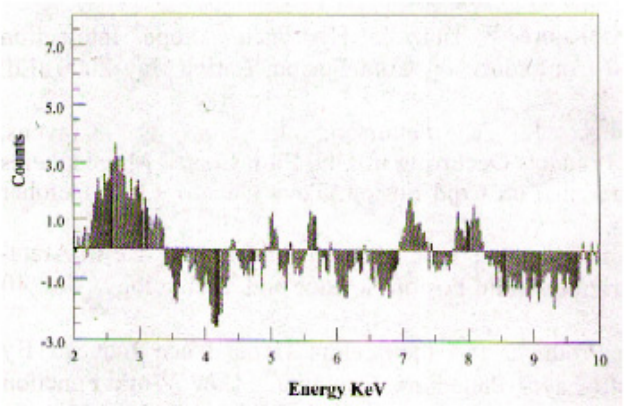

Figure 2. Count rate in excess of background for an inactive Ni cathode reported by Violante et al. [15].

pulses from the detector were fed to an electronic circuit where the pulses were amplified and used to charge a resistor–capacitor circuit to produce an average voltage that was recorded. Consequently, the plotted values are arbitrary units for which only a change is important. The average background was about 60 counts/min for the large-area detector.

A second GM (GM No. 2) of the same type was located about 30 cm from the source (Fig. 6), such that any radiation from the source had to pass through 1 cm of steel and the back of the detector before it entered the active region of GM No. 2. As a result, ambient background radiation was detected along with only very energetic radiation that might be emitted by the sample or less energetic radiation originating at GM No. 1. The background flux at GM No. 2 was found to be essentially constant during the studies.

The sample was contained in an aluminum cup that could be heated in H_2 to 350°C with pressures up to 5 atm. The samples were exposed to a variety of conditions in order to activate the material, a process important to achieving success.

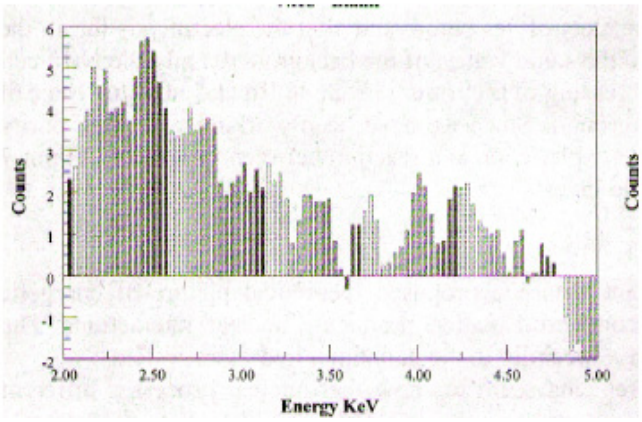

Figure 3. Count rate in excess of background for an active Ni cathode reported by Violanti et al. [15].

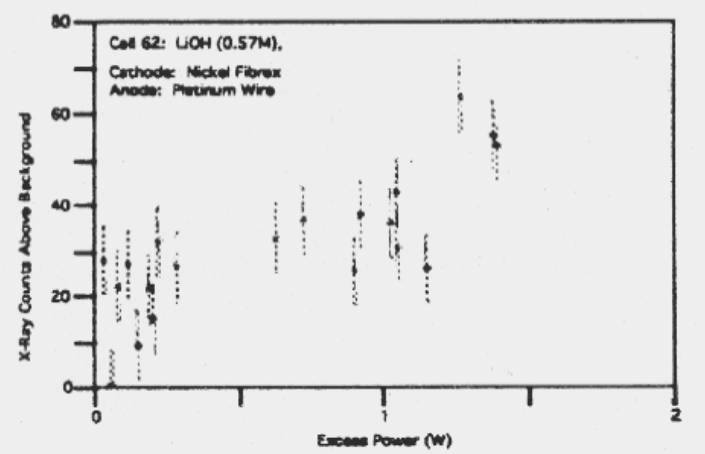

Figure 4. Radiation detected by Bush and Eagleton [17] from a cell having a Ni cathode and H_2O electrolyte while it was making excess power.

2.2. Sample preparation

The samples consisted of palladium or nickel sheet on which various metals were deposited by electroplating or sputtering.

The palladium samples were prepared by reducing the thickness of stock palladium to a convenient value using a rolling mill. The sample was then heated near the melting point using a propane–oxygen torch in air. This treatment

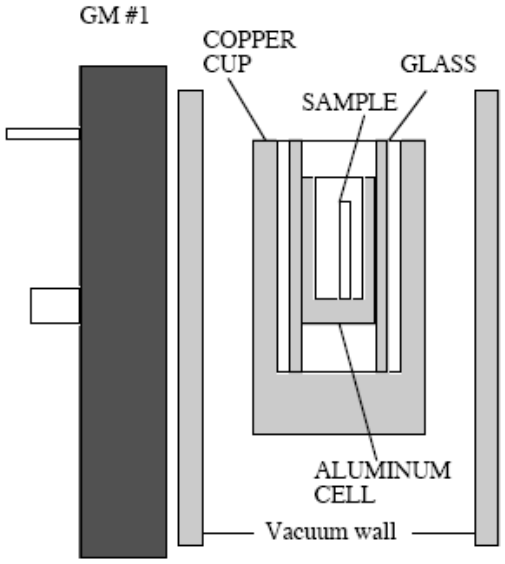

Figure 5. Cross-section of region around sample and relationship to GM No. 1.

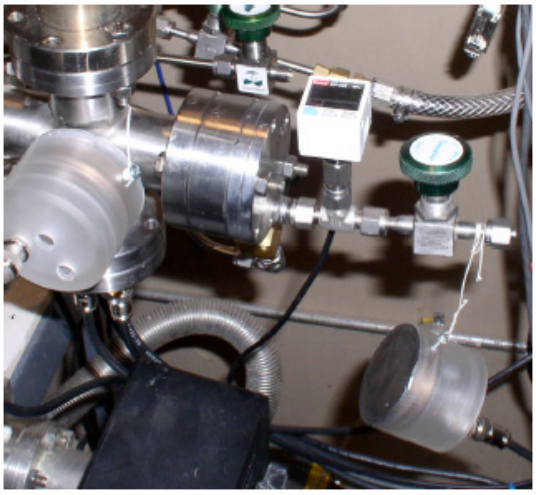

Figure 6. Photograph of apparatus with GM No. 1 attached to the apparatus and GM No. 2 hanging by a wire off to the right.

purified the surface and created a thin oxide coating. Heating to 200–280°C followed by cooling in 30 psi H_2 resulted in the sample coming to equilibrium with the H_2 and acquiring a H/Pd ratio between 0.70 and 0.72. This step was used to make sure the Pd was clean and would react quickly and completely with H_2. The hydrogen was then removed by heating in vacuum to 200°C before the metal coating was applied.

One sample was made by applying Cr to the clean Pd surface by sputtering to give a thickness of 101 nm on both sides. This was followed by 262 nm of Pd and another 101 nm layer of Cr. The sample was heated in 4.8 atm of H_2 to 213°C and cooled in order to bond the layers to the base material. When the sample cooled in H_2, the Pd expanded as it formed beta-PdH resulting in H/Pd = 0.70, which caused stress in the Cr layer to form the required voids.

A second sample was made by applying 101 nm of Ni, and 252 nm of Pd on the Pd substrate. The sample was heated in vacuum to 415°C and cooled in 4.9 atm of H_2. This caused the sample to reach a composition of H/Pd = 0.73, which would produce stress in the Ni layer as the Pd expanded while forming beta-PdH and the Ni did not.

A sheet of Ni was cleaned by electrolysis in NaOH solution followed by applying an electroplated layer of Cu 552 nm thick. This was heated to 481°C in vacuum followed by heating in H_2. The surface is shown in Fig. 7 on which the sought-for pits are clearly seen. Subsequent studies showed that such pits were characteristic of Ni–Cu interaction although radiation was seldom produced.

The active regions were not stable so that the amount of radiation was not constant with time or conditions. Nevertheless, the samples were active long enough to obtain useful measurements and could even be removed to air for weighing without losing the ability to produce radiation once returned to the system.

Table 1. Effective stopping power of material between sample and GM No. 1.

0.9 mm Al = 0.24 g/cm^2
2 mm Cu = 1.79 g/cm^2
1 mm Pyrex = 0.22 g/cm^2
2 mm stainless steel = 1.61 g/cm^2
Total = 3.86 g/cm^2

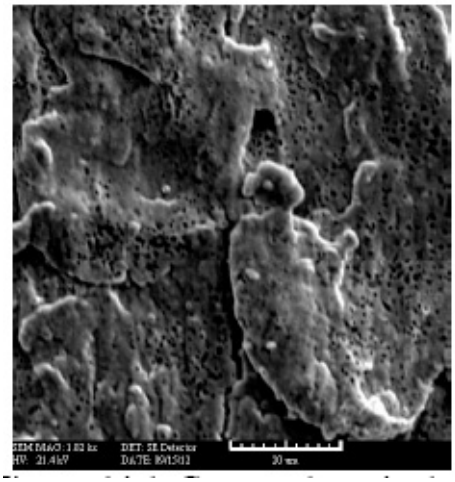

Figure 7. Surface of Ni on which Cu was deposited after heating in vacuum at 481°C.

The voids proposed to be the nuclear active environment (NAE) appeared to have a range of sizes, some of which were too small to be resolved in the images. Figures 8 and 9 show a topical void formation at different magnifications for samples of Ni applied to Pd. Figure 10 shows the surface after study of a sample created by applying Cr to Pd. This layer delaminated from the Pd at some point during the study, probably when the radiation abruptly stopped at the end of the study.

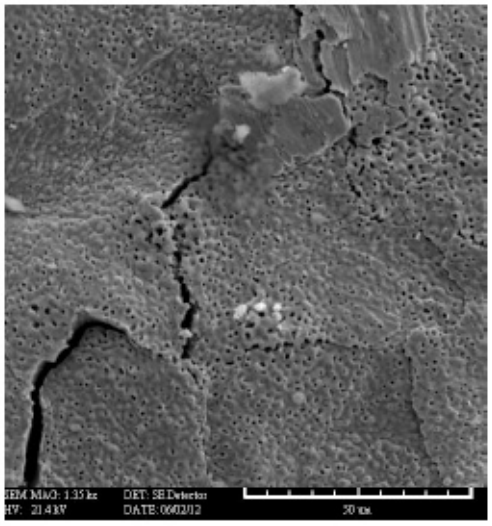

Figure 8. SEM image of a surface of Ni on Pd after the study containing voids and cracks.

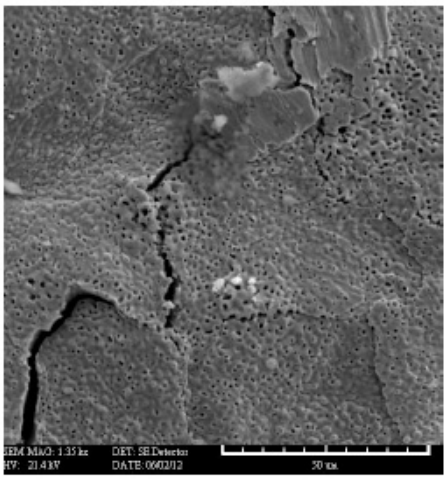

Figure 9. Detailed SEM examination of the Pd–Ni surface after the study.

3. Results

Four samples were found to produce radiation after being prepared using a variety of conditions, three of which are described here. The most important requirement is that the layer not detach from the substrate metal and the pit structure form. These pits are expected to be the mouth of voids that extend into the material. Their formation requires a narrow range of conditions, some of which are described here. Nevertheless, such structures are not always active probably

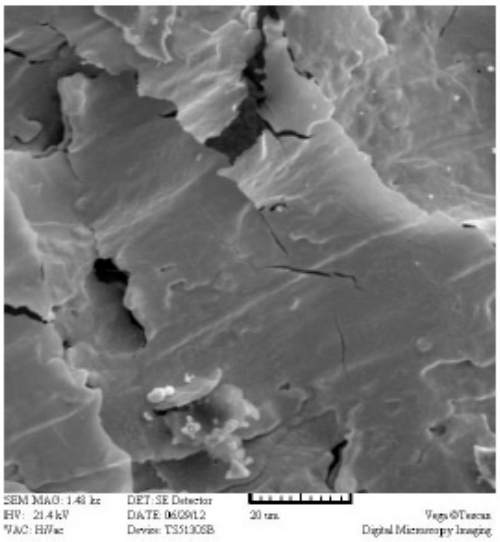

Figure 10. SEM image of surface of Cr on Pd after the study.

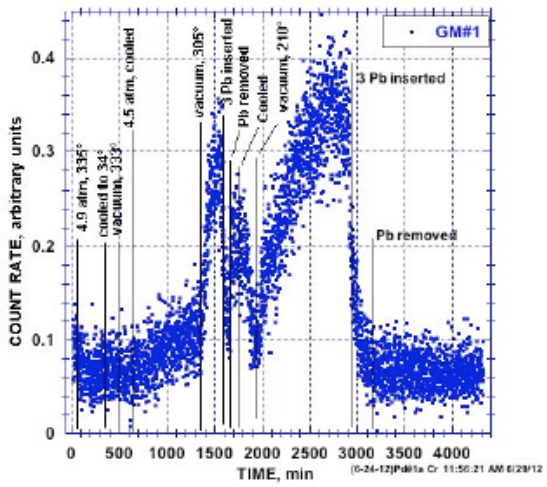

Figure 11. History of sample of Pd coated by Cr.

because the small required size was not formed.

3.1. Pd–Cr

Figure 11 shows the counting history for a sample of Pd coated with 100 nm of Cr followed with about 200 nm of Pd. In this case the voids are produced in a volume of about 0.0001 cm^3 of Cr, which emphasizes the small volume of material from which radiation is typically emitted. A brief exposure to H_2 was done before this sequence was started. Several heating and vacuum cycles were required before significant radiation was started at 1350 min while the sample was at 305°C and H_2 was being pumped out. Such treatment would cause the gap in cracks that had formed during previous treatments to become smaller as hydrogen was lost causing the PdH to contract. Presumably this smaller size was required for the process to function and radiation to be produced. Only this sample required loss of H_2 to produce radiation.

The effect of inserting sheets of lead absorber (1.3 g/cm^2) is shown in Fig. 12. Every time an absorber was inserted, all samples showed an immediate reduction in radiation followed by slow decay. The absorber changed the distance between GM No. 1 and the sample by no more than 2 mm. Once the absorber had been removed, an immediate increase in radiation occurred that was followed by slow increase to a steady value. The effect when Pb was inserted can be seen clearly in Fig. 13, but unfortunately the radiation stopped before the Pb could be removed. This abrupt termination of radiation near 3000 min is presumed to have resulted when the coating detached from the Pd substrate, the consequence of which can be seen in Fig. 10. GM No. 2, located at a distance from the sample, also shows unusual behavior. Radiation was being detected by GM No. 2, which slowly decreased when an absorber stopped radiation from the sample from reaching GM No. 1, as seen in Fig. 13. This means the radiation being detected by GM No. 2 originated from GM No. 1, not from the apparatus. This behavior was observed on several occasions when other samples were treated in the same way.

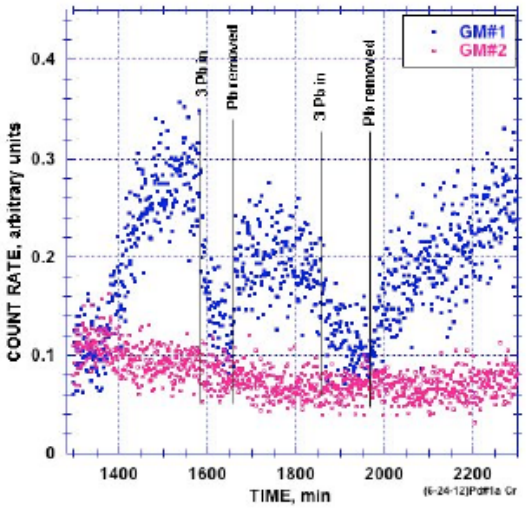

Figure 12. Sample of Pd coated by Cr. Time sequence taken from Fig. 12.

3.2. Pd–Ni

This sample was heated at various temperatures under as much as 5 atm of H_2 over a period of 3000 min before any radiation was detected. The sample was at 33°C under of 4.4 atm of H_2 when radiation was detected. Figure 14 shows onset of radiation and the effect of inserting a Pb absorber. Once again, immediate reduction was produced followed by

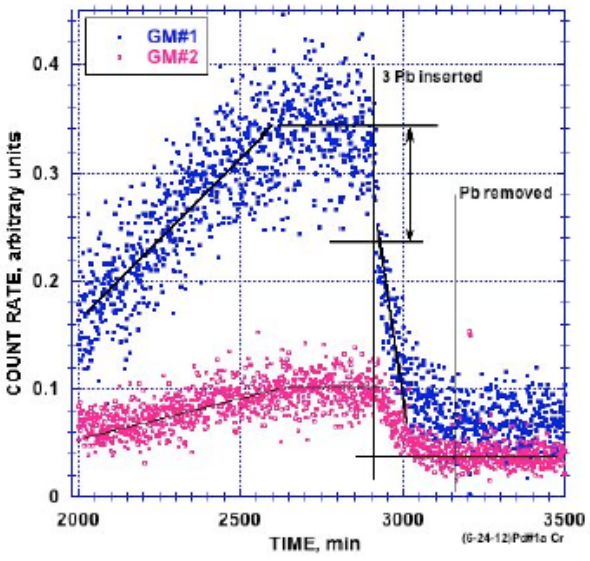

Figure 13. Sample of Pd coated by Cr. Time sequence taken from Fig. 11.

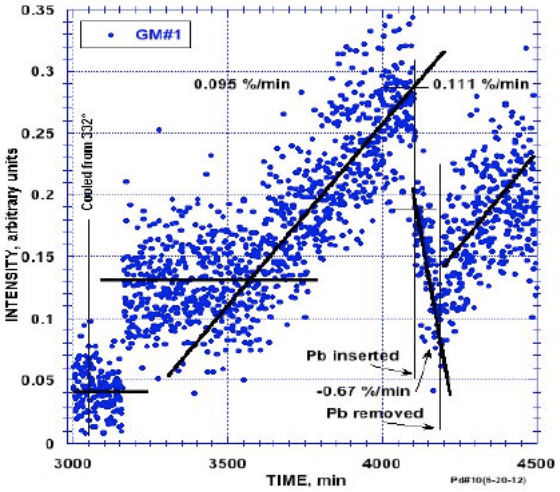

Figure 14. Example of inserting a lead absorber using Pd coated by Ni.

slow decay having a half-life of about 40 min, as calculate using the linear least-squares fit of ln (rate) versus time during the decay phase (Fig. 15). The rate was obtained by subtracting the GM No. 1 signal when no radiation was produced from the value measured for each point during the decay. When the absorber was removed, radiation immediately increased followed by a slow increase with a slope close to the increase observed before the absorber was inserted.

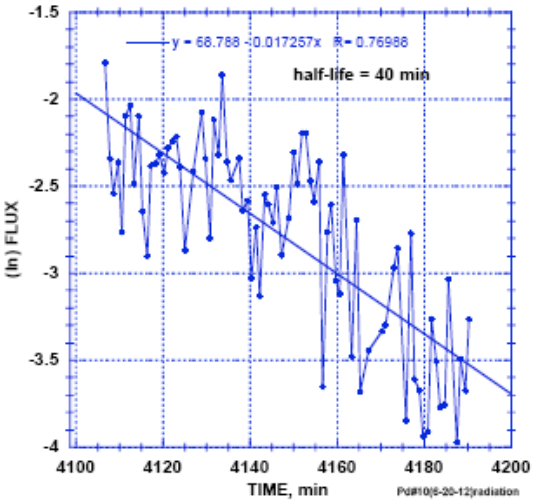

Figure 15. ln (flux) vs time for decay after absorber is inserted.

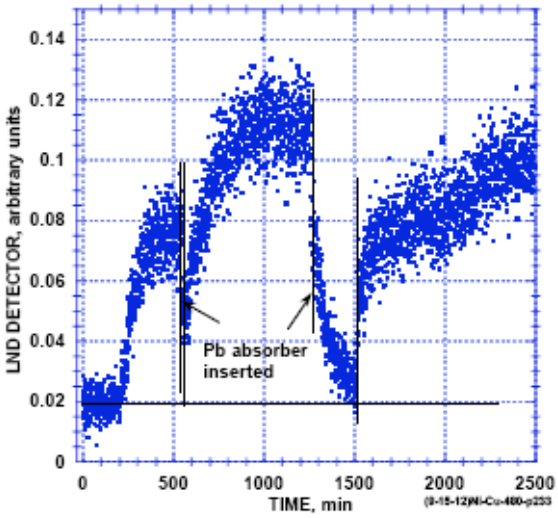

Figure 16. Behavior of radiation during the full study while Ni–Cu was being heated in H_2.

3.3. Ni–Cu

The sample was heated through 212°C in 3.7 atm of H_2 when the radiation intensity first increased at 200 min. Lead (Pb) was briefly inserted at 548 min and then removed. Lead was again inserted at 1260 min, which had the effect shown in Fig. 16. The decay in Fig. 17 had a longer average half-life (Fig. 18) compared to a shorter time shown in Fig. 15, with an indication that the initial decay had a shorter half-life than the average. This shorter initial decay rate might account for the smaller half-life obtained from the smaller data set shown in Fig. 15.

3.4. Radon

When a fan was used to circulate air around GM No. 1 and the apparatus, the count rate increased and then decreased after the fan is turned off over a period of about an hour. This change is attributed to radon in the air that is made available to the apparatus on which it deposits. Only the count rate of GM No. 1 next to the apparatus was affected. This extra count rate was not present in the absence of the fan. Inactive samples, of which many were studied, and the empty cell show a steady count rate at the normal background level. All data were obtained in the absence of the fan. Figure 19 shows the behavior of a typical inert sample exposed to H_2.

4. Discussion

A recently published explanation of LENR proposes that the nuclear reactions are initiated in voids or cracks [2]. Consequently, these experiments were designed to generate cracks in various materials while photon radiation was measured outside the apparatus using a Geiger-Muller detector. Because the energy of photons is not altered by penetration through matter, only a small flux that leaks from the apparatus is required to identify a source of radiation even though most is stopped by the apparatus.

Two sources of radiation are detected. One source is produced by the sample and can be stopped almost completely by 1.6 g/cm^2 of lead in addition to the 3.9 g/cm^2 provided by the apparatus. This radiation is proposed to originate

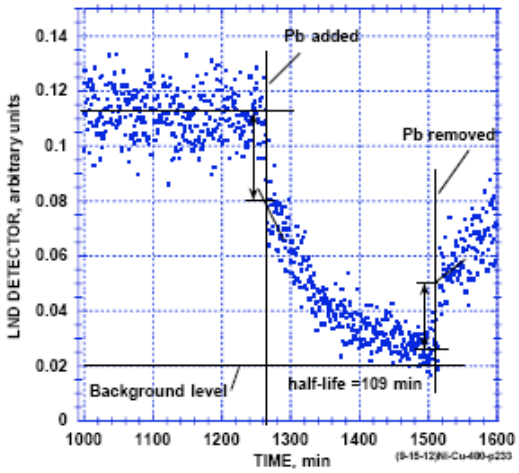

Figure 17. Effect of inserting a Pb absorber between 1262 and 1510 min shown in Fig. 16.

from samples containing characteristic voids in which a fusion reaction can take place. Although the visible voids are too large to be nuclear active, the observed voids are expected to have a wide range of size, suggesting some may have the required small size.

This primary radiation initiates a reaction within GM No. 1 that emits radiation, called secondary radiation. This secondary radiation grows slowly while the primary radiation from the sample bathes GM No. 1 and decays away when an absorber intercepts the primary radiation. As a result, GM No. 1 detects the sum of primary and secondary radiation. Insertion of an absorber immediately stops radiation from the sample, which stops further activation. The secondary

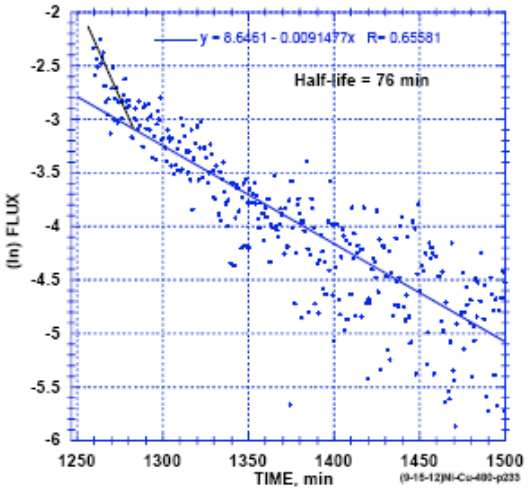

Figure 18. Half-life calculation for decay shown in Fig. 17.

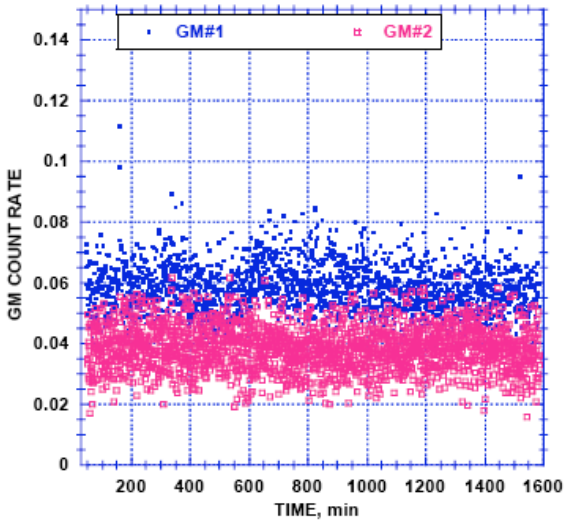

Figure 19. Behavior of GM No. 1 and GM No. 2 when a typical inert sample is in the apparatus. The difference between the two GM count rates is arbitrary. Only the constant value over time is important.

radiation has enough energy to be detected as a small flux by GM No. 2 located well away from the primary source. Because this radiation was created by a reaction inside the GM, it could not be studied by stopping it with absorbers.

The secondary radiation results from a reaction having an average half-life of about 76 min with a faster initial decay after the primary is first removed. When the absorber is removed, activation starts again and the concentration of activated source slowly increases, causing a slow increase in count rate that becomes constant when the activation rate equals the decay rate of the activated source.

The activated nuclei cannot be Al, Si, O, Ni, Fe, or Cr, because these elements are present in the sample and in construction materials, which show no such activation. Only the mica window of GM No. 1 contains elements not present anywhere else. These elements are listed in Table 2 based on EDX analysis. Only C and K are present in the detector and nowhere else, both of which have unstable isotopes. A GM detector having a plastic window containing carbon rather than one made from mica did not show this activation. Consequently, the likely activated nucleus is K^{40}.

The radiation being emitted by the sample is proposed to result from a fusion reaction that produces coherent photons. These photons are proposed to react with K^{40} nuclei in the mica window of GM No. 1 to stimulate its decay by beta and gamma emission that is detected by the GM. Some of the energetic gamma from this decay can reach GM No. 2 and cause a slight increase in count, as shown in Fig. 13.

Table 2. Composition of mica window based on EDX analysis.

C	**55 wt.%**
O	16 wt.%
Si	10 wt.%
Al	9 wt.%
K	**5 wt.%**
Fe	3 wt.%
Mg, Ti, Na	$<$ 1 wt.%

The role of radon in this study is important to acknowledge and address. Radon could be concentrated on the apparatus by a fan blowing air on the apparatus. The radioactive gas accumulated slowly and continued to activate GM No. 1 as long as the fan operated. The radiation slowly decayed away when the fan was turned off. This radiation did not produce secondary radiation and it did not reach GM No. 2. All of the measurements shown here were taken while the fan was off. Many samples were studied without the fan being on and only the three described here produced significant radiation. These facts give confidence that the measured radiation was not caused by spontaneous accumulation of radon. Nevertheless, this study needs to be repeated using a NaI detector when active material can again be made. As is characteristic of this phenomenon, replication of the effect has been difficult.

This study raises many questions that are not answered and demonstrates some very unexpected behavior. Having this behavior made known without delay is more important than taking time to answer all questions before publication. Therefore, this paper should be viewed as a progress report about an important behavior and is made known to encourage further study.

5. Conclusion

Several kinds of material when treated in a manner to produce voids are found to radiate photons typical of a nuclear reaction when exposed to H_2. This radiation is able to activate a nucleus exposed to this radiation, which decays with an average half-life of about 76 min. This photon radiation can be produced using Cr, which is not magnetic, and Ni, which is magnetic after the metals are subjected to stress by creating concentration gradients. Ni also reacts with Cu to form the same type of structure, after which photon radiation is produced when the alloy is exposed to H_2.

References

[1] E.K. Storms, *The Science of Low Energy Nuclear Reaction* (World Scientific, Singapore, 2007), p. 312.

[2] E.K. Storms, An explanation of low-energy nuclear reactions (cold fusion), *J. Cond. Matter Nucl. Sci.* **9** (2012) 85–107.

[3] E.K. Storms, Cold fusion from a chemist's point of view, *Infinite Energy* (2013) (in print).

[4] E.K. Storms, The role of voids as the location of LENR, *J. Cond. Matter Nucl. Sci.* **11** (2013) (in print).

[5] R.K. Rout et al., Reproducible, anomalous emissions from palladium deuteride/hydride, *Fusion Technol.* **30** (1996) 273.

[6] B.F. Bush et al., Helium production during the electrolysis of D_2O in cold fusion experiments, *J. Electroanal. Chem.* **304** (1991) 271–278.

[7] I.B. Savvatimova, G. Savvatimov and A.A. Kornilova, Gamma emission evaluation in tungsten irradiated by low energy deuterium ions, in *8th International Workshop on Anomalies in Hydrogen/Deuterium Loaded Metals*. 2007, Catania, Sicily, Italy, The International Society for Condensed Matter Science, p. 258.

[8] E.K. Storms and B. Scanlan, *Detection of radiation from LENR,* in *14th International Conference on Condensed Matter Nuclear Science,* 2008, Washington, DC, www.LENR.org. p. 261-287.

[9] A.G. Lipson et al. , Strong enhancement of DD-reaction accompanied by X-ray generation in a pulsed low voltage high-current deuterium glow discharge with a titanuim cathode, in *Tenth International Conference on Cold Fusion*, 2003, Cambridge, MA, World Scientific, Singapore, p. 635.

[10] A.B. Karabut, Y.R. Kucherov and I.B. Savvatimova, Excess heat measurements in glow discharge using flow "calorimeter-2", in *5th International Conference on Cold Fusion,* 1995, Monte-Carlo, Monaco, IMRA Europe, Sophia Antipolis Cedex, France, p. 223.

[11] E.G. Campari et al., Photon and particle emission, heat production and surface transformation in Ni–H system, in *11th International Conference on Cold Fusion,* 2004, Marseilles, France, World Scientific, Singapore, p. 405.

[12] S. Focardi et al., *Evidence of electromagnetic radiation from Ni-H systems,* in *11th International Conference on Cold Fusion,* 2004, Marseilles, France, World Scientific, Singapore, p. 70.

[13] A. Takahashi, Progress in condensed matter nuclear science, in *12th International Conference on Cold Fusion,* 2006, Yokohama, Japan, World Scientific, Singapore, pp. 1–25.

[14] E.G. Campari et al., Nuclear reactions in Ni–H systems. in *6th International Workship on Anomalies in Hydrogen/Deuterium Loaded Metals*, 2005, Siena, Italy.
[15] V. Violante et al., X-ray emission during electrolysis of light water on palladium and nickel thin films, in *The 9th International Conference on Cold Fusion, Condensed Matter Nuclear Science,* 2002, Tsinghua Univ., Beijing, China, Tsinghua Univ. Press, p. 376.
[16] T. Matsumoto, Cold fusion experiments with ordinary water and thin nickel foil, *Fusion Technol*. **24 (**993) 296–306.
[17] R.T. Bush and R.D. Eagleton, Experimental studies supporting the transmission resonance model for cold fusion in light water: II. Correlation of X-ray emission with excess power, in *Third International Conference on Cold Fusion, "Frontiers of Cold Fusion",* 1992, Nagoya Japan, Universal Academy Press, Tokyo, Japan, p. 409.
[18] A. Rossi, *J.f Nucl. Phy.,* 2012, http://www.journal-of-nuclear-physics.com/.